Making the Heaviest Elements in the Universe: A Review of the Rapid Neutron Capture Process

John J. Cowan*

HLD Department of Physics & Astronomy,
University of Oklahoma,
440 W. Brooks St.,
Norman, OK 73019,
USA

Christopher Sneden†

Department of Astronomy,
University of Texas, 2515 Speedway,
Austin, TX 78712-1205,
USA

James E. Lawler‡

Physics Department,
University of Wisconsin-Madison,
1150 University Avenue,
Madison, WI 53706-1390,
USA

Ani Aprahamian§ and Michael Wiescher¶

Department of Physics and Joint Institute for Nuclear Astrophysics,
University of Notre Dame,
225 Nieuwland Science Hall,
Notre Dame, IN 46556,
USA

Gabriel Martínez-Pinedo** and Karlheinz Langanke††

GSI Helmholtzzentrum für Schwerionenforschung,
Planckstraße 1, 64291 Darmstadt,
Germany
Institut für Kernphysik (Theoriezentrum),
Technische Universität Darmstadt,
Schlossgartenstraße 2,
64298 Darmstadt,
Germany

Friedrich-Karl Thielemann‡‡

Department of Physics,
University of Basel,
Klingelbergstrasse 82, 4056 Basel,
Switzerland
GSI Helmholtzzentrum für Schwerionenforschung,
Planckstraße 1, 64291 Darmstadt,
Germany

(Dated: January 4, 2019)

The production of about half the heavy elements (beyond Fe and Ni) found in nature is assigned to a specific astrophysical nucleosynthesis process: the rapid neutron capture process (r process). Although this idea has been postulated more than six decades ago, the full understanding faces two types of uncertainties/open questions: (a) The nucleosynthesis path in the nuclear chart runs close to the neutron-drip line, where presently only limited experimental information is available, and one has to rely strongly on theoretical predictions for nuclear properties. (b) While for many years the occurrence of the r process has been associated with supernovae, where the innermost ejecta close to the central neutron star were supposed to be neutron-rich, more recent studies have cast substantial doubts on this environment. Possibly only a weak r process, not producing

the third r-process peak, can be accounted for, while much more neutron-rich conditions, including an r-process path with fission-cycling, are likely responsible for the majority of the heavy r-process elements. Such conditions could result during the ejection of initially highly neutron-rich matter, as found in neutron stars, or during the fast ejection of matter which has prior experienced strong electron-captures at high densities. Possible scenarios are the mergers of neutron stars, neutron-star black hole mergers, but include also rare classes of supernovae/hypernovae with polar jet ejecta (and possibly also accretion disk outflows in case of black hole formation) related to the collapse of fast rotating massive stars with high magnetic fields. The composition of the ejecta from each event determines the temporal evolution of the r-process abundances during the "chemical" evolution of the Galaxy. Stellar r-process abundance observations, have provided insights into, and constraints on the frequency of and conditions in the responsible stellar production sites. One of them, neutron star mergers, just identified thanks to the observation of the r-process kilonova electromagnetic transient, AT 2017gfo, following the Gravitational wave event GW170817. These observations, increasingly more precise due to improved experimental atomic data and high resolution observations, have been particularly important in defining the heavy element abundance patterns of the old halo stars, and thus determining the extent, and nature, of the earliest nucleosynthesis in our Galaxy. Combining new results and important breakthroughs in the related nuclear, atomic and astronomical fields of science, this review attempts to provide an answer to the question "How Were the Elements from Iron to Uranium Made?"

CONTENTS

* jjcowan1@ou.edu
† chris@astro.as.utexas.edu
‡ jelawler@wisc.edu
§ aapraham@nd.edu
¶ Michael.C.Wiescher.1@nd.edu
** g.martinez@gsi.de
†† k.langanke@gsi.de
‡‡ f-k.thielemann@unibas.ch

I. INTRODUCTION AND HISTORICAL REVIEWS

At present we know of 118 elements from charge number $Z = 1$ (H) to $Z = 118$ (Og). 80 of them have at least one stable isotope (up to $Z = 82$, Pb) with $Z = 43$ (Tc) and $Z = 61$ (Pm) being unstable. Another 11 elements up to $Z = 94$ (Pu) [with the exception of $Z = 93$, Np] are naturally occurring on earth with sufficiently long half-lives, while the remaining ones with short half-lives have only been either produced in laboratory or possibly also astrophysical environments. The question of how this took place in the Universe is a long-standing one. Presently we know that of the natural elements/isotopes only ^{1,2}H, ^{3,4}He and ^{7}Li originate in the Big Bang, with problems remaining in understanding the abundance of ^{7}Li (Cyburt *et al.*, 2016; Pitrou *et al.*, 2018). All other elements were synthesized in stars, the first ones forming a few hundred million years after the Big Bang. The majority of stars, which have long evolutionary phases, are powered by fusion reactions. During their evolution, and in explosive end phases, massive stars can synthesize (among others) elements up to, and including, the iron-peak elements (e.g., $21 \leq Z \leq 30$ from Sc to Zn). Major concepts were laid out in the 1950s (Burbidge *et al.*, 1957; Cameron, 1957), and one of the main conclusions was that the production of heavier nuclei up to Pb, Bi, and the actinides requires free neutrons.

A (very) small number of these heavy isotopes are produced as a result of charged-particle and photon-induced reactions in explosive nucleosynthesis, the so called (proton-rich) p process (e.g. Arnould and Goriely, 2003; Travaglio *et al.*, 2018; Nishimura *et al.*, 2018, and references therein), and possibly a further contribution results from interactions with neutrinos in such environments, including the ν process (Woosley *et al.*, 1990; Sieverding *et al.*, 2018) and νp process (Fröhlich *et al.*, 2006; Pruet *et al.*, 2006; Wanajo, 2006).

The two main processes involving the capture of free neutrons are the slow (s) process and the rapid (r) process, with the s process taking place during stellar evolution and passing through nuclei near stability with a process timescale of hundreds to thousands of years. For many of these nuclei experimental data are available (see e.g. Käppeler *et al.*, 2011; Karakas and Lattanzio, 2014; Reifarth *et al.*, 2014). The r process operates (over a timescale of seconds) far from stability requiring high neutron densities in regimes where still little experimental data are known and the quest for its stellar origin involved a large number of speculations for many decades (e.g. Cowan *et al.*, 1991; Arnould *et al.*, 2007). [There are also observational indications of intermediate neutron capture processes between the s and the r process, e.g., the i process (Cowan and Rose, 1977), possibly occurring in super-AGB stars (Jones *et al.*, 2016a).] Fig. 1 gives an overview of the major contributions to the solar system abundances. We note, however, that the contributions of the i, p, ν, and νp processes are minor and thus are not readily apparent in this figure. The focus of this review will be on the r process and the understanding how the corresponding isotopes were synthesized in nature.

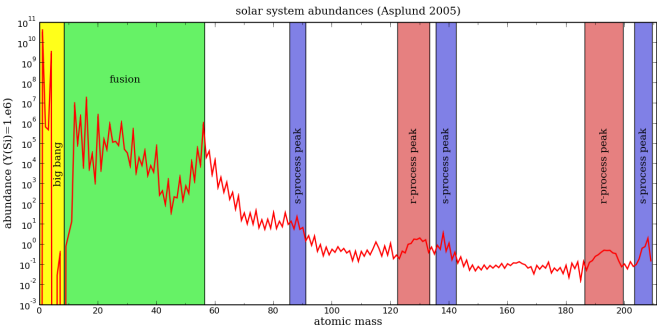

FIG. 1 Abundances, Y_i, of elements and their isotopes in the solar system as a function of mass number $A_i = Z_i + N_i$, with a normalization leading to an abundance of 10^6 for ^{28}Si, rather than $\sum_i A_i Y_i = 1$, as introduced later in the text. Element ratios are obtained from solar spectra, the isotopic rations from primitive meteorites and terrestrial values (Asplund *et al.*, 2009; Lodders *et al.*, 2009). These values represent a snapshot in time of the abundances within the gas that formed the solar system. It formed from contributions of the Big Bang (light elements H, He, Li and their isotopes ^{1,2}H, ^{3,4}He and ^{7}Li, given in yellow) plus stellar sources, contributing via winds and explosions to the interstellar medium until the formation of the solar system. The abundances result from charged-particle fusion reactions up to the Fe-group in stellar evolution and explosions (green), and neutron capture processes. The latter are a superposition of (understood) slow neutron captures (s process) in helium burning of stars (with abundance maxima at closed neutron shells for stable nuclei, blue), and a rapid neutron capture process (r process) leading to abundance maxima shifted to lighter nuclei in comparison to the s process (red). The r process and its stellar origins represent the focus of this article.

Over the years there have been a number of comprehensive reviews on this topic (for a selected list see e.g. Hillebrandt, 1978; Cowan *et al.*, 1991; Qian and Wasserburg, 2007; Arnould *et al.*, 2007; Sneden *et al.*, 2008; Thielemann *et al.*, 2011; Thielemann *et al.*, 2017a,b; Horowitz *et al.*, 2018, and references therein). In order to get clues on the r process origin, a wide range of subtopics need to be addressed: (1) nuclear input to understand the nucleosynthesis path far from stability, (2) nucleosynthesis modeling to find out conditions for neutron densities and temperatures which can reproduce the r-process abundances found in nature, (3) determining whether proposed astrophysical sites can match such conditions, (4) observations of stellar abundances throughout galactic history in order to find out which of these sites can contribute during which period of galactic evolution, (5) in order to do so with good precision a detailed study of the atomic physics is required for identifying the strengths of absorption lines needed to determine abundances, and (6) detections of long-lived

radioactive species that can hint towards understanding the frequencies of r-process events in the Galaxy. Thus, a number of connected fields, including atomic physics, nuclear physics, stellar spectroscopy, stellar (explosion) modeling, and galactic chemical evolution are involved in attempting to answer the long-standing problem of "How Were the Elements from Iron to Uranium Made?", one of the *Eleven Science Questions for the New Century* addressed by the National Academy of Sciences in 2003 (Council, 2003). Detailed discussions will come in the appropriate sections, but we want to mention at this point already a number of suggested scenarios, in order to whet the appetite for these upcoming sections.

While there have been many parametric studies in the early days, assuming a set of neutron densities and temperatures (e.g. Seeger *et al.*, 1965; Kodama and Takahashi, 1975; Kratz *et al.*, 1986; Kratz *et al.*, 1988, 1993; Freiburghaus *et al.*, 1999a; Pfeiffer *et al.*, 2001), the long-standing question is, where an r process with neutron densities of 10^{26} cm^{-3} and higher, producing highly unstable neutron-rich isotopes of all heavy elements and permitting a fast build-up of the heaviest elements up to the actinides, can take place.

There have been many suggestions relating the site of the strong r process to

1. the innermost ejecta of regular core-collapse supernovae (e.g. Schramm, 1973; Sato, 1974; Hillebrandt *et al.*, 1976; Hillebrandt, 1978; Woosley *et al.*, 1994; Takahashi *et al.*, 1994; Witti *et al.*, 1994; Qian and Woosley, 1996; Hoffman *et al.*, 1997; Thompson *et al.*, 2001; Wanajo *et al.*, 2001; Terasawa *et al.*, 2001; Qian and Wasserburg, 2007; Farouqi *et al.*, 2010; Roberts *et al.*, 2010, 2012; Martínez-Pinedo *et al.*, 2012; Arcones and Thielemann, 2013; Mirizzi, 2015; Fischer *et al.*, 2018). However, despite all remaining uncertainties in the explosion mechanism, recent conclusions are that at most a weak r process can occur under these conditions (Wanajo *et al.*, 2011; Martínez-Pinedo *et al.*, 2012; Roberts *et al.*, 2012; Curtis *et al.*, 2018), because weak interactions with electron neutrinos and anti-neutrinos will either make initially neutron-rich matter less neutron-rich or even proton-rich or, if matter is neutron-rich, sufficiently high entropies are not attained.

2. Outer layers of supernova explosions, e.g. the helium layer where neutrons are created by (α, n)-reactions, were also suggested (Truran *et al.*, 1978; Thielemann *et al.*, 1979; Cowan *et al.*, 1980; Hillebrandt *et al.*, 1981; Klapdor *et al.*, 1981; Cameron *et al.*, 1983; Cowan *et al.*, 1983; Thielemann *et al.*, 1983; Cowan *et al.*, 1985; Epstein *et al.*, 1988; Nadyozhin and Panov, 2007; Banerjee *et al.*, 2011; Qian, 2014), later also the collapsing ONeMg core of massive stars (Wheeler *et al.*, 1998). Further options include—for low abundances of heavy elements in the early Galaxy—sufficient amounts of neutrons in He-shell, provided via neutrino interactions (Epstein *et al.*, 1988). But this scenario, with low neutron number densities, would not be able to produce the solar r-process pattern with its correct peak locations (Banerjee *et al.*, 2011, 2016).

3. A special class of core-collapse supernovae (MHD-jet supernovae) with fast rotation, high magnetic fields and neutron-rich jet ejecta along the poles (Symbalisty *et al.*, 1985; Cameron, 2003; Fujimoto *et al.*, 2008; Ono *et al.*, 2012; Winteler *et al.*, 2012; Mösta *et al.*, 2014; Nishimura *et al.*, 2015a; Mösta *et al.*, 2015; Nishimura *et al.*, 2017; Mösta *et al.*, 2018; Halevi and Mösta, 2018; Obergaulinger *et al.*, 2018) showed quite some promise. A further option related to massive stars with fast rotation goes back to Pruet *et al.* (2003, 2004) and Siegel *et al.* (2018). If collapsing to black holes, i.e. leading to collapsars, magnetic field effects could cause the production of medium mass r-process elements in the black hole accretion disk.

4. Ejecta from binary neutron star (or BH-neutron star) mergers (e.g. Lattimer and Schramm, 1974; Symbalisty and Schramm, 1982; Eichler *et al.*, 1989; Freiburghaus *et al.*, 1999b; Rosswog *et al.*, 2000, 2014; Wanajo *et al.*, 2014; Goriely *et al.*, 2011; Just *et al.*, 2015a; Eichler *et al.*, 2015; Goriely *et al.*, 2015; Ramirez-Ruiz *et al.*, 2015; Mendoza-Temis *et al.*, 2015; Shibagaki *et al.*, 2016; Wu *et al.*, 2016; Lippuner *et al.*, 2017; Thielemann *et al.*, 2017b), becoming of special interest after the recent detection of a neutron star merger (GW170817, Metzger, 2017b).

But before discussing these sources in detail, a lot of groundwork has to be laid out. Section II provides an overview of observations (including the atomic physics for their correct interpretation), section III the basic working of an r process and which conditions are needed for its successful operation, sections IV and V discuss the impact played by nuclear physics (with experimental and theoretical investigations), and section VI passes through the astrophysical sites which can fulfill the required conditions, section VIII combines these astrophysical sites and how their role in galactic evolution connects to section II. Finally in the summary (section IX), after having presented all possible connections, we discuss remaining issues and open questions, i.e. whether a single r-process site has been identified by now, or whether we still might need several sources to explain observations throughout galactic evolution.

II. OBSERVATIONS

A. Stellar Abundances of Neutron-Capture Elements in Metal-Poor Stars

Stellar abundance observations over decades have provided fresh evidence about the nature and extent of heavy element nucleosynthesis. In the case of the s process there is direct observational evidence of in situ stellar nucleosynthesis with the observation of the radioactive element Tc, discovered first by Merrill (1952). Additional stellar abundance studies have strongly linked this type of nucleosynthesis to very evolved He shell-burning asymptotic giant branch stars (e.g., Busso *et al.* 1999, Käppeler *et al.* 2011, Karakas and Lattanzio 2014). There is no similar example for the r process, related to nucleosynthesis during stellar evolution; its need for explosive neutron floods ensures that its action is part of the death thores of massive stars or dynamic events around compact objects. Some elements are only formed exclusively or almost so in the r process, such as Eu, Os, Ir, Pt, Th and U (see Figure 2). Their presence in old very metal-poor Galactic halo stars is a clear indication that this neutron process occurred in some violent astrophysical site early in the history of the Galaxy and the Universe (see e.g. Sneden *et al.*, 2008; Thielemann *et al.*, 2017b, and references therein).

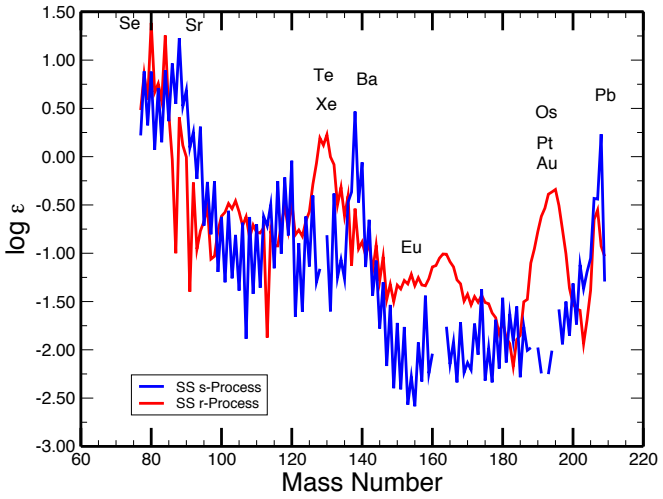

FIG. 2 Breakdown of the solar system abundances into the s and the r process (Cowan and Thielemann, 2004).

Identification of r-process-rich stars began with the discovery of n-capture overabundances in the field red giant HD 115444 (Griffin *et al.*, 1982). This was followed by the identification of an r-process pattern in the well known bright giant HD 122563, even though its overall n-capture element level is depressed relative to Fe (Sneden and Parthasarathy 1983, see also the more extensive analysis of Honda *et al.* 2006). An initial n-capture abundance survey in metal-poor stars (Gilroy *et al.*, 1988) considered 20 red giants, finding a common and easily spotted pattern of increasing overabundances from Ba ($Z = 56$) to Eu ($Z = 63$) among the rare-earth elements. With better echelle spectrographic data came discoveries of many more r-process-rich stars, leading Beers and Christlieb (2005) to sub-classify them as "r-I" with $0.3 \leq$ [Eu/Fe] $\leq +1.0$ and [Ba/Eu] < 0, and as "r-II" with [Eu/Fe] $> +1.0$ and [Ba/Eu] < 0.

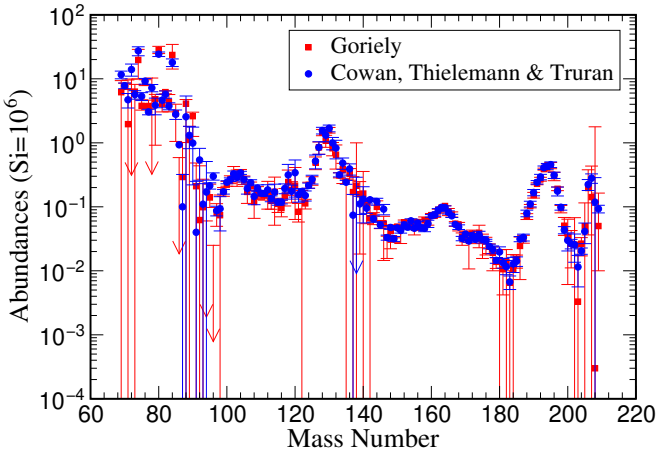

FIG. 3 Solar r-process abundances as determined by Goriely (1999) and Cowan *et al.* (1991). The largest uncertainties are clearly visible for $A \lesssim 100$ (weak s process region) and around lead.

As discussed in the introduction, in general elements heavier than iron are formed via various nucleosynthetic mechanisms, dominantly by the r and s processes. The most detailed deconvolution of abundances into nucleosynthetic contributions exists for the solar system, as we have accurate abundances down to the isotopic lever as a result of meteoritic and solar atmospheric measurements (e.g., Cameron 1959, Asplund *et al.* 2009, Lodders *et al.* 2009, see Fig. 1). Identifying the r-process contributions to the solar system n-capture abundances is usually accomplished by first determining the s-process fractions, (e.g. Käppeler, 1999; Arlandini *et al.*, 1999; Burris *et al.*, 2000; Käppeler *et al.*, 2011). The remaining (residual) amount of the total elemental abundance is assumed to be the solar r-process contribution (see Figures 2 and 3). Aside from the so-called p process (Arnould and Goriely 2003; Rauscher *et al.* 2013; Nishimura *et al.* 2018) that accounts for the minor heavy element isotopes on the proton-rich side of the valley of instability, as well as the ν process (Woosley *et al.*, 1990) and the νp processs (Fröhlich *et al.*, 2006), only the s and r processes are needed to explain nearly all of the solar heavy element abundances.

Early observations of CS 22892-052 (Sneden *et al.* 1994, Sneden *et al.* 2003) and later CS 31082-001 (Hill *et al.* 2002, Siqueira Mello *et al.* 2013 and references therein), indicated a "purely" or "complete" solar system r-process abundance pattern (see Figure 4). (The

total abundances of these, mostly rare-earth, elements in the stars were smaller than in the Sun but with the same relative proportions, i.e., scaled.) This indicated that these stars, that likely formed early in the history of the Galaxy, experienced already a pollution by a robust r process, operating over billions of years in a similar manner.

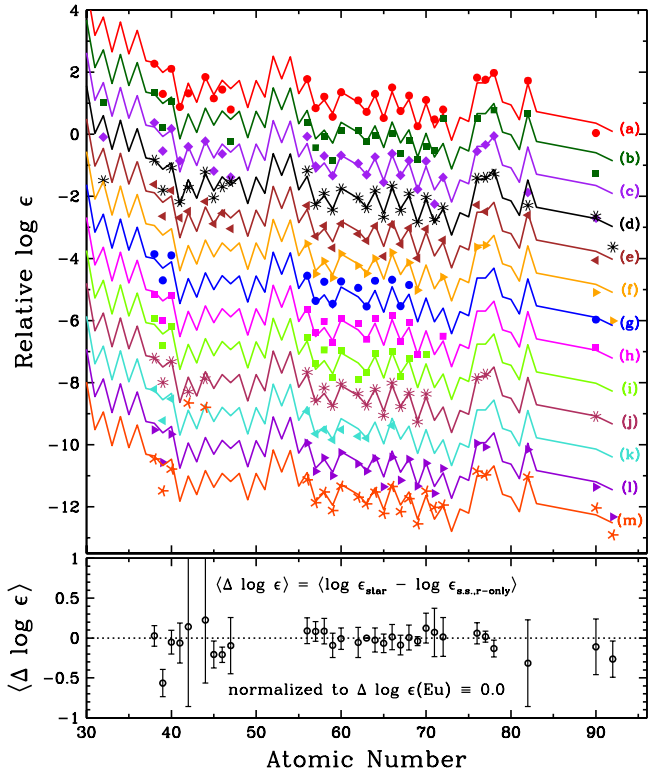

FIG. 4 Top panel: n-capture abundances in 12 r-II stars (points) and the scaled solar-system r-process-only abundances of (Siqueira Mello *et al.*, 2013), mostly adopted from (Simmerer *et al.*, 2004). The stellar and solar system distributions have been normalized to agree for element Eu (Z = 63), and than vertical shifts have been applied in each case for plotting clarity. The stellar abundance sets are: (a) CS 22892-052, (Sneden and Cowan, 2003); (b) HD 115444, (Westin *et al.*, 2000); (c) BD+17 3248, (Cowan *et al.*, 2002); (d) CS 31082-001, (Siqueira Mello *et al.*, 2013); (e) HD 221170, (Ivans *et al.*, 2006); (f) HD 1523+0157, (Frebel *et al.*, 2007); (g) CS 29491-069, (Hayek *et al.*, 2009); (h) HD 1219-0312, (Hayek *et al.*, 2009); (i) CS 22953-003, (François *et al.*, 2007); (j) HD 2252-4225, (Mashonkina *et al.*, 2014); (k) LAMOST J110901.22+075441.8, (Li *et al.*, 2015); (l) RAVE J203843.2-002333, (Placco *et al.*, 2017); (m) 2MASS J09544277+5246414, (Holmbeck *et al.*, 2018a). Bottom panel: mean abundance differences for the 12 stars with respect to the solar system values.

However, the growing literature on abundance analyses of very metal-poor stars has added to our knowledge of the average r-process pattern, and has served to highlight departures from that pattern. Additions to the observational results since the review of Sneden *et al.* (2008) include Roederer *et al.* (2010b, 2014); Li *et al.* (2015); Roederer *et al.* (2016); Roederer (2017); Aoki *et al.* (2017); Yong *et al.* (2017); Hansen *et al.* (2018). These additional observations have shown that there is a complex relationship between light and heavy n-capture elements: Travaglio *et al.* (2004); Cowan *et al.* (2005); Hansen and Primas (2011); Aoki *et al.* (2013); Ural *et al.* (2015); Wu *et al.* (2016). In particular it has been found in some stars that there is significant observed star-to-star abundance scatter of lighter n-capture elements (Z ≤ 50), opposite to the heavier ones (Z ≥ 56), as shown in Fig. 4. For heavy n-capture elements, particularly among the well-studied rare earths, an r process origin does not always mean perfect agreement with the solar r-process pattern. So-called "truncated" r-process stars have been identified with sharp abundance falloffs toward the heavy end of the rare earths (Honda *et al.*, 2006, 2007; Roederer *et al.*, 2010a; Boyd *et al.*, 2012). These observed abundance patterns can be described as having a range of r-process "completeness" with some stars showing only a partial agreement. The differences in these abundance patterns have led to a flurry of stellar models and calculations to identify a site or sites for r process, and to determine why stars show differences in these heavy element patterns. In addition to the suggestion to the operation of a "weak" r process, two additional processes have gained currency: the so-called Lighter Element Primary Process (LEPP; Travaglio *et al.* 2004), and the i process (Cowan and Rose 1977; see also Denissenkov *et al.* 2017 and references therein). (While the LEPP and the i process may explain certain individual stellar abundances, their contributions to the total solar s process (SS) abundances appear to be very small.)

An r-process pattern (defined here as [Eu/Ba] > +0.3) can be seen even in metal-poor stars with bulk deficiencies in n-capture elements: In Fig. 5 we show abundances differences between observed stellar abundances and those of the solar system attributed only to the r process. Fig. 5 is similar in structure to those of Honda *et al.* (2007) and Roederer *et al.* (2010a). As defined in the figure, if $\Delta \log \epsilon = 0$, then the stellar n-capture abundance set is identical to the solar-system r-process-only distribution. This is clearly the case for elements in the atomic numbers range $Z = 57$–78, e.g. La–Pt in CS31082-001 (Siqueira Mello *et al.*, 2013). All extremely r-process-rich stars (classified as "r-II": [Eu/Fe] > +1) have similar abundance runs in the heavy n-capture elements, as discussed above. However, many metal-poor stars with a clear dominance of the r process, as defined by [Eu/Ba] > +0.3, have abrupt drop-offs in abundances through the rare-earth domain. The most dramatic examples are the truncated r-process stars shown in Fig. 5: HD 122563 (Honda *et al.*, 2006) and HD 88609 (Honda *et al.*, 2007). Intermediate cases are abound, as shown in Roederer *et al.* (2010b).

To understand the types and nature of the nucleosyn-

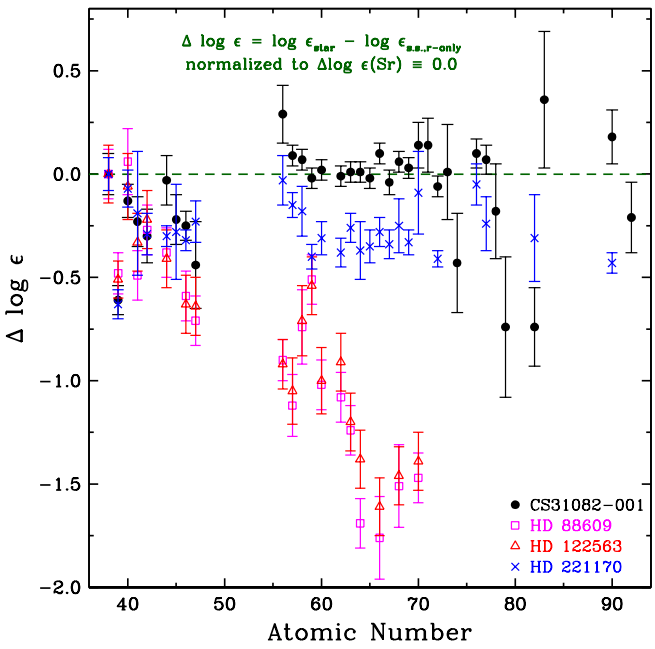

FIG. 5 Differences between stellar and r-process-only solar system (s.s.) abundances for four very metal-poor stars with r-process abundance mixes, after Figure 5 of Honda *et al.* (2007) and Fig. 11 of Roederer *et al.* (2010b). The "s.s.,r-only" abundances are those of Siqueira Mello *et al.* (2013), mostly from Simmerer *et al.* (2004). The stellar abundance sets are: CS31082-001, (Siqueira Mello *et al.*, 2013); HD 88609, (Honda *et al.*, 2007); HD 122563, (Honda *et al.*, 2006); and HD 221170, (Ivans *et al.*, 2006).

thesis, along with identifying the stellar sites and the identities of the first stars in our Galaxy, demands highly precise stellar abundance observations. Those require both high-resolution spectrographic measurements and accurate atomic data. Thus, the discovery of Metal Poor (MP) stars renewed efforts to improve atomic data for many heavy (beyond the Fe-group) n-capture elements (see e.g., Sneden *et al.*, 2009), as discussed below in section II.B.

B. Atomic Data for the Analysis of n-capture Elements in Metal-Poor Stars

Although there was a great need for improved transition probabilities, the identification of lines from n-capture elements in stellar spectra was possible for most elements using readily available laboratory data from about the middle of the 20th Century. Wavelengths of spectral lines of such elements were measured during the first half of the 20th Century using large grating spectrographs such as 10 m Rowland circle instruments. These early wavelength measurements often achieved 1 part per million (ppm) accuracy and were compiled in the well known Atomic Energy Level series by Moore (1971) and for the Rare-Earth Elements by Martin *et al.* (1971). The latter of these two works includes more data from Fourier transform spectrometers (FTSs) and thus achieved $\simeq 0.01$ ppm or 10 ppb accuracy in many cases. All of these spectroscopic data are now available online from the Atomic Spectra Database of the National Institute of Standards and Technology[1]. Although modern optical frequency comb lasers could add many additional digits to energy levels, this technology has not yet been widely applied because of the difficulty in simultaneously using it on large numbers of spectral lines.

The situation with respect to transition probabilities changed with the development of tunable dye lasers originally by Sorokin and Lankard (1966) in the US and Schäfer *et al.* (1966) in Germany. Although it took some time to thoroughly control dye laser performance, many research groups had organic dye lasers with broad tunability, narrow bandwidths (comparable to or less than Doppler widths), short (few nsec) pulse durations, and repetition rates in the 10s of Hz. Non-linear techniques, using crystals and/or gas cells, are needed to access IR and UV wavelengths, and those were also increasingly available. The remaining challenge is to make free atoms and ions of various elements in the periodic table in an optically thin sample with a low collision rate. There are several methods, including sputtering metal cathodes, in a low pressure gas cell (Hannaford and Lowe, 1981), laser driven plasma sources (e.g. Svanberg *et al.* 1994), and the hollow cathode atom/ion beam source developed and favored at the Univ. of Wisconsin-Madison (Duquette *et al.* 1981, Salih and Lawler 1983). The broadly tunable organic dye lasers, in combination with a technique to make low pressure samples of metal atoms and ions, opened the possibility of using time-resolved laser-induced-fluorescence (TRLIF) to measure accurate and precise (about a few %) radiative lifetimes of upper levels on interest in atoms and ions. These lifetimes provide an accurate and precise total decay rate for transition probabilities from the selected upper level.

Emission branching fractions (BFs) in rich spectra still represented a challenge. The same visible and UV capable FTS instruments (e.g. Brault 1976), used to improve energy levels, became the "work horse" of efforts on BFs in complex spectra. Reference Ar I and II lines became internal standards for many laboratory spectra from hollow cathode lamps recorded using FTS instruments (Whaling *et al.* 1993 and references therein). The advantages of interferometric instruments such as the 1 m FTS of the National Solar Observatory on Kitt Peak, AZ were critical for BF measurements in complex spectra. This instrument has a large etendue among all interferometric spectrometers, wavenumber accuracy to 1 part in 10^8, a

[1] http://physics.nist.gov/asd

limit of resolution as small as 0.01 cm^{-1}, broad spectral coverage from the UV to IR, and the capability of recording a million point spectrum in minutes (Brault 1976). Hollow cathode lamps yield emission spectra for neutral and singly ionized atoms of essentially the entire periodic table.

Interest in rare-earth elements is a natural part of studies of n-capture elements in MP stars. Atoms and ions with open f-shells have a great many transitions in the optical. Rare-earths have important applications in general lighting and in optoelectronics because of their rich visible spectra. Rare-earth elements in MP stars are convenient for spectroscopic studies in the optical region accessible to ground based telescopes. Europium is a nearly pure r-process element and lanthanum is a nearly pure s-process element in solar system material. Although none of the r-process peaks are in the rare-earth row, the accessibility from the ground is a major advantage for rare earths. Hubble Space Telescope (HST) observing time is heavily oversubscribed even today.

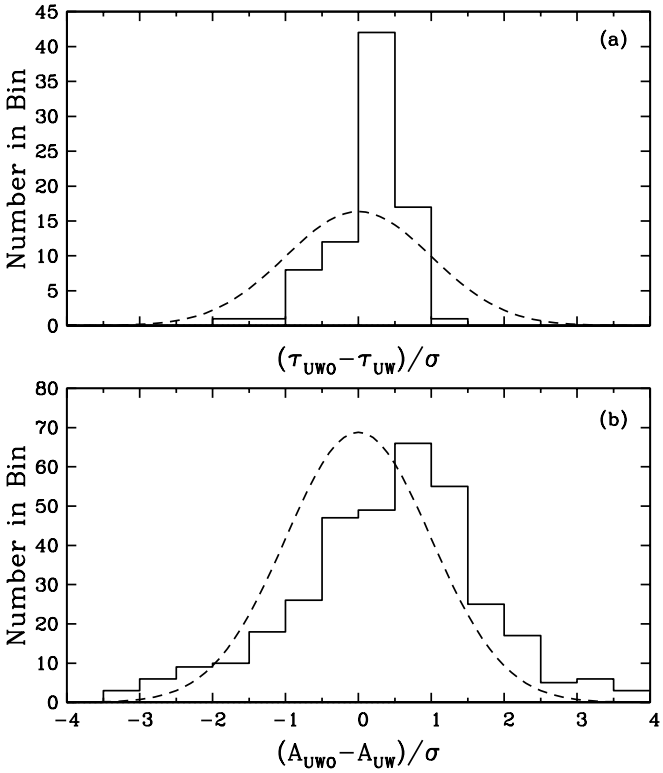

FIG. 6 Comparisons of laboratory data on Sm II from University of Western Ontario (UWO) and University of Wisconsin (UW) groups, adapted from Figs. 4 and 5 of Lawler *et al.* (2008). In panel (a) a histogram of differences in lifetimes (τ divided by their uncertainties added in quadrature) is shown, along with a dashed line representing a one standard deviation Gaussian. In panel (b) we show a similar histogram and Gaussian representation for transition probabilities (A-values).

Rare-earth elements tend to be singly ionized in the photospheres of F, G, and K stars of interest for many elemental abundance studies. The spectrum of singly ionized samarium (Sm II) received attention almost simultaneously by the Univ. of Wisconsin-Madison (UW) laboratory astrophysics team and by a team at the Univ. of Western Ontario (UWO) (Lawler *et al.* 2006, Rehse *et al.* 2006). Publications from these groups did not include comparisons to the measurements from the other group. Lawler *et al.* (2008) completed comparisons from the two sets of measurements in a separate note. Fig. 6 shows a histogram of lifetime measurement differences in common to the two studies with a one standard deviation Gaussian superposed, and a similar histogram comparison for Einstein A coefficients which include BFs. It is clear from these histograms that radiative lifetime uncertainties are overly conservative and BFs uncertainties are satisfactory but perhaps slightly too optimistic in at least one of two sets of measurements.

Uncertainties in radiative lifetimes from TRLIF experiments have proven to be easier to minimize than uncertainties in emission BFs. Various techniques can conveniently be used to check for optical depth (vary the atom/ion beam intensity), to check for collisional effects (throttle a vacuum pump), and to eliminate errors from Zeeman quantum beats (zero the B-field in the experimental region for short lifetimes and introduce a high, 30 Gauss, B-field for long lifetimes). Most importantly benchmark lifetimes in simple spectra such as He I, Be I, Be II, Mg II, etc., which are well known from accurate theory, can be periodically re-measured as an end-to-end test of the TRLIF experiment (Den Hartog *et al.*, 2002). There are multiple challenges in BF measurements. It is essential to have a reliable relative radiometric calibration, and have a source that is optically thin for strong lines of interest. Of course one must resolve lines of interest from nearby blending partners and line identifications must be correct. These latter two constraints are most easily achieved using FTS instruments due to their exceptional resolving power and absolute wave number accuracy and precision. Weak lines from an upper level of interest are clearly most vulnerable to blending, poor signal-to-noise ratios (S/N), and other problems. Uncertainty migrates to weak lines because BFs from an upper level of interest sum to unity by definition.

Elements with wide hyperfine and/or isotopic structure require some additional effort, but in most cases the needed hfs data can be extracted from FTS spectra. The existence of even a few hfs data from single frequency laser measurements is helpful since such data can serve to constrain nonlinear least square fitting of partially resolved hfs patterns in FTS data. Laboratory transition probability measurements on rare-earth ions were summarized during a study of Ce II by Lawler *et al.* (2009) and were applied to five r-process rich very MP stars in a companion paper by Sneden *et al.* (2009). The most striking conclusion from the decade long rare-earth study

is that the relative r-process abundance pattern is stable over time and space. Third r-process peak elements, including Os, Ir, and Pt were observed in MP stars by Cowan *et al.* (2005). Some useful lines of Os I and Ir I are accessible to ground based studies. Unfortunately lines suitable for abundance studies of many lighter n-capture elements are not accessible to ground based observations. Elements near the first r-process peak such as a As and Se have their valence electrons in nearly closed p-shells. The huge gap between the ground and first resonance levels exists in both the neutral and ion energy level structure, although the neutral atom population is dominant in most stars of interest for both of these elements. A similar problem arises for Te at the second r-process peak with only deep UV lines. Fortunately HST time was allocated for a study of Te I lines in multiple MP stars (Roederer *et al.* 2012). The success of the Te study inspired a careful search through the HST archives for one or more stars with sufficiently deep UV spectral coverage for observations on all three r-process peaks (Roederer and Lawler 2012). Unfortunately the star HD 160617 is likely the only such star with sufficient deep UV spectral coverage. Laboratory data sets for many of the lighter r-process elements are included with references in Roederer and Lawler (2012). Laboratory data sets for many of the lighter r-process elements could be improved, but a successor telescopes to HST with a high resolution spectrograph and UV capability will be needed to exploit improvements in the laboratory data.

The discovery of a single line of U II in an MP star by (Cayrel *et al.*, 2001) was a milestone in stellar spectroscopy. Although the single line is on the shoulder of a much stronger Fe I line, there is some confidence in its identification. Thorium is also an element of choice for stellar chronometry (e.g. Sneden *et al.* 2003).

C. Abundance trends in Galactic and Extragalactic Stars

As already discussed in section II.A, the metal-poor Galactic stars show indications of neutron-capture abundances, in fact, it appears as if ALL such stars (to an observational limit) exhibit some level of n-capture abundances. In addition, observations have indicated the presence of n-capture elements such as Ba in nearby dwarf spheroidal galaxies (Shetrone *et al.*, 1998, 2003; Venn *et al.*, 2003). More recently there has been evidence of these elements in ultra-faint dwarf (UFD) galaxies, structures of only about 10^4 $M_\odot$ and possibly being also the building blocks and substructures of the early Galaxy. The 10 up to now discovered UFDs around our Galaxy are very metal-poor with metallicities of [Fe/H] ≈ -3 (Kirby *et al.*, 2013; Frebel and Norris, 2015), and most of them show very low r-process enhancements. However, one of them, Reticulum II, shows highly r-process enhanced stars comparable to Galactic r-process rich stars such as CS 22892-052 (Roederer, 2013; Ji *et al.*, 2016; Roederer, 2017; Ji and Frebel, 2018) which seems to go back to one very early r-process event. In addition to Reticulum II, a further dwarf galaxy, Tuscana III, has very recentlly been observed and also shows these features (Marshall *et al.*, 2018).

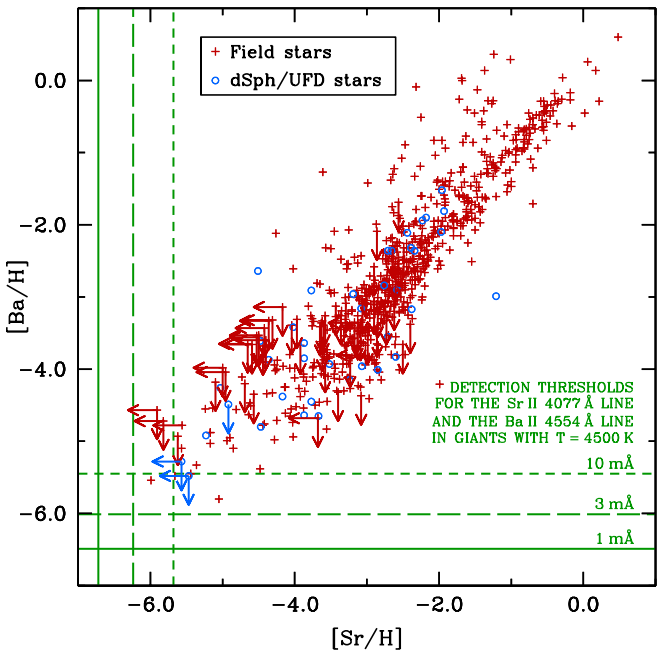

FIG. 7 Abundances of [Sr/Fe] vs. [Ba/Fe] in a large number of Galactic and extragalactic stars from Roederer (2013) and references therein.

We show in Fig. 7, (taken from Roederer, 2013, and references therein), a compilation of abundances in both Galactic and extragalactic stars. In these observations the Sr abundance acts as a surrogate for the overall metallicity of these stars and Ba indicates the enrichment of n-capture elements. The figure illustrates that stars down to the lowest metallicities contain Sr and/or Ba. In a solar mix these are predominantly s-process elements, i.e. their s-process isotopes dominate in present solar abundances. If massive stars with fast rotation rates contributed already some s process in early Galactic evolution (Frischknecht *et al.*, 2016), this could be due to such s-process sources. However, global trends, where observed elemental or isotopic ratios can be deconvolved into s- and r-process contributions, show an s-process appearance only in later periods of Galactic evolution. Thus, this compilation strongly suggests that all of these stars have been enriched in r-process material, which also has implications for early nucleosynthesis in galaxies.

Clues about early Galactic nucleosynthesis are also found in comparison of elements with different nucleosynthesic origin. We show one such comparison in Figure 8, observed in halo stars, i.e. containing elements synthe-

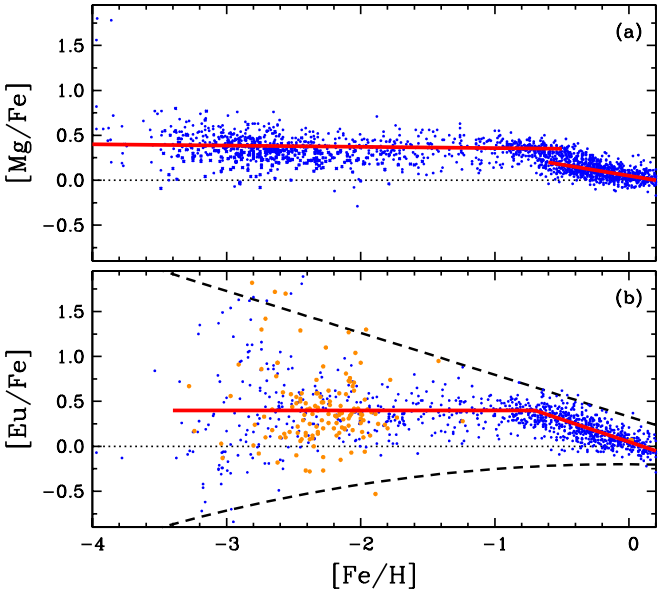

FIG. 8 Abundances as a function of metallicity for [Mg/Fe] (panel a) and [Eu/Fe] (panel b). This is an update of Fig. 14 in (Sneden *et al.*, 2008). Red straight lines are approximate fits to the averages of halo, thick disk, and thin disk stars. Black dashed lines in panel (b) highlight the growing star-to-star scatter in [Eu/Fe] with decreasing metallicity. Individual data points are taken from Fulbright (2000); Hill *et al.* (2002); Reddy *et al.* (2003); Cayrel *et al.* (2004); Simmerer *et al.* (2004); Cohen *et al.* (2004); Barklem *et al.* (2005); Reddy *et al.* (2006); François *et al.* (2007); Bensby *et al.* (2014); Roederer *et al.* (2014); Battistini and Bensby (2016).

sized prior to the formation of these stars. It is evident that alpha elements (such as Mg) appear early in Galactic evolution at low metallicities, originating from fast evolving massive stars and core-collapse supernovae as their final endpoints. Such events occur with a high frequency during galactic evolution and show little scatter. Common r-process elements, like Eu, display an extensive scatter, indicating that they are made in rare events which contribute significant amounts of material, when they occur (see Fig. 8). Such abundance comparisons can be used to put constraints on the site (or sites) for the r process and to understand the history of element formation in the Galaxy (i.e., Galactic Chemical Evolution, GCE). We will return to these issues later in section VIII, after having presented the nucleosynthesis yields of different astrophysical sites.

The eventual demise of the Hubble Space Telescope, able to obtain high-quality UV observations, will hamper future progress in the observation of heavy elements in low-metallicity stars. The James Webb Space Telescope (JWST), the scientific "successor" of HST, will have no UV capability but an IR capability. Identification of n-capture element lines in the IR region could provide new avenues for understanding the operation and nature of the r process (see subsection II.B).

D. The role of long-lived radioactive species

Identification and detailed spectroscopic analysis of a handful of r-II stars, e.g., CS 22892-052 (Sneden *et al.* 1994, Sneden *et al.* 2003) CS 31082-001 (Hill *et al.* 2002, Siqueira Mello *et al.* 2013 and references therein), and HE 1523-0901 (Frebel *et al.* 2007) brought forth detections of the long-lived very heavy n-capture radioactive elements Th ($t_{1/2}$ = 13.0 Gyr) in all of these stars, U ($t_{1/2}$ = 4.6 Gyr), which can only be made in the r process, and in addition an n-capture atomic number range from $Z \approx 30$ to 92, indicating also an r-process pattern. This makes detailed observation vs. theory r-process comparisons possible. More Th detections have been made since then, and more recently U has also been detected in some halo stars. Due to its shorter half-life, its abundance is inherently smaller and detections are difficult. Shown in Fig. 9 from (Holmbeck *et al.*, 2018a) is a uranium detection in 2MASS J09544277+5246414, the most actinide-enhanced r-II star known.

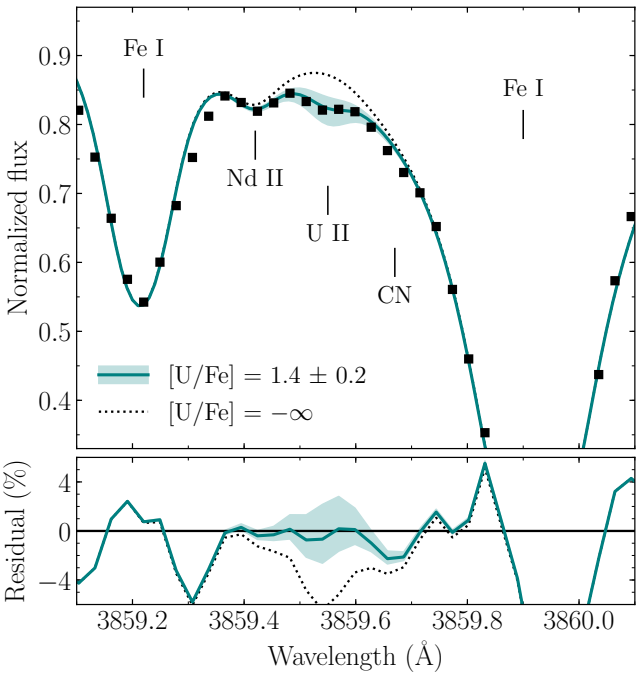

FIG. 9 Synthesis and derived abundance for U in the star MASS J09544277+524641 from Figure 4 of (Holmbeck *et al.*, 2018a).

These Th and U discoveries led to cosmochronology estimates, independent of a cosmological model, based solely on decay half-lives of involved isotopes. This method requires Th/U ratios from theoretical predictions for r-process sources plus observed abundance ratios. This made possible estimates on the decay-time since the birth of a star (when the addition of new material from other nucleosynthesis sites stopped) and promising results were obtained (Cowan *et al.*, 1991; Cowan

et al., 1999; Kratz *et al.*, 2000; Schatz *et al.*, 2002). The same can in principle also be done utilizing the Th/Eu ratio for some stars yielding values in concordance with cosmological age estimates (see above). The fact that some stars seem to have experienced an "actinide boost", i.e. an enhanced amount of Th and U in comparison to lighter r-process elements, could point back to a non-universal r-process production pattern and possibly varying r-process compositions from different productions sites. This made the [Th/Eu] chronology uncertain or non-reliable for such stars (e.g. Cayrel *et al.*, 2001; Honda *et al.*, 2004), having experienced a non-solar r-process contribution, while the [U/Th] did not show these anomalies (Mashonkina *et al.*, 2014). Such an actinide boost is found in a few stars with metallicities of about [Fe/H] = −3. This indicates that (a) an r process was already contributing in very early Galactic evolution, but also (b) with possibly varying conditions for producing the heaviest elements, dependent on the r-process site. Unfortunately it has proved difficult to obtain U detections in many stars, but it is surprising that an actinide boost has not been seen at higher metallicities (see Fig. 10 from Holmbeck *et al.*, 2018a).

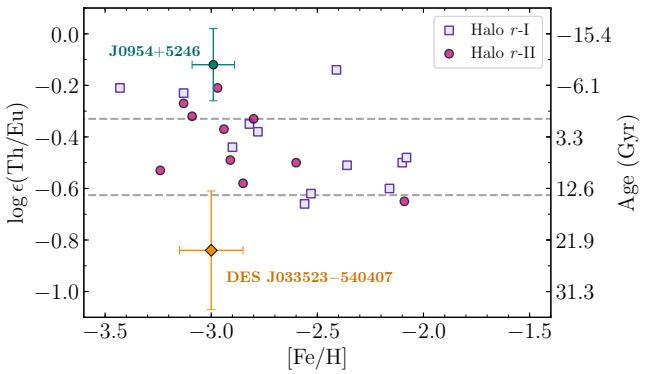

FIG. 10 Th/Eu ratios for stars with detected thorium abundances from Holmbeck *et al.* (2018a). One can see that at low metallicities around [Fe/H]≈-3 quite a number of so-called actinide boost stars can be found. If utilizing initial r-process production ratios which fit solar r-abundances (Schatz *et al.*, 2002), unreasonable, and even negative, ages of these stars are obtained, not at all consistent with their metallicity, which points to the formation of these stars in the very early Galaxy.

In addition to observations of long-lived radioactive species seen via the spectra of stars throughout galactic evolution, there have also been detections in deep-sea sediments, indicating more recent additions of these elements to the earth. While the discussion in II.C points to rare strong r-process events in the early galaxy, the latter detections, suggest the same in recent history. Long-lived radioactive species can act as witness of recent additions to the solar system, dependent on their half-lives. For a review on the signature of radioactive isotopes alive in the early solar system see e.g. Davis and McKeegan (2014). Two specific isotopes have been utilized in recent years to measure such activities in deep sea sediments. One of them, ^{60}Fe, has a half-life of 2.6×10^6 yr and can indicate recent additions from events occurring up to several million years ago. ^{60}Fe is produced during the evolution and explosion of massive stars, leading to supernovae (Thielemann *et al.*, 2011; Wanajo *et al.*, 2013; Limongi and Chieffi, 2018; Thielemann *et al.*, 2018). It is found in deep-sea sediments which incorporated stellar debris from a nearby explosion about two million years ago (Knie *et al.*, 2004; Ludwig *et al.*, 2016; Wallner *et al.*, 2016; Sørensen *et al.*, 2017). Such a contribution is consistent with a supernova origin and related occurrence frequencies, witnessing the last nearby event. Another isotope utilized, ^{244}Pu, has a half-life of 8.1×10^7 yr and would contain a collection from quite a number of such supernova events. If the strong r process would take place in every core-collapse supernova from massive stars, about 10^{-4}–10^{-5} $M_\odot$ of r-process matter would need to be ejected per event in order to explain the present day solar abundances (see Fig. 42). The recent ^{244}Pu detection (Wallner *et al.*, 2015) is lower than expected from such predictions by two orders of magnitude, suggesting that actinide nucleosynthesis is very rare (permitting substantial decay since the last nearby event). This indicates that (regular) core-collapse supernovae did not contribute significantly to the strong r process in the solar neighborhood for the past few hundred million years. Thus, in addition to the inherent problems of (regular) core-collapse supernova models (to be discussed in later sections) to provide conditions required for a strong r process—also producing the actinides—these observational constraints from nearby events also challenge them as source of main r-process contributions. A recent careful study of the origin of the strong r process with continuous accretion of interstellar dust grains into the inner solar system (Hotokezaka *et al.*, 2015) concluded that the experimental findings (Wallner *et al.*, 2015) are in agreement with an r-process origin from a rare event. This can explain the ^{244}Pu existing initially in the very early solar system as well as the low level of more recent additions witnessed in deep-sea sediments over the past few hundred million years.

E. Kilonovae observations

For many years a connection between observations of short-duration gamma-ray bursts (sGRBs), supernova-like electromagnetic transients (macronovae/kilonovae), and compact binary mergers has been postulated (see e.g. Piran, 2004). The first observational evidence, relating a sGRB and an afterglow came in 2013 with the observa-

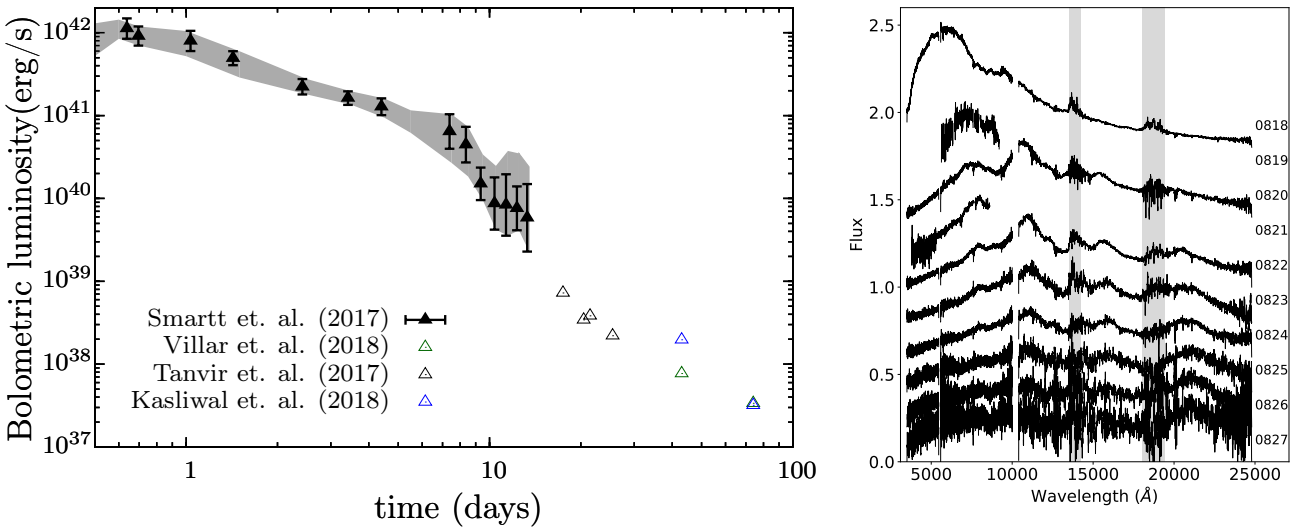

FIG. 11 (right panel) Bolometric light curve of AT 2017gfo, the kilonova associatted with GW170817. The filled black triangles are from Smartt *et al.* (2017). Uncertainties derived from the range of values given in the literature (Waxman *et al.*, 2018; Cowperthwaite *et al.*, 2017; Smartt *et al.*, 2017) are shown as a grey band. Also shown are lower limits (empty triangles) on the late-time luminosity as inferred from the Ks band with VLT/HAWK-I (Tanvir *et al.*, 2017) (black) and the 4.5 μm detections by the *Spitzer Space Telescope* from Villar *et al.* (2018) (green) and Kasliwal *et al.* (2018) (blue) (adapted from Wu *et al.*, 2018). (right panel) Evolution of the kilonova flux spectra during the first 10 days. Each spectra is labelled by the observation epoch. The shaded areas mark the wavelength ranges with very low atmospheric transmission (figure from Pian *et al.*, 2017).

tion of GRB 130603B by Tanvir *et al.* (2013)[2]. First predictions for light curves, accompanying such events due to the decay of radioactive species, were done by Metzger *et al.* (2010b); Roberts *et al.* (2011); Goriely *et al.* (2011). These initial studies used grey opacities appropriate to the Fe-rich ejecta in type Ia SNe and predicted peak luminosities at timescales of a day in the Blue. However, the opacity of heavy r-process elements is substantially higher due to the high density of line transitions associated with the complex atomic structure of Lanthanides and Actinides. This lead to a light curve peak at timescales of a weak in the Red/Near-infrared (Kasen *et al.*, 2013; Barnes and Kasen, 2013; Tanaka and Hotokezaka, 2013). Metzger *et al.* (2015) speculated on the possibility that in fast expanding ejecta unburned neutrons are left and lead via their decay to a Ultraviolet/Blue precursor event. Then finally on 17 August 2017 the gravitational wave event GW170817 was observed (Abbott *et al.*, 2017) and identified as merger of two neutron stars. With the combination of gravitational wave signals and multi-messenger observations its location was identified (Abbott *et al.*, 2017a), a (weak) sGRB detected (Abbott *et al.*, 2017b) (weak probably due to an off-axis observation Wu and MacFadyen, 2018), accompanied by secondary X-ray and radio signals. The amount of dynamical ejecta has been estimated in the range $M_{\rm ej} = 10^{-3}$–10^{-2} M$_\odot$ based on Gravitational wave data (Abbott *et al.*, 2017a). Such amount of ejecta is enough to produce an electromagnetic transient. Within eleven hours of the merger the electromagnetic transient, named AT 2017gfo, was observed in the ultraviolet, optical and near infrared wavelength bands in the galaxy NGC 4993 (Arcavi *et al.*, 2017; Chornock *et al.*, 2017; Coulter *et al.*, 2017; Cowperthwaite *et al.*, 2017; Drout *et al.*, 2017; Evans *et al.*, 2017; Kasliwal *et al.*, 2017; Nicholl *et al.*, 2017a; Pian *et al.*, 2017; Smartt *et al.*, 2017; Soares-Santos *et al.*, 2017; Tanvir *et al.*, 2017). The left panel of Fig 11 shows the bolometric light curve for the two-week-long epoch of detailed observations adapted from (Wu *et al.*, 2018). The figure also includes late-time observations from the Ks band with the VLT/HAWK-I (Tanvir *et al.*, 2017) and the 4.5 μm detections by the *Spitzer Space Telescope* (Villar *et al.*, 2018; Kasliwal *et al.*, 2018). The right panel shows the evolution of the kilonova flux spectra during the first 10 days from Pian *et al.* (2017). The luminosity and its evolution agreed with predictions for the light powered by the radioactive decay of heavy nuclei synthesized via the r process in the neutron-rich merger ejecta (Li and Paczyński, 1998; Metzger *et al.*, 2010b; Roberts *et al.*, 2011; Barnes and Kasen, 2013; Rosswog *et al.*, 2018) (see also section VII). Additional evidence is provided by the spectral/color evolution. The presence of luminous visual wavelength

[2] see https://kilonova.space for an up to date catalog of kilonova observations

("blue") emission at early times was interpreted by most groups as arising from the fastest outer layers of the ejecta, which contained exclusively light r-process nuclei with a relatively low visual wavelength opacity (Metzger and Fernández, 2014; Nicholl *et al.*, 2017a; Drout *et al.*, 2017) (see, however Waxman *et al.*, 2018; Kawaguchi *et al.*, 2018). The observed transition of the emission colors to the near-infrared confirmed predictions for the inner ejecta layers containing lanthanide elements, with atomic mass number $A \gtrsim 140$ (Kasen *et al.*, 2013; Barnes and Kasen, 2013; Tanaka and Hotokezaka, 2013). In order to explain the color evolution of the emission models with at least two-components are necessary. However, three component models are necessary to account for the ejecta components found in neutron star mergers: dynamic, winds, and secular outflows from the disk (Perego *et al.*, 2017a). Combining all observations Villar *et al.* (2017) find a best-fit kilonova model consisting of three-components: a "blue" lanthanide-poor component (opacity $\kappa = 0.5$ cm^2 g^{-1}) with $M_{\rm ej} \approx 0.020$ M$_\odot$, moving with a velocity of approximately 0.27 c, an intermediate opacity "purple" component ($\kappa = 3$ cm^2 g^{-1}) with $M_{\rm ej} \approx 0.047$ M$_\odot$ at 0.15 c, and a "red" lanthanide-rich component ($\kappa = 10$ cm^2 g^{-1}) with $M_{ej} \approx 0.011$ M$_\odot$ at 0.14 c. The three-component model is compatible with a two-component model containing only blue and red components. The blue component is expected to contain light r-process elements with a negligible mass fraction of Lanthanides/Actinides $X_{\rm lan} \lesssim 10^{-4}$ (Kasen *et al.*, 2017). The mass fraction of Lanthanides/Actinides necessary to account for the reddening of the spectra has been inferred to be $X_{\rm lan} \sim 10^{-3}$–10^{-2} (Kasen *et al.*, 2017; Tanaka *et al.*, 2017; Waxman *et al.*, 2018) and hence contains both light and heavy r-process material assuming Solar proportions. The purple component corresponds to ejecta with a small, but non-negligible, lanthanide fraction. The blue-component is expected to be produced by material ejected in the polar direction and associated to dynamical ejecta, the purple and red components are expected to originate from post-merger accretion disk ejecta given their smaller velocities and larger masses (Kasen *et al.*, 2017; Perego *et al.*, 2017a) (see section VI.B). This milestone observation provided the first direct indication that r-process elements are produced in neutron-star mergers including the amount of ejecta, composition and morphology. Additional information about kilonova modeling and the connection of these observations with models of compact binary mergers can be found in section VII.

III. BASIC WORKING OF THE R PROCESS AND NECESSARY ENVIRONMENT CONDITIONS

A. Modeling Composition Changes in Astrophysical Plasmas

Before discussing the working of the r process in detail, a short introduction into the methods should be given, how the build-up of elements in astrophysical plasmas can be described and determined. The mechanism to model composition changes is based on nuclear reactions, occurring in such environments at a given temperature and density. The overall probability for reactions to happen is obtained by integrating the reaction cross section $\sigma(E)$ over the velocity or energy distribution of reacting partners (abbreviated as $\langle \sigma v \rangle$), being for most conditions in stellar evolution and explosions a Maxwell-Boltzmann distribution, which can be generally derived from a Boltzmann transport equation (e.g. Clayton, 1968; Rolfs and Rodney, 1988; Iliadis, 2007; Lippuner and Roberts, 2017). Changes of species can also occur via decays, where the decay constant λ is related to the half-life of a nucleus $t_{1/2}$ via $\lambda = \ln 2/t_{1/2}$. Interactions with photons (photodisintegrations), described by a black-body spectrum for the local temperature, are determined by an integration of the relevant cross section over the energies of the photon Planck distribution. This results also in an effective (temperature-dependent) "decay constant" $\lambda(T)$. Reactions with electrons (electron captures on nuclei) (e.g. Fuller *et al.*, 1980; Langanke and Martínez-Pinedo, 2001; Langanke and Martínez-Pinedo, 2003; Juodagalvis *et al.*, 2010) or neutrinos (e.g. Langanke and Kolbe, 2001, 2002; Kolbe *et al.*, 2003) can be treated in a similar way, also resulting in effective decay constants λ, which can depend on temperature and density (determining for electrons whether degenerate or non-degenerate Fermi distributions are in place), while the λ's for neutrinos require their energy distributions from detailed radiation transport, not necessarily reflecting the local conditions, but rather the transport from their place of origin (see e.g. Liebendörfer *et al.*, 2005, 2009; Richers *et al.*, 2017; Pan *et al.*, 2018b; Burrows *et al.*, 2018).

All the reactions discussed above contribute to three types of terms in reaction network equations. The nuclear abundances Y_i enter in this set of equations and their time derivative can be written in the form

$$\frac{dY_i}{dt} = \sum_j P^i_j \; \lambda_j Y_j + \sum_{j,k} P^i_{j,k} \; \frac{\rho}{m_u} \langle j,k \rangle Y_j Y_k + \sum_{j,k,l} P^i_{j,k,l} \; \frac{\rho^2}{m_u^2} \langle j,k,l \rangle Y_j Y_k Y_l. \quad (1)$$

One has to sum over all reaction partners given by the different summation indices. The P's include an integer

(positive or negative) factor N^i (appearing with one, two or three lower indices for one-body, two-body, or three-body reactions), describing whether (and how often) nucleus i is created or destroyed in this reaction. Additional correction factors $1/m!$ are applied for two-body and three-body reactions in case two or even three identical partners are involved. This can be written as $P^i_j = N^i_j$, $P^i_{j,k} = N^i_{j,k}/m(i,j)!$, or $P^i_{j,k,l} = N^i_{j,k,l}/m(i,j,k)!$. m(i,j) in the second term is equal to 1 for $i \neq j$ and 2 for $i = j$, m(i,j,k) can have the values 1 (for non-identical reaction partners), 2 for two identical partners, and 3 for the identical partners. Thus, this (additional) correction factor (without considering the N^i's) is 1 for non-identical reaction partners, 1/2=1/2! for two identical partners or even 1/6=1/3! for three identical partners. The λ's stand for decay rates (including decays, photodisintegrations, electron captures and neutrino-induced reactions), $\langle j,k\rangle$ for $\langle\sigma v\rangle$ of reactions between nuclei j and k, while $\langle j,k,l\rangle$ includes a similar expression for three-body reactions (Nomoto *et al.*, 1985; Görres *et al.*, 1995), being in reality a sequence of two two-body reaction with a highly unstable intermediate nucleus resulting from the first reaction, which is in chemical equilibrium (see e.g, the next paragraph). A survey of computational methods to solve nuclear networks is given in Hix and Thielemann (1999); Timmes (1999); Hix and Meyer (2006); Lippuner and Roberts (2017). The abundances Y_i are related to number densities $n_i = \rho Y_i/m_u$ and mass fractions of the corresponding nuclei via $X_i = A_i Y_i$, where A_i is the mass number of nucleus i, $\sum X_i = 1$, ρ denotes the density of the medium, and m_u the atomic mass unit. The solution of the above set of differential equations provides the changes of individual nuclear abundances for any burning process in astrophysical environments, requiring the inclusion of all possible reactions and the relevant nuclear input[3]. In astrophysical applications the composition changes determined by Eq. 1 cause related energy generation which can be dynamically coupled to the thermodynamics and hydrodynamics of the event (Mueller, 1986). For large reaction networks that can be computationally rather expensive. For this reason the most often applied approach is splitting the problem in a hydrodynamics/thermodynamics part with a limited reaction network, sufficient for the correct energy generation, and a postprocessing of the obtained thermodynamic conditions with a detailed nucleosynthesis network (see e.g. Ebinger *et al.*, 2018; Curtis *et al.*, 2018, and references therein).

In case matter experiences explosive burning at high temperatures and densities, the reaction rates for fusion reactions are high, and the photodisintegration rates (due to a Planck photon distribution extending to high energies) are high as well. This will lead to chemical equilibria, i.e. balancing of forward and backward flows in reactions, in particular also for proton or neutron capture reactions $p+(Z,A) \rightleftarrows (Z+1,A+1)+\gamma$ and $n+(Z,A) \rightleftarrows (Z,A+1)+\gamma$, corresponding to a relation between the chemical potentials $\mu_p + \mu(Z,A) = \mu(Z+1,A+1)$ and $\mu_n + \mu(Z,A) = \mu(Z,A+1)$, as the chemical potential of photons vanishes. If this is not only the case for a particular reaction, but across the whole nuclear chart, it leads to a complete sequence being in chemical equilibrium, i.e. $Z\mu_p + N\mu_n = \mu(Z,A)$, termed complete chemical or also nuclear statistical equilibrium (NSE) (e.g. Clayton, 1968; Hix and Thielemann, 1999). When the involved particles can be described by a Boltzmann distribution (which is the case in general in astrophysical plasmas, with the exception of highly degenerate conditions, where Fermi distributions have to be utilized for the chemical potentials), the abundances of nuclei can be expressed by nuclear properties like the binding energies $B(Z,A)$, the abundances of free neutrons and protons, and environment conditions like temperatures T and densities ρ, leading to the abundance of nucleus i (with Z_i protons and N_i neutrons or $A_i = Z_i + N_i$ nucleons)

$$Y_i = Y_n^{N_i} Y_p^{Z_i} \frac{G_i(T) A_i^{3/2}}{2^{A_i}} \left(\frac{\rho}{m_u}\right)^{A_i-1} \times \left(\frac{2\pi\hbar^2}{m_u kT}\right)^{3(A_i-1)/2} \exp\left(\frac{B_i}{kT}\right), \quad (2)$$

where B_i is the nuclear binding energy of the nucleus. G_i corresponds to the partition function of nucleus i, as the ground and excited state population is in thermal equilibrium. β-decays, electron captures, and charged-current neutrino interactions, change the overall proton to nucleon ratio $Y_e = \sum Z_i Y_i$ and occur on longer time scales than particle captures and photodisintegrations. They are not necessarily in equilibrium and have to be followed explicitly. Thus, as a function of time the NSE will follow the corresponding densities $\rho(t)$, temperatures $T(t)$, and $Y_e(t)$, leading to two equations based on total mass conservation and the existing Y_e

$$\sum_i A_i Y_i = Y_n + Y_p + \sum_{i,(A_i>1)} (Z_i + N_i) Y_i(\rho, T, Y_n, Y_p) = 1 \quad (3)$$

$$\sum_i Z_i Y_i = Y_p + \sum_{i,(Z_i>1)} Z_i\ Y_i(\rho, T, Y_n, Y_p) \ = Y_e.$$

In general, very high densities favor large nuclei, due to the high power of ρ^{A_i-1}, and very high temperatures favor light nuclei, due to $(kT)^{-3(A_i-1)/2}$ in Eq. (2). In

[3] for data repositories see e.g. https://jinaweb.org/reaclib/db, https://nucastro.org/reaclib.html, http://www.kadonis.org, and http://www.astro.ulb.ac.be/pmwiki/Brusslib/HomePage.

the intermediate regime $\exp(B_i/kT)$ favors tightly bound nuclei with the highest binding energies in the mass range $A = 50 - 60$ of the Fe-group, but depending on the given Y_e. The width of the composition distribution is determined by the temperature (see already early derivations in Clayton, 1968).

Under certain conditions, i.e. not sufficiently high temperatures when not all reactions are fast enough, especially due to small reaction rates caused by too small Q-values across magic proton or neutron numbers (closed shells), not a full NSE emerges but only certain areas of the nuclear chart are in equilibrium, called quasi-equilibrium groups (or QSE). This happens e.g. during early or late phases of explosive burning, before or after conditions for a full NSE have been fulfilled. A typical situation is a break-up in three groups, the Fe-group above Ca ($N = Z = 20$), the Si-group between Ne ($N = Z = 10$) and Ca, the light group from neutrons and protons up to He, and nuclei not in equilibrium from there up to Ne, as discussed in great detail in (Hix and Thielemann, 1999).

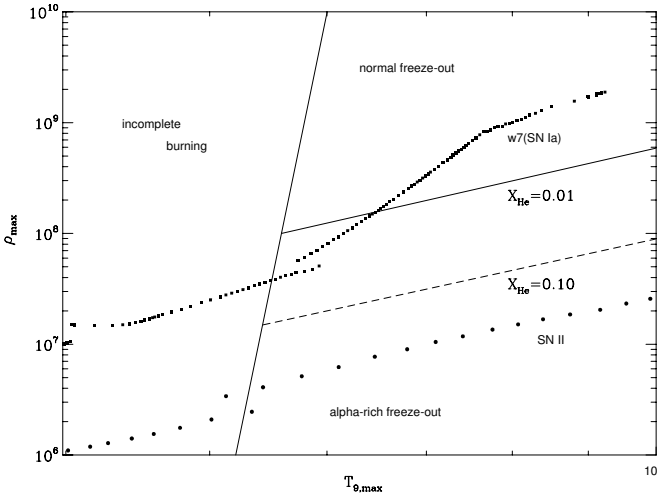

FIG. 12 Plane of maximum temperatures and densities attained during explosive Si-burning, indicating the boundaries of conditions after freeze-out of charged-particle reactions for an adiabatic expansion with an electron fraction $Y_e = 0.498$. For high densities, permitting "three-body" reactions to build-up C (and heavier nuclei), the outcome is a normal freeze-out NSE composition. For lower densities, unburned α-particles remain, i.e. the final outcome is a so-called α-rich freeze-out (see the lines of remaining He mass fractions $X_{\rm He}$). The figure also includes typical conditions experienced in Si-burning mass zones of type Ia and core-collapse supernovae (SNe II), influencing the nucleosynthesis outcome of such explosions.

A so-called α-rich freeze-out is a special case of such QSE conditions, when the build-up of nuclei beyond He is hampered by the need of reaction sequences involving highly unstable ^{8}Be (e.g. $\alpha + \alpha + \alpha \rightarrow ^{12}$C or $\alpha+\alpha+n \rightarrow ^9$Be) which are strongly dependent on the density of matter. The first part of these reaction sequences involves a chemical equilibrium for $\alpha + \alpha \leftrightarrow ^8$Be which is strongly shifted to the left side of the reaction equation, due to the half life of ^{8}Be ($t_{1/2} = 6.7 \times 10^{-17}$s). Reasonable amounts of ^{8}Be, which permit the second stage of these reactions via an alpha or neutron-capture, can only be built-up for high densities. The reation rates for the combined reactions have a quadratic dependence on density in comparison to a linear density dependence in regular fusion reactions. Therefore, for low densities the NSE cannot be kept and an overabundance of alpha particles (helium) remains, permitting only a (much) smaller fraction of heavier elements to be formed than in an NSE for the intermediate temperature/density regime (determined by binding energies of nuclei). This result is, if cooling causes a freeze-out of charged-particle reactions, called an α-rich freeze-out and leads to the fact that (a) the abundance of nuclei heavier than He is (strongly) reduced in comparison to their NSE abundances, and (b) the abundance maximum of the (fewer) heavy nuclei is shifted (via final alpha captures) to heavier nuclei in comparison to an NSE. While this maximum would normally be around Fe and Ni (the highest binding energies) with A=50-60, it can be shifted up to A about 90.

Other quasi-equilibrium conditions are encountered in proton or neutron-rich environments. Such an environment can be essentially free of neutrons, but permitting proton captures and reverse photodisintegrations (e.g. for accretion of a solar abundance composition, which is H-dominated, onto neutrons stars in binary systems, leading to X-ray bursts). This causes QSE-clusters along isotonic lines in the nuclear chart, connected via β^+-decays and/or (α, n)-reactions on longer timescales (see e.g. Rembges *et al.*, 1997). In a similar way Burbidge *et al.* (1957) (followed up later by Seeger *et al.* (1965)), postulated already in their 1957 review that isotopic lines in the nuclear chart are in quasi-equilibrium for neutron-rich r-process conditions (i.e. via neutron captures and their reverse photodisintegrations), connected via beta$^-$-decays on longer tinescales. The latter will be discussed in more detail with respect to the r process. It should be mentioned that both latter applications act close to the proton or neutron drip-lines. This means that small reaction Q-values are involved for proton or neutron captures, and thus also only small photon energies for the inverse reactions are needed to establish such an equilibrium. This changes temperature requirements somewhat. While a full NSE, also close to stability with Q-values of the order 8–10 MeV, is only established for temperatures around 4–5 GK (as a rule of thumb temperatures need to exceed $kT \gtrsim Q/30$), for Q-values of the order 1–2 MeV close to the drip-lines such equilibria can still be established at temperatures exceeding about 1–1.5 GK.

B. Special features of the r process and the role of neutron densities and temperatures

The previous subsection explained in all generality how, due to charged-particle reactions, neutron captures, photo-disintegrations, etc. a complete NSE or also just QSE-subgroups can be established. Here we want to discuss the special case of QSE-subgroups along isotopic chains, before entering a description of the possible sites which permit such quasi-equilibria. When charged-particle reactions are frozen, the only connection between isotopic chains is given by weak processes, i.e. β-decay (for large nuclear masses fission and alpha decay set in lighter nuclei). High neutron densities make the timescales for neutron capture much faster than those for β-decay and can produce nuclei with neutron separation energies $S_n \sim 2$ MeV and less. This is the energy gained (Q-value) when capturing a neutron on nucleus $A-1$ and or the photon energy required to release a neutron from nucleus A via photo-disintegration. Such a process runs close to the neutron-drip line, where S_n goes down to 0. For temperatures around 1 GK (γ, n), describing the photodisintegrations in a thermal plasma, can still be very active for such small reaction S_n-values, as only temperatures about $30\,kT \gtrsim S_n$ are required for these reverse reactions to dominate. With both reaction directions being faster than process timescales (and β-decays) a chemical equilibrium can set in between neutron captures and photodisintegrations. In such a case, many (quasi-)equilibrium clusters exist, representing each of them an isotopic chain of heavy nuclei. The abundance distribution in each isotopic chain follows the ratio of two neighboring isotopes

$$\frac{Y(Z,A+1)}{Y(Z,A)} = n_n \frac{G(Z,A+1)}{2G(Z,A)} \left[\frac{A+1}{A}\right]^{3/2} \times \left[\frac{2\pi\hbar^2}{m_u kT}\right]^{3/2} \exp\left(\frac{S_n(A+1)}{kT}\right), \quad (4)$$

with partition functions G, the nuclear-mass unit m_u, and the neutron-separation (or binding) energy of nucleus $(Z, A+1)$, $S_n(A+1)$, being the neutron-capture Q-value on nucleus (Z, A). This relation for a chemical equilibrium of neutron captures and photo-disintegrations in an isotopic chain can either be derived by utilizing chemical equilibria and the appropriate chemical potentials (as discussed in the previous subsection) or in an equivalent way due to the fact that the cross sections for these reactions and their reverses are linked via detailed balance between individual states in the initial and the final nucleus of each capture reaction. This causes the appearance of partition functions G for population of excited states. The abundance ratios are dependent only on $n_n = \rho Y_n/m_u$, T, and S_n. S_n introduces the dependence on nuclear masses, i.e. a nuclear-mass model for these very neutron-rich unstable nuclei. Under the assumption of an $(n,\gamma) \rightleftarrows (\gamma, n)$ equilibrium, no detailed knowledge of neutron-capture cross sections is needed.

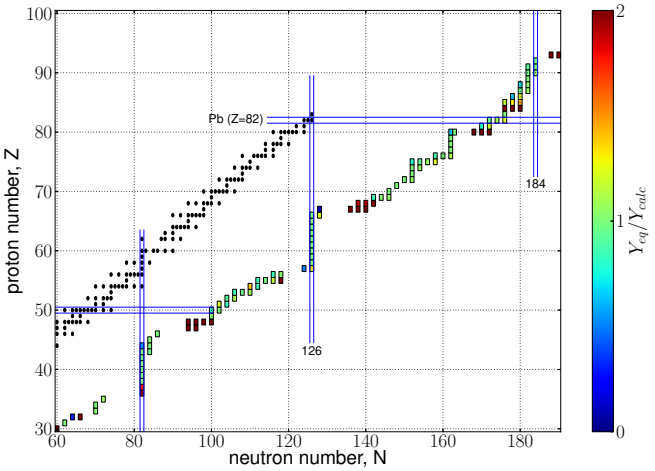

FIG. 13 Shown is (a) the line of stability (black squares) and (b) an r-process path. The special conditions here are taken from a neutron star merger environment which will be discussed further below (Eichler *et al.*, 2015). The position of the path follows from a chemical equilibrium between neutron captures and photo-disintegrations in each isotopic chain ($(n,\gamma) \rightleftarrows (\gamma, n)$ equilibrium). However, the calculation was performed with a complete nuclear network, containing more than 3000 nuclei. The colors along the path indicate how well the full network calculation follows such an $(n,\gamma) \rightleftarrows (\gamma, n)$ equilibrium. It can be seen that such full calculations agree with this equilibrium approach within a factor of 2 along the r-process path, which continues to the heaviest nuclei.

One fact which can be easily deduced, given that $Y(A+1)/Y(A)$ first rises with increasing distance from stability, becomes close to 1 at the abundance maximum of the isotopic chain, and finally decreases, is that the abundance maxima in each isotopic chain are only determined by the neutron number density n_n and the temperature T. Approximating $Y(Z,A+1)/Y(Z,A) \simeq 1$ at the maximum and keeping all other quantities constant, the neutron-separation energy S_n has to be the same for the abundance maxima in all isotopic chains, defining the so-called r-process path.

Fig. 13 shows such r-process path for $S_n \simeq 2$ MeV, when utilizing masses based on the Finite Range Droplet Model (FRDM) (Möller *et al.*, 1995, for a detailed discussion of nuclear properties far from stability see the following sections IV and V). In addition, it displays the line of stability. As the speed along the r-process path is determined by β-decays, and they are longest closer to stability, abundance maxima will occur at the top end of the kinks in the r-process path at neutron shell closures $N = 50, 82, 126$. This causes abundance maxima at the related mass numbers A after decay back to stability at the end of the process, which correspond to smaller mass numbers A than those for stable nuclei with the

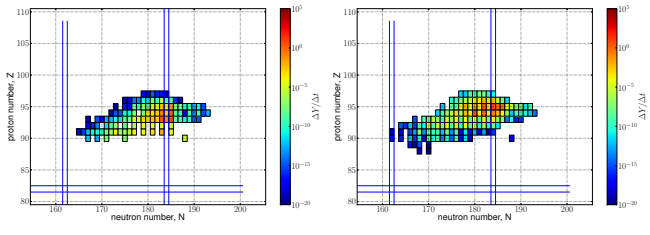

(a)β-delayed fission (b)neutron-induced fission

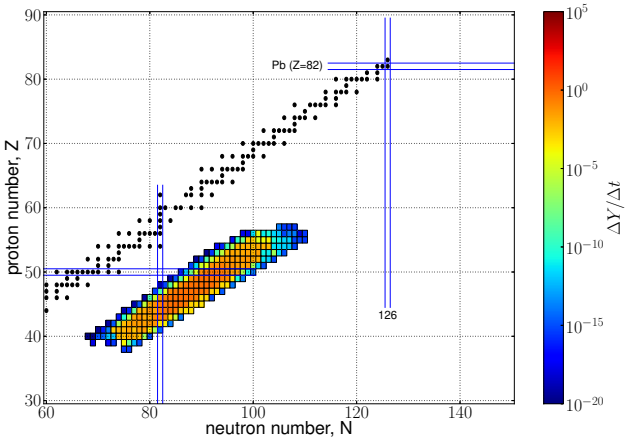

(c)fission fragments

FIG. 14 Shown are (color-coded) time derivatives of nuclear abundances Y during an r-process simulation (Eichler *et al.*, 2015), (a) describing the destruction via neutron-induced and β-delayed fission (Panov *et al.*, 2010) and (b) the production of fission fragments (Kelic *et al.*, 2008). The largest destruction rates occur at and close to the neutron closure $N = 184$, due to the smallest fission barriers encountered at these locations. Fission fragments are produced in a broad distribution, ranging in mass numbers A from 115 to 155.

same neutron shell closures. The latter —experiencing the smallest neutron capture cross sections and determining the speed of the s process— cause s-process maxima at higher mass numbers. In environments with sufficiently high neutron densities, the r process continues to extremely heavy nuclei and finally encounters the neutron shell closure $N = 184$, where fission plays a dominant role.

Fig. 14 shows the regions of the nuclear chart where fission dominates and the location of fission fragments for the given mass models and fission barriers. Nuclear properties like mass models, fission, and weak interactions will be discussed in extended detail in the following two sections.

Early r-process calculations always made use of an $(n, \gamma) \rightleftarrows (\gamma, n)$ equilibrium as discussed above, but had to assume neutron densities, temperatures, and a specific duration time (plus the final decay back to stability,

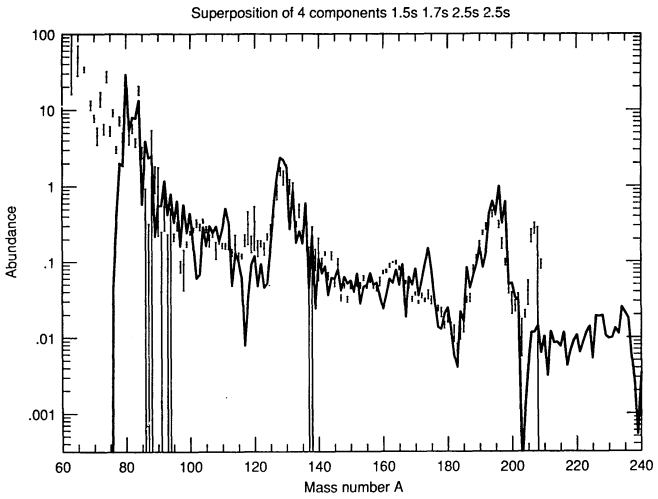

FIG. 15 Global r-abundance curve, obtained from simulations, in comparison to the solar-system r-process component. The predictions utilized time-dependent calculations with constant n_n and T for a duration time τ, followed afterwards by the decay back to stability, including the smoothing of abundances via β-delayed neutron emission. Shown is a superposition of components with four sets of n_n, T, and duration time τ and different (declining) weights applied.

including β-delayed neutron emission) (Burbidge *et al.*, 1957; Seeger *et al.*, 1965; Kodama and Takahashi, 1975). They realized that with such calculations not a unique set of conditions could reproduce solar r-process abundances. Within this approach, and with increasing knowledge of nuclear properties, Kratz and collaborators provided a large series of parameter studies (see e.g. Kratz *et al.*, 1993; Pfeiffer *et al.*, 2001). Fig. 15 shows such a superposition of four components in order to obtain an optimal fit for the three r-process peaks and the amount of matter produced in the actinides.

Dynamical calculations with varying $n_n(t)$, and $T(t)$, and discarding the $(n, \gamma) \rightleftarrows (\gamma, n)$ equilibrium, follow the abundance changes in detail (e.g. Blake and Schramm, 1976; Truran *et al.*, 1978; Cowan *et al.*, 1980; Cameron *et al.*, 1983; Cowan *et al.*, 1985). These calculations showed that the r process can operate under two different regimes with very different nuclear physics demands (Wanajo, 2007; Arcones and Martínez-Pinedo, 2011): a "hot" r process in which the temperatures are large enough to reach $(n, \gamma) \rightleftarrows (\gamma, n)$ equilibrium and a "cold" r process in which the temperatures are so low that photodissociation reactions are irrelevant (Blake and Schramm, 1976). Notice that the differentiation between "hot" and "cold" refers to the temperature conditions during the neutron capture phase and not during the earlier phase when the seeds are build (see next section). Material could be initially very cold and later reheated by nuclear processes, resulting in a hot r process or initially very hot and during the expansion cool to low temperatures producing a cold r process. In general, astrophys-

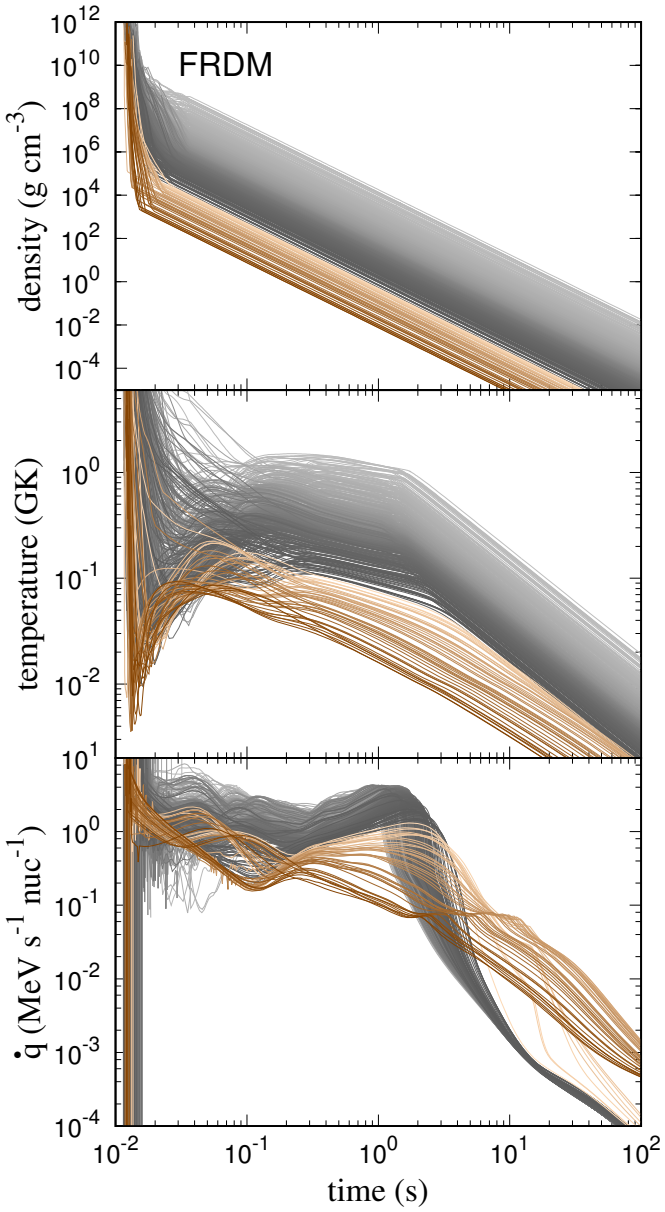

FIG. 16 Evolution of temperature, density, and nuclear energy generation for different trajectories corresponding to material ejected dynamically in neutron star mergers. Gray (brown) lines correspond to the "slow (fast) ejecta" discussed in section VI.B.1. For both gray and brown lines, light (dark) colors correspond to hotter (colder) conditions (adapted from Mendoza-Temis *et al.*, 2015)

.

ical environments produce a broad range of conditions in which both high and low temperatures are reached, this is illustrated in Fig. 16. In some cases the material can reach such low densities that free neutrons remain after the r process (brown lines in the figure) with potentially important observational consequences (Metzger *et al.*, 2015). The figure also shows the nuclear energy generation during the r process (lower panel) that is particularly relevant for very neutron-rich conditions as expected in dynamic ejecta from neutron star mergers (see section VI.B.1) and for kilonova r-process electromagnetic transients (see section VII).

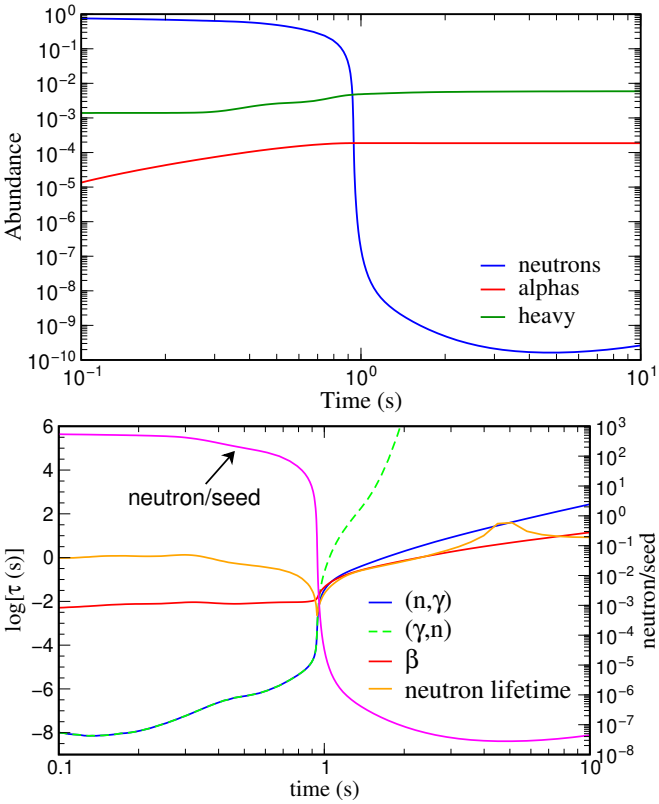

FIG. 17 (Upper panel) Evolution of the abundances of neutrons, alphas and heavy nuclei during the r process. (Bottom panel) Evolution of the neutron-to-seed ratio and average timescales for neutron captures, photodissociation and β-decays (courtesy of M.-R. Wu).

The r process consists typically of two phases: an initial phase dominated by neutron captures and, depending on temperature, photodissociations and a later phase in which neutron captures and β-decays operate on very similar time scales during the decay to stability in what is typically known as r-process freeze-out. The transition between both phases occurs when the neutron-to-seed ratio (i.e. the ratio of free neutrons to heavy nuclei) reaches values close to one. This is illustrated in Fig. 17. The upper panel shows the evolution of the abundances of neutrons, alphas and heavy nuclei for a typical trajectory from those shown in Fig. 16. The lower panel shows the effective neutron lifetime, τ_n, the average radiative neutron capture timescale per nucleus, $\tau_{(n,\gamma)}$, the average photodissociation timescale per nucleus, $\tau_{(\gamma,n)}$, and the average β-decay timescale per nucleus, τ_β, defined as the inverse of their average destruction rates per nucleus for the respective processes (note that $n_n = Y_n \rho / m_u$):

$$\frac{1}{\tau_n} = \left| \frac{1}{Y_n} \frac{dY_n}{dt} \right| \tag{5a}$$

$$\frac{1}{\tau_{(n,\gamma)}} = \frac{\sum_{Z,A} Y(Z,A) n_n \langle \sigma v \rangle_{A,Z}}{\sum_{Z,A} Y(Z,A)} \tag{5b}$$

$$\frac{1}{\tau_{(\gamma,n)}} = \frac{\sum_{Z,A} Y(Z,A) \lambda_\gamma(Z,A)}{\sum_{Z,A} Y(Z,A)} \tag{5c}$$

$$\frac{1}{\tau_\beta} = \frac{\sum_{Z,A} Y(Z,A) \lambda_\beta(Z,A)}{\sum_{Z,A} Y(Z,A)} \tag{5d}$$

Thus, the latter three equations provide the neutron capture rate on an average seed nucleus (averaged over all nuclei with their abundances $Y(Z,A)$), the photodisintegration (γ,n) rate and the β-decay rate, respectively, being the inverse to the corresponding average reaction time scales.

For the calculation shown in Fig. 17 the initial neutron-to-seed (nucleus) ratio, n_s, is ~ 600 allowing for several fission cycles before the end of the r process. The impact of fission can be seen in the upper panel of the figure by the increase in the abundance of heavy nuclei. A similar increase is also seen in the abundances of alpha particles mainly due to the α-decay of translead nuclei. At early times the neutron abundance is large and changes slowly with time. This is a consequence of the almost identical (n,γ) and (γ,n) timescales as the temperatures are large enough to maintain $(n,\gamma) \rightleftarrows (\gamma,n)$ equilibrium. Neglecting the production of neutrons by β-decay and fission one finds the following relation for $1/\tau_n$, corresponding to Eq.(5a), which is equal to the difference between average neutron destructions via neutron capture and productions via photodisintegrations per nucleus, divided by the neutron-to-seed (nucleus) ratio n_s

$$\frac{1}{\tau_n} = \frac{1}{n_s} \left(\frac{1}{\tau_{(n,\gamma)}} - \frac{1}{\tau_{(\gamma,n)}} \right) \tag{6}$$

illustrating the important role played by the neutron-to-seed ratio. Whenever the $n_s > 1$, the effective neutron lifetime is large and there is enough time for the r process to reach a β-flow equilibrium (Kratz *et al.*, 1993; Freiburghaus *et al.*, 1999a) in which the elemental abundances are proportional to effective β-decay half-lives of an isotopic chain, (see Fig. 18), defined as:

$$\frac{1}{t^{\rm eff}_{1/2}(Z)} = \frac{1}{\sum_N Y(Z,N)} \sum_N \frac{Y(Z,N)}{t_{1/2}(Z,N)} \tag{7}$$

During this phase, the r-process path is mainly determined by the two-neutron separation energies, S_{2n} as

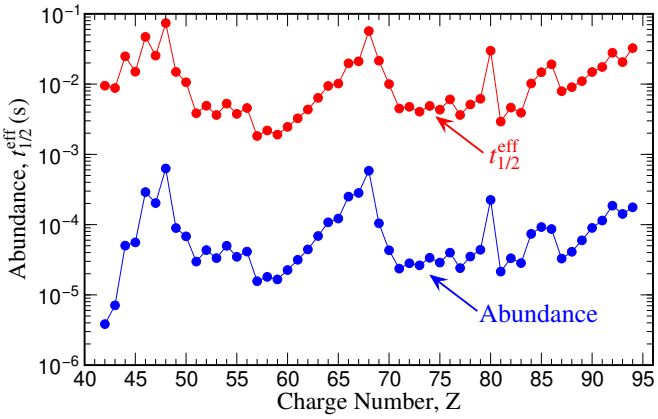

FIG. 18 r-process elemental abundances compared with the effective β-decay half-live of an isotopic chain.

only even neutron number nuclei are present (see Fig. 13). Typically, S_{2n} values decrease smoothly with neutron excess with a sudden decrease at magic neutron numbers. However, for several mass models the S_{2n} are either constant or show saddle point behavior in regions where there is a transition from deformed to spherical nuclei (or vice-versa) just before or after magic shell closures. This translates in the appearance of gaps in the r-process path (see Fig. 13) producing troughs in the abundance distribution (Arcones and Martínez-Pinedo, 2011) before the onset of the freeze-out of neutron captures. This troughs have been extensively discussed in the literature (see e.g. Chen *et al.*, 1995) as a signature of quenching of the $N = 82$ shell gap, however they are most likely related to the behaviour of neutron separation energies discussed above (see e.g. Grawe *et al.*, 2007).

Before freeze-out the nuclei with the strongest impact in the r-process dynamics are those with the longest β-decay half-lives. These are the nuclei closest to the stability at or just after the magic shell closures. Uncertainties in the nuclear physics properties of those nuclei may have a strong impact on the final abundances. This is particularly the case for nuclei located after the $N = 82$ shell closure. (long-lived nuclei with $N = 82$ have known masses and β-decay half-lives.) This is confirmed by sensitivity studies (see e.g. Mumpower *et al.*, 2016) that explore the impact on r-process abundances due to variations of nuclear properties.

Once the r process reaches $n_s \approx 1$, there is an important change in the dynamics. Nuclei start to compete for the few available neutrons and the effective neutron lifetime decreases dramatically, see Eq. (6). The neutron lifetime increases again once the β-decay timescale becomes shorter than the (n,γ) timescale, resulting in a more gradual decline of n_s at later times. The evolution after $n_s \lesssim 1$ is known as r-process freeze-out. During this phase, the timescales of neutron captures and β-decays become similar. It is precisely the competition

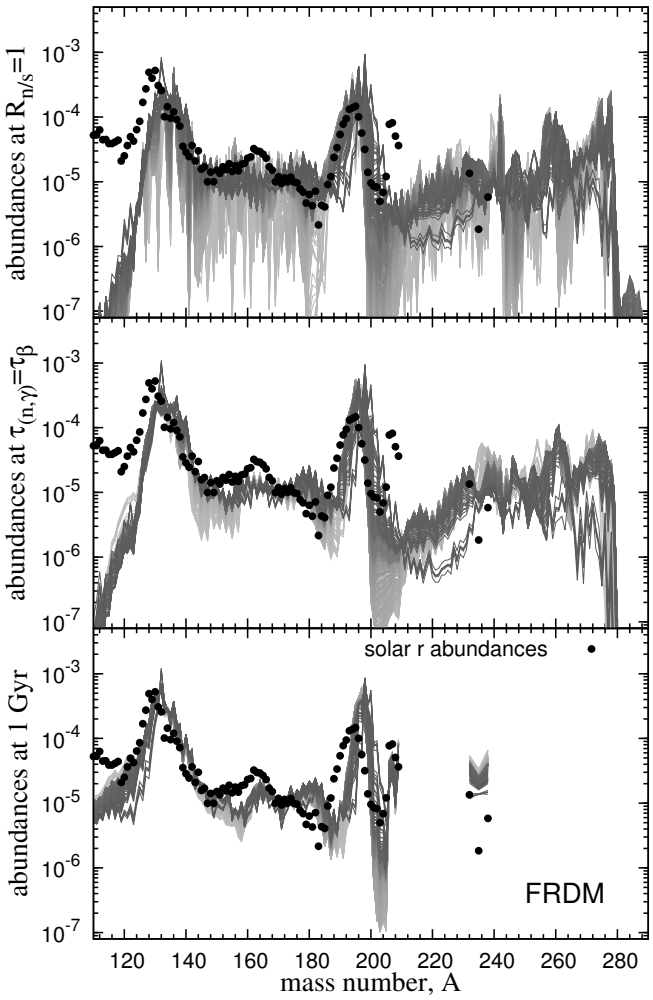

FIG. 19 Evolution of the r-process abundances during freeze-out (adapted from (Mendoza-Temis *et al.*, 2015))

between neutron captures and β-decays (often followed by neutron emission) during the decay to stability that is responsible of smoothing the r-process abundances. Just before the freeze-out the abundances exhibit strong oscillations versus mass number. However, after freeze-out they are rather smooth in agreement with the solar system r-process abundances. This is a characteristic feature of the r process when compared with the s process. In this case, there is never a competition between β-decays and neutron captures and hence the abundances show strong sensitivity on A.

Any process that produces neutrons during freeze-out can potentially affect the final abundances. This includes β-delayed neutron emission and fission with the first one dominating for $n_s \lesssim 150$. One should keep in mind that the impact of neutron production is non-local, in the sense that neutrons can be produced in a region of nuclear chart and captured in another. The freeze-out is responsible of shaping the final abundances. The rare-earth peak is known to be formed during the r-process freeze-out. At low n_s, this is due by a competition between neutron captures and β-decays (Surman *et al.*, 1997), at high n_s, when fission is important, the fission yields play also an important role (Steinberg and Wilkins, 1978; Panov *et al.*, 2008; Goriely *et al.*, 2013; Eichler *et al.*, 2015). The freeze-out has also a strong impact on the abundances at the r-process peaks at $A \sim 130$ and 195. This is illustrated in Fig. 19 that shows the evolution during freeze-out of the abundances for a subset of the trajectories shown in Fig. 16. Due to the large n_s, material accumulates at the $N = 184$ shell closure with $A \sim 280$. During the decay to β-stability the material fissions, producing nuclei with $A \lesssim 240$ and neutrons. Depending on the fission yields used it may result in very different final abundances (Eichler *et al.*, 2015; Goriely and Martínez-Pinedo, 2015). For the calculations shown in Fig. 19, the fission yields produce the $A \sim 130$ peak. Neutrons emitted by fission have a strong impact on the abundances of the 3rd r-process peak. Depending on the masses of nuclei around $N = 130$ (Mendoza-Temis *et al.*, 2015) and the β-decay rates of nuclei with $Z \gtrsim 80$ (Eichler *et al.*, 2015) the peak could be shifted to higher mass numbers when compared with solar system abundances.

After having discussed here the general working of and the nuclear input for an r process, the following subsection discusses how to obtain the required neutron-to-seed rations, before discussing the astrophysical sites section VI. However, independently, the influence of nuclear uncertainties should be analyzed, which will be done in sections IV and V. They can also affect the validity of suitable astrophysical environments. Recent tests with respect to mass models, β-decay half-lives, and fission fragment distributions have been (among others) performed by Arcones and Martínez-Pinedo (2011); Eichler *et al.* (2015); Goriely (2015); Mendoza-Temis *et al.* (2015); Mumpower *et al.* (2016); Marketin *et al.* (2016b); Panov *et al.* (2016); Mumpower *et al.* (2018).

C. How to obtain the required neutron-to-seed ratios

Explosive environments with high temperatures exceeding about 5 GK, lead to a nuclear statistical equilibrium NSE, consisting of neutrons, protons, and α-particles, as discussed subsection III.A. The Y_e which affects the NSE composition is given by the initial abundances and the weak interactions which determine the overall neutron to proton (free and in nuclei) ratio. Essentially all sites of interest for the r process, whether starting out with hot conditions or emerging from cold neutron star material, which heats up during the build-up of heavier nuclei, pass through such a phase. Thus, both cases will lead to similar compositions of light particles and nuclei before the subsequent cooling and expansion of matter, still being governed initially by the trend of keeping matter in NSE.

In hot environments the total entropy is dominated by the black-body photon gas (radiation) and proportional to T^3/ρ (Hartmann *et al.*, 1985; Woosley and Hoffman, 1992; Meyer, 1993; Witti *et al.*, 1994), i.e. the combination of high temperatures and low densities leads to high entropies. Thus, high entropies lead to an α-rich freeze-out (see Fig. 12), and - dependent on the entropy - only small amounts of Fe-group (and heavier) elements are produced, essentially the matter which passed the three-body bottle neck reactions (triple-alpha or $\alpha\alpha$n) transforming He to Be and/or C. This can also be realized when examining Fig. 20, obtained from detailed nucleosynthesis calculations, not assuming any equilibrium conditions. Initially NSE has been obtained. However, dependent on the entropy, different types of charged-particle freeze-out occur, paving the way to the subsequent evolution.

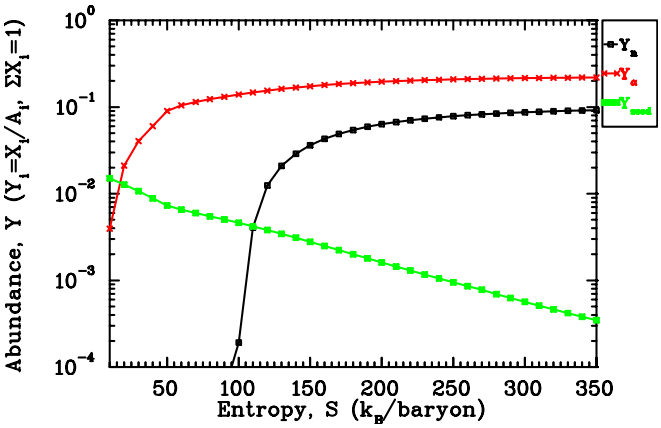

FIG. 20 Abundances of neutrons Y_n, ^{4}He (α-particles) Y_α, and so-called seed nuclei Y_{seed} (in the mass range $50 \leq A \leq 100$), resulting after the charged-particle freeze-out of explosive burning (for a $Y_e = 0.45$), as a function of entropy in the explosively expanding plasma, based on results by Farouqi *et al.* (2010). It can be realized that the ratio of neutrons to seed nuclei ($n_s = Y_n/Y_{\rm seed}$) increases with entropy. The number of neutrons per seed nucleus determines whether the heaviest elements (actinides) can be produced in a strong r process, requiring $A_{\rm seed} + n_s \gtrsim 230$.

The calculation for Fig. 20, start out with matter in an NSE composition for $Y_e = 0.45$, at $T_0 = 8$ GK and a density ρ_0 corresponding to the given entropy. The expansion from those conditions follows on a so-called free-fall timescale $t_{ff} = (3\pi/(32G\rho_0))^{1/2}$ (the timescale on which a homogeneous gas cloud of initial density ρ_0 would contract). This timescale is comparable to the expansion caused by an explosion. Fig. 20 shows how - with increasing entropies - the alpha mass-fraction ($X_\alpha = 4Y_\alpha$) is approaching unity and the amount of heavier elements (which would provide the seed nuclei for a later r process) is going to zero. This is similar to the big bang, where extremely high entropies permit essentially only elements up to He, and tiny amounts of Li. Opposite to

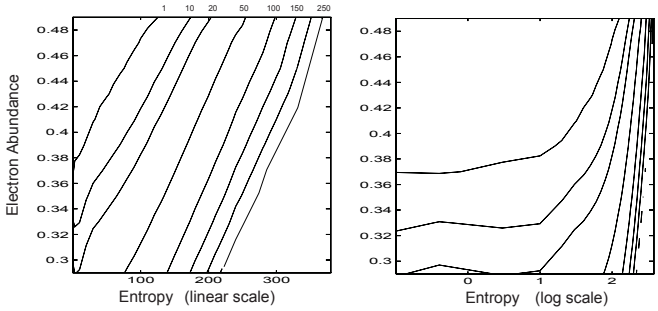

FIG. 21 neutron-to-seed, n_s, ratios (shown as contour lines) resulting in expanding hot plasmas from explosive burning as a function of the electron abundance Y_e and the entropy (measured in k_b per baryon). A strong r process, producing the actinides with n_s of 150, requires for moderate Y_e's, of about 0.45, entropies beyond 250 (Freiburghaus *et al.*, 1999a). The alternative is that for vanishing entropies, i.e. cold matter like in neutron stars, the n_s curves turn over and become independent of entropy. Then an n_s ratio of 150 requires a Y_e of about 0.15 or less.

the Big Bang, experiencing very proton-rich conditions, the $Y_e = 0.45$ chosen here is slightly neutron-rich, leading at high entropies predominantly to He and free neutrons. The small amount of heavier nuclei after this charged-particle freeze-out (in the mass range of $A = 50$–100), depending on the entropy or α-richness of the freeze-out, can then act as seed nuclei for capture of the free neutrons. Once the charged-particle freeze-out has occurred, resulting in a high neutron-to-seed ratio n_s, the actual r process - powered solely by the rapid capture of neutrons - can start, at temperatures below 3 GK. Whether this r process is a "hot" or "cold" one, as discussed in subsection III.B, i.e. governed by an $(n,\gamma) \rightleftarrows (\gamma,n)$ equilibrium or the competition of neutron captures and β-decays, depends on the resulting neutron densities and temperatures.

For both cases, a prerequisite for an r process, the neutron-to-seed ratio depends of the mass range of nuclei to be produced. Starting with $A = 50$–100 nuclei, the production of lanthanides requires $n_s \sim 50$ while the one of actinides $n_s \sim 150$. Figure 21 shows the lines of constant n_s as a function of entropy and Y_e, illustrating the dependence $n_s \sim s^3/(Y_e^3 \tau_{dyn})$ of the neutron-to-seed ratio as a function of entropy, Y_e and expansion dynamical timescale $\tau_{\rm dyn} = [(d\rho/dt)/\rho]^{-1}$ (Hoffman *et al.*, 1997; Freiburghaus *et al.*, 1999a).

When considering the result of these investigations, there remain two options for a strong r process in matter which was heated sufficiently to pass through NSE: (a) for moderately neutron-rich conditions with Y_e not much smaller than 0.5, only very high entropies can provide the necessary environment. (b) For very low entropies, the n_s ratio becomes essentially entropy-independent, $n_s \approx A_{\rm seed}[Z_{\rm seed}/(A_{\rm seed}Y_e) - 1]$, such that only very neutron-rich matter ($Y_e \lesssim 0.15$) can support a strong

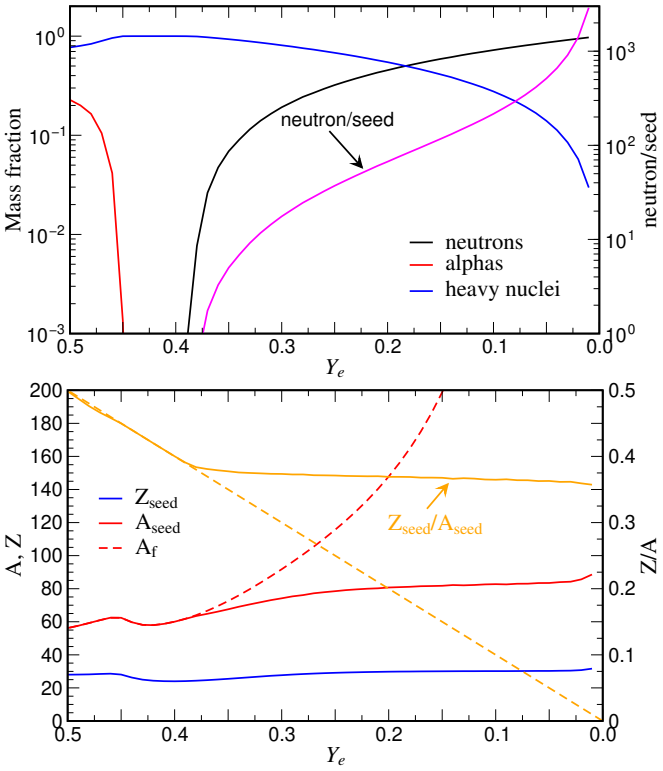

FIG. 22 (top panel) Evolution of the mass fractions of neutrons, alphas and heavy nuclei versus Y_e (left y-axis scale) and neutron-to-seed (right y-axis scale) at a temperature of 3 GK for an adiabatic expansion with an entropy per nucleon $s = 20\ k_B$. (lower panel) Evolution of the average mass, A, and proton number Z of the seeds and the final mass number $A_f = A_{\rm seed} + n_s$ versus Y_e (left y-axis scale). The evolution of Z/A is also shown (right y-axis scale). As a reference Y_e is shown as a diagonal dashed line.

r process. Fig. 22 shows such a case of low entropies per nucleon using $s = 20\ k_B$, typical for matter ejected in neutron star mergers. It shows several quantities as a function of Y_e. Comparing with Fig. 20 at $S = 20$ and for $Y = 0.45$ one finds consistent results, i.e. essentially only alphas and heavy nuclei (no free neutrons) with typical charges $Z_{\rm seed} \approx 28$ and $A_{\rm seed} \approx 63$. Only for $Y_e \lesssim 0.38$ free neutrons start to appear and Lanthanides are produced for $Y_e \lesssim 0.25$ (see Lippuner and Roberts, 2015, for a systematic study of the astrophysical conditions necessary to produce Lanthanides).

IV. EXPERIMENTAL DEVELOPMENTS FOR R-PROCESS STUDIES

The r-process path runs through nuclei with extreme neutron excess. Most of these nuclei have yet not been produced in the laboratory and their properties are experimentally unknown. Hence the nuclear input required for r-process simulations must largely be modelled. This has always been a source of noticeable uncertainties. This situation has already improved as some intermediate-mass r-process nuclei could be produced at existing radioactive ion-beam facilities like CERN/Isolde, GSI and, in particular, RIKEN. Significant advance, however, is expected in the future when key r-process nuclei, including those around the third r-process peak, become accessible at the next-generation RIB facilities like FAIR and FRIB. This will be discussed in more detail in the following sections. Data taken at these facilities will not only directly substitute theory predictions, but will also serve as stringent and valuable constraints to advance model predictions for even then not accessible nuclei.

The next two sections deal with the nuclear ingredients needed for r-process simulations. At first we will discuss the various experimental approaches to produce and study neutron-rich nuclei and summarize the experimental data relevant for r-process nucleosynthesis which have been achieved recently. In the next section we present the nuclear models applied to interpret the experimental results and derive the vast nuclear data sets needed for large scale simulations. We will focus on theoretical advances achieved by improved models and experimental constraints and guidance, and finally discuss the impact on the improved nuclear data on our understanding of r-process nucleosynthesis.

There has been considerable experimental effort over the last forty years to explore the nuclear physics of the r-process and the structure and properties of r-process nuclei along the projected reaction path; a goal that is nearly equivalent with exploring the evolution of nuclear structure towards the limits of stability. This was one of the strong motivations towards the development of facilities capable of producing radioactive ion beams. The experiments have concentrated on measurement of masses, β decay and β-delayed neutron emission probabilities of neutron rich nuclei towards and on occasion even at the anticipated r-process path. A multitude of experimental probes have been used to facilitate the production and separation of very neutron rich short-lived nuclei and to measure their specific properties. The traditional tools in the past ranged from extracting fission products from reactors to the use of spontaneous fission sources, to the analysis of short-lived reaction products at ISOL and fragmentation facilities. The enormous progress in producing neutron-rich isotopes with increasing intensity and resolution was enabled by the simultaneous progress in the development of new experimental techniques and detectors. The traditional approach of tape-collection and decay analysis leading to half-life and β-endpoint determination for single separation products was replaced by large scale ring experiments for measuring hundreds of masses at once, or complementary to that by sophisticated trapping experiments for determining the masses and decay properties of individual neutron-rich nuclei with unprecedented accuracy.

While the utilization of these facilities and techniques

produced a wealth of data, it primarily addressed the needs for knowledge about the collective properties of neutron-rich nuclei near or at the r-process path. These studies provided important information and input for the early r process simulations based on the $(n,\gamma) \rightleftarrows (\gamma,n)$ equilibrium assumptions. Specific challenges remained, such as the (n,γ) nuclear cross section reaction data for simulating the r-process nucleosynthesis after freeze-out. The associated reaction cross sections and reaction rates that are now used in dynamic r-process simulations rely entirely on statistical model calculations, utilizing Hauser-Feshbach codes like SMOKER, NON-SMOKER[4], and TALYS[5]. While this approach is commonly used, it is not clear how reliable these predictions for the (n,γ) reaction rates are and how valid they are for reactions on neutron-rich closed-shell nuclei that are characterized by low Q-values (Rauscher *et al.*, 1997). In fact, it is expected that close to the stability the direct capture component dominates, permitting possibly an $(n,\gamma) \rightleftarrows (\gamma,n)$ equilibrium down to lower temperatures (Mathews *et al.*, 1983), but how reliable are the predictions for the strength of such direct capture components (Goriely, 1998; Arnould *et al.*, 2007)? A direct measurement of neutron capture reactions on short-lived neutron-rich nuclei is challenging and certainly not feasible within the near future. The experimental developments have focused on two approaches that combine theory and experiment in order to get at the neutron capture cross-sections, the β-Oslo method (Spyrou *et al.*, 2014, 2017; Tornyi *et al.*, 2014; Guttormsen *et al.*, 1987) and surrogate reactions (Escher *et al.*, 2012), mostly (d,p) to get access to (n,γ) rates. New initiatives have also recently been proposed for direct neutron capture studies at ring experiments (Reifarth *et al.*, 2017). This proposal is particularly challenging since the idea is to combine, for the first time, a method that couples radioactive beam with radioactive target experiments. Below, we discuss the facilities and approaches presently used for the production of neutron-rich nuclei on or near the r-process path, along with some of the noteworthy experimental developments in tools and techniques that allow measurements of nuclear masses, β-decay rates, β-delayed neutron emission probabilities, and neutron capture rates of nuclei required as inputs for reliable simulations of the r process.

A. Production of neutron-rich isotopes

The biggest challenge in experimentally studying isotopes near or at the r-process path is the production of these isotopes in sufficient abundances to explore their properties. This is closely correlated with the selectivity of the separators necessary to select the isotopes in question and the sensitivity of the detectors for measuring the respective properties. The overall production of rare isotopes has not significantly improved over the last decades due to the cross section limitations in the production reactions, or the energetics of the facilities to produce beams. However, substantial improvements have been made in the selection process due to innovative techniques in the isotope separation through electro-magnetic systems and the increasing utilization of laser based separation techniques. Also, enormous progress has been made on the detection side, and the development of ion trapping techniques has overcome many of the statistical limitations in the more traditional measurements of lifetimes, masses, and direct measurements of β-delayed neutron emission probabilities of the very neutron-rich nuclei. This section addresses the production of neutron rich nuclei in reactors, in spontaneous fission sources, in fission products in accelerators, at spallation sources or ISOL facilities, and at fragmentation facilities.

1. Nuclear reactors and fission product sources

One of the traditional methods for the production of neutron-rich nuclei is the extraction and separation of neutron-rich fission products from high flux nuclear reactors. Pioneering work has been done at the TRISTAN separator (McConnell and Talbert, 1975; Talbert *et al.*, 1979) at the Ames Laboratory Research Reactor in Iowa. The TRISTAN separator was moved in the mid 1970's to the 60 MW High Flux Beam Reactor (HFBR) at Brookhaven National Laboratory (Crease and Seidel, 2000). The fission products were ionized, extracted from a ^{235}U target placed in an ion source located in a beam line close to the reactor core, and separated. A similar separator was installed at the at the High Flux Reactor of the Institute Laue Langevin (ILL) in Grenoble, France, where the LOHENGRIN fission fragment separator is used to extract and analyze fission products to order to study their decay properties (Armbruster *et al.*, 1976). This facility was complemented by the installation of thermoionization separators, OSTIS I & II, at the ILL. The OSTIS separator concept (Wünsch, 1978; Münzel *et al.*, 1981) was based on the use of an external neutron guide line bombarding an external ^{235}U source. This approach allowed the measurement of shorter-lived fission products since it reduced the transport times to the ion-source. Studies of neutron-rich nuclei were also performed at smaller reactors as long as separators were available to select the desired fission product. Measurements of masses, decay half-lives, β-delayed neutron emission probabilities, and γ-ray decay properties were performed with the best techniques available utilizing moving tape systems. The measurement of neutron-rich

[4] https://nucastro.org/reaclib.html
[5] http://www.talys.eu/more-about-talys

isotopes reached close to some of the r-process trajectories, in particular for the alkali isotopes. The measurements on the neutron-rich Rubidium isotopes made at that time (Lhersonneau *et al.*, 1995) are only rivaled now some twenty-five years later. The main handicaps, for reaching the r-process path and mapping the very neutron-rich nuclei, were the fission product distribution and long extraction times for the fission products. All of these measurements had limitations that were overcome with the new advances and technical developments in detectors, including new neutron detection technologies based on ^{6}Li-glass, ^{3}He tubes, and ^{3}He spectrometer systems (Kratz *et al.*, 1979; Yeh *et al.*, 1983). Fission studies with traditional approaches limited the access to the very short-lived nuclei along the r-process path, but the development of new and more sensitive detection systems such as traps or laser ionization, used in conjunction with spallation or spontaneous fission sources or with the use of storage rings at fragmentation facilities, has revolutionized the studies of neutron-rich r-process nuclei.

2. Spallation sources and ISOL techniques

The on-line separators for fission products were complemented by ISOLDE (Isotope Separator On-Line DEtector), designed in the mid-sixties for separating spallation products that were produced by impinging 600 MeV protons from the synchro-cyclotron at CERN on a stationary target. The spallation of the heavy target nuclei produced a variety of fragments, which were extracted and filtered to yield the desired isotope. The time required for extraction placed a lower limit on the half life of isotopes which could be produced by this method. Once extracted, the isotopes were directed to one of several detector stations for measuring the decay properties. The ISOLDE separator was moved in 1990 to the CERN PS booster to increase the yield of the spallation products (Kugler *et al.*, 1992). In a two-step process, the 1 GeV proton beam from the PS-Booster impinging on a Ta or W rod positioned in close proximity to the uranium-carbide target produced the fast spallation neutrons to induce fission. This method was essential for suppressing the proton-rich isobaric spallation products that dominated the spallation yield. The new ISOLDE system was one of the most successful sources for neutron-rich isotopes and dominated the production of neutron-rich isotopes for nearly two decades. The implementation of laser ion-source techniques for the selection of specific Z-selectivity, and hence selection of specific elements, was a significant improvement to studies of neutron-rich nuclei. The laser ionization of the fission products led to a significant reduction in isobar background. This was further improved by using the hyperfine splitting to select or separate specific isomers in neutron-rich isotopes. These gradual improvements of ion source and separator techniques finally led to the detailed measurement of the r-process waiting point nucleus ^{130}Cd, the first milestone in reaching and mapping the r-process path (Dillmann *et al.*, 2003), as well as the recent mass measurements of $^{129-131}$Cd nuclei (Atanasov *et al.*, 2015) near the doubly closed magic shell nucleus of ^{132}Sn, a capability that is unmatched to date.

3. Fragmentation sources

Another successful technique for the production of neutron-rich isotopes is the use of fragmentation for the production of neutron-rich, or fusion-evaporation for the production of neutron-deficient, isotopes in heavy ion reactions. The GSI Online Mass Separator was one of the first instruments to utilize fusion-evaporation for studying isotopes far from stability using heavy-ion beams from the UNILAC accelerator. The reaction products were stopped in a catcher inside an ion source, from where they were extracted as singly charged (atomic or molecular) ions and re-accelerated to 60 keV. These beams were implanted, yielding sources for β or particle decay spectroscopy (Bruske *et al.*, 1981). This method, however, was more suitable for the study of neutron-deficient isotopes and remained not competitive with fission product or spallation based production of neutron-rich isotopes. This instrument was gradually replaced by the Projectile Fragment Separator FRS to focus on the neutron-rich side of the line of stability (Geissel *et al.*, 1992). Fragmentation was based on smashing a high energy heavy ion beam on light target material and collecting the fragments through electromagnetic separator systems for subsequent on-line analysis. The great advantage of this technique over the traditional ISOL approach was that even short-lived isotopes could be studied if properly separated. Fragmentation played an increasingly important role for β-decay studies of r-process isotopes both at the fragment separators at GSI (Kurcewicz *et al.*, 2012), at NSCL/MSU in the US (Quinn *et al.*, 2012), and RIKEN in Japan (Lorusso *et al.*, 2015). The measurement of a very neutron-rich, doubly closed shell nucleus, ^{78}Ni, at the on-set of the r process, presented a particularly impressive example on the new relevance of fragment separators for the study of r-process nuclei (Hosmer *et al.*, 2005). The simultaneous measurement of the half-lives of 110 neutron-rich nuclei near the $N = 82$ closed shell gap at RIKEN (Lorusso *et al.*, 2015) proved a substantial step forward for studies of r-process nuclei (see Fig. 23). Another example is the systematic study of β-decay half-lives and β-delayed neutron emission processes using the BELEN ^{3}He detector array for 20 heavier isotopes of Au, Hg, Tl, Pb, and Bi in the neutron-rich mass region above the neutron shell closure $N = 126$ (Caballero-Folch *et al.*, 2016) to probe the feeding pattern of the third r-process abundance peak

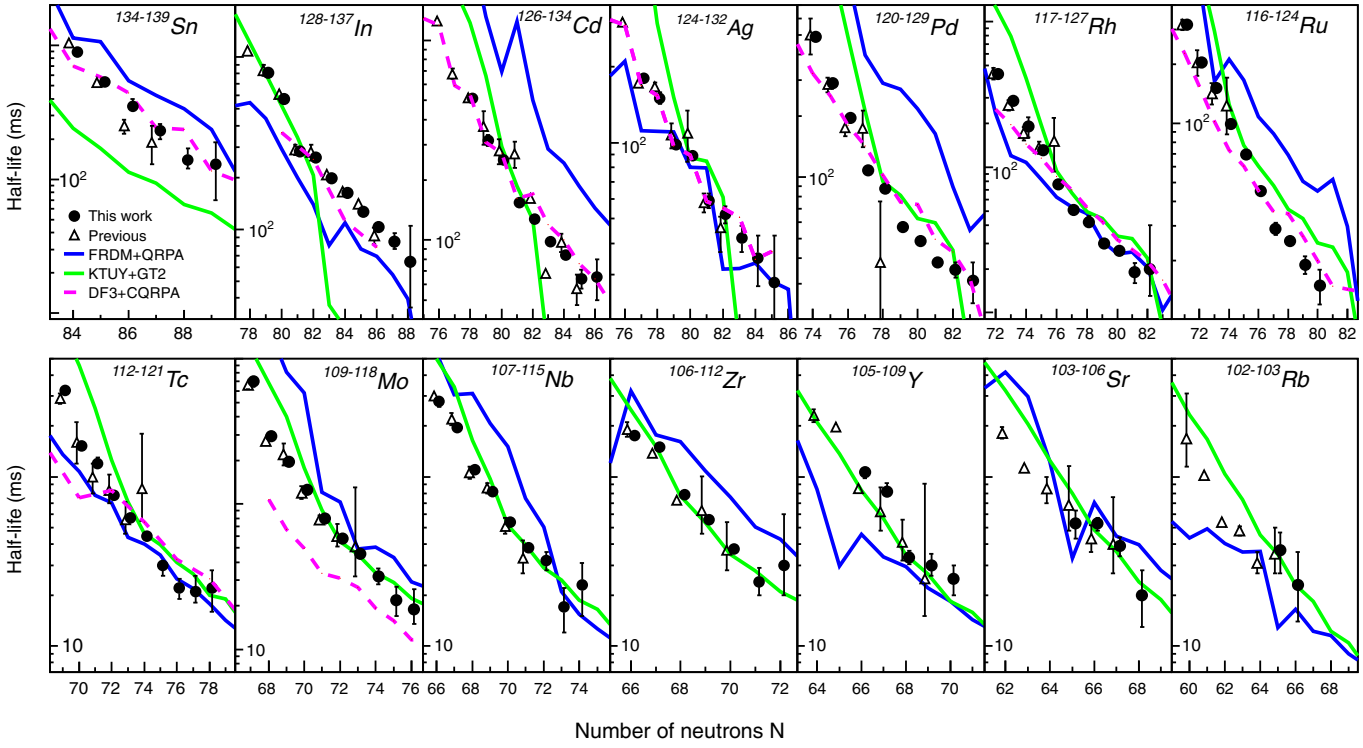

FIG. 23 β-decay half-lives measured by Lorusso *et al.* (2015) (solid circles) for a number of isotopic chains as a function of neutron number, compared with previous data (Audi *et al.*, 2012) (open triangles) and the predictions of the models FRDM-QRPA (blue) (Möller *et al.*, 2003), KTUY-GT2 (green) (Tachibana *et al.*, 1990; Koura *et al.*, 2005), and DF3-CQRPA (magenta) (Borzov *et al.*, 2008) when available. (figure from Lorusso *et al.*, 2015)

at $A \approx 195$, needed in astrophysical studies (Caballero *et al.*, 2014; Eichler *et al.*, 2015).

B. Experimental Achievements in Measuring Nuclear Properties

Progress at ISOL-based systems, both at reactors as well as at spallation facilities, was incremental. The production of neutron-rich isotopes was mainly limited by the chemistry and extraction time from the ion source. Large effort went in the development of suitable target materials and ion source techniques (Ravn *et al.*, 1975). The choice of isotopes for the study of masses, half-lives and other decay properties was often dictated by the availability of isotope products rather than by physics priorities. The measurements were tedious and the picture of nuclear structure development towards the very neutron rich side of stability emerged only slowly. The experimental uncertainties were substantial since mass-determinations depended mostly on the reliability of Q_β measurements, which depended on the statistical significance of the data and were therefore only reliable to a certain extent. Despite these handicaps for the experimental community, by the early 21st century significant progress had been made in measurements of very neutron-rich isotopes in the Fe–Ni group and in the mass range feeding $A \approx 130$ r-process abundance peak associated with the $N = 82$ closed neutron shell. Most notably, the properties of the ^{130}Cd and the double closed shell nucleus ^{132}Sn had been studied at that time (Kratz, 2001). However, during the last decade fragmentation techniques improved enormously. Not only did they allow the measurement of much shorter lived neutron-rich radioisotopes, they also were not handicapped by ion-source chemistry considerations and with the right target and projectile combination they were able to reach far beyond the range accessible by ISOL facilities. There were exceptions, but with advantageous chemistry conditions ISOL facilities were still very competitive with fragmentation techniques.

In the last decades several new technical developments led to an enormous improvement in the study of r-process masses and decay properties, partly driven by the development of larger high efficiency detection devices but also by new techniques using storage ring technology to determine masses of multiple isotopes at once instead of painstakingly extracting and probing one isotope after the other. Other advances were based on the development of laser traps designed to trap only a few of the selected and collected neutron-rich isotopes and determine their masses and decay characteristics with unprecedented accuracy. In addition to these studies of the

decay properties of r-process or near r-process nuclei first attempts are being made in determining neutron capture rates far off stability using surrogate reaction techniques, and new innovative ideas are being brought forward for facilities that allow a direct and model independent measurements of neutron capture reaction cross sections on very short-lived neutron rich isotopes. The most significant or impactful developments of these techniques will be discussed in the following sections.

1. The experimental study of nuclear masses

Mass measurements of selected isotopes near stability were traditionally performed using mass spectrometers based on magnetic and electric sector fields for separating single isotopes. Modern experimental methods of mass measurement of rare isotopes are generally based on three experimental techniques. Time-of-flight mass spectrometry (TOF-MS) is based on the velocity measurement of short-lived isotopes produced in fragment processes that are analyzed in single-pass spectrometers. The other techniques are frequency-based spectrometry of isotopes in storage rings using Schottky pick-up signals of rapidly circulating particles (Litvinov *et al.*, 2004) and Penning traps capable of making measurements with even single trapped particles (Blaum, 2006; Blaum *et al.*, 2013). The TOF and frequency-based methods are often mentioned together as direct mass measurement methods because unknown masses (in fact, mass-to-charge ratios) are directly determined by calibration with well-known masses.

Indirect methods usually rely on the measurement of the energy balance in reaction or decay processes of the isotopes in question. The un-known mass is calculated from known ones in the reaction or decays, plus the determined Q values. This is the classical approach, which requires a substantial production of the radioactive isotopes in question to ensure sufficient statistical reliability of the data.

Mass measurements in storage rings

Spectrometry of masses at storage rings allows the simultaneous measurements of many nuclei. The ions produced at fragmentation facilities typically are then stored in storage rings where the relative frequencies of ion revolutions or relative revolution times of the stored ions are related to their relative mass to charge ratios and velocities (Yan *et al.*, 2016). In order to measure the masses of the ions in storage rings, the ions are typically cooled in order to minimize the velocity spread. The cooling process requires time, and therefore limits the half-lives that can be measured. This was the principle of the Schottky Mass Measurement Method (Radon *et al.*, 2000; Litvinov *et al.*, 2004). Another approach, named the Isochronous Mass Spectrometry (Hausmann *et al.*, 2000, 2001; Sun *et al.*, 2008) removed the limitation on half-lives since it does not depend on cooling. This ISM approach resulted in a reduction of the velocity spread by injection of the ions into the isochronous ion optical mode of the ring. That is, the fast and slow ions of the same species are deliberately placed in the longer and shorter orbital paths, respectively, of the ring in order to yield essentially the same revolution frequency and therefore a reduced velocity spread. Two facilities use these methods for mass measurements at storage rings, the GSI Helmholtz Center in Germany and the Institute of Modern Physics in Lanzhou, China. While these two methods have been used mainly for neutron-deficient nuclei, the masses of ^{129,130,131}Cd have been recently measured at GSI (Knöbel *et al.*, 2016). There are ongoing plans to implement the same approaches at the Radioactive Ion Beam Factory in RIKEN, Japan and the future FAIR facility at GSI.

Mass measurements in traps

Measurements of masses in traps have yielded the most precise and accurate mass measurements to date, and present a significant advance over any other methods, including the storage rings and the traditional β-endpoint measurements. There are basically two types of traps. Paul traps are based on radio-frequency confinement of ions and Penning traps use electromagnetic fields to trap ions (magnetic fields for radial confinement and electrostatic ones for axial trapping). Coupling of traps to fragmentation or spallation facilities or coupling to spontaneous fissioning sources has tremendously extended the reach of high precision and high accuracy measurements, setting new worldwide standards for studies of this very fundamental property of the nucleus and its special impact on simulations of the r process. There are now numerous facilities worldwide, including the Canadian Penning Trap at Argonne National Laboratory; LEBIT at the National Superconducting Cyclotron Laboratory at MSU in the USA; TITAN at TRIUMF in Canada; JYFLTRAP in Jyvaskyla, Finland; SHIPTRAP at GSI Darmstadt and MAFFTRAP in Munich, Germany; ISOLTRAP at CERN; and RIKEN trap at the SLOWRI facility in Japan. Many of the facilities have implemented or intend to implement MRTOF devices (multi-reflection time-of-flight spectrographs) to increase the purity of the ions as well as the range of short-lived exotic nuclei that can be measured. ISOLTRAP at CERN was a pioneer in the field of traps, reaching an uncertainty of a few parts in 10^8 with a resolving power of up to 10^6 with nuclear half-lives in the order of seconds (Eliseev *et al.*, 2013). Exotic neutron rich nuclei with shorter half-lives required much greater re-

solving power and led to the introduction of the phase-imaging ion-cyclotron resonance technique (Eliseev *et al.*, 2013). This new technique is based on determining the frequency of the ion by the projection of the ion motion in the trap onto a high resolution position sensitive micro-channel plate detector. The method has been shown to increase the resolving power forty-fold, and at the same time, to tremendously increase the speed with which measurements can be made. The higher precision of the measurements have a strong impact on attempts to distinguish sites of the r process, as shown in resulting publications (Mumpower *et al.*, 2015, 2016, 2017b). Recent highlights include precision mass measurement of neutron-rich Neodymium and Samarium Isotopes at the CARIBU facility (Orford *et al.*, 2018), of neutron-rich rare-earth isotopes at JYFLTRAP (Vilen *et al.*, 2018), and neutron-rich Gallium isotopes at TITAN (Reiter *et al.*, 2018).

2. Beta Decay

Beta decay measurements are typically challenged by the detection efficiency of electrons and neutron-rich ions. New results of half-lives measured at RIKEN include stacking of eight silicon double sided strip detectors such as WAS3ABi (Lorusso *et al.*, 2015; Wu *et al.*, 2017a) surrounded by an array of 84 HP germanium detectors of the EURICA array (Söderström *et al.*, 2013). Tremendous detection power, coupled with the most intense radioactive ion beams available, has made a significant contribution to the measurements of half-lives. While silicon has been the ideal choice, other detector materials such as Ge with higher Z have recently been commissioned at the NSCL fragmentation facility for use with β-decay experiments. The GeDSSD detector shows 50% electron efficiency and greater mechanical stability in allowing the manufacture of thicker detectors (Larson *et al.*, 2013). TRIUMF in Canada has also developed the Scintillating Electron-Positron Tagging Array (SCEPTAR) comprised of 20 thin plastic scintillator beta detectors that surround the implantation point of radioactive ion beams inside a central vacuum chamber surrounded by 16 Clover type, large volume Germanium detectors. SCEPTAR has been shown to have an efficiency of ∼80% for electrons emitted from radioactive decays, and also provides information on their directions of emission in order to veto background in the surrounding GRIFFIN HPGe detectors from the bremsstrahlung radiation produced by the stopping of the energetic beta particles. Neutron rich nuclei are transported to the center of GRIFFIN by a moving tape collector (MTC) system.

3. Beta-delayed neutron emission probability measurements

Beta delayed neutron emission changes the availability of neutrons in a given r-process scenario and is particularly important since the delayed neutrons can significantly change the abundances of neutron-rich nuclei during freeze-out. While the probabilities of β-delayed neutron emission (P_n) are of great impact for r-process simulations, as well as nuclear power reactor designs (for early work see e.g. Kratz *et al.*, 1982), the experimental situation is quite poor since very few of the P_n-values have been measured. Facilities capable of producing neutron-rich nuclei by fragmentation, spallation, or fission sources have invested in a variety of approaches to measure theses P_n-values.

A number of neutron detection techniques were applied, but multiple counter systems consisting of a number of ^{3}He counters embedded in a paraffin matrix to thermalize the neutrons for better efficiency emerged as a standard approach for these kind of studies. One more recent example was the neutron counter NERO (Pereira *et al.*, 2010) that was developed at the NSCL/MSU to measure the P_n-values of neutron-rich isotopes in the lower mass range that was accessible using fragment production and separation at the A1900 separator. NERO consists of sixty ^{3}He counters embedded in a polyethylene matrix surrounding the collection station to maximize counting efficiency. The efficiency was tested using a ^{252}Cf spontaneous fissioning source and the energy detection range of the detectors was expanded using (α, n) reactions on various target materials. NERO was utilized primarily for the study of lighter r-process nuclei in the Co to Cu mass region (Hosmer *et al.*, 2010) and in the range of of very neutron rich Y, Mo, and Zr isotopes near the r-process path (Pereira *et al.*, 2009), pushing the experiments to nuclei in the N=82 closed neutron shell region (Montes *et al.*, 2006).

The BELEN (BEta-deLayEd Neutron) detector array is a more recent development of a neutron counter that follows the same concept as NERO. BELEN was conceived as a modular detector that has been developed in preparation for experiments at FAIR. Specifically, the DEcay SPECtroscopy (DESPEC) experiment at FAIR is planned for the measurement of β-decays in an array of Double Sided Silicon Detectors (DSSD) called AIDA, in coincidence with the ^{3}He neutron detectors of BELEN, in order to measure P_n-values of exotic nuclei. BELEN-20 consists of two concentric rings of ^{3}He counters (8 and 12 counters, respectively), arranged inside a polyethylene neutron moderator. Early measurements included testing the system by transporting a beam of ions to the center of the neutron detector in front of a Si detector to measure the β-decay (Gómez-Hornillos *et al.*, 2011). The most current version of BELEN includes 48 ^{3}He tubes (Calvino *et al.*, 2014; Agramunt *et al.*, 2016) and was recently tested, similarly to BELEN-20, at Jy-

vaskyla, with fission products produced from the proton-induced fission of Thorium. Fission products were swept away by a Helium gas jet system into a double Penning trap system that acts as a mass separator, resulting in a relatively pure beam of β-decaying products. The transport system takes some time, on the order of a few hundred milliseconds and imposes a limitation on the lifetimes that can be studied. The BELEN detector is soon to become a part of the largest ever neutron detector of its kind as a part of a 160 ^{3}He counter arrangement being built by the BRIKEN collaboration for measurements of exotic nuclei at RIKEN. The challenges that remain are the trade-offs between the highest efficiencies and the best energy resolutions for the detection of neutrons. First, measurements at the GSI fragment separator focused on the study of massive radioactive nuclei of the N=126 closed shell in the Au to Rn range, in order to determine the half-lives of these isotopes, the β-delayed neutron emission probabilities, and the P_n-values, to compare with theoretical model predictions (Caballero-Folch *et al.*, 2016). This work demonstrated that the FRDM+QRPA predictions typically used in r-process simulations differ sometimes by up to an order of magnitude from the experimental values. These discrepancies between theoretical predictions and experimental result underline the importance of these kind of studies for exploring the evolution of nuclear structure towards the r-process path and beyond.

Recently, a new technique was demonstrated in which the challenges of neutron detection are circumvented by measuring the nuclear recoil (Yee *et al.*, 2013) instead of the neutron energy using traps. The traps can confine a radioactive ion and basically β-decay at rest. The emitted radiation emerges with minimal scattering, allowing the measurement of the ion recoil. The β is measured in coincidence with the ion recoiling as a result of neutron emission resulting in a time of flight spectrum. The proof of principle was demonstrated using a fission source of ^{252}Cf, where fission fragments are thermalized in a large volume gas catcher, extracted, bunched, trapped and mass separated in a Penning trap, then delivered into a β-decay Paul Trap (BPT). The β-particles are detected in a ΔE-E plastic scintillator while the recoil ions are detected in a microchannel plate detector. The technique allows the measurements of exotic isotopes with half-lives as short as 50 ms while avoiding some of the complications of neutron measurements.

C. Experiments towards Neutron Capture Rates

For a long time, the determination of neutron capture rates on neutron-rich nuclei has been considered of secondary relevance for the simulation of r-process nucleosynthesis and scenarios. This is due to the fact that the r process is governed by an $(n,\gamma) \rightleftarrows (\gamma,n)$ equilibrium, where the actual reaction rates cancel out as described earlier. However, after freeze-out the equilibrium is no longer maintained and neutron capture reactions on the neutron-rich r-process reaction products may well shift the abundance distribution towards heavier nuclei. Sensitivity studies with variations of the neutron capture rates by factors of ten result in significant variations in the resulting abundances of the heavy elements as a function of the astrophysical trajectories that are used (Mumpower *et al.*, 2015), but the experimental measurements of neutron capture on exotic beams pose significant challenges, both in the production of the exotic nuclei as well as the neutrons and in turn the measurements of the reaction rates.

While the direct measurement of neutron capture reactions on stable and even long-lived radioactive for the s process has been very successful (Guerrero *et al.*, 2017), a similar approach to study neutron capture on short-lived neutron rich isotopes provides considerable challenges. Most of the r-process neutron capture rates rely on theoretical predictions based on the Hauser-Feshbach statistical model formalism (Rauscher *et al.*, 1997; Goriely, 1998). To test and verify these predictions a number of indirect methods have been developed over the last decade as a first step towards this goal. This includes the so-called Oslo method (Guttormsen *et al.*, 1987) as well as the surrogate reaction technique (Escher *et al.*, 2012), while new methods are being envisioned towards a direct experimental approach.

1. Neutron Capture on neutron rich nuclei: β-Oslo method

The Oslo method involves the extraction of level densities and γ-ray strength functions by the measurements of the total de-excitation of a nucleus as a function of energy. The different excitation ranges to be studied are populated by different nuclear reaction modes that can range from light ion transfer reaction to inelastic scattering techniques. This approach requires high intensity beams and the direct measurements of cross sections (Guttormsen *et al.*, 1987) to obtain the level density and strength function data with sufficient statistics for extracting neutron capture cross sections. The recent adaptation of the Oslo method has been demonstrated in the β-Oslo method in which the β-decay of a neutron-rich nucleus populates the levels at high excitation range and the subsequent γ-decay is measured using total absorption spectroscopy (Spyrou *et al.*, 2017). A first version of this approach was developed on the basis of β-decay data obtained at the ILL Grenoble and at ISOLDE at CERN (Kratz *et al.*, 1983; Leist *et al.*, 1985). A benchmark test for quantifying the method was the successful comparison between the level density analysis from the study of ^{87}Br$(\beta^-n)^{86}$Kr through neutron unbound states in ^{87}Kr and the direct ^{86}Kr$(n,\gamma)^{87}$Kr resonant neutron

capture data (Raman *et al.*, 1983). An important aspect in this work is the fact that the extracted level density is based on the analysis of the neutron decay data and not on the γ-decay analysis.

The present approach, the so-called β-Oslo method, however, rests mostly on the analysis γ-decay of highly excited states. Neutron unbound states, populated by the β-decay are less likely to be observed because they primarily decay into the particle rather than the γ channel as observed in the early studies (Raman *et al.*, 1983). Nevertheless, the study of the β-delayed γ-decay is a useful tool for determining level densities up to the threshold. The new approach relies on the use of a 4π summing detector device instead of a single Ge detector to analyze the γ-decay pattern. The spectra are then unfolded as a function of excitation energy in order to determine the nuclear level density and the γ-strength function. The neutron capture cross section is derived by folding the level density and γ-ray strength function with a nucleon-nucleus optical model potential, adopting statistical asumptions for the neutron transmission channels. The analysis depends critically on a number of assumptions with respect to level density normalization and the optical potential, which possibly introduces systematic uncertainties. However, the largest uncertainty is in the assumption of the density of neutron unbound states above the threshold and the associated neutron strength distribution. This is typically determined from systematics and statistical model simulations. It works well near the stability where the level density above the neutron threshold is high. It becomes more questionable when the method is applied to nuclei at the r-process path, where the neutron thresholds and therefore the level density are much lower. A number of measurements have been performed and the extracted results agree well with the predictions of Hauser-Feshbach simulations (Spyrou *et al.*, 2014) and the uncertainty range in the prediction is claimed to be significantly reduced (Liddick *et al.*, 2016). The approach suggests a certain redundancy since the experimental data do not consider the neutron strength function above the threshold, but adopt the one predicted by the same statistical model against which the predicted reaction rates are being tested. A study of the systematic uncertainties (Spyrou *et al.*, 2017) suggests that the overall uncertainty in the rates obtained by the β-Oslo method is within a factor of ~ 3 which is comparable to the uncertainty range of case-optimized Hauser Feshbach calculations (Beard *et al.*, 2014).

2. Neutron capture by (d, p) surrogate reactions

Single particle transfer reactions such as (d, p) have emerged as a powerful tool for probing the single particle structure of neutron-rich nuclei near the r-process path. First (d, p) transfer measurements, using radioactive ^{130,132}Sn beams on CD2 (deuterated polyethylene) targets at the Holifield Radioactive Ion Beam Facility (HRIBF) radioactive beam facility in Oak Ridge National Laboratory, led to a better understanding of the single particle structure of bound states in ^{131,133}Sn (Kozub *et al.*, 2012; Jones *et al.*, 2010). The extracted single particle spectroscopic factors allowed calculating the direct reaction components for neutron capture reactions. Higher energy unbound states were not observed. The observation of such states is critical for extracting reliably the single resonant or statistical resonant contributions expected for high level density compound nuclei in (n, γ) reactions.

The study of the unbound regions of neutron-rich compound nuclei in (n, γ) reactions near the r-process path is the primary goal of the surrogate reaction approach where single particle transfer reactions are utilized to bypass the challenges of measuring neutron capture cross sections on short lived nuclei. Neutron transfer reactions such as (d, p) or $(d, p\gamma)$ are frequently highlighted as surrogates for direct neutron capture studies (Escher *et al.*, 2012). In surrogate reactions the neutron is carried within a "trojan" projectile and brought to react with the target. The neutron-capture cross sections on the target nucleus can be extracted by measuring the proton in the final stage (Escher and Dietrich, 2006; Forssén *et al.*, 2007). First benchmark experiments have been performed at the 88-inch cyclotron at Lawrence Berkeley National Laboratory probing the ^{171,173}Yb(n, γ) cross section via the surrogate reaction ^{171,173}Yb$(d, p\gamma)$, using a high intensity deuterium beam (Hatarik *et al.*, 2010). The extracted neutron capture cross sections agreed within 15% with direct measurements (Wisshak *et al.*, 2000) at energies above 90 keV. At lower energies corresponding to the stellar energy range considerably larger discrepancies are observed.

In the case of neutron capture on short-lived nuclei, inverse kinematics techniques will be necessary with short-lived radioactive beams interacting with a deuterium target. Neutron-transfer measurement on a radioactive r-process nucleus needs large area silicon detector arrays at backward angles in coincidence with an ionization counter at forward angles to detect the beam-like recoils to reduce the beam induced background. Such a system was developed as the Oak Ridge - Rutgers University Barrel Array (ORRUBA) (Pain *et al.*, 2007). The ORRUBA detector has been used in the center of the Gammasphere Ge-array in a combination called Gammasphere Orruba Dual DEtectors for $(d, p\gamma)$ studies using stable ^{95}Mo beams (Cizewski *et al.*, 2018) but no conclusive results have been presented. Extracting the neutron capture cross section out of the surrogate reaction measurements offers its own challenges since it requires proper treatment of nuclear model parameters. Deviations between the results of direct measurements and surrogate reaction studies may reflect insufficient treat-

ment and separation between different reaction mechanisms, such as direct transfer and break-up components (Avrigeanu and Avrigeanu, 2016). While promising as a method, a deeper understanding of the reaction mechanism seems necessary (Potel *et al.*, 2015).

3. n-capture in ring experiments

Recently a new method has been proposed for the direct study of neutron capture on short-lived nuclei, using high intensity radioactive beams in a storage ring on a thermalized neutron target gas produced on-line by proton-induced spallation reactions. (Reifarth *et al.*, 2017). The cross section of the neutron capture reactions would be measured in inverse kinematics, detecting the heavy ion recoils in the ring, using for example the Schottky method developed at the GSI storage ring facilities (Nolden *et al.*, 2011). This concept is an expansion of earlier work that proposed the use of the high neutron flux in a reactor core as possible target environment with the radioactive beam passing through the reactor core in a storage ring (Reifarth and Litvinov, 2014). A number of simulations demonstrate that both methods seems feasible albeit technically challenging, since it requires the combination of a storage ring facility with either a spallation or fission neutron source. There is a half-life limit that is mostly determined by the production rate at the radioactive ion facility or the beam intensity and the beam losses due to interactions with the rest gas in the ring. Yet, such a facility would allow for the first time to address the challenges of neutron capture reaction measurements on neutron rich radioactive isotopes with half lives less than a minute in the decay products of r-process neutron-rich nuclei.

V. NUCLEAR MODELING OF R-PROCESS INPUT

A. Nuclear masses

The most basic nuclear property for any r-process calculation is the mass of the nuclei involved. It determines the threshold energy for the main reactions during the r process: β decay, neutron capture and photodissociation. Neutron separation energies, S_n, are particularly important if the r process proceeds in $(n,\gamma) \rightleftarrows (\gamma,n)$ equilibrium, as the reaction path is then fixed at a constant value of S_n, for given values of neutron density and temperature of the astrophysical environment. The most commonly used mass tabulations can be grouped in three different approaches: a) microscopic-macroscopic models like the finite-range droplet model (FRDM) approach (Möller *et al.*, 1995, 2012a,b, 2015, 2016), the Extended Thomas-Fermi model with Strutinski Integral (ETFSI) approach (Aboussir *et al.*, 1995), the extended Bethe-Weizsäcker formula (Kirson, 2008) and the Weizsäcker-Skyrme mass models (Wang *et al.*, 2010; Liu *et al.*, 2011); b) a microscopically inspired parametrization based on the averaged mean field extracted from the shell model and extended by Coulomb, pairing and symmetry energies (Duflo and Zuker, 1995); and c) microscopic models based on the non-relativistic (Goriely *et al.*, 2016) or relativistic (Sun and Meng, 2008) mean-field models.

TABLE I Comparison of the root mean square deviation, in keV, for the mass models FRDM-1992 (Möller *et al.*, 1995), HFB-21 (Goriely *et al.*, 2010), DZ10, DZ31 (Duflo and Zuker, 1995), and WS3 (Liu *et al.*, 2011) with experimental taken from the 2003 (Audi *et al.*, 2003) and 2012 (Wang *et al.*, 2012). The columns labeled "full" consider all masses present in each evaluation while the column labeled "new" includes only masses found in AME-2012 but not in 2003.

Model	AME-2003 (full)	AME-2012 (new) (new)	AME-2012 (full)
FRDM-1992	655	765	666
HFB-21	576	646	584
WS3	336	424	345
DZ10	551	880	588
DZ31	363	665	400

All mass models have in common that, by fitting a certain set of parameters to known experimental data, they are then being used to predict the properties of all nuclei in the nuclear landscape. The models reproduce the experimentally known masses quite well, with mean deviations between 350 keV and 600 keV (see Table I). It is quite satisfying to see that, when in 2012 a new atomic mass evaluation (AME) (Wang *et al.*, 2012), including 219 new experimental masses, became available the agreement with data worsened only slightly compared to the comparison with the previous AME. However, when considering only the new experimental masses found in AME-2012 the agreement deteriorates. As the new masses typically involve more exotic nuclei than those found in a previous evaluation, they provide a measure of the capabilities of each model to extrapolate to regions far from stability. This is in general one the most challenging aspects to determine when using a given mass model in r-process calculations. Neufcourt *et al.* (2018) has recently applied Bayesian machine-learning techniques to assess the predictive power of global mass models towards more unstable neutron-rich nuclei and provide uncertainty quantification of predictions. Nevertheless, deviations between model and data for neutron-rich nuclei are typically related to bulk properties that may not dramatically affect the abundance predictions, e.g. the symmetry energy whose value is known with an uncertainty 3.8 MeV to be the range 29.7–33.5 MeV (Hebeler *et al.*, 2013).

Fig. 24 provides a closer comparison between models

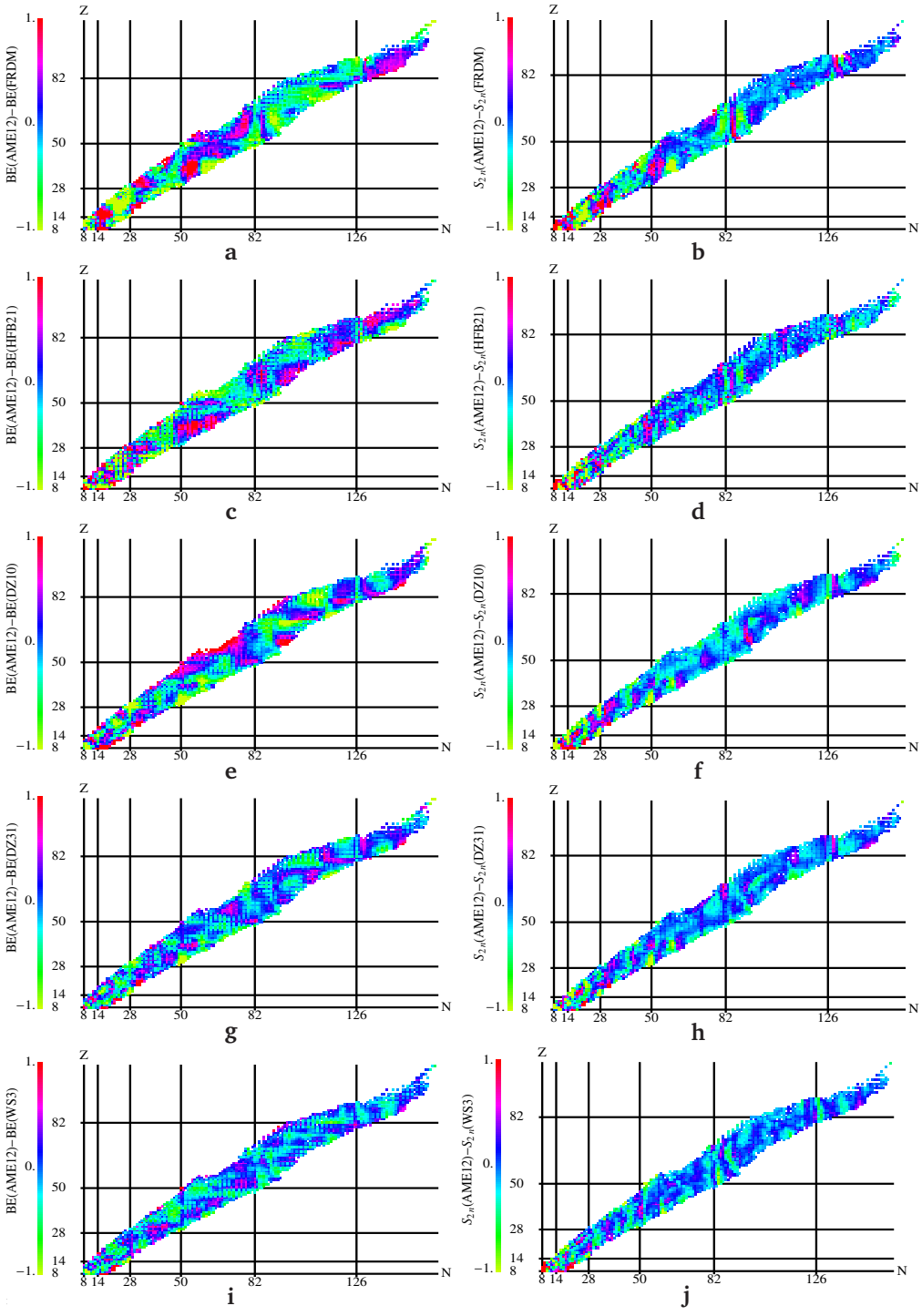

FIG. 24 Differences, in MeV, between experimental, taken from the 2012 version of the atomic mass evaluation AME12 (Wang *et al.*, 2012), and theoretical binding energies (left panels) and two-neutron separation energies (right panels). The following mass models are shown: (FRDM-1992 Möller *et al.*, 1995, a, b), (HFB-21 Goriely *et al.*, 2010, c, d), (DZ10 Duflo and Zuker, 1995, e, f), (DZ31 Duflo and Zuker, 1995, g, h), (WS3 Liu *et al.*, 2011, i, j). (Figure from Mendoza-Temis, 2017).

and data. One notices systematic deviations between models and data, i.e. for neutron numbers around $N \sim 90$ and 130 just above the neutron shell closures at $N = 82$ and 126 (Fig. 24). These mass regions are known as 'transitional regions' where nuclear shapes change from spherical to deformed configurations, accompanied by a sudden drop in neutron separation energies. The description of these shape changes is very sensitive to correlations which are not fully accounted for in the current mass models. Noticeable differences among the various mass

models, and the data, are also observed in the differences of neutron separation energies for odd-A and odd-odd nuclei (Arzhanov, 2017), likely pointing to the need for an improved description of neutron-proton correlations. A better description, in particular of the transitional region, requires beyond-mean-field techniques. A first attempt has been presented in Rodríguez *et al.* (2015), based on the Generator Coordinator Method which considers superpositions of different shapes and restores the breaking of particle number and angular momentum as inherent in the Hartree-Fock-Bogoliubov (HFB) approach. However, first calculations of nuclear masses show only rather slight effects for nuclei in the $N \sim 90$ range.

Although the differences in the transitional regions at $N \sim 90$ and 130 between the various mass models might be rather minute, they can have noticeable impact in r-process simulations. The FRDM (Möller *et al.*, 1995) and version 21 of the Brussels Hartree-Fock-Bogoliubov mass model (HFB21 Goriely *et al.*, 2010) predict noticeably smaller neutron separation energies than the Duflo-Zuker (Duflo and Zuker, 1995) or the Weizsäcker-Skyrme (WS3 Wang *et al.*, 2010; Liu *et al.*, 2011) models in the $N \sim 130$ mass range. As a consequence, for the former two mass tabulations, these nuclei act as obstacles in the r-process mass flow and produce a third r-process abundance peak which is narrower in width, overestimated in height, slightly shifted to larger mass numbers and followed by an abundance trough just above the peak if compared to simulations using the Duflo-Zuker and WS3 masses (and to data) (see Fig. 25). At $N \sim 90$ the FRDM predicts very low neutron separation energies, in contrast to the other mass models! (Arcones and Martínez-Pinedo, 2011). As is discussed in Mendoza-Temis *et al.* (2015) these low S_n values have consequences for the matter flow between the second and third r-process peaks and result in a narrow peak around $A \sim 136$ in the r-process abundances at freeze-out, which is, however, washed out at later times due to continuous productions of material in this region by fission. Similar effects have also been observed in Martin *et al.* (2016) using masses derived from Skyrme energy density functionals based on different optimization protocols. This allows for systematic studies of uncertainty bands under the same underlying physical model for the description of nuclear masses.

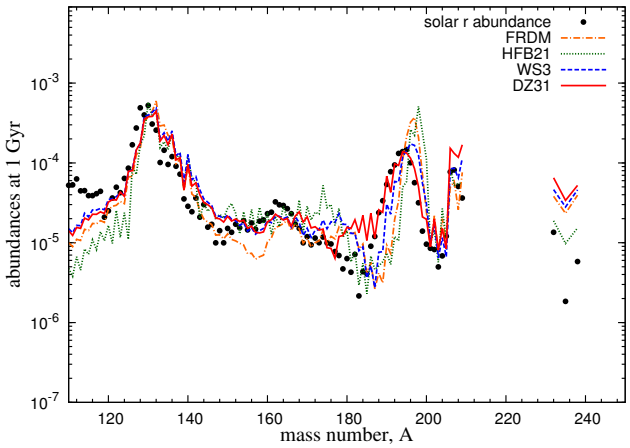

FIG. 25 Final mass-integrated r-process abundances obtained in a neutron-star merger simulation using four different mass models (adopted from Mendoza-Temis *et al.*, 2015)

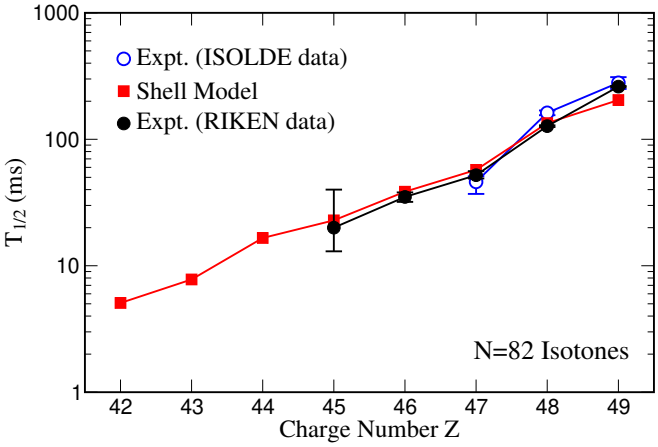

FIG. 26 Comparison of experimental (Pfeiffer *et al.*, 2001; Dillmann *et al.*, 2003; Fogelberg *et al.*, 2004; Lorusso *et al.*, 2015) and shell-model halflives (Zhi *et al.*, 2013) for $N = 82$ r-process nuclei

B. Beta half lives

Nuclear beta decays, which change a neutron into a proton, are responsible for the mass flow to elements with increasingly heavier Z-number. As the r process occurs in a dynamical environment, the time, which is needed for the succession of beta decays to produce thorium and uranium from the seed nuclei available after freeze-out of charged-particle fusion reactions, is competing with the dynamical timescale of the explosion, which transports matter to larger radii (and lower densities), thus suppressing the neutron number density required for the mass flow to heavier nuclei by neutron captures. Particularly important are beta decays of nuclei with magic neutron numbers $N_{\rm mag}$, as the matter flow is hindered by the reduced neutron separation energies of the nuclei with $N_{\rm mag} + 1$. Furthermore, due to the extra binding of the magic nuclei, the Q-value of their beta decays is relatively reduced, resulting in longer lifetimes.

Calculations of beta decays require two ingredients: the relative energy scale between parent and daughter nuclei (Q value) and the transition strength distribution in the daughter nucleus. We note that the Q values are large for r-process nuclei due to the extreme neutron excess. As a consequence uncertainties in this quantity (usually of order 0.5–1 MeV) have a mild effect on the half lifes, despite the strong energy dependence of the involved phase

space (E^5 for allowed Gamow-Teller transition, and even higher powers for forbidden transitions). However, this strong energy dependence makes the half life sensitive to the detailed low-lying strength distribution, which is also crucial to determine whether the beta decay is accompanied by the emission of neutrons, i.e. whether the transition proceeds to states in the daughter nucleus above or below the neutron threshold (which is only 2–3 MeV in r-process nuclei). This so-called β-delayed neutron emission is a source of free neutrons and plays an important role in determining the final r-process abundances during the freeze-out of neutron captures (Arcones and Martínez-Pinedo, 2011).

Nucleon-nucleon correlations are responsible for the strong fragmentation of the transition strengths and for its suppression compared to the Independent Particle Model. These correlations are accounted for in the interacting shell model (Caurier *et al.*, 2005), and in fact large-scale shell model calculations have been proven as the appropriate tool to describe nuclear Gamow-Teller distributions (Caurier *et al.*, 1999; Cole *et al.*, 2012) for stellar weak interaction processes (Langanke and Martínez-Pinedo, 2000, 2003). Shell-model calculations proved also very valuable for the calculation of the half lives of r-process key-nuclei with magic neutron numbers. For ^{78}Ni the shell model predicted a half life of 127 ms (Langanke and Martínez-Pinedo, 2003), which was significantly shorter than the value estimated by global models at the time, and was subsequently experimentally verified (110 ± 40 ms, Hosmer *et al.*, 2005). As is shown in Fig. 26, the half lives for the $N = 82$ r-process nuclei recently measured at RIKEN (Lorusso *et al.*, 2015) agree very well with the earlier shell model values (Zhi *et al.*, 2013), once the quenching of GT transitions is adjusted to the new ^{130}Cd half-live. The shell model calculations imply that the half lives for the $N = 50$ and 82 r-process nuclei are dominated by Gamow-Teller transitions and forbidden strengths contribute only on the few-percent level. This is different for the $N = 126$ r-process waiting points. Here two independent large-scale shell model calculations (Suzuki *et al.*, 2012; Zhi *et al.*, 2013) give evidence that, due to the presence of intruder states with different parity, forbidden transitions contribute significantly and make the half lives about a factor of 2 shorter than estimated for pure allowed transitions. In turn, the shorter half lives allow for a faster mass flow through the $N = 126$ waiting points. We note that the relevant forbidden transitions are at low excitation energies, where due to their enhanced phase space energy dependence they can compete with allowed transitions, and hence they have a strong impact on the β-delayed neutron emission probability.

The shell model is the method-of-choice for β-decay calculations. However, due to the model spaces involved, calculations are only possible for r-process nuclei near closed neutron shells. Thus, the global beta decay rates for r-process simulations have to be modelled by less sophisticated many-body models. Traditionally these studies were performed by calculation of the Gamow-Teller strength distributions within the Quasiparticle Random Phase Approximation on the basis of the Finite Range Droplet Model (Möller *et al.*, 1997) or the ETFSI approach (Extended Thomas Fermi Model with Strutinsky Integral, Borzov and Goriely, 2000). Experimental data for half-lives of r-process nuclei around $N = 50$ and 82 (Pfeiffer *et al.*, 2001; Lorusso *et al.*, 2015) showed that these estimates were systematically too long. The FRDM+QRPA model was subsequently extended to include forbidden transitions within the phenomenological "gross theory" (Möller *et al.*, 2003). A new promising road towards globally calculating half lives for r-process nuclei has recently been developed by performing QRPA studies on top of the self-consistent Hartree-Fock-Bogoliubov (HFB+QRPA, Engel *et al.*, 1999) method or density functionals either non-relativistic (Borzov, 2003) or relativistic (Marketin *et al.*, 2007). Recent covariant density functional theory (D3C*+QRPA Marketin *et al.*, 2016a) and Skyrme finite-amplitude (Mustonen and Engel, 2016; Shafer *et al.*, 2016) studies, which accounted for allowed and forbidden transitions, yielded noticeably shorter half lives for medium and heavy nuclei than obtained by the FRDM+QRPA approach.

Shorter half lives for r-process nuclei with $Z > 80$ have a strong impact on the position of the third r-process peak (Eichler *et al.*, 2015) and enhance the mass flow through the $N = 126$ waiting points (Mendoza-Temis *et al.*, 2015). The latter implies more material available for fission, thus affecting the abundances of the second r-process peak, and the late-time α decays from the decaying r-process matter in a neutron star merger event (Wu *et al.*, 2018). Studies of the influence on beta decays on the r-process abundances for different astrophysical sites have been reported in (Mumpower *et al.*, 2016; Shafer *et al.*, 2016; Kajino and Mathews, 2017).

In principle, the transformation of neutrons into protons can also be achieved by charged-current (ν_e, e^-) reactions. In fact, there have been various suggestions how neutrino-induced reactions on nuclei might affect r-process nucleosynthesis (e.g. Qian *et al.*, 1997; Haxton *et al.*, 1997; Meyer *et al.*, 1998; Otsuki *et al.*, 2000; Terasawa *et al.*, 2004). All these studies were based on the assumption that the r-process operates in the neutrino-driven wind scenario in the presence of strong neutrino fluxes. These assumptions are not supported by modern supernova simulations. In the neutron star merger scenario neutrino fluxes once the r-process operates are too low to substantially influence the abundances by charged-current reactions (Roberts *et al.*, 2017). However, the initial proton-to-neutron ratio of the matter ejected in neutron star mergers and its spatial and time dependence is set by neutrino reactions on free nucleons (see section VI)

C. Neutron captures

During the r-process phase, in which the temperature is large enough ($T \gtrsim 1$ GK), neutron captures and its inverse reaction, photo-dissociation, are in equilibrium. The rates become, however, relevant once the nucleosynthesis process drops out of this equilibrium. As the temperature is cooler during this period, it is mainly neutron capture that matters.

The neutron capture and photo-dissociation rates for r-process nuclei (the latter can be derived by detailed balance from the former) are traditionally determined within the statistical model. This assumes a sufficiently high density of states in the daughter nucleus at the relevant capture energies just above the neutron threshold which is not given for the most neutron-rich nuclei close to the neutron dripline. A systematic estimate about the range of nuclei for which the statistical model is applicable to calculate neutron capture rates is given in (Rauscher *et al.*, 1997). It has been proposed that for the most neutron-rich nuclei the capture rates should be calculated within a direct-capture approach based on a potential (Mathews *et al.*, 1983; Otsuki *et al.*, 2010; Xu and Goriely, 2012; Xu *et al.*, 2014). In such an approach the rate is often determined by a single resonance in the Gamow window (Loens *et al.*, 2012). This makes rate predictions quite uncertain, as nuclear models are not capable to predict the resonance energies with sufficient accuracy. It has therefore been suggested to describe the final states by a level density rather than by discrete levels (Goriely, 1997; Ejnisman *et al.*, 1998). Calculations of neutron capture rates which include a statistical component and a direct contribution are reported in (Mocelj *et al.*, 2007).

The main ingredients of statistical model calculations within the Hauser-Feshbach approach are the nuclear level density, the γ-strength function for the decay of the compound state, and various light-particle potentials. The γ transition can occur with different multipolarities requiring either different ($E1$) or equal parities ($M1$, $E2$) between the involved states. To additionally fulfil the angular momentum selection rules, requires the knowledge of parity- and angular-momentum-dependent level densities.

There has been significant progress in modelling nuclear level densities in recent years. With the Shell Model Monte Carlo approach (SMMC) (Johnson *et al.*, 1992; Koonin *et al.*, 1997) a tool became available which allowed level densities in unprecedently large model spaces. The method to derive level densities within the SMMC was presented in Ormand (1997); Nakada and Alhassid (1997); Langanke (1998) and then systematically extended to explore the parity-dependence (Alhassid *et al.*, 1999) and angular-momentum-dependence (Alhassid *et al.*, 2007). In Özen *et al.* (2015) the collective vibrational and rotational enhancement factors have been explored, finding that the decay of these enhancement factors is correlated with the pairing and shape phase transitions. The vanishing of pairing and its effect on the level density has been studied in Langanke (2006). In the Bethe Fermi Gas (BFG) level density formula this vanishing has been described by a temperature-dependent pairing parameter (Mustafa *et al.*, 1992; Junghans *et al.*, 1998) for which Langanke (2006) gives a parametrization on the basis of the SMMC calculations. SMMC calculations have been performed for many mid-mass and heavy nuclei. These include even-even, odd-A and odd-odd nuclei, allowing to microscopically test the standard prescription in the BFG level density to describe the systematic differences in these nuclei due to the pairing effect by a pairing shift parameter (e.g. Cowan *et al.*, 1991; Rauscher and Thielemann, 2000).

Despite these advances, a calculation of level densities for all nuclei involved in r-process nucleosynthesis is out of scope. However, these calculations have initiated and guided attempts to extend a microscopically derived parity dependence into phenomenological level density formulae like the BFG approach. This is achieved by deriving the excitation-energy dependent parity ratio in the level density by the assumption of Poisson distributed independent quasi-particles combined occupation numbers obtained from the BCS (Bardeen-Cooper-Schrieffer) model, in this way including pairing (Alhassid *et al.*, 2000). In Mocelj *et al.* (2007) this approach has been applied to the large set of r-process nuclei (incorporating also a temperature-dependent pairing parameter suggested from SMMC studies) and its effects on astrophysically relevant reaction rates was studied in Loens *et al.* (2008). This improved level density description is part of the statistical model packages NON-SMOKER and SMARAGD developed by Rauscher (Rauscher and Thielemann, 2001; Rauscher, 2011).

A different path to derive parity- and angular-momentum-dependent level densities has been followed by Goriely and co-workers, based on a combinatorial approach within HFB calculations. Also this approach has been incorporated into a statistical model package and applied to the calculation of neutron capture rates for r-process nuclei within the Brussels Nuclear Library for Astrophysics Applications (BRUSLIB)[6] data compilation (Koning *et al.*, 2008; Goriely *et al.*, 2008; Hilaire *et al.*, 2010; Goriely *et al.*, 2012).

Traditionally the different γ-strength functions have been described by global parametrizations (Cowan *et al.*, 1991) which were adjusted to photo-dissociation for $E1$ transitions or electron scattering data for $M1$ transitions (e.g. Cowan *et al.*, 1991). Recently $E1$ strength functions became available which were microscopically calculated

[6] http://www.astro.ulb.ac.be/bruslib

for individual nuclei within the framework of the HFB model (Goriely and Khan, 2002; Goriely *et al.*, 2004) or based on the relativistic mean field model (Litvinova *et al.*, 2009). These calculations support the presence of enhanced dipole strength at energies just above the neutron threshold. Experimentally such enhanced strength is observed as 'pygmy dipole strength' in nuclei with large neutron excess, like those involved in r-process nucleosynthesis (Adrich *et al.*, 2005). As shown in Goriely (1998) this enhanced dipole strength can have significant impact on neutron capture cross sections.

Dipole γ-strength functions determined from particle-γ coincidence data in neutron pick-up and inelastic scattering data for several mid-mass nuclei exhibit a remarkable upbend of the strength towards $E_\gamma = 0$ (e.g. Guttormsen *et al.*, 2005; Larsen *et al.*, 2006, 2007). The data also allow for the derivation of the nuclear level density, making a few assumptions (the Oslo method, Schiller *et al.*, 2000) (see section IV.C.1). The impact of this upbend on neutron capture rates for r-process nuclei has been studied in (Larsen and Goriely, 2010; Larsen *et al.*, 2015) and a potential increase of the capture rate by up to two orders of magnitude has been calculated. The origin of the low-energy upbend has yet not been completely identified. Coherent adding of magnetic moments of high-j orbitals has been suggested as a possible mechanism for low-energy $M1$ enhancement (Schwengner *et al.*, 2013; Brown and Larsen, 2014; Schwengner *et al.*, 2017), while a low-energy upbend in the $E1$ strength was obtained within finite-temperature relativistic QRPA calculations (Litvinova and Belov, 2013). An upbend in the $M1$ strength function has also been found in large-scale shell model calculations for selected pf-shell nuclei (Sieja, 2017) and $A \gtrsim 100$ (Sieja, 2018). Goriely *et al.* (2018) have performed large scale calculations of $E1$ and $M1$ strength functions by a combination of shell-model and Gogny-HFB+QRPA calculations.

Several general questions regarding basic assumptions made in statistical model evaluations of capture rates have been addressed in large-scale shell model calculations of the $M1$ strength functions for several mid-mass nuclei (similar studies for $E1$ transitions are yet prohibited by computing limitations as they require the inclusion of two major shells, Loens *et al.*, 2012). The results are briefly summarized as: a) The shell-model $M1$ strength functions turned out to give smaller cross sections than the usually adopted parametrizations; b) the scissors mode, a fundamental orbital $M1$ excitation observed in deformed nuclei at low energies (Bohle *et al.*, 1984), might lead to a noticeable enhancement of the capture rates; c) the assumption of the Brink hypothesis, i.e. the strength function is the same for all nuclear states (Brink, 1955; Brink, 1957) is only valid with moderate accuracy; and d) the cross section calculated microscopically by a state-by-state approach had the largest contribution from a single state with $M1$ excitations just in the Gamow window. Such a nuclear structure effect cannot be caught by any global parametrization. The potential impact of the $M1$ scissors mode on r-process neutron capture cross sections has subsequently been revisited by Mumpower *et al.* (2017a).

The transmission coefficients required in statistical model calculations of astrophysical rates (Cowan *et al.*, 1991; Rauscher and Thielemann, 2000) are calculated on the basis of global optical potentials. For the proton and neutron potentials several rather reliable potentials exist (e.g., Jeukenne *et al.*, 1977; Bauge *et al.*, 2001; Koning and Delaroche, 2003; Goriely and Delaroche, 2007). The situation is different for the α-optical potential. Although several global potentials exist (e.g., McFadden and Satchler, 1966; Demetriou *et al.*, 2002, 2003; Kiss *et al.*, 2009; Mohr *et al.*, 2013), none of them is able to consistently describe the existing data at low energies in statistical model approaches. Using ^{64}Zn as an example, Mohr *et al.* (2017) explores the sensitivity of the α-induced reaction cross section to the variation of different alpha optical potential (and other parameters in the statistical model). Attempts have been made to cure the problem. Rauscher suggested that the consideration of Coulomb excitation leads to a better agreement with data (Rauscher, 2013). In Demetriou *et al.* (2002) it was shown that a modified imaginary part of the optical potential can improve the reproduction of experimental reaction data at low energies. Based on a large set of α-induced reaction data at sub-Coulomb energies Avrigeanu *et al.* (2014); Avrigeanu and Avrigeanu (2015) have presented a global α-optical potential for nuclei in the mass range $45 \leq A \leq 209$.

D. Fission

Fission plays an important role in the r process, in particular within the NS-NS merger scenario. Fission determines the region of the nuclear chart at which the flow of neutron captures and beta decays stop (Thielemann *et al.*, 1983; Petermann *et al.*, 2012; Giuliani *et al.*, 2018). In the particular case of dynamic cold ejecta from mergers, several fission cycles are expected to operate before all neutrons are used (Korobkin *et al.*, 2012; Goriely, 2015; Goriely and Martínez-Pinedo, 2015). Fission has been suggested to be responsible for producing a robust r-process pattern (Korobkin *et al.*, 2012; Rosswog *et al.*, 2014; Goriely, 2015), in which the abundances of nuclei with $A \lesssim 140$ are determined during the r-process freeze-out from the fission yields of nuclei with $A \lesssim 280$ (see Mendoza-Temis *et al.*, 2015, and Fig. 19).

The description of fission for r-process nuclei is very challenging as it sensitively depends on the knowledge of the fission barriers for a broad range of very neutron-rich nuclei. In addition, the evolution of the shell structure as function of neutron excess is very uncertain. Several

competing reaction channels need to be modelled, including neutron capture, neutron-induced fission, beta decay, β-delayed fission, spontaneous fission, alpha decay and gamma-induced fission. Hence, parallel to the calculation of fission barriers one has to develop models for all these different reaction channels. Several studies have computed barriers for r-process nuclei (Howard and Möller, 1980; Myers and Świątecki, 1999; Mamdouh *et al.*, 2001; Goriely *et al.*, 2009; Erler *et al.*, 2012; Möller *et al.*, 2015). It has been shown that the dominating fission channel during r-process nucleosynthesis is neutron-induced fission (Panov *et al.*, 2005; Martínez-Pinedo *et al.*, 2007; Petermann *et al.*, 2012). However, the necessary reaction rates have been computed for a strongly limited set of barriers (Thielemann *et al.*, 1989; Panov *et al.*, 2005; Goriely *et al.*, 2009; Panov *et al.*, 2010). This hinders studies of the sensitivity of the r-process abundances to the fission barriers. Due to the dominance of neutron-induced fission, the fission barrier itself is the most important quantity for the determination of reliable fission rates, as the fission process occurs at energies just above the fission barrier. In this case, the inertial mass parameter plays a minor role as tunneling through the barrier has only a negligible contribution. This fact, however, simplifies calculations considerably as the calculation of the inertial mass parameter is rather challenging (Sadhukhan *et al.*, 2013; Giuliani *et al.*, 2014; Giuliani *et al.*, 2018).

In addition to the description of the different fission reaction channels, also the corresponding fission yields, which depend on the excitation energies of the compound nucleus (Kelic *et al.*, 2008, 2009; Schmidt *et al.*, 2016; Sadhukhan *et al.*, 2016; Zhang *et al.*, 2016; Schmitt *et al.*, 2018; Schmidt and Jurado, 2018), have to be known for r-process simulations. As discussed above, the fission yields determine the abundance of r-process elements in the second r-process peak and above and can play an important role for abundance distribution of rare-earth elements (Bengtsson and Howard, 1975; Steinberg and Wilkins, 1978; Panov *et al.*, 2008; Goriely *et al.*, 2013; Eichler *et al.*, 2015; Vassh *et al.*, 2018).

It should be emphasized that during the last phase of the r-process alpha decays compete with fission. This competition determines the final abundances of Pb, U and Th and of long-lived actinides. Consequently, an improved description of transuranic nuclides is necessary for the determination of the r-process abundances produced in the dynamic ejecta from neutron star mergers, with important consequences for the kilonova lightcurves (Hotokezaka *et al.*, 2016; Barnes *et al.*, 2016; Rosswog *et al.*, 2017; Zhu *et al.*, 2018; Wanajo, 2018; Wu *et al.*, 2018).

E. Nuclear Equation of State

Most environments expected to be sites of a strong r process involve objects at highest densities, whether related to core-collapse, compact binary mergers, or the inner areas of black hole accretion disks. The nuclear and supra-nuclear equation of state is of highest importance for modelling these sites, providing the pressure response during dynamic phases, the nuclear and particle composition, the existence of electron/positron pairs and their degeneracy, and last but not least determining maximum neutron star masses, which are important e.g. for answering the question whether in compact binary mergers a hypermassive neutron star lives for period or remains as a final outcome. The recent discovery of massive ~ 2 $M_\odot$ neutron stars (Demorest *et al.*, 2010; Antoniadis *et al.*, 2013) had a major impact. Thus, simulations of neutron-star mergers and core-collapse supernovae are quite sensitive to the adopted Equation of State (EoS), particularly its stiffness, mainly related to the symmetry energy (for some recent literature see e.g., Lattimer, 2012; Hebeler *et al.*, 2013; Steiner *et al.*, 2013; Lattimer, 2014; Fischer *et al.*, 2014; Baldo and Burgio, 2016; Steiner *et al.*, 2016; Özel and Freire, 2016; Lattimer and Prakash, 2016). Oertel *et al.* (2017) give an excellent overview about the various EoS implementations available, as well as the experimental nuclear and astronomical constraints.

VI. ASTROPHYSICAL SITES AND THEIR EJECTA COMPOSITION

In section I we have whetted the appetite already by mentioning possible sources/sites for the origin of the heavy r-process elements. Section III has discussed the optimal conditions that any astrophysical site should attain in order to produce r-process nuclei. They reduce to particular combinations of entropy, expansion time scale, and Y_e in the ejecta. As a minimum requirement the ejecta should be characterized by a high neutron-to-seed nuclei ratio. This is certainly the case for neutron-rich matter, pointing naturally to neutron stars as an important reservoir of neutrons. However, ejecting material from the deep gravitational field of a neutron star requires a cataclysmic event. Thus could be either associated to the birth of a neutron star in a supernova explosion or to ejecta from a compact binary merger involving a neutron star. This leads logically to the most promising sites for a strong r process: (i) The innermost ejecta of regular core-collapse supernovae. But opposite to initial expectations (e.g. Hillebrandt *et al.*, 1976), the ejecta of a neutrino-driven core-collapse supernova are not very neutron-rich. However, for high entropies high neutron-to-seed ratios could be obtained, permitting a strong r process (Woosley *et al.*, 1994; Takahashi

et al., 1994; Hoffman *et al.*, 1997; Qian and Wasserburg, 2007; Farouqi *et al.*, 2010; Roberts *et al.*, 2012; Martínez-Pinedo *et al.*, 2012; Arcones and Thielemann, 2013; Martínez-Pinedo *et al.*, 2014; Mirizzi *et al.*, 2015; Fischer *et al.*, 2018b). (ii) A special class of core collapse supernovae (magneto-rotational MHD-jet supernovae or collapsars), with fast rotation and high magnetic fields responsible for their explosion mechanism, can come with neutron-rich jet ejecta along the poles or from accretion disk outflows (Fujimoto *et al.*, 2006, 2007, 2008; Ono *et al.*, 2012; Winteler *et al.*, 2012; Mösta *et al.*, 2014; Nishimura *et al.*, 2015a; Mösta *et al.*, 2015; Shibagaki *et al.*, 2016; Nishimura *et al.*, 2017; Mösta *et al.*, 2018; Halevi and Mösta, 2018; Siegel *et al.*, 2018). (iii) Ejecta from binary neutron star mergers are naturally neutron-rich (Lattimer and Schramm, 1974, 1976; Eichler *et al.*, 1989; Freiburghaus *et al.*, 1999b; Nishimura *et al.*, 2006; Korobkin *et al.*, 2012; Bauswein *et al.*, 2013; Wanajo *et al.*, 2014; Just *et al.*, 2015a; Eichler *et al.*, 2015; Goriely, 2015; Ramirez-Ruiz *et al.*, 2015; Mendoza-Temis *et al.*, 2015; Shibagaki *et al.*, 2016; Just *et al.*, 2016; Radice *et al.*, 2016; Wu *et al.*, 2016; Rosswog *et al.*, 2017; Lippuner *et al.*, 2017; Siegel and Metzger, 2017; Bovard *et al.*, 2017; Baiotti and Rezzolla, 2017; Thielemann *et al.*, 2017b), all predicted before the observation of GW170817.

A common feature of these scenarios is that matter reaches such high temperatures that neutrinos become the main cooling mechanism. Those neutrinos and in particular electron flavor neutrinos can interact with the ejecta and reset the composition that is commonly determined by a balance between the following reactions:

$$\nu_e + n \rightleftarrows p + e^- \tag{8}$$

$$\bar{\nu}_e + p \rightleftarrows n + e^+. \tag{9}$$

In the case of neutrino-driven winds and potentially also for neutron star mergers ejecta, the material is subject long enough to the processes above to reach an equilibrium between neutrino and antineutrino captures (Qian and Woosley, 1996; Martínez-Pinedo *et al.*, 2016), resulting in

$$Y_e = Y_{e,\rm eq} = \left[1 + \frac{L_{\bar{\nu}_e} W_{\bar{\nu}_e}}{L_{\nu_e} W_{\nu_e}} \frac{\varepsilon_{\bar{\nu}_e} - 2\Delta + \Delta^2/\langle E_{\bar{\nu}_e}\rangle}{\varepsilon_{\nu_e} + 2\Delta + \Delta^2/\langle E_{\nu_e}\rangle}\right]^{-1}. \tag{10}$$

with L_{ν_e} and $L_{\bar{\nu}_e}$ being the neutrino and antineutrino luminosities, $\varepsilon_\nu = \langle E_\nu^2\rangle/\langle E_\nu\rangle$ the ratio between the second moment of the neutrino spectrum and the average neutrino energy (similarly for antineutrinos), $\Delta = 1.2933$ MeV the neutron-proton mass difference, and $W_\nu \approx 1 + 1.01\langle E_\nu\rangle/(m_n c^2)$, $W_{\bar{\nu}} \approx 1 - 7.22\langle E_{\bar{\nu}}\rangle/(m_n c^2)$ the weak-magnetism correction to the cross sections for neutrino and antineutrino absorption (Horowitz, 2002) with m_n the nucleon mass.

These reactions turn matter neutron-rich provided the following condition is fulfilled:

$$\varepsilon_{\bar{\nu}_e} - \varepsilon_{\nu_e} > 4\Delta - \left[\frac{L_{\bar{\nu}_e} W_{\bar{\nu}_e}}{L_{\nu_e} W_{\nu_e}} - 1\right](\varepsilon_{\bar{\nu}_e} - 2\Delta). \tag{11}$$

One should keep in mind an important difference between neutrino emission from protoneutron stars formed in core-collapse supernovae and the emission from a neutron-star merger remnant (see Fig. 27). In the supernova case, we deal with the deleptonization of a hot neutron star and consequently we expect slightly higher fluxes for ν_e's than $\bar{\nu}_e$'s. However, due to the fact that the $\bar{\nu}_e$ spectrum is slightly hotter than the ν_e spectrum, the luminosities of both flavors are rather similar. According to Eq. (11) this implies that the average energies between $\bar{\nu}_e$ and ν_e should differ by at least $4\Delta \approx 5.2$ MeV. Such large differences are not reached in any modern neutrino-wind simulation (Hüdepohl *et al.*, 2010; Fischer *et al.*, 2010; Martínez-Pinedo *et al.*, 2012; Roberts *et al.*, 2012; Martínez-Pinedo *et al.*, 2014; Mirizzi *et al.*, 2015). In the case of a neutron star merger the initial configuration corresponds to a cold very neutron-rich neutron star. Due to the merger dynamics the final merger remnant and accretion disk is heated to large temperatures. The large temperatures favor the production of electron-positron pairs and the material tends to protonize towards the new equilibrium Y_e on timescales of hundreds of ms as determined by the weak interaction timescale in matter affected by neutrino interactions (Beloborodov, 2003; Arcones *et al.*, 2010). During this phase the luminosities and average energies of $\bar{\nu}_e$ are much larger than those of ν_e (see right panels of Fig. 27), reducing the required energy difference of Eq. (11). Hence, even if the impact of neutrino process in mergers is expected to be substantial (Wanajo *et al.*, 2014; Perego *et al.*, 2014; Sekiguchi *et al.*, 2015; Martin *et al.*, 2015; Sekiguchi *et al.*, 2016; Foucart *et al.*, 2016; Martin *et al.*, 2018) the (late) ejecta affected by neutrino interactions are expected to be still neutron-rich enough to produce a (weak) r process, while early dynamic ejecta, emerging from spiral arms after the collision, stay in any case very neutron-rich and lead to a strong r process.

There is also an important difference between the nucleosynthesis operated in neutrino heated ejecta for supernova and mergers. In the supernova case, due to the high entropies and moderate electron fractions the material suffers an α-rich freeze-out (see Fig. 20). Under this conditions, if the material is subject to strong neutrino fluxes during the phase of alpha formation, the so-called α-effect (Meyer *et al.*, 1998) will drive the composition to $Y_e \approx 0.5$, hindering the occurrence of an r process. In the case of merger ejecta due to the more moderate entropies no alpha formation takes place for $Y_e \lesssim 0.45$ (see Fig. 17) and hence the α-effect plays no role.

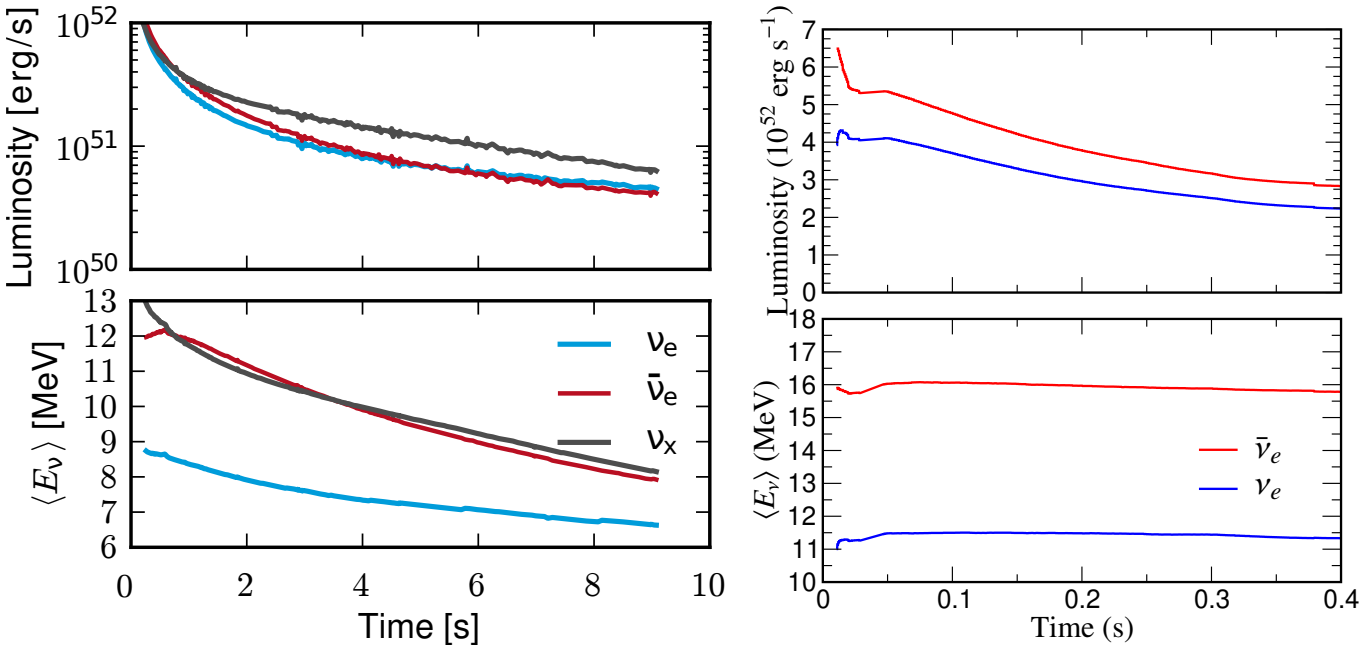

FIG. 27 (left panel) Evolution of the luminosities and average energies of neutrinos emitted during the protoneutron star cooling phase following a core-collapse supernova explosion (adapted from Martínez-Pinedo *et al.*, 2014). (right panel) Luminosities and average energies of neutrinos emitted after a NS-NS merger that forms and hypermassive neutron star surrounded by an accretion disk. (based on the simulations from Perego *et al.*, 2017b, courtesy of Albino Perego).

The discussion above neglects neutrino flavor transformations and their impact on the Y_e of the ejected material. In the supernova case, the very similar spectra for all neutrino flavors hinders the impact of neutrino active-active flavor transformations (see e.g. Wu *et al.*, 2015). Active-sterile transformations, involving sterile neutrinos on the eV mass scale, as suggested by the reactor (Mention *et al.*, 2011) and Gallium (Giunti *et al.*, 2012) anomalies, tend to drive the composition more neutron-rich (Nunokawa *et al.*, 1997; McLaughlin *et al.*, 1999; Wu *et al.*, 2014; Pllumbi *et al.*, 2015). As discussed above in the case of mergers the $\bar{\nu}_e$ fluxes dominate over those of ν_e. Hence, the neutrino self-interaction potential has a different sign than the neutrino matter potential in the Hamiltonian that describes flavor transformations. This induces conversions via matter-neutrino resonances (Malkus *et al.*, 2012; Foucart *et al.*, 2015; Malkus *et al.*, 2016; Zhu *et al.*, 2016; Frensel *et al.*, 2017) and fast pairwise conversions (Wu and Tamborra, 2017; Wu *et al.*, 2017b). The existing investigations clearly point to a potential impact on Y_e and thus on the resulting nucleosynthesis.

After this general outline, disussing in detail how weak interactions are setting the stage for the resulting Y_e (and entropy), being the dominant criteria for the operation of an r process, we want to go through environments/sites suggested so far in a more detailed way than in the introduction. However, we want to leave out the r process in He-layers, initiated by ^{13}C$(\alpha, n)^{16}$O reactions but ruled out since realistic stellar models are in existence (Woosley *et al.*, 2002), and straight forward assumptions of neutron-rich ejecta from the collapsed core of a massive star (e.g. Hillebrandt *et al.*, 1976), ruled out since the neutrino-powered explosion mechnism has been established (Bethe, 1990). Here we will pass through suggested sites related either to massive stars or compact objects in binary systems.

A. Possible r-process sites related to massive stars

1. Neutrino winds from core-collapse supernovae

Supernovae have been thought to be the origin of the strong r process for many years, with the intrinsic expectation that the innermost ejecta, coming from regions close to the neutron star, should be neutron-rich (see e.g. the reviews by Cowan *et al.*, 1991; Sumiyoshi *et al.*, 2001; Arnould *et al.*, 2007). While the prompt explosion mechanism has been shown to fail (Bethe, 1990), the development of multidimensional neutrino radiation transport simulations has shown that the neutrino delayed explosion mechanism remains the most promising scenario to explain the observations (see Kotake *et al.*, 2012; Burrows, 2013; Foglizzo *et al.*, 2015; Janka *et al.*, 2016; Müller, 2016; Hix *et al.*, 2016; Janka, 2017; Burrows *et al.*, 2018; Cabezón *et al.*, 2018, for reviews). These simulations predict that after the onset of the supernova explosion the hot proto-neutron star enters

the so-called Kelvin-Helmholtz cooling phase. During this phase that lasts around 10 s, the proto-neutron star deleptonizes, emitting neutrinos of all flavors. Those neutrinos are responsible of producing an outflow of matter known as neutrino-driven wind (Duncan *et al.*, 1986) that is expected to operate in each supernova explosion that produces a neutron star. The basic properties of the wind are well understood, based on semianalitical models (Duncan *et al.*, 1986; Qian and Woosley, 1996; Hoffman *et al.*, 1997; Thompson *et al.*, 2001; Otsuki *et al.*, 2000; Arcones and Thielemann, 2013). These models relate the nucleosynthesis relevant conditions (see sect. III.C) to fundamental properties including neutrino luminosities, average energy, and mass and radius of the proto-neutron star. Early simulations and parametric models (Woosley and Hoffman, 1992; Meyer *et al.*, 1992; Woosley *et al.*, 1994; Witti *et al.*, 1994; Takahashi *et al.*, 1994; Freiburghaus *et al.*, 1999a; Farouqi *et al.*, 2010; Arcones and Martínez-Pinedo, 2011; Kratz *et al.*, 2014) led to impressive results. However, large uncertainties remained, particularly in the determination of entropy and Y_e. Fig. 28, taken from Kratz *et al.* (2014), shows a close to excellent fit to solar r-process abundances, especially when utilizing modern input from nuclear mass models, but also requiring a superposition of entropies of up to 280 k_B per baryon (and a $Y_e < 0.5$).

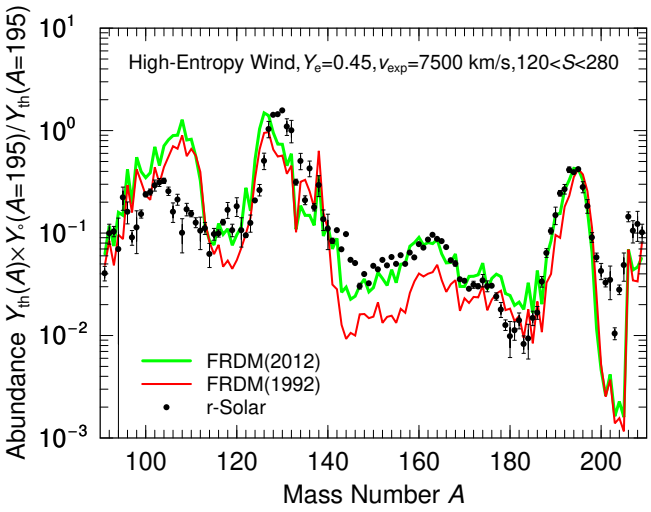

FIG. 28 Results from an r-process calculation, assuming an initial Y_e of 0.45, the adiabatic expansion of matter in a so-called neutrino wind with a given expansion speed v_{exp} of ejected mass shells, and that a superposition of entropies S between 120 and 280 k_B/baryon can be attained. The abundance plot assumes that similar amounts of matter are ejected per entropy interval and indicates the changes which occur due to utilizing an improved nuclear mass model (Möller *et al.*, 2012a, 2016).

The development of hydrodynamics simulations (Arcones *et al.*, 2007; Arcones and Janka, 2011) showed that such high entropies were out of reach. Nevertheless, they still allowed for the occurrence of a weak r process (Roberts *et al.*, 2010; Arcones and Montes, 2011). Further progress, including the development of neutrino radiation hydrodynamics simulations that follow the whole cooling phase (Hüdepohl *et al.*, 2010; Fischer *et al.*, 2010; Roberts, 2012), improvements in the treatment of neutrino opacities in the decoupling region (Martínez-Pinedo *et al.*, 2012; Roberts *et al.*, 2012; Horowitz *et al.*, 2012; Rrapaj *et al.*, 2015; Janka, 2016; Roberts and Reddy, 2017; Martínez-Pinedo *et al.*, 2014; Bollig *et al.*, 2017; Fischer *et al.*, 2018b), and the treatment of convection in the proto-neutron star (Roberts *et al.*, 2012; Mirizzi *et al.*, 2016) have shown that most or all of the ejecta are proton-rich. Under these conditions the nucleosynthesis proceeds via the νp process (Fröhlich *et al.*, 2006; Pruet *et al.*, 2006; Wanajo, 2006), producing neutron deficient isotopes, including light p-process nuclei like ^{92}Mo, as illustrated in Fig. 29 (see Martínez-Pinedo *et al.*, 2014; Pllumbi *et al.*, 2015; Wanajo *et al.*, 2018; Eichler *et al.*, 2018a).

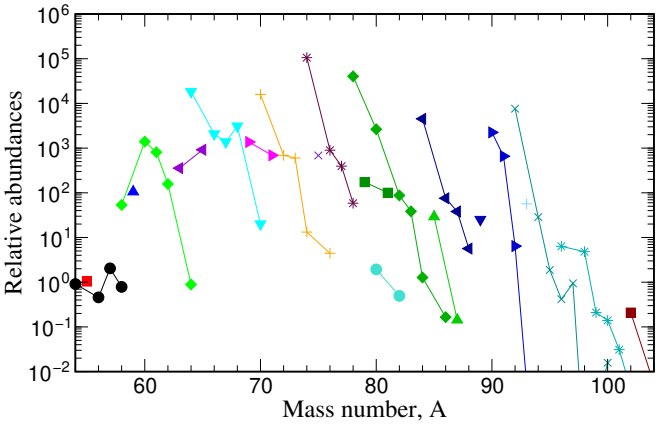

FIG. 29 Isotopic abundances relative to solar abundances of nuclei produced in neutrino driven winds (adapted from Martínez-Pinedo *et al.*, 2014).

The above result can be understood by considering that in neutrino driven winds matter is ejected by neutrino energy deposition and is subject to neutrino reactions for sufficient amounts, permitting Y_e to attain the equilibrium value given in Eq. (10). For the very similar spectra of ν_e and $\bar{\nu}_e$ (see Fig. 27) predicted by modern simulations, this results in proton-rich ejecta. These results are robust against the inclusion of neutrino flavor transformations between active flavors (Wu *et al.*, 2015; Pllumbi *et al.*, 2015) but may be affected by the active-sterile flavor transformations (Wu *et al.*, 2014; Pllumbi *et al.*, 2015).

2. Electron-capture supernovae

A way out of the problem that neutrino irradition is turning matter proton-rich is by considering matter that

is ejected promptly with little exposure to neutrinos. This occurs in the so-called electron-capture supernovae in the stellar mass range 8-10 $M_\odot$ (Jones *et al.*, 2014), which could lead to a weak r process (Kitaura *et al.*, 2006; Janka *et al.*, 2008; Wanajo *et al.*, 2009; Wanajo *et al.*, 2011), possibly producing nuclei up to Eu, but not up to and beyond the third r-process peak (for more details see Mirizzi *et al.*, 2016). However, there are strong indications based on multidimensional hydrodynamic simulations of the oxygen deflagration (Jones *et al.*, 2016b) and nuclear physics data on the electron capture rate on ^{20}Ne (Kirsebom *et al.*, 2019) that intermediate mass stars may end their lives as a thermonuclear supernova triggered by electron captures on ^{20}Ne (see Nomoto and Leung, 2017a, for a recent review).

3. Neutrino-induced r process in the He-shell

One of the major requirements for an r process to take place is to attain a sufficiently high neutron-to-seed ratio. As already discussed above for the high entropy wind, this can also be achieved via a (very) low seed abundance. Banerjee *et al.* (2011) and Banerjee *et al.* (2016), following on an idea by Epstein *et al.* (1988), could show that for core-collapse supernovae with metallicities as low as [Fe/H] ≤ 3, i.e. indicating a very low seed abundance, the neutrons released in the He-shell by ^{4}He$(\bar{\nu}_e, e^+n)^3$H can be captured to produce nuclei with mass numbers up to $A = 200$ in the stellar mass range of 11–15 $M_\odot$. The caveat of this environment is, that while a sufficiently high neutron-to-seed ratio permits the production of heavy nuclei via neutron captures, the relatively low neutron density n_n leads to a larger S_n for the maximum in each isotopic chain (with $Y(Z, A+1)/Y(Z, A) \approx 1$, see Eq. 4) and thus a process path closer to stability than for a regular r process (see the discussion in III.B). Such a path, in between an r-process and an s-process path leads to abundance peaks shifted to higher masses numbers than found for the solar r-abundances. Thus, such a process cannot be an explanation for solar as well as the r-process abundance patterns observed in low-metallicity stars.

4. Quark deconfinement supernovae

This suggested scenario considers objects which undergo core collapse at the end of their evolution and form a central compact proto-neutron star, but the neutrino emission from the hot proto-neutron star and accreted matter is not sufficient to prevent a further collapse with ongoing mass accretion. The question is whether this second collapse leads directly to black hole formation or can come to a halt (Fischer *et al.*, 2018a). A specific equation of state effect was initially introduced by (Sagert *et al.*, 2009; Fischer *et al.*, 2011), with a quark-hadron phase transition taking place just at the appropriate density/temperature conditions. When adjusting the equation of state properties to presently observed maximum neutron star masses, Fischer *et al.* (2018) could show that in such supernovae explosions, expected for a certain stellar mass range, an r process can take place. When examining their results, they show that abundance up to the third r-process peak can be obtained, however, the abundances beyond the second r-process peak show a subsolar behavior. Thus, while there remains hope that core-collapse supernovae can produce r-process elements, they probably do not support a solar-type r process up to the third r-process peak.

5. Magneto-rotational supernovae with jets

Core-collapse with fast rotation and strong magnetic fields is considered to lead to neutron stars with extremely high magnetic fields of the order 10^{15}G (magnetars, see e.g. Duncan and Thompson, 1992; Kramer, 2009; Kaspi and Beloborodov, 2017) and connected to a special class of supernovae (Kasen and Bildsten, 2010; Greiner *et al.*, 2015; Nicholl *et al.*, 2017b). Such supernovae, induced by strong magnetic fields and/or fast rotation of the stellar core, i.e., magneto-hydrodynamic supernovae (MHD-SNe), are considered to provide an alternative and robust astronomical source for the r process (Symbalisty *et al.*, 1985). Nucleosynthetic studies were carried out by Nishimura *et al.* (2006), based on adiabatic MHD simulations which exhibited a successful r process in jet-like explosions. One important question is whether these earlier results, assuming axis symmetry, also hold in full three-dimensional (3D) simulations, i.e., lead to the ejection of jets along the polar axis. 3D MHD simulations with an improved treatment of neutrino physics were performed by Winteler *et al.* (2012) for a 15 $M_\odot$ progenitor, utilizing an initial dipole magnetic field of 5×10^{12} G and a ratio of magnetic to gravitational binding energy, $E_{mag}/W = 2.63 \times 10^{-8}$. These calculations supported and confirmed the ejection of polar jets in 3D, attaining magnetic fields of the order 5×10^{15} G and $E_{mag}/W = 3.02 \times 10^{-4}$ at core-bounce, with a successful r process up to and beyond the third r-process peak at $A = 195$ (see e.g. Winteler *et al.*, 2012, and Fig. 30).

More recent general relativistic simulations in 3D-MHD (Mösta *et al.*, 2014), involving a 25 $M_\odot$ progenitor with an initial magnetic field of 10^{12} G, led in the early phase to jet formation, but experienced afterwards a kink instability which deformed the jet-like feature. Possibly the difference between the two latter investigations in 3D hydrodynamics marks a transition due to passing critical limits in stellar mass, the initial rotation, and magnetic fields between a clear jet-like explosion and a deformed explosion. When we see the time evolution of jet-like ex-

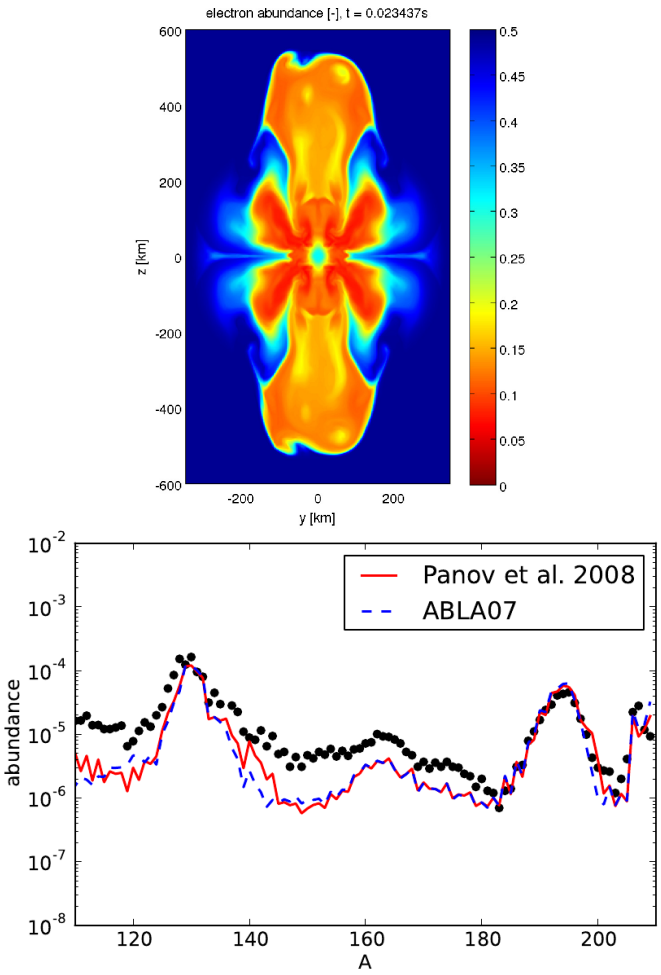

FIG. 30 In an MHD-jet supernova the winding up of magnetic field lines causes the "squeezing-out" of polar jets, along the rotation axis (Winteler *et al.*, 2012). This environment leads to quite low entropies, much lower than those discussed in Fig. 20. But opposite to the Y_e-values utilized for Fig. 20, the collapse to high densities resulted in large amounts of electron captures and Y_e-values close to 0.1-0.15 (see top part of this figure and the right part of Fig. 21 as well as Fig. 22). Such low Y_e's, similar to neutron star merger conditions (where even values as low as 0.03-0.05 can be attained, see next subsection) lead also to a strong r process - even at low entropies - and the abundance predictions displayed here in the bottom part result (shown for two fission fragment distributions utilized Kelic *et al.*, 2008; Panov *et al.*, 2008). As Y_e is moderately low, the effect of late neutron-capture by fission neutrons is also moderate, avoiding a final shift of the third r-process peak as indicated in Fig. 19.

plosions with the hydrodynamic instability (see results in Mösta *et al.*, 2014, 2015), the region with the highest magnetic pressure contains essentially the matter corresponding to the initially forming jets before the deformation. Further investigations by Mösta *et al.* (2018); Obergaulinger *et al.* (2018) underlined, that very high magnetic fields are required to avoid such kink instabilities (and ensure a strong r process). Further studies by Halevi and Mösta (2018) also analyze the dependence on the alignment between rotation axis and magnetic fields, where the most aligned cases result in the strongest r process.

A number of 2D axissymmetric simulations tested nucleosythesis features (e.g. Nishimura *et al.*, 2015a; Shibagaki *et al.*, 2016), the most recent ones also resolving the magnetorotational (Nishimura *et al.*, 2017). The latter simulations analyzed a whole variety of conditions in terms of rotation rates, initial magnetic fields, and ratios of neutrino luminosities vs. magnetic field strengths, under the assumption that the fields are high enough in order to avoid kink instabilities. Their study included a series of long-term explosion simulations, based on special relativistic MHD (Takiwaki *et al.*, 2009; Takiwaki and Kotake, 2011), following the amplification of magnetic fields due to differential rotation (winding of magnetic fields) and the launch of jet-like explosions. One finds possible outcomes from prompt-magnetic-jet over delayed-magnetic-jet explosions up to dominantly neutrino-powered explosions, determined by the ratio of magnetic field strengths in comparison to neutrino heating. This causes also a variation of r-process nucleosynthesis results, from full-blown strong r process environments (see Fig. 31), over a weak r process, not producing nuclei of the third r-process peak, down to no r process at all.

A fully self-consistent treatment requires high resolution simulations which can resolve magneto-rotational instabilities (MRI) and predict reliably the possible amplificaton of magnetic fields during the explosion. While the latter is actually possible by now (Nishimura *et al.*, 2017), present calculations still depend on the uncertain and therefore assumed initial conditions, that either cause strong jet ejection or can develop kink instabilities of the jets. Based on initial conditions, somewhat parametrized in terms of the impact, either neutrino heating or magnetic pressure is causing the supernova explosion. The production for heavy neutron capture elements varies strongly, being either Fe and Zn dominated like in regular core-collapse SNe or Eu dominated, indicating a strong r process. This is shown in Fig. 32.

In terms of applications to galactic chemical evolution it should be noticed that the MHD-jet supernovae discussed here are expected to occur as a fraction of 0.1-1 percent of all core-collapse supernovae, probably being somewhat metallicity dependent. Higher metallicities lead to stronger stellar wind loss which will be accompanied by a loss of angular momentum, thus reducing the fast rotation necessary for this type of SN explosions. Another feature is that these events can lead to only small amounts of Fe-group ejecta for the cases of strong r processing (Nishimura *et al.*, 2015b, 2017). As indicated in Fig. 32, with respect to the relative influence of neutrino heating vs. magnetic field effects, one can see that the Ni/Eu-ratio (and similarly the Fe/Eu-ratio) varies

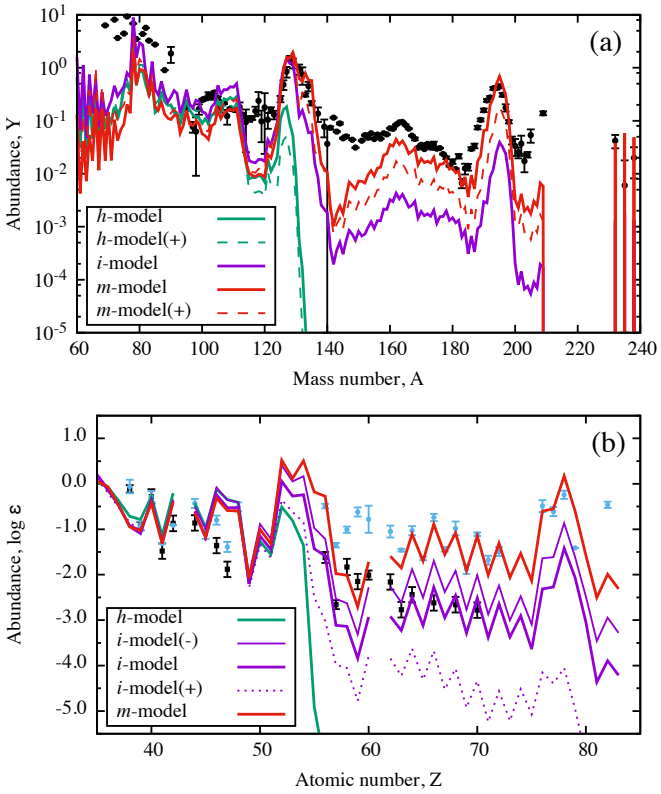

FIG. 31 Abundances from nucleosynthesis calculations with varying ratios of magnetic field strength with respect to the neutrino heating mechanims of regular core-collaspe SNe, increasing for the models h, i-, i, i+, and m (for details see Nishimura *et al.*, 2017). For comparison also (a) solar r-process abundances are shown (black dots Arlandini *et al.*, 1999), (b) abundances from metal-poor stars with a weak r process, i.e. HD122563 (black dots Honda *et al.*, 2006), and solar-type r-process observations from CS22892-052 (blue dots Sneden *et al.*, 1996). Abundances are normalized for Z = 40 of HD122563. Observations of low metallicity stars with strong r-process contributions vary for abundances below Z=50 (Sneden *et al.*, 2008).

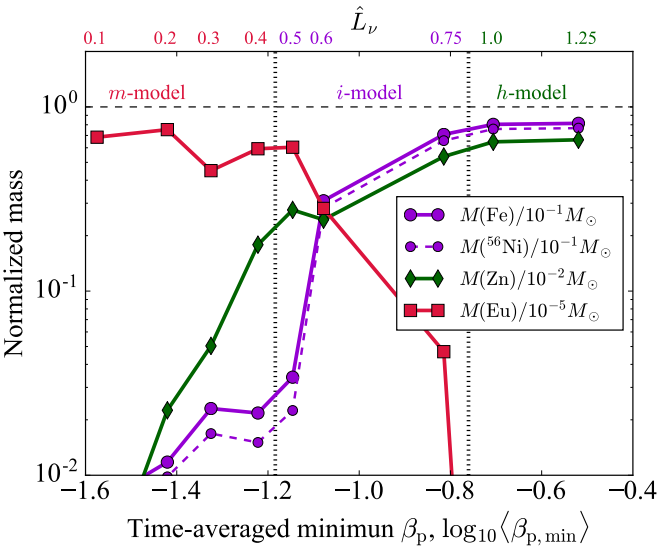

FIG. 32 Nucleosymthesic features of rotating core-collapse SN models (h, i-, i, i+, m) with varying ratios of neutrino luminosity and magnetic field strengths as in Fig. 31. Model m represents a strong MHD-jet supernova. One can see the transition from a regular core-collapse SN pattern, dominated by ^{56}Ni, total Fe (after decay), and Zn, to a strong r-process pattern with a high Eu abundance (for details see Nishimura *et al.*, 2017).

strongly. Thus, if these types of supernovae would contribute already at low metallicities, they alone would be able to provide a large spread in Eu/Fe and might even explain the variations in actinides vs. Eu, seen in a number of cases at low metallicities (see e.g. Wehmeyer *et al.*, 2015; Thielemann *et al.*, 2017a).

6. Collapsars, Hypernovae, long-duration Gamma-Ray Bursts

One of the most interesting developments in the study of supernovae (SNe) is the discovery of some very energetic supernovae (see e.g. Nomoto *et al.*, 2006), dubbed hypernovae, whose kinetic energy (in spherically symmetric analysis, see also Piran, 2004) exceeds 10^{52} erg, about 10 times the value of normal core-collapse SNe (10^{51} erg). The most luminous and powerful of these objects, the Type Ic supernova (SN Ic) 1998bw, was probably linked to the gamma-ray burst GRB 980425, thus establishing for the first time a connection between (long-duration) gamma-ray bursts (lGRBs) and the well-studied phenomenon of core-collapse SNe. However, SN 1998bw was exceptional, indicating that it synthesized ~ 0.5 M$_\odot$ of ^{56}Ni with an estimated explosion energy of $E \sim 3 \times 10^{52}$ erg.

The question is where these events should be placed in the stellar mass range and which other features should be related. We know that for non-rotating cases only the (regular) supernova "branch" (with neutron stars as final outcome) can be attained, probably followed towards increasing stellar mass by a faint or failed supernova branch (leading eventually to black holes, but not to gamma-ray bursts and high ejecta masses). Thus, massive stars, which fail to explode as supernovae via neutrino-powered explosions, will eventually experience the formation of a central black hole (BH) (see e.g. Pan *et al.*, 2018a; Kuroda *et al.*, 2018). However, rotating BHs and the formation of accretion disks with accretion rates of about ≈ 0.1 M$_\odot$ s^{-1} can lead - for certain conditions (strong magnetic fields) - to long duration gamma-ray bursts (lGRBs) or hypernovae, also dubbed collapsars as they result from a core-collapse to the formation of a black hole. Many authors have contributed to the discovery and shaping of first ideas (for theoretical explanations see e.g. the review by Piran, 2004). The collapsar model was proposed by Woosley, MacFadyen and others (see

also MacFadyen and Woosley, 1999; MacFadyen *et al.*, 2001; Nagataki *et al.*, 2007; Sekiguchi and Shibata, 2011; Nagataki, 2011), based on neutrino heating from the accretion disk and/or the winding of strong magnetic fields and MHD jets (e.g. Ono *et al.*, 2012; McKinney *et al.*, 2013; Janiuk *et al.*, 2018). Early hydrodynamic simulations (injecting explosion energies artificially) were performed either by introducing high explosion energies (up to 10^{52} erg) in a sperically symmetric way or aspherically in order to understand jet-like explosions (Nakamura *et al.*, 2001; Nomoto *et al.*, 2006, 2013; Nomoto, 2017).

The basic (consensus) picture has been the following: explosion energies can be found up to 5×10^{52} erg, ^{56}Ni ejecta up to 0.5 $M_\odot$, and there exist relativistic jets responsible for lGRBs. Many attempts have been undertaken to model such events. There exists uncertainty in predicting Y_e, due to weak interactions and especially neutrino transport in disks and jets. The observational constraint of high ^{56}Ni ejecta argues for a dominant Y_e in matter of the order of 0.5. High explosion energies also lead to high entropies and a strong α-rich freeze-out, including interesting amounts of ^{45}Sc, large amounts of ^{64}Zn (from ^{64}Ge-decay), and also other Fe-group elements. Nakamura *et al.* (2001) and Nomoto (2017) concluded that larger abundance ratios for (Zn, Co, V, Ti)/Fe and smaller (Mn, Cr)/Fe ratios are expected than for normal SNe, a feature which seems to be consistent with observations in extremely metal-poor (EMP) stars, as will be discussed later.

Self-consistent modeling of the complete event, from collapse, black hole formation, accretion disk modeling, jet ejection, and GRB occurrence are only forthcoming slowly. There have been investigations with respect to the role of weak interactions and resulting nucleosynthesis in the accreation disk and corresponding outflows (for specific nucleosynthesis results see e.g. Pruet *et al.*, 2003; Beloborodov, 2003; Pruet *et al.*, 2004; Surman *et al.*, 2006; Janiuk, 2014; Siegel and Metzger, 2017; Janiuk, 2017; Siegel *et al.*, 2018).

Beloborodov (2003) found conditions for the minimum accretion rate required, leading to neutron-rich environments with low Y_e's at a given radius:

$$\dot{M}_n = 0.0152 \times \left(\frac{r}{3r_g}\right)^{1/2} \left(\frac{\alpha}{0.1}\right) \left(\frac{M_{\rm BH}}{M_\odot}\right)^2 \ {\rm M}_\odot \ {\rm s}^{-1} \tag{12}$$

Here r_g is the gravitational Schwarzschild radius, α the disk viscosity, M_{BH} the mass of the central black hole. I.e. for typical accretions rates of 0.1 $M_\odot$ s^{-1}, this can lead to a low Y_e at small radii in the disk. Larger accretion rates are in favor of reducing Y_e, so are larger BH masses (as the Schwarzschild r_g radius is linear in M_{BH}, an overall power of 3/4 on the BH mass results).

Fig. 33 shows the Y_e distribution obtained by Janiuk (2014) as a function of the radius. While the central parts of the disk experience a low Y_e, its value reaches $Y_e \approx 0.5$ in the outermost regions and even exceeds beyond 0.5 in intermediate regions. If the disk outflow occurs from the outer regions, this is consistent with the large ^{56}Ni ejecta (observed and) found e.g. by Pruet *et al.* (2004); Surman *et al.* (2006); Janiuk (2014, 2017). However, Pruet *et al.* (2004) also speculated that in case of strong magnetic fields low Y_e matter can be flung out from more central regions of the disk along magnetic field lines, possibly causing r-process production. Additionally, MHD-driven collapsar models, involving black hole accretion disk systems (Nagataki *et al.*, 2007; Fujimoto *et al.*, 2008; Harikae *et al.*, 2009), have argued that the jets produced by the central engine of long duration gamma-ray-bursts can produce heavy r-process nuclei (Fujimoto *et al.*, 2007, 2008; Ono *et al.*, 2012; Nakamura *et al.*, 2015). However, it should be mentioned that early studies assumed a quite simplified treatment of the black hole and the required microphysics. Siegel and Metzger (2017); Siegel *et al.* (2018); Janiuk (2018), having performed multi-D MHD simulations for accretion disk outflows, argue that large amounts, up to ($\approx 1 M_\odot$) of r-process material can be ejected. If this scenario materializes, it would be sufficient to have about one such event per 10 000 core-collapse supernovae to explain the solar r-process abundances.

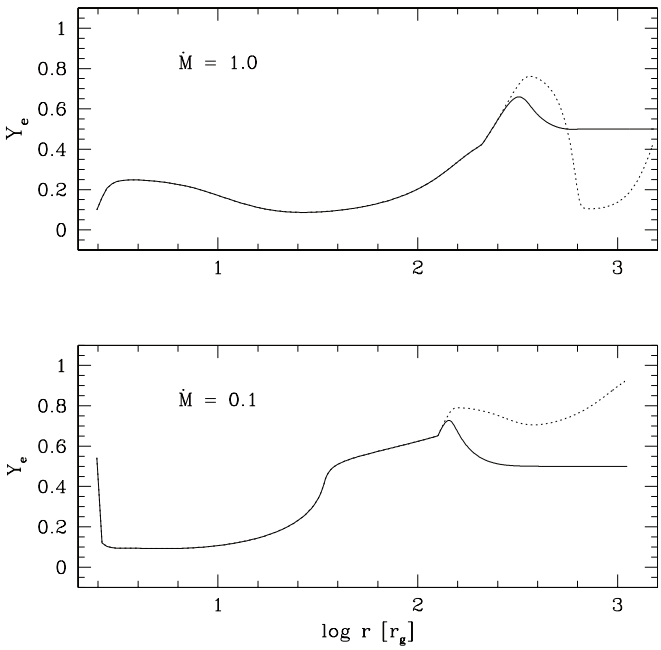

FIG. 33 Radial distribution of Y_e in the disk for different accretion rates. r_g, the gravitational radius, stands for the Schwarzschild radius of the black hole. Y_e indicates very neutron-rich conditions deep inside the disk but developes aymptotically to values of 0.5 in the outer layers above 100 r_g from where the nucleosynthesis outflow will occur (from Janiuk, 2014))

The open question is whether both, large amounts of ^{56}Ni expected for hypernovae as well as r-process ejecta can be produced in the same event? Siegel *et al.* (2018) argue that the ^{56}Ni would have to come from a preceding supernova explosion phase, leaving an intermittent neutron star before further accretion causes black hole formation and a black hole accretion disk. This brings up the following questions: (a) At which stellar progenitor masses do we have a transition from the formation of neutron stars to the formation of black holes after collapse? (b) In which transition region are initially neutron stars formed, causing a regular supernova explosion, but ongoing accretions leads to a black hole? (c) For which progenitor masses are black holes formed directly during collapse and how can this be observed? (d) What is the role of rotation and magnetic fields to cause lGRBs and can we give reliable nucleosynthesis yields for such events? (e) Is there a separation in different types of events, depending on the parameters in (d), leading either to hypernovae and strong ^{56}Ni ejecta or systems with a large outflow of r-process elements? (f) Are jets and lGRBs occurring in both types of events?

The scenario suggested by Siegel *et al.* (2018) would relate to case (b), but it is not clear whether for such a case a strong supernova explosion with lots of Ni production takes place before the accretion disk outflows eject r-process material. It could, however, also be possible that such an event does not cause a hypernova and only creates r-process outflows. Further observations will have to constrain such events.

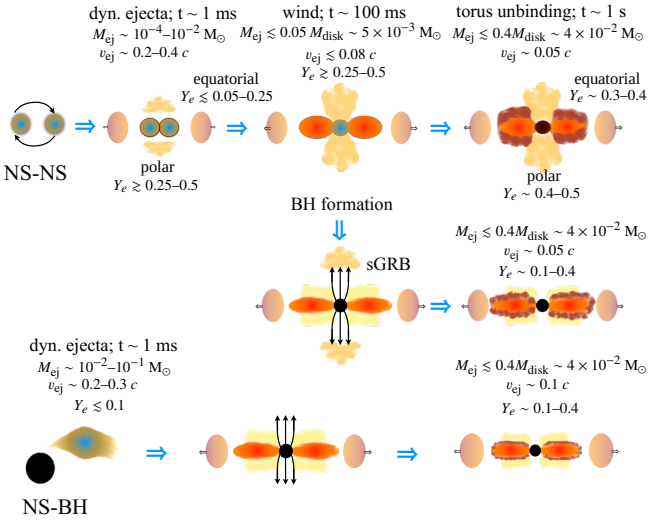

FIG. 34 Ejection channels in compact binary mergers including estimates based on simulations of the ejecta mass, Y_e and velocity during the different ejection phases. The NS-NS merger system is shown in the upper part including the two possible outcomes: a log lived massive neutron star and a hypermassive neutron star that collapses to a black hole on a timescale shorter than the disk lifetime. The BH-NS merger is shown in the lower part. (Adapted from Rosswog *et al.*, 2017)

B. Neutron-star and neutron-star / black hole mergers

Neutron stars, postulated by Landau (1932) even before the discovery of the neutron (Yakovlev *et al.*, 2013), were predicted as the final fate of massive stars, ending in supernova events (Baade and Zwicky, 1934). Their existence was proven in the 1960's after the first observations of pulsars (Hewish and Okoye, 1965). We have by now an extensive knowledge of the distribution of neutron star masses and the underlying equation of state, (e.g. Lattimer and Prakash, 2016; Özel and Freire, 2016; Oertel *et al.*, 2017), with the most precise determinations existing for binary systems. Shortly after the discovery of the binary pulsar by Hulse and Taylor (1975), with an energy loss in agreement with the emission of gravitational waves predicted by General Relativity, it was found that this system would merge in $\sim 10^8$ years (Weisberg and Huang, 2016). In parallel came the prediction that neutron star or neutron star - black hole mergers would eject r-process nuclei (Lattimer and Schramm, 1974, 1976; Symbalisty and Schramm, 1982), followed up by a first detailed analysis of possible abundance distributions (Meyer and Schramm, 1988). Later predictions included that such mergers would be accompanied by neutrino bursts and gamma-ray bursts (Eichler *et al.*, 1989). The very first and later more precise estimates of the mass ejection from neutron star mergers in Newtonian approximation followed (Davies *et al.*, 1994; Ruffert *et al.*, 1996; Rosswog *et al.*, 1999, 2000), together with the very first detailed nucleosynthesis predictions (Freiburghaus *et al.*, 1999b).

More recently, extensive investigations have been undertaken with respect to nucleosynthesis predictions (Panov and Thielemann, 2004; Panov *et al.*, 2008; Goriely *et al.*, 2011; Korobkin *et al.*, 2012; Panov *et al.*, 2013; Bauswein *et al.*, 2013; Goriely *et al.*, 2013; Hotokezaka *et al.*, 2013; Rosswog *et al.*, 2014; Wanajo *et al.*, 2014; Just *et al.*, 2015a; Goriely *et al.*, 2015; Perego *et al.*, 2014; Eichler *et al.*, 2015; Martin *et al.*, 2015; Mendoza-Temis *et al.*, 2015; Ramirez-Ruiz *et al.*, 2015; Hotokezaka *et al.*, 2015; Shibagaki *et al.*, 2016; Just *et al.*, 2016; Wu *et al.*, 2016; Radice *et al.*, 2016; Roberts *et al.*, 2017; Martin *et al.*, 2018; Wojczuk and Janiuk, 2018; Papenfort *et al.*, 2018). Initial Newtonian approaches have been replaced with conformally flat and fully relativistic treatments (e.g. Ruffert *et al.*, 1996; Shibata and Uryū, 2000; Ruffert and Janka, 2001; Oechslin *et al.*, 2002, 2004; Shibata and Uryū, 2006; Oechslin *et al.*, 2007; Shibata and Taniguchi, 2011; Bauswein and Janka, 2012; Bauswein *et al.*, 2013; Hotokezaka *et al.*, 2013; Wanajo *et al.*, 2014; Sekiguchi *et al.*, 2015, 2016; Radice *et al.*, 2016; Baiotti and Rezzolla, 2017; Bovard *et al.*, 2017; Papenfort *et al.*, 2018), and further followed by the inclusion of magnetic

fields (Price and Rosswog, 2006; Anderson *et al.*, 2008; Liu *et al.*, 2008; Giacomazzo *et al.*, 2009; Obergaulinger *et al.*, 2010; Zrake and MacFadyen, 2013; Kiuchi *et al.*, 2015; Giacomazzo *et al.*, 2015) as well as their interplay with neutrinos (Palenzuela *et al.*, 2015; Guilet *et al.*, 2017)

In parallel to neutron star (NS-NS) mergers also neutron star - black hole (NS-BH) mergers have been investigated (e.g. Rosswog, 2005; Shibata and Uryū, 2006; Chawla *et al.*, 2010; Shibata and Taniguchi, 2011; Korobkin *et al.*, 2012; Wanajo and Janka, 2012a; Kyutoku *et al.*, 2013; Foucart *et al.*, 2014a; Mennekens and Vanbeveren, 2014; Rosswog *et al.*, 2017; Brege *et al.*, 2018). Both NS-NS and NS-BH mergers are accompanied by the formation of a massive accretion disk surrounding the central compact object (Ruffert *et al.*, 1997).

From the point of view of r-process nucleosynthesis, simulations should predict the amount of ejecta, their properties (particularly Y_e), spatial distribution and temporal evolution. In the following, we discuss the major phases of ejection and the general dependencies with the merging system. The discussion is mostly based on a presentation of Shibata (2018). Fig. 34 summarizes the main ejection channels in compact binary mergers and provides summarizes the estimates of ejecta mass, Y_e and velocity discussed below.

Due to the emission of gravitational waves, that reduces the eccentricity of the orbit, at times close to coalescence NS-NS systems are expected to have almost circular orbits and spins much smaller than the orbital frequency (Rosswog, 2015). During the coalescence phase matter is ejected dynamically due to angular momentum conservation on timescales of milliseconds with mildly relativistic speed $v \sim 0.2$–0.4 c (Rosswog *et al.*, 1999, 2000; Bauswein *et al.*, 2013; Hotokezaka *et al.*, 2013b; Palenzuela *et al.*, 2015; Sekiguchi *et al.*, 2015, 2016; Radice *et al.*, 2016; Foucart *et al.*, 2016).

The amount of dynamic ejecta and their properties depend on the compactness of the neutron stars and their mass ratio (Bauswein *et al.*, 2013; Hotokezaka *et al.*, 2013b; Radice *et al.*, 2018b). Two components can be distinguish: cold tidal ejecta in the equatorial plane and shock heated ejecta originating from the contact interface with a more isotropic distribution. Systems with small mass ratios tend to eject larger amounts of material mainly in the equatorial region, while for similar mass ratios the shock heated component dominates (Bauswein *et al.*, 2013; Hotokezaka *et al.*, 2013b; Palenzuela *et al.*, 2015; Lehner *et al.*, 2016). While the cold tidal ejecta maintain the original low Y_e of the neutron star crust from which they are ejected, the shock component is heated to very large temperatures. This drives electron and positron captures that contribute to increase Y_e from a very low initial value. As the material moves away, it is further increased by ν_e and $\bar{\nu}_e$ absorption (Wanajo *et al.*, 2014; Goriely *et al.*, 2015; Martin *et al.*, 2015; Sekiguchi *et al.*, 2016; Radice *et al.*, 2016; Martin *et al.*, 2018). The impact of neutrino absorptions is sensitive to the evolution of the central remnant (Sekiguchi *et al.*, 2015) as will be discussed below. The total amount of dynamic ejecta is in the range 10^{-4}–10^{-2} $M_\odot$ (Bauswein *et al.*, 2013; Hotokezaka *et al.*, 2013b; Sekiguchi *et al.*, 2015, 2016; Lehner *et al.*, 2016; Radice *et al.*, 2018b) with an angular mass distribution well approximated by $F(\theta) = \sin^2\theta$ (Perego *et al.*, 2017a) and a Y_e distribution that can reach up to $Y_e \sim 0.5$ in the polar region (Shibata *et al.*, 2017; Radice *et al.*, 2018b). Magnetohydrodynamic instabilities, operating during the merger, can produce a third component denoted as "viscous-dynamical" ejecta by (Radice *et al.*, 2018a) with asymptotic velocities extending up to ~ 0.8 c. Population synthesis studies (Belczynski *et al.*, 2008), formation studies (Tauris *et al.*, 2017), pulsar observations (Özel and Freire, 2016), and the gravitational wave signal from GW170817 (Abbott *et al.*, 2017; De *et al.*, 2018; Abbott *et al.*, 2018) favour binary NS systems with nearly equal-mass stars ~ 1.35 $M_\odot$. For such systems the ejecta are mainly sensitive to the compactness of the neutron stars. The analysis of the tidal deformability from the Gravitational Wave observations of GW170817 (Most *et al.*, 2018; De *et al.*, 2018; Abbott *et al.*, 2018), the observation of an electromagnetic transient which disfavors a prompt collapse to a black hole (Margalit and Metzger, 2017; Bauswein *et al.*, 2017; Shibata *et al.*, 2017; Coughlin *et al.*, 2018), together with nuclear physics constraints (Fattoyev *et al.*, 2018; Annala *et al.*, 2018; Tews *et al.*, 2018) favors moderately compact neutron stars with a radius in the range 8.9–13.2 km. In this case, the major source of ejecta is the contact interface between the neutron stars (Bauswein *et al.*, 2013; Sekiguchi *et al.*, 2015; Radice *et al.*, 2018b). The maximum mass of a neutron star has been constrained to $M_{\rm max} \lesssim 2.17$ $M_\odot$ (Margalit and Metzger, 2017; Shibata *et al.*, 2017; Rezzolla *et al.*, 2018; Ruiz *et al.*, 2018) following the observation of GW170817.

In the case of NS-BH systems, in order to eject material it is necessary that the NS is disrupted before entering the innermost stable circular orbit of the BH. Tidal disruption means that the BH tidal force is larger than the self-gravity of the NS and requires a large NS radius, a small BH mass or small BH/NS mass ratio, or a high spin for the BH. Population synthesis studies favor a BH/NS mass ratio ~ 7 (Belczynski *et al.*, 2010). This, together with the NS radius constraints mentioned above, suggests that mass ejection will only take place for BH with spin parameter $\chi = cJ/(GM^2) \gtrsim 0.5$ (Foucart *et al.*, 2013, 2014b; Kyutoku *et al.*, 2015; Brege *et al.*, 2018; Kyutoku *et al.*, 2018). The tidal dynamic ejecta are much more anisotropic than those of NS-NS mergers. They are mainly concentrated around the orbital plane and often sweeps out only half of the plane. The ejected mass can reach ~ 0.1 $M_\odot$ with asymptotic velocities of 0.2–0.3 c. The material is very neutron-rich $Y_e \lesssim 0.1$

and not affected by neutrino irradiation (Foucart *et al.*, 2014b; Kyutoku *et al.*, 2018).

An equally common outcome of compact binary mergers is the production of a rotating torus surrounding the newly-formed central object with a typical mass of 0.1 $M_\odot$ (Radice *et al.*, 2018b). In the case of BH-NS mergers the central remnant is a BH and we deal with a neutrino cooled disk that evolves on viscous timescales of seconds. Such systems have been studied based on α-viscosity prescriptions (Fernandez and Metzger, 2013; Fernández *et al.*, 2015; Just *et al.*, 2015a) and more recently by three-dimensional General-Relativistic Magnetohydrodynamic simulations (Siegel and Metzger, 2017; Siegel and Metzger, 2018; Fernández *et al.*, 2019). These works find that up to 40% of the disk mass, depending on the BH spin, is unbound in a quasi-spherical fashion. The electron fraction in the outflow is in the range $Y_e \sim 0.1$–0.4 with velocities $v \approx 0.1$ c (Siegel and Metzger, 2018; Fernández *et al.*, 2019). For the case of NS-NS mergers, the possibilities for the central object are a stable NS, a long-lived massive neutron star (MNS, i.e. a NS with a mass above the maximum mass for a non-spinning NS and below the one for a uniformly rotating NS), a hypermassive neutron star (HMNS, i.e. a NS with a mass above the maximum mass for a uniformly rotating NS, Baumgarte *et al.*, 2000) or a black hole (BH) depending primarily on the total mass of the binary, M_t (Hotokezaka *et al.*, 2013a; Shibata, 2018). If M_t exceeds a critical value M_c, the central object produced by the merger collapses promptly to a BH on the dynamical time scale of a few ms (Sekiguchi *et al.*, 2011). On the other hand, if $M_t < M_c$ the resulting HMNS is at least temporarily supported against gravitational collapse by differential rotation and thermal pressure (Hotokezaka *et al.*, 2013a; Kaplan *et al.*, 2014). The value of M_c depends on the uncertain EoS of nuclear matter, particularly its stiffness, mainly related to the symmetry energy (Baldo and Burgio, 2016; Oertel *et al.*, 2017). The discovery of massive ~ 2 $M_\odot$ neutron stars (Demorest *et al.*, 2010; Antoniadis *et al.*, 2013), places a lower limit to $M_c \gtrsim 2.6 - 2.8$ $M_\odot$ (Hotokezaka *et al.*, 2013a). Hydrodynamical simulations of neutron star mergers for a large sample of temperature-dependent equations of state, show that the ratio between critical mass and the maximum mass of a non-rotating NS are tightly correlated with the compactness of the non-rotating NS (Bauswein *et al.*, 2013). This allows to derive semi-analytical expressions for the critical mass (Bauswein and Stergioulas, 2017; Bauswein *et al.*, 2016) that combined with the GW170817 constraints on the maximum mass and radius of NS give $M_c \approx 2.8$ $M_\odot$. It thus appears likely that the canonical 1.35 + 1.35 $M_\odot$, including GW170817, binary merger goes through a HMNS phase. The duration of this phase depends on the EoS: for a soft EoS that results in rather compact initial neutron stars before the merger, the HMNS collapses to a black hole on timescales of several 10s of milliseconds, while for a stiff EoS the HMNS is long-lived with a lifetime longer than the timescales relevant for matter ejection. The NS radius constraints mentioned above favor the first case. For the case of prompt collapse to a BH, the BH-torus system evolves similarly to the BH-NS merger case considered before. However, systems with large M_t are expected to eject little mass dynamically and produce a low mass accretion disk. In these cases, the total amount of ejecta, dynamical plus accretion disk, is $\sim 10^{-3}$ $M_\odot$ of neutron-rich material, $Y_e \lesssim 0.1$ (Shibata, 2018).

The HMNS-torus is characterized by a more important role of neutrino heating that increases the amount of ejecta and raises their Y_e to values that depend on the lifetime of HMNS remnant (Metzger and Fernández, 2014; Perego *et al.*, 2014; Kaplan *et al.*, 2014; Martin *et al.*, 2015; Lippuner *et al.*, 2017; Fujibayashi *et al.*, 2018). The ejecta consist of two-components being either neutrino-driven or viscous-driven (also known as secular). The neutrino-driven component is ejected mainly on the polar direction with velocities $v \lesssim 0.08$ c and $Y_e \gtrsim 0.25$ and containing around 5% of the disk mass (Martin *et al.*, 2015; Perego *et al.*, 2017a). The viscous-driven component occurs mainly in the equatorial direction with a velocity $v \sim 0.05$ c and contains around 40% of the disk mass (Metzger and Fernández, 2014; Lippuner *et al.*, 2017; Fujibayashi *et al.*, 2018). The Y_e distribution depends on the lifetime of the HMNS (Fujibayashi *et al.*, 2018). If the HMNS survives at least for the timescale of neutrino cooling of the disk (~ 10 s), neutrino heating drives Y_e to values above 0.25. If the HMNS collapses to a black hole on a timescale shorter than the disk lifetime, the Y_e distribution is in the range 0.1–0.4, similar to the BH-torus case.

There exists extensive literature relating these events to short duration Gamma-Ray Bursts (sGRBs) and/or macronovae/kilonovae as electromagnetic counterparts (for literature before GW170817 see e.g., Li and Paczyński, 1998; Nakar, 2007; Metzger and Berger, 2012; Tanvir *et al.*, 2013; Piran *et al.*, 2013; Tanaka and Hotokezaka, 2013; Kasen *et al.*, 2013; Grossman *et al.*, 2014; Rosswog *et al.*, 2014; Metzger and Fernández, 2014; Wanderman and Piran, 2015; Rosswog, 2015; Fryer *et al.*, 2015; Hotokezaka *et al.*, 2016; Barnes *et al.*, 2016; Fernández and Metzger, 2016; Rosswog *et al.*, 2017; Metzger, 2017a). Although these objects are also of major importance as strong sources for gravitational wave emission (Shibata and Taniguchi, 2011; Baiotti and Rezzolla, 2017), especially after GW170817 (Abbott *et al.*, 2017a), underpinning the importance of multi-messenger observations, we will essentially focus here on the ejected nucleosynthesis composition. In the following subsections we will concentrate on (i) the dynamic ejecta, (ii) the post-merger neutrino wind ejecta, and (iii) the late time viscous or secular outflow from the accretion disk.

1. Dynamic ejecta

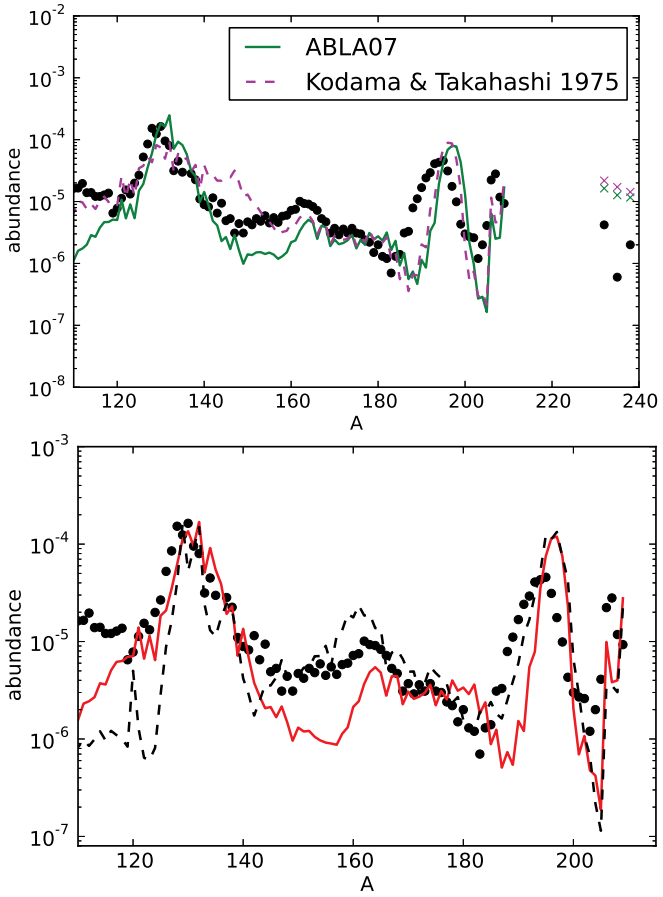

FIG. 35 Top: Resulting r-process abundances for dynamic tidal ejecta (in comparison to solar values - black dots) from neutron star merger simulations (Eichler *et al.*, 2015), making use of β-decay half-lives from Möller *et al.* (2003) together with a relatively old (Kodama and Takahashi, 1975) and a modern set (Kelic *et al.*, 2008) of fragment distributions from fissioning nuclei. However, in both cases a shift of the third r-process peak seems to occur in the final phases, driven by neutron capture of the released fission neutrons. Bottom: Same as above, but utilizing recent β-decay half-life predictions (Marketin *et al.*, 2016a, dashed black line) in comparison to an older set (red line, identical to the green line from top figure). Faster β-decays for heavy nuclei cause a speed-up of the r process and deliver (also in the final phases) nuclei which are prone to fission at an earlier time. This way, the late release of fission neutrons occurs earlier, to a large extent before the freeze-out from $(n,\gamma) \rightleftarrows (\gamma,n)$ equilibrium. Therefore, final neutron captures after freeze-out, which can distort this distribution, are strongly reduced. This can be seen when comparing the top and bottom figure.

As discussed above the dynamic ejecta consist of two components: a cold component consisting of very neutron-rich matter originating from the neutron star crust that is "thrown out" via tidal interaction in the equatorial plane, and a hotter component originating from the contact interface. The first component is the only one present in NS-BH mergers and the second represents most of the unbound material in NS-NS mergers. The tidal component was originally found in Newtonian simulations (see for first investigations Davies *et al.* 1994; Rosswog *et al.* 1999 and more detailed discussions Korobkin *et al.* 2012), while the contact interface component was found in relativistic simulations, first within the conformal flatness approximation (Oechslin *et al.*, 2007; Goriely *et al.*, 2011; Bauswein *et al.*, 2013) and then in fully relativistic simulations (Hotokezaka *et al.*, 2013b). Those simulations neglected the impact of weak processes in the ejecta and hence the ejected material kept the very neutron-rich conditions corresponding to β-equilibrium in the cold neutron star crust, $Y_e \lesssim 0.01$.

The nucleosynthesis in low Y_e ejecta, as found in BH-NS mergers and the tidal component of NS-NS mergers, has been extensively studied (Freiburghaus *et al.*, 1999b; Korobkin *et al.*, 2012; Bauswein *et al.*, 2013; Rosswog *et al.*, 2014; Mendoza-Temis *et al.*, 2015; Eichler *et al.*, 2015; Martin *et al.*, 2016; Mumpower *et al.*, 2016; Bovard *et al.*, 2017) and found to be independent of the astrophysical conditions (Korobkin *et al.*, 2012) but rather sensitive to the nuclear physics input (Panov and Thielemann, 2004; Panov *et al.*, 2008; Bauswein *et al.*, 2013; Eichler *et al.*, 2015; Mendoza-Temis *et al.*, 2015; Goriely, 2015; Goriely and Martínez-Pinedo, 2015; Martin *et al.*, 2016; Mumpower *et al.*, 2016; Shibagaki *et al.*, 2016; Thielemann *et al.*, 2017b). For very neutron-rich ejecta, we deal with rather large neutron-to-seed ratios that can even reach several 1000, hence the nucleosynthesis becomes insensitive to the initial composition and the material loses memory of the exact thermodynamic conditions at ejection. The temperature evolution is characterized by having a high temperature plateau, $T_{\rm max}$, (see Fig. 16) whose value is determined by a competition between the r-process energy generation rate, $\dot{Q}$, and the expansion dynamical timescale (Mendoza-Temis *et al.*, 2015):

$$T_{\rm max} \approx 0.8\ {\rm GK} \left[\left(\frac{\rho}{10^5\ {\rm g\ cm^{-3}}} \right) \left(\frac{\dot{Q}}{4\ {\rm MeV\ s^{-1}}} \right) \left(\frac{\tau_{\rm dyn}}{10\ {\rm ms}} \right) \right]^{1/4} , \quad (13)$$

Hence, independent of the initial conditions, during the phase of neutron captures one can have a hot ($T \gtrsim 0.7$ GK) or cold ($T \lesssim 0.3$ GK) r process, see section III and Fig. 16 where dark gray and brown lines correspond to cold r process conditions and light gray lines to hot r process conditions. Typically the expansion of the material is "slow" enough to allow for all neutrons to be captured. This leads to the occurrence of several fission cycles with large amounts of very heavy nuclei prone to fission, mainly around $A \sim 280$, remaining at freeze-out, see Figs. 14 and 19. During the final freeze-out phase the fission yields of the heaviest nuclei determine the final abundances of nuclei with $A \lesssim 140$ (Goriely and Martínez-Pinedo, 2015). Fission also produces large amounts of

neutrons that tend to be captured on the third r-process peak material. Depending on the amount of neutrons produced and the speed at which they are released the third r-process peak can be shifted to higher mass numbers when compared with solar abundances (see Fig. 35 from Eichler *et al.*, 2015, and for more details on the effects of fission subsection V.D). The final impact depends on the mass model considered, see Fig. 25, and β-decay half-lives (Marketin *et al.*, 2016a; Panov *et al.*, 2016). Shorter β-decay half-lives for very heavy nuclei result in smaller abundances in the fissioning region and hence less and faster release of neutrons during the freeze-out (Eichler *et al.*, 2015).

Fission rates and yields for neutron-rich superheavy nuclei are then fundamental for the determination of the r-process abundances (Goriely, 2015). This requires not only the determination of the region of the nuclear chart where fission occurs (Thielemann *et al.*, 1983; Petermann *et al.*, 2012; Giuliani *et al.*, 2018; Giuliani *et al.*, 2019) but also the modeling of all relevant fission channels including neutron-induced fission, β-delayed fission, and spontaneous fission (Thielemann *et al.*, 1983; Panov *et al.*, 2005; Panov and Thielemann, 2004; Goriely *et al.*, 2009; Panov *et al.*, 2010; Mumpower *et al.*, 2018; Vassh *et al.*, 2018) and corresponding yields (Kelic *et al.*, 2009; Goriely *et al.*, 2013; Schmidt *et al.*, 2016; Schmitt *et al.*, 2018; Schmidt and Jurado, 2018). Low Y_e ejecta produce a final abundance distribution that closely follows the solar r-process abundance distribution for $A > 140$ independently of the fission yields used (Goriely and Martínez-Pinedo, 2015). The production of lighter nuclei is rather sensitive to the fission rates and yields used and typically no nuclei below $A \sim 110$ are produced in substantial amounts (Panov *et al.*, 2008; Goriely *et al.*, 2013; Mendoza-Temis *et al.*, 2015; Eichler *et al.*, 2015; Vassh *et al.*, 2018). Fission is also important for the production of actinides with important consequences for late time kilonova light curves (Barnes *et al.*, 2016; Rosswog *et al.*, 2017; Wanajo, 2018; Wu *et al.*, 2018; Holmbeck *et al.*, 2018b; Zhu *et al.*, 2018) and U/Th cosmochronometry (see section VIII.D).

Several studies (Goriely *et al.*, 2014; Metzger *et al.*, 2015; Mendoza-Temis *et al.*, 2015; Radice *et al.*, 2018a; Fernández *et al.*, 2019; Ishii *et al.*, 2018) have shown that part of the material, up to 10% in mass, is ejected very fast and reaches such low densities that the timescale for neutron captures becomes much longer than the expansion timescale (Mendoza-Temis *et al.*, 2015) (see brown lines on Fig. 16). Under such conditions most of the neutrons are not captured, despite of having a large neutron-to-seed ratio. The final abundances of this "frustrated" r process does not correspond to solar abundances (see Fig. 36) and hence it cannot constitute a major component of the total ejected mass, assuming mergers are a major r-process site. However, it can drive an early (timescales of hours) electromagnetic emission that is

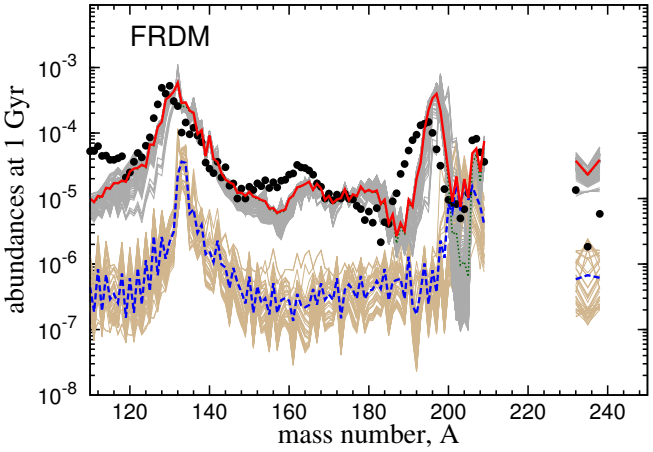

FIG. 36 R-process abundances at a time of 1 Gyr for all trajectories shown in Fig. 16. The grey (brown) curves correspond to the abundances of the trajectories of the slow (fast) ejecta. The mass-averaged abundances for all trajectories (red curves), the slow ejecta (green curves), and the fast ejecta (blue curves) are also shown. The abundances for the slow and fast trajectories and their averages have been scaled by the value of their fractional contribution to the total ejecta. (Figure adapted from Mendoza-Temis *et al.*, 2015).

powered by the radioactive decay of the free neutrons left after completion of the r process (Metzger *et al.*, 2015).

Wanajo *et al.* (2014) showed that weak processes operating on the shock heated ejecta of NS-NS mergers can increase the Y_e. They are particular efficient in the polar region, where the large neutrino fluxes from the HMNS increase substantially the Y_e of the ejecta, provided the HMNS does not collapse promptly to a BH. Depending on the neutrino luminosities, Y_e could be increased to values between 0.25 and 0.4. While it is currently accepted that weak processes increase the Y_e of the ejecta, an aspect confirmed by the kilonova observations discussed in section VII, there is still a relatively large spread between the predictions of different groups (Shibata *et al.*, 2017; Sekiguchi *et al.*, 2016, 2015; Radice *et al.*, 2016, 2018b; Foucart *et al.*, 2016; Bovard *et al.*, 2017; Foucart *et al.*, 2018) related to the different approximations in the treatment of neutrino radiation transport. Dynamic ejecta from NS-NS mergers are expected to contribute to the synthesis of a broad range of r-process nuclei, including both light and heavy, once weak processes are considered (Wanajo *et al.*, 2014; Goriely *et al.*, 2015; Martin *et al.*, 2018). However, it should be kept in mind that the predicted amount of high Y_e matter is typically much smaller that the one found in accretion disk outflows.

2. Neutrino Winds and the Effect of Neutrinos

In addition to the dynamic ejecta, related directly to the merging/collision, post merger ejecta will emerge as well. One component is a "neutrino-wind" as found in

core-collapse supernovae. For the typical merging system, the hot central NS remnant, supported by high temperatures and differential rotation, will not collapse to a black hole immediately, and will be surrounded by a hot and dense torus. Hence, the structure of the wind is quite different from the isolated NSs usually found in core-collapse supernova. The wind outflow occurs mainly in the polar direction (Rosswog *et al.*, 2014; Perego *et al.*, 2014; Metzger and Fernández, 2014; Martin *et al.*, 2015). Matter is exposed to neutrinos long enough for the material to reach an equilibrium between electron neutrino and antineutrino absorption, changing Y_e, see Eq. (10), from the initial (neutron-rich) conditions towards higher values that can even be above $Y_e = 0.5$. Due to the much larger $\bar{\nu}_e$ luminosities and energy differences between $\bar{\nu}_e$ and ν_e, found during the post-merger evolution when compared with core-collapse supernova (see Fig. 27), the peak of the Y_e distribution is expected to be neutron-rich with $Y_e \gtrsim 0.25$ (Martin *et al.*, 2015; Lippuner *et al.*, 2017; Fujibayashi *et al.*, 2017, 2018). This leads to a weak r process and produces mainly matter below the second r-process peak, i.e. no lanthanides are produced.

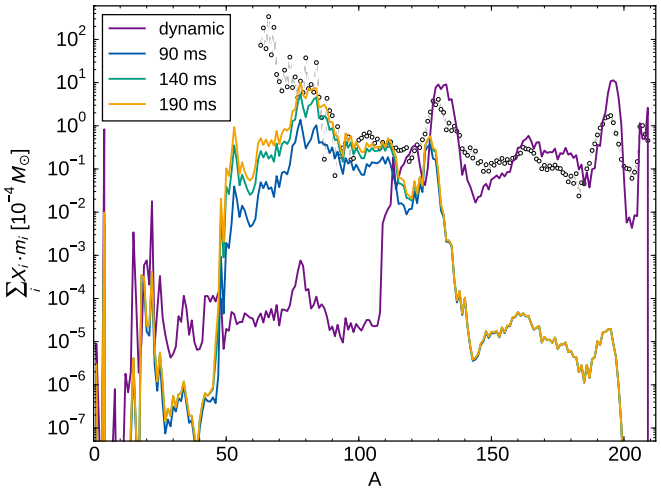

FIG. 37 Neutrino wind contribution to neutron star merger ejecta, dependent on the delay time between the merger and BH formation (Martin *et al.*, 2015). In comparison also the dynamic, tidal ejecta of (Korobkin *et al.*, 2012) are shown. The neutrino wind, ejected dominantly in polar regions, contributes nuclei with $A < 130$, due to the effect of the neutrinos on Y_e.

Fig. 37 displays the results of Martin *et al.* (2015) for the neutrino wind component as a function of the delay time until black hole formation sets in. It can be seen that predominantly nuclei below $A = 130$ are produced, complementing nicely the abundance features originating from prompt/dynamic low Y_e ejecta, also displayed. The latter, resulting here from the Newtonian simulations (Korobkin *et al.*, 2012).

Similarly to the situation in core-collapse supernova, the properties of neutrino-wind ejecta, and particularly Y_e, are expected to be sensitive to the spectral differences between ν_e and $\bar{\nu}_e$. This requires an accurate prediction of neutrino luminosities and spectra. Supernova neutrino-wind transport simulations are nowadays based on exact numerical solutions of the Boltzmann transport equation (e.g. Hüdepohl *et al.*, 2010; Fischer *et al.*, 2010; Roberts, 2012) exploiting the spherically symmetric nature of the problem. In the case of mergers, due to the multidimensional nature of the problem, simulations so far are based on neutrino leakage schemes (Perego *et al.*, 2014; Metzger and Fernández, 2014; Radice *et al.*, 2016; Ardevol-Pulpillo *et al.*, 2018) and $M1$ schemes (Just *et al.*, 2015a,b; Foucart *et al.*, 2015; Fujibayashi *et al.*, 2017, 2018). There are indications that they may not properly capture the energy densities and fluxes of neutrinos in the polar regions (Just *et al.*, 2015a), hence, affecting the Y_e estimates in the polar region (Foucart *et al.*, 2016; Foucart *et al.*, 2018). Additional opacity reactions so far not considered, like neutrino-pair annihilation, may also play an important role in determining the properties of the ejecta (Just *et al.*, 2016; Fujibayashi *et al.*, 2017; Perego *et al.*, 2017b; Fujibayashi *et al.*, 2018; Foucart *et al.*, 2018).

Y_e can also be affected by modifications of neutrino and antineutrino spectra due to neutrino flavor conversion. There have been a number of tests to verify such neutrino conversions via matter-neutrino resonances (Malkus *et al.*, 2012; Foucart *et al.*, 2015; Malkus *et al.*, 2016; Zhu *et al.*, 2016; Frensel *et al.*, 2017) and fast pairwise flavor conversions (Wu and Tamborra, 2017; Wu *et al.*, 2017b). Due to the more complicated geometry of a disk environment in comparison to core-collapse supernovae, most of the calculations are based on single-angle approximations. Spherically symmetric test calculations show that the matter-neutrino resonance still occurs in multiangle models (Vlasenko and McLaughlin, 2018) but with reduced efficiency. Nevertheless, the existing investigations clearly point to the potential effect on Y_e, and thus the resulting nucleosynthesis can be affected.

3. Accretion Disks outflows

The long-term evolution, $t \sim 1$–10 s, of the accretion disc produces outflows of material powered by viscous heating and nuclear recombination (Lee and Ramirez-Ruiz, 2007; Beloborodov, 2008; Metzger *et al.*, 2009; Fernandez and Metzger, 2013). Those outflows can contain up to 40% of the disk mass. The amount of ejected mass increases with the lifetime of the MNS formed in the merger, but most importantly for nucleosynthesis the Y_e distribution is dramatically affected by the lifetime of the MNS (Metzger and Fernández, 2014). For a long lived MNS, $t \gtrsim 1$ s, neutrino irradiation from the MNS results in ejecta with $Y_e > 0.3$ (Metzger and Fernández, 2014;

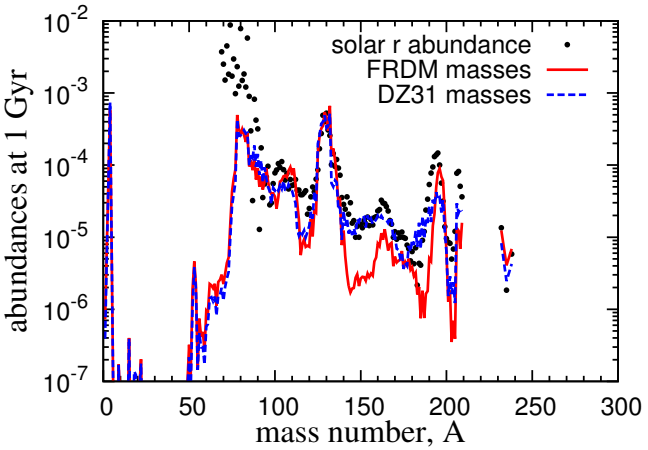

FIG. 38 Resulting r-process abundances (in comparison to solar values - black dots) from black hole accretion disk simulations (Wu *et al.*, 2016), making use of a black hole mass of 3 $M_\odot$, a disk mass of 0.03 $M_\odot$, an initial Y_e of 0.1, entropy per baryon of $8k_b$, an alpha parameter of the viscous disk of 0.03, and a vanishing black hole spin. The figure illustrate the impact of two different mass models, FRDM and DZ31, in the final abundances

Lippuner *et al.*, 2017; Fujibayashi *et al.*, 2018). The nucleosynthesis in these ejecta is simular to the neutrino-wind ejecta discussed in the previous subsubsection.

For a short-lived MNS, $t \lesssim 1$ s, the impact of neutrino-irradiation is small and from the point of view of nucleosynthesis outflows from accretion disks formed in NS-NS and BH-NS mergers gives similar results. Early nucleosynthesis studies where mainly parametric and considered mainly the "neutrino-driven" wind outflow from the surface of the disk (Pruet *et al.*, 2003; Fujimoto *et al.*, 2003, 2004; Pruet *et al.*, 2004; McLaughlin and Surman, 2005; Surman *et al.*, 2006; Metzger *et al.*, 2008; Surman *et al.*, 2008; Dessart *et al.*, 2009; Kizivat *et al.*, 2010; Wanajo and Janka, 2012b; Surman *et al.*, 2014). Detailed simulations have been performed in recent years based on α-viscosity prescriptions (Fernandez and Metzger, 2013; Metzger and Fernández, 2014; Just *et al.*, 2015a; Fernández and Metzger, 2016; Just *et al.*, 2016; Wu *et al.*, 2016; Wojczuk and Janiuk, 2018; Fujibayashi *et al.*, 2018) and more recently on three-dimensional General-Relativistic Magnetohydrodynamic simulations (Siegel and Metzger, 2017; Siegel and Metzger, 2018; Fernández *et al.*, 2019). These simulations show that neutrino winds from the accretion disk eject little mass and that most of the material is ejected by viscous heating (Just *et al.*, 2015a). The results for disk outflows by Wu *et al.* (2016) are displayed in Fig. 38, which shows the integrated abundance pattern of all tracer particles. This underlines that, in principle, disk outflows alone can produce the whole range of r-process nuclei, with a significant production of $A \lesssim 130$ nuclei. Disk outflows also reach the third peak at $A = 195$ in most of the simulations. The detailed results depend on the disk viscosity, the initial mass or entropy of the torus, the black hole spin, and (of course) the nuclear physics input. The latter is illustrated in Fig. 38 that compares the nucleosynthesis results for two different mass models, FRDM (Möller *et al.*, 1995) and Duflo-Zuker (Duflo and Zuker, 1995). The production of heavy ($A \gtrsim 195$) nuclei is also affected by uncertainties of the disk properties discussed above (Just *et al.*, 2015a; Wu *et al.*, 2016). However, such a possible deficit can be counterbalanced by the dynamic ejecta, as the total nucleosynthesis of the merger includes the components of the dynamic ejecta, the neutrino wind, and the accretion disk.

Nucleosynthesis studies in mergers are commonly based on simulation data that follow the evolution of the ejecta for timescales shorter, $\sim$ ms, than the r-process nucleosynthesis timescale, $\sim$ s. This makes it necessary to extrapolate the time evolution of thermodynamic properties like temperature and density in order to follow the nucleosynthesis to completion. It is commonly assumed that the expansion is homologous, $\rho \sim t^{-3}$, with the temperature evolution determined by the nuclear energy production of the r process. The nuclear energy production during the r process, originating mainly from β decays, is in the range $\dot{Q} \approx 1-4$ MeV s^{-1} nuc^{-1} (see lower panel of Fig. 16). Rosswog *et al.* (2014) have performed long-term simulations and found that the r-process energy release does not qualitatively alter the properties of dynamic ejecta. Wu *et al.* (2016) found that r-process heating can increase the amount of ejecta up to a factor 2 in viscous outflows from accretion disks and remove an anomalously high abundance of $A = 132$ nuclei (see Fig. 38 and Lippuner *et al.*, 2017; Siegel and Metzger, 2018). R-process heating can increase the amount of ejecta and critically shape the dynamics of marginally bound ejecta responsible for fall-back accretion on timescales of the second to minutes (Metzger *et al.*, 2010a; Desai *et al.*, 2018). Late-time fall-back accretion has been suggested as possible mechanism to explain the extended X-ray emission observed in some short GRBs (Rosswog, 2007). R-process heating on timescales of days to weeks after the merger has been found responsible for powering the "kilonova" electromagnetic emission (Li and Paczyński, 1998; Metzger *et al.*, 2010b) as will be discussed in the next section.

VII. ELECTROMAGNETIC SIGNATURES OF R-PROCESS NUCLEOSYNTHESIS

As discussed above the r process produces very neutron rich unstable nuclei on timescales of a few seconds. Once produced they decay to stability by a combination of beta, alpha and fission decays. These decays produce large amounts of energy and can potentially lead to an observable electromagnetic emission. The first suggestion of such a electromagnetic emission was due

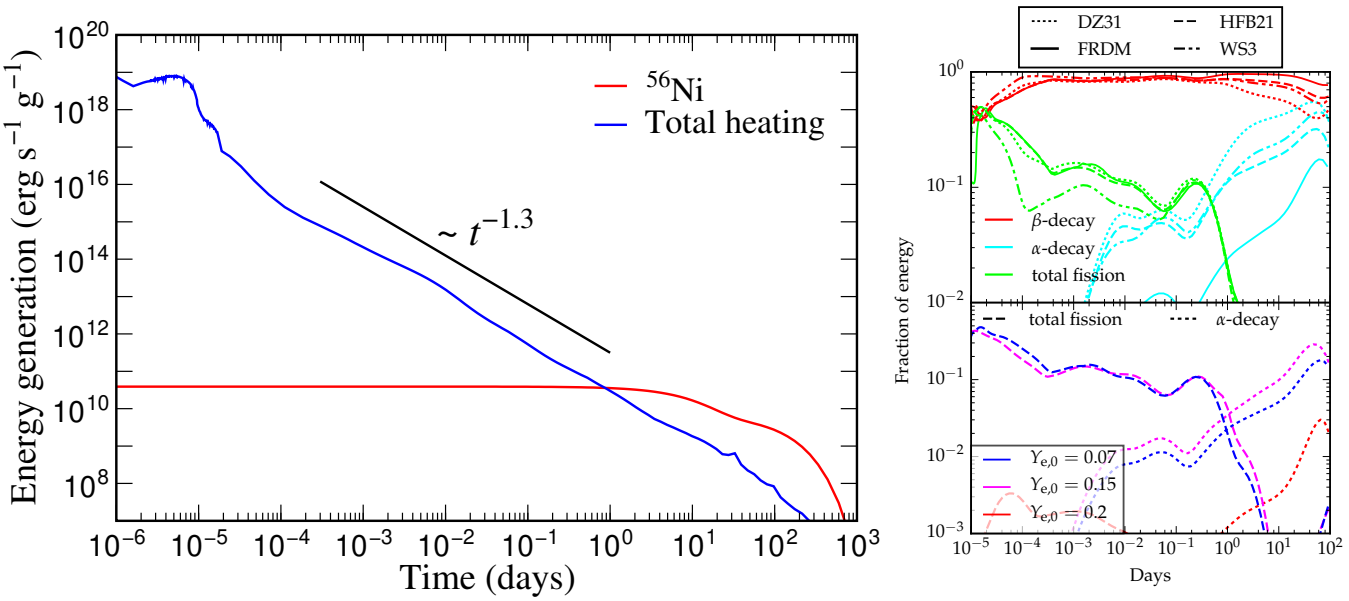

FIG. 39 (left panel) Specific energy generation rate, $\dot{Q}$, in r-process ejecta (black line). For comparison the energy production from the decay chain $^{56}\mathrm{Ni} \rightarrow {}^{56}\mathrm{Co} \rightarrow {}^{56}\mathrm{Fe}$ (red) and the analytical estimate $\dot{Q} \sim t^{-1.3}$ are also shown (adapted from Metzger *et al.*, 2010b). (right panel) top: the fraction of total radioactive energy produced by β-decays, α-decays, and fission for a representative trajectory corresponding to low Y_e NS-NS merger dynamical ejecta for four nuclear mass models While β-decay dominates, fission (α-decay) can be important at early (late) times. Agreement between the four mass models shown is within an order of magnitude. Bottom: energy released in α-decays and fission, for the FRDM mass model, for a range of initial $Y_{e,0}$ conditions. Lower electron fractions favor the assembly of the heavy elements that later decay by fission and α-emission. As $Y_{e,0}$ increases, these processes become less important, and are negligible for $Y_{e,0} > 0.2$ (from Barnes *et al.*, 2016).

to Burbidge *et al.* (1956) who attributed type Ia supernova light curves to the decay of ^{254}Cf produced by the r process. Nowadays, we know that both type Ia and type II supernova light curves are due mainly to the decay of ^{56}Ni (Bersten and Mazzali, 2017; Zampieri, 2017). The study of light curves and spectra does not only constraint the nucleosynthesis yields (Diehl and Timmes, 1998; Seitenzahl *et al.*, 2014) but also provide information about the physical parameters of the progenitor system and the explosion itself (Bersten and Mazzali, 2017; Zampieri, 2017). This illustrates the physics potential of an electromagnetic transient observation associated with r-process ejecta. It identifies one the sites where the r process occurs (Metzger *et al.*, 2010b) and serves as a promising electromagnetic counterpart to the gravitational wave detection following a neutron star merger (Metzger and Berger, 2012). All these aspects were confirmed by the electromagnetic transient AT 2017gfo observed following the gravitational wave event GW170817 (Abbott *et al.*, 2017a).

Li and Paczyński (1998) were the first to propose that radioactive ejecta from a NS-NS merger could power a supernova-like transient. However, they did not posses a physical model to describe the origin of the radioactive heating, $\dot{Q}$, and considered two possible limiting cases: an exponential-law decay and a power-law $\dot{Q} \sim t^{-1}$. In both cases the normalization was left an a free parameter.

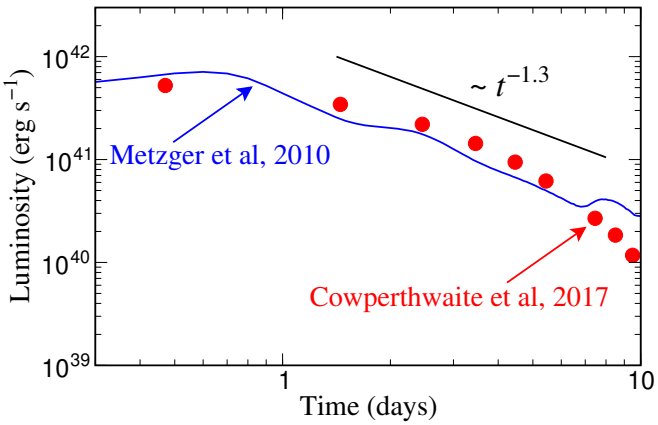

FIG. 40 Bolometric light curve of the optical/infrared counterpart, AT 2017gfo, of GW170817 (red circles) from multiband photometry (Cowperthwaite *et al.*, 2017) compared with the fiducial model of Metzger *et al.* (2010b). For comparison a line with the approximate power-law decay $\dot{Q} \sim t^{-1.3}$ for r-process heating (see Fig. 39).

Hence, even if the model predicted the right timescale for the peak luminosity, it could not determine the absolute luminosity, spectral peak frequency and time-evolution of the luminosity. Indeed, their fiducial model reached extremely high values of the luminosity $\sim 10^{44}$ erg s^{-1} with a spectral peak in the ultra-violet. Kulkarni (2005)

considered two possible origins for the heating: neutron and ^{56}Ni decay; and named such events "macronova". Metzger *et al.* (2010b) were the first to relate the late time radioactive heating to the decay of freshly produced r-process nuclei. Based on heating rates derived self-consistently from a nuclear reaction network, they showed that the heating rate follows a power law at time scales of a day with a steeper dependence than the one assumed by (Li and Paczyński, 1998), $\dot{Q} \sim t^{-1.3}$. As shown in Fig. 39, the heating evolves very differently for r-process material than for supernova-like ejecta dominated by ^{56}Ni. A power law dependence is expected whenever the heating is dominated by a broad distribution of nuclei all of them decaying exponentially. It can be understood from basic physics of β-decay and the properties of neutron-rich nuclei (Metzger *et al.*, 2010b; Hotokezaka *et al.*, 2017). A similar dependence is found for the decay rate of terrestrial radioactive waste (Way and Wigner, 1948).

The work of Metzger *et al.* (2010b) predicted peak luminosities $\sim 3 \times 10^{41}$ erg s^{-1} for 0.01 M$_\odot$ of ejecta expanding at $v \sim 0.1\ c$ and spectral peak at visual magnitude. As such value corresponds to 1000 times the luminosity of classical novae they named these events "kilonova". Fig. 40 compares their prediction with the recent observation of AT 2017gfo (Cowperthwaite *et al.*, 2017). Similar results were also found by Roberts *et al.* (2011) and Goriely *et al.* (2011).

The physical processes determining the kilonova light curve are (see Fernández and Metzger, 2016; Metzger, 2017a; Tanaka, 2016, for reviews):

a. Radioactive heating. The radioactive heating of r-process products is expected to follow a power law whenever a large statistical ensemble of nuclei is produced. This is the case for ejecta with $Y_e \lesssim 0.2$. For higher Y_e ejecta, the heating rate has 'bumps' as a function of time caused by being dominated by a few nuclei (Grossman *et al.*, 2014; Martin *et al.*, 2015; Lippuner and Roberts, 2015; Rosswog *et al.*, 2018; Wanajo, 2018). However, when averaged over Y_e distributions as predicted by simulations the heating rate at timescales of days to a week (of greatest relevance to determine the peak luminosity) lies within a factor of a few for $Y_e \lesssim 0.4$ (Lippuner and Roberts, 2015; Wu *et al.*, 2018). At early times of a few hours the heating may be dominated by neutron decay, assuming the presence of free neutrons in the outermost layers of the ejecta, producing a Ultraviolet/Blue precursor to the kilonova emission (Metzger *et al.*, 2015; Metzger, 2017a). At times between 10 and 100 days, the heating is dominated by a few decays, (see Wu *et al.*, 2018, for a complete listing), due to the scarcity of nuclei with the appropriate half-life. R-process nuclei decay in a variety of channels including β-decay, α-decay and fission. The energy production in each individual channel is important as the absorption of the energy depends on the decay products being electrons, photons, alphas and fission products. For high Y_e ejecta, heating is dominated by β-decay and only electrons and photons are relevant with neutrinos being just an energy loss. For low Y_e ejecta, actinides are produced and alpha decay and fission become important (see Fig. 39). The right panel of Fig. 39 shows that the contribution alphas and fission to the energy production can be substantial and sensitive to the underlying mass model (Barnes *et al.*, 2016; Rosswog *et al.*, 2017; Wu *et al.*, 2018).

b. Thermalization efficiency. At early times the ejecta is very dense and the energy produced by radioactive decay, except neutrinos, is completely reabsorbed. However, as the density decreases an increased fraction of the energy is lost and cannot be used to drive a thermal electromagnetic emission. Hence, one normally introduces a time dependent thermalization efficiency that corrects the energy produced by radioactive processes (Barnes *et al.*, 2016). The efficiency depends on bulk properties of the ejecta like mass and velocity as they determine the evolution of the density. It also depends on the presence of magnetic field and its geometry. Furthermore, it varies with the decay product and time evolution of the heating at each particular decay channel (Kasen and Barnes, 2018), i.e. whether we have a statistical distribution of decaying nuclei or a heating dominated by a few isotopes which is probably more appropiate for late times. Earlier works considered the thermalization of γ-rays (Hotokezaka *et al.*, 2016) and were later extended to consider charged particles (Barnes *et al.*, 2016). This work has been recently extended to the case of a few decays dominating the heating (Kasen and Barnes, 2018; Wu *et al.*, 2018). Qualitatively one finds that the thermalization efficiency for γ-rays decreases very rapidly and becomes negligible on timescales of a few 10's of days. The thermalization efficiency for changed particles and particularly alphas and fission products remains substantial at late times. This makes kilonova light curves rather sensitive the heating contribution of alpha decays and fission (Barnes *et al.*, 2016; Rosswog *et al.*, 2017; Wu *et al.*, 2018; Zhu *et al.*, 2018; Vassh *et al.*, 2018).

c. Atomic opacities. A significant electromagnetic luminosity is only possible once the density decreases sufficiently that photons can escape the ejecta on the expansion time-scale (Arnett, 1980, 1982). Assuming an homogeneous spherical distribution of ejecta with mass M, expanding homologously with velocity v and radius $R = vt$, the diffusion time scale of the ejecta can be approximated as $t_{\rm diff} \approx \rho\kappa R^2/(3c)$, with $\rho = 3M/(4\pi R^3)$ the density and κ the opacity of the ejecta. Once the ejecta expands enough to become transparent, it releases

the thermal radiation. This occurs when the diffusion timescale, $t_{\rm diff}$, becomes comparable to the dynamical timescale, $t = R/v$. This defines the time at which the maximum of the luminosity is reached (see e.g. Metzger *et al.*, 2010b; Fernández and Metzger, 2016):

$$t_{\rm peak} \approx \left(\frac{\kappa M}{4\pi c v}\right)^{1/2} \tag{14}$$
$$\approx 1.5 \text{ days} \left(\frac{M}{0.01 M_\odot}\right)^{1/2} \left(\frac{v}{0.1c}\right)^{-1/2} \left(\frac{\kappa}{\rm cm^2 g^{-1}}\right)^{1/2}$$

At timescales beyond the peak time the luminosity can be approximated using the Arnett's Law (Arnett, 1980, 1982): $L(t) = M\dot{Q}_{\rm dep}(t)$. $\dot{Q}_{\rm dep}$ is the energy deposition rate corrected by the thermalization efficiency and can be approximated as $\dot{Q}_{\rm dep} \approx \varepsilon \times 10^{10} \, (t/\text{day})^{-\alpha}$ erg s^{-1}g^{-1}, with $\varepsilon < 1$ the thermalization efficienty. At peak time the kilonova luminosity is given by:

$$L_{\rm peak} \approx 1.1\varepsilon \times 10^{41} \text{ erg s}^{-1} \tag{15}$$
$$\left(\frac{M}{0.01 M_\odot}\right)^{1-\alpha/2} \left(\frac{v}{0.1c}\right)^{\alpha/2} \left(\frac{\kappa}{\rm cm^2 g^{-1}}\right)^{-\alpha/2}$$

The effective temperature of emission can be obtained from the luminosity using the Stefan-Boltzmann Law that together with the Wien displacement law gives the characteristic wavelength of the emission:

$$\lambda_{\rm peak} \approx 514 \text{ nm} \tag{16}$$
$$\left(\frac{M}{0.01 M_\odot}\right)^{\alpha/8} \left(\frac{v}{0.1c}\right)^{(2-\alpha)/8} \left(\frac{\kappa}{\rm cm^2 g^{-1}}\right)^{(2+\alpha)/8}$$

The above formulas illustrate several characteristic features of kilonova light curves. Even if the emission mechanism is similar to supernova the typical ejecta mass is much smaller and the velocity larger. The equations illustrate the important role played by the opacity that is dominated by Doppler-broadened atomic line bound-bound transitions (Kasen *et al.*, 2013; Fontes *et al.*, 2015; Tanaka *et al.*, 2018). Ejecta containing light r-process elements ($A \lesssim 140$) with d-shell valence electrons possess an opacity $\kappa \lesssim 1$ cm^2 g^{-1}. In this case the emission peaks in around a day in the Blue. This was, indeed, the case for AT 2017gfo (Nicholl *et al.*, 2017a). If the ejecta contains lanthanide or actinide nuclei ($A \gtrsim 140$), then the optical opacity is very high $\kappa \gtrsim 10$–100 cm^2 g^{-1} due to the complex structure of f-shell valence electrons for these elements, resulting in a dense forest of lines (Kasen *et al.*, 2013; Barnes and Kasen, 2013; Tanaka and Hotokezaka, 2013; Fontes *et al.*, 2017). Having a kilonova observation, like in the case of AT 2017gfo, it is possible to adjust the multi-wavelength evolution of the light curve using a variation of the model described above and determine the amount of ejecta, velocity and opacity that is a proxy for composition. As discussed in section II.E, to reproduce the AT 2017gfo observations requires at least two different ejecta components with three-component models being slightly favored (see e.g. Villar *et al.*, 2017). This result is consistent with the existence of several ejecta components in mergers giving rise to different nucleosynthesis products (see section VI.B). The analysis of sGRB observations (Wu and MacFadyen, 2018) and kilonova transient (Perego *et al.*, 2017a) favors an off-axis viewing angle of $\sim 30°$ deg. Hence, the early blue phase of the kilonova light curve has been suggested to originate from Lanthanide poor polar ejecta (see e.g. Kasen *et al.*, 2017), however see Kawaguchi *et al.* (2018) for an alternative explanation. This result is consistent with simulations that predict that weak processes including electron (anti)neutrino absorption drive the composition to $Y_e \gtrsim 0.25$. It may be interpreted as an observational evidence of the important role of neutrinos in determining the composition of the ejecta. However, there is a tension between the velocity of the ejecta $v \approx 0.27$ c that is consistent with simulations of dynamical ejecta and the large ejecta mass, $M_{\rm ej} \approx 0.020$ M$_\odot$, that is not. Additional Lanthanide-poor ejecta is expected to originate from the post-merger neutrino-wind ejecta. However, its velocity is expected to be smaller, unless the wind is magnetically accelerated by the strongly magnetized HMNS remnant (Metzger *et al.*, 2018). The amount of material and velocity of material involved in the "purple" and "red" components suggest that they originate from post-merger outflows from the accretions disk (see e.g. Kasen *et al.*, 2017). Simulations predict that the ejecta contains a broad distribution of Y_e and is able to produce both light and heavy r-process material including the Lanthanides/Actinides necessary to account for the high opacity (Just *et al.*, 2015a; Wu *et al.*, 2016).

It is, indeed, the observation of the Lanthanide-rich "red" emission that provided the first observational evidence that neutron-star mergers produce r-process nuclei. However, so far no direct spectroscopic evidence has been obtained pointing to the production of a particular element. The high density of lines for lanthanides/actinides together with the large velocities of the ejecta produces line blending and smoothness the spectra (Chornock *et al.*, 2017). This aspect has been used to determine the velocity of the ejecta from spectroscopic information (see e.g. Chornock *et al.*, 2017). Nevertheless, the spectra presents peaks that may probe the abundance of individual elements (see figure 4 of Kasen *et al.*, 2017). However, uncertainties in current atomic data hinder a detailed spectral analysis. The lanthanide/actinide opacities are uncertain because the atomic states and line strengths of these complex elements are not measured experimentally. Theoretically, such high-Z atoms represent a challenging problem in many-body quantum mechanics, and hence are based on statistical models that must

be calibrated to experimental data (Kasen *et al.*, 2013; Fontes *et al.*, 2015; Tanaka *et al.*, 2018). Beyond identifying the line transitions themselves, there is considerably uncertainty in how to translate these data into an effective opacity. The commonly employed "line expansion opacity" formalism (Pinto and Eastman, 2000a,b), based on the Sobolev approximation and applied to kilonovae by Barnes and Kasen (2013) and Tanaka and Hotokezaka (2013), may break down if the line density is sufficiently high that the wavelength spacing of strong lines becomes comparable to the intrinsic thermal width of the lines (Kasen *et al.*, 2013; Fontes *et al.*, 2015; Fontes *et al.*, 2017).

Lacking a direct spectroscopic identification of the abudance of individual elements, recent work has focused in identifying fingerprints of heavy elements in kilonova light curves. Particularly promising are late-time observations as the decay heating can be dominated by a few nuclei (Wu *et al.*, 2018). Kasliwal *et al.* (2018) suggest heavy isotopes (e.g. ^{140}Ba, ^{143}Pr, ^{147}Nd, ^{156}Eu, ^{191}Os, ^{223}Ra, ^{225}Ra, ^{233}Pa, ^{234}Th) with β-decay half-live around 14 days. Wu *et al.* (2018) has shown that at times of weeks to months, the decay energy input may be dominated by a discrete number of α-decays, ^{223}Ra (half-life $t_{1/2} = 11.43$ d), ^{225}Ac ($t_{1/2} = 10.0$ d, following the β-decay of ^{225}Ra with $t_{1/2} = 14.9$ d), and the fissioning isotope ^{254}Cf ($t_{1/2} = 60.5$ d) (see also Zhu *et al.*, 2018), which liberate more energy per decay and thermalize with greater efficiency than β-decay products. Late-time nebular observations of kilonovae which constrain the radioactive power provide the potential to identify signatures of these individual isotopes, thus confirming the production of heavy nuclei. In order to constrain the bolometric light to the required accuracy, multi-epoch and wide-band observations are required with sensitive instruments like the James Webb Space Telescope.

An alternative mechanism to probe the in situ production of r-process nuclei is the identification of X-ray or γ-ray lines from their decay similar to the observations of ^{44}Ti γ-rays in Cas A (Vink *et al.*, 2001; Renaud *et al.*, 2006) and SN 1987A (Grebenev *et al.*, 2012) remnants. Qian *et al.* (1998, 1999) has provided estimates of γ-ray fluxes for several r-process nuclei and Ripley *et al.* (2014) has extended those estimates to X-ray lines. The predicted fluxes are too low to be detected by current missions, however improvements in detection techniques may allow to detect the last merger that took place in our Galaxy.

VIII. ABUNDANCE EVOLUTION IN THE GALAXY AND ORIGIN OF THE R PROCESS

After we have summarized in section II the status of abundance observations of neutron-capture (especially r-process) elements, and passed in the intermediate sections through the nucleosynthesis working and required nuclear input, we presented in section VI the most favorable astrophysical sites and the related abundance predictions. This section addresses their features, in addition to abundance predictions their occurrence frequency and its time evolution throughout galactic history, with the aim to provide an understanding of the impact of these individual sites on the evolution of the Galaxy. The goal is to identify those astrophysical site(s) responsible for the total solar r-process abundances as well as the observed features during galactic evolution.

A. Supernova vs. r-process imprints in early galactic evolution

Based on the nucleosynthesis predictions for (regular) core-collapse and for type Ia supernovae, plus their occurrence rates, one finds that the early phase of the evolution of galaxies is dominated by the ejecta of (fast evolving) massive stars, i.e. those leading to core-collapse supernovae. While there might exist differences for the ejecta composition of e.g. 13, 15, 20, 25 or 40 $M_\odot$ stars, average production ratios in the interstellar gas will be found after some time delay when many such explosions and the mixing of their ejecta with the interstellar medium have taken place. These averaged abundance ratios reflect integrated ejecta yields over the initial mass function of stars, i.e. weighted with the probability of finding stars in a certain mass interval. As type Ia supernovae originate from exploding white dwarfs in binary systems, i.e. (a) from stars with initially less than 8 $M_\odot$ in order to become a white dwarf and (b) requiring mass transfer in a binary system before the type Ia supernova explosion, such events are delayed in comparison to the explosion of massive single stars. This follows (a) because low and intermediate mass stars experience longer evolution phases and (b) binary evolution adds to the delay. For these reasons type Ia supernovae, dominating the overall production of Fe and Ni (typically 0.5–0.6 $M_\odot$ per event), are only important at later phases in galactic evolution. As core-collapse supernovae produce larger amounts of O, Ne, Mg, Si, S, Ar, Ca, Ti (so-called α-elements) than Fe-group nuclei like Fe and Ni (only of the order 0.1 $M_\odot$), their average ratio of α/Fe is larger than the corresponding solar ratio.

For most stars their surface abundances represent the composition of the interstellar gas out of which they formed. This is not the case for already evolved stars which blew off part of their envelope by stellar winds or stars in binary systems with mass exchange. With these exceptions we can look back into the early history of the Galaxy via the surface abundances of unevolved low-mass stars, witnessing the composition of the interstellar medium at the time of their birth. In Fig. 8 of section II.A some of these aspects were displayed, with

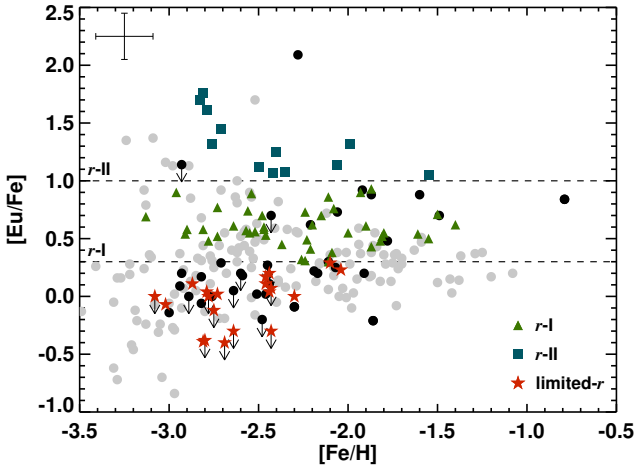

FIG. 41 Derived [Eu/Fe] abundances for the sample, as a function of metallicity: r-I stars (green triangles), r-II stars (blue squares), limited-r (red stars), and non r- process-enhanced stars (black dots); upper limits are shown with black arrows (Hansen *et al.*, 2018)

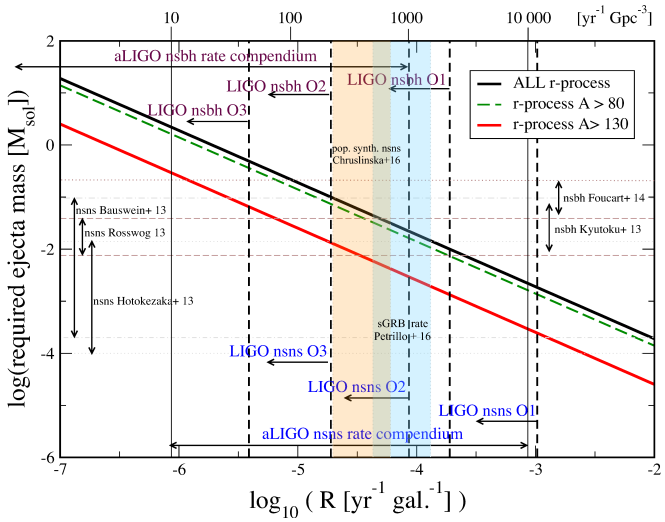

FIG. 42 Figure taken from Rosswog *et al.* (2017), indicating the required r-process ejecta masses as a function of the occurrence frequency of the production site (for references we refer to the original paper). The figure shows that on a typical SN frequency of 1/100 yrs about 10^{-4} to 10^{-5} $M_\odot$ of r-process matter would need to be produced, for binary merger ejecta with about 10^{-2} $M_\odot$ the frequency must be rarer by a factor of 100 to 1000, and if even 1 $M_\odot$ of r-process matter would be ejected in specific events, the frequency must be again lower by another factor of 100.

the ratio [Mg/Fe] plotted as a function of metallicity [Fe/H] for stars in our Galaxy. For Mg (a typical α-element and representative for many elements from O to Ti) one sees—with a relatively small scatter—a flat value of [Mg/Fe] between 0.3 and 0.5 up to [Fe/H] ≤ -1, which decreases down to solar values at [Fe/H] $= 0$. This can be explained, as discussed above, by the early appearance of core-collapse supernovae from fast evolving massive, single stars, producing on average [Mg/Fe] $= 0.4$ (see e.g. Woosley *et al.*, 2002; Woosley and Heger, 2007; Limongi and Chieffi, 2018) before type Ia supernovae set in. The properties of the latter have been reviewed by Hillebrandt *et al.* (2013); Maoz *et al.* (2014); Goldstein and Kasen (2018); Livio and Mazzali (2018) as well as their nucleosynthesis features (Seitenzahl and Townsley, 2017; Nomoto and Leung, 2017b). These basic features of galactic evolution have been understood reasonably well for a majority of elements (Matteucci and Greggio, 1986; Nomoto *et al.*, 2013), while still many open questions exist in stellar evolution and the supernova explosion mechanisms. (This includes also the question of the role of more massive stars, probably ending as black holes and related to so-called hypernovae / long-duration gamma-ray bursts, and even more massive pair instability supernovae Heger *et al.*, 2003; Ertl *et al.*, 2016; Sukhbold *et al.*, 2016).

The solar abundance of Eu is to more than 90% dominated by those isotopes which are produced in the r process (Bisterzo *et al.*, 2015, 2017). Therefore it is considered as a major r-process indicator. The ratio [Eu/Fe], already displayed in Fig. 8 of section II.A and its recent update in Fig. 41 (above), shows a huge scatter by more than two orders of magnitude at low metallicities, corresonding to very early in galactic evolution. While the evolution of the average ratio resembles that of the alpha elements, being of a core-collapse supernova origin and also experiencing a decline to solar ratios for [Fe/H] ≥ -1, it is far more complex to understand Eu than α-elements like Mg. In this section, we will discuss the suggested origins for the r process and the possibility of their discrimination. A large scatter seems to indicate a not yet well mixed or averaged interstellar medium and thus a lower occurrence rate for r-process events, compensated by larger amounts of their ejecta (see Fig. 42) in order to be consistent with total solar abundances.

Also rare events, if consistent with the overall solar r-abundances, would need to support the averaged [Eu/Fe] ratios at low metallicities, combined with a scatter of individual observations. The observed approach to the average [Eu/Fe] ratio with a small scatter occurs only in the interval $-2 \leq$ [Fe/H] ≤ -1. This shift in comparison to the behavior of [Mg/Fe] (see Figs. 8 and 41) is consistent with the fact that the much higher supernova rate, responsible for Mg (but also e.g. Zn and Ge), leads to a much earlier approach to average values already at metallicities of about [Fe/H] $= -3$.

A further interesting aspect of this analysis is related to the question whether r-process elements are correlated or not correlated with other nucleosynthesis products, in order to determine whether they were co-produced in the same nucleosynthesis site or require a different origin. In

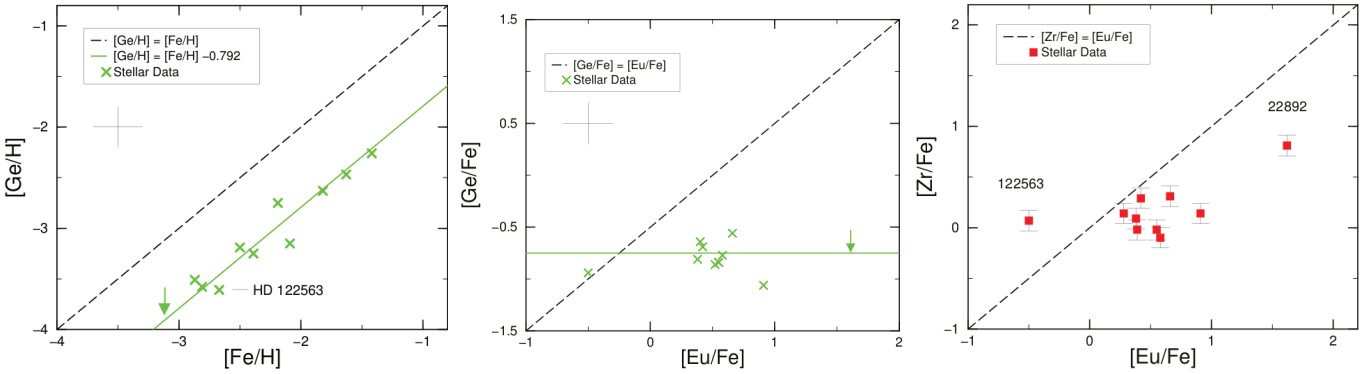

FIG. 43 Left: [Ge/H] vs. [Fe/H] ratios from low metallicity observations. One sees a correlated rise of Ge and Fe, i.e. at these low metallicities (where type Ia supernovae do not yet contribute significantly) this points to a joint origin, where Ge and Fe co-produced, i.e. in core-collapse supernovae. Center: [Ge/Fe] vs. [Eu/Fe]. While Ge/Fe is already almost constant, related to the ratio displayed in the top panel, Eu/Fe shows large variations, due to rare (non-supernova?) events which were contributing in a different way. Right: [Zr/Fe] vs. [Eu/Fe]. One sees a slight/weak correlation, indicating that Zr is partially co-produced with heavy (strong) r-process elements like Eu. However, the very weak correlation points also to a combination of different and joint origins, possibly also a contribution from a weak r process or other nucleosynthetic origin from core-collapse supernovae (Cowan *et al.*, 2005).

Fig. 43 we show the behavior of Ge, Zr, and Eu with respect to Fe. In case of different origins of e.g. Fe, Ni, Zn, and Ge (from regular core-collapse SNe) vs. r-process elements, there should be no correlation between Fe and Eu, as actually observed (Cowan *et al.*, 2005).

Combining these considerations, we come to the following preliminary conclusions for the sites discussed in section VI:

a. Electron-capture supernovae can possibly produce a weak r process, not a strong one, and they are probably not rare, if containing stars from the interval of 8 to 10 $M_\odot$ of the initial mass function.

b. The neutrino-induced processes in He-shells of low-metallicity massive stars (Epstein *et al.*, 1988; Banerjee *et al.*, 2011, 2016) would also be frequent events at low metallicities, and not lead to a large scatter of e.g. [Eu/Fe]. In addition, the related peaks would not be consistent with a strong r process.

c. The regular neutrino-driven core-collapse SNe which produce Fe, but at most a weak r process (e.g. Wanajo *et al.*, 2011; Martínez-Pinedo *et al.*, 2012; Roberts *et al.*, 2012, for an extended set of references see section VI.A.1) are excluded as site of a strong r process, because they do not produce the correct abundance pattern and would also be too frequent, not permitting a large scatter in [Eu/Fe] at low metallicities.

d. Quark deconfinement supernovae could be rare, if existent, but present predictions display not a full strong r process up to the third peak.

e. Magneto-rotational supernovae, leading to magnetars (i.e. neutron stars with magnetic fields of 10^{15} G) rely still on parameter studies and depend on assumptions on rotation rates and magnetic field strengths. Due to these somewhat extreme initial conditions before collapse, they will be rare events, possibly as infrequent as 1 in 100 to 1 in 1000 of regular core-collapse supernovae. This would produce a large [Eu/Fe] scatter and also be consistent with the required total r-process production (see Fig. 42) and abundances pattern, but this site requires observational confirmation.

f. Collapsars, if resulting in events as predicted by Siegel *et al.* (2018), could also be consistent with observations, if they would occur even rarer than magneto-rotoational supernovae by a factor of 100. At a first glance they would contradict the observational finding that r-process sites should not co-produce Fe (see Fig. 43). However, in solar abundances the ratio of Fe/r-process elements is of the order 1000. If collapsars would produce 0.5 $M_\odot$/1 $M_\odot$, this would result in ratios of about 0.5, being off by more than three orders of magnitude. These negligible Fe contributions in comparison to r-process matter with respect to solar would not be visible in a plot like Fig. 43.

g. Compact binary mergers (NS-NS as well as NS-BH mergers) would lead to a similar total ejecta mass and (rare) occurrence frequency as discussed in case (e). Their occurrence and contribution to heavy elements is observationally proven via gravitational wave, (short) GRB, as well as macronova/kilonova observations. Abundance predictions are consistent with overall solar

r-abundances.

Summarizing the sites above, we have (of the sites consistent with the observational constraints of Figs. 42 and 43), as well as the reproduction of a solar r-process pattern, the following ones remaining: (e) magneto-rotational supernovae (magnetars), (f) collapsars, and (g) compact binary mergers. Of these (e) and (f) would belong to massive stars, i.e. occurring during the earliest instances of galactic evolution. (g) is related to the coalescence of compact objects produced via the collapse of massive stars and would possibly experience a delay in their occurrence. Such differences might be recognizable in galactic evolution modeling.

The following subsection will address the question how rare and frequent events can be modeled consistently in galactic chemical evolution. Another aspect is how actually early galactic evolution takes place. There exist indications that (ultra-faint) dwarf galaxies are the earliest building blocks of galactic evolution and their merger will finally lead to the evolution of the early Galaxy as a whole. Due to different gas densities they might experience different star formation rates and due to a low gravitational pull they might lose explosive ejecta more easily. This can have an effect on the point in time (and metallicity) when the first imprints of explosive ejecta can be observed. These features will be addressed as well.

B. Galactic Chemical Evolution Modelling

1. Homogeneous evolution models

Chemical evolution of galaxies has made strong advances since its early days. Initially all approaches made use of the instantaneous recycling approximation in the sense, that the ejecta of stellar end stages were utilized without delay immediately after the corresponding star formation, assuming that the stellar evolution time scale is short in comparison to galactic evolution. If, in addition, the instantaneous mixing approximation was applied, i.e. assuming that the ejecta were instantaneously mixed throughout the galaxy, the whole galaxy acts as homogeneous box. Neglecting this complete mixing throughout the Galaxy can explain radial gradients, but would still assume mixing within large and extended volumes (e.g. radial shells). Further developments included infall of primordial matter into and outflow of enriched material out of the Galaxy (for a review of these early investigations see e.g. Audouze and Tinsley, 1976; Tinsley, 1980). When relaxing the instantaneous recycling approximation, i.e. taking into account that (explosive) stellar ejecta enter the interstellar medium (ISM) delayed with respect to the birth of a star by the duration of its stellar evolution, detailed predictions for the evolution of element abundances can be made. Based on nucleosynthesis predictions for stellar deaths, a number of detailed analyses have been performed, from light elements up to the Fe-group (e.g. Matteucci and Greggio, 1986; Wheeler *et al.*, 1989; Timmes *et al.*, 1995; Matteucci and Chiappini, 2001; Kobayashi *et al.*, 2006; Pagel, 2009; Matteucci, 2012; Nomoto *et al.*, 2013). Such approaches have also been applied to understand the enrichment of heavy elements in the Galaxy (including r-process contributions) as a function of time or metallicity [Fe/H] (see e.g. Travaglio *et al.*, 1999; Ishimaru and Wanajo, 1999; De Donder and Vanbeveren, 2004; Wanajo and Ishimaru, 2006; Matteucci *et al.*, 2014; Ishimaru *et al.*, 2015; Vangioni *et al.*, 2016; Côté *et al.*, 2017; Hotokezaka *et al.*, 2018; Côté *et al.*, 2018a).

The instantaneous mixing approximation (IMA) simplifies a chemical evolution model in terms of mass movement. In detail, all event outputs are expected to cool down and mix with the surrounding ISM instantaneously. Such approaches always result in an average value of element ratios and do not exhibit a spread which can be observed at low metallicities. Thus, the greatest problem of the IMA simplification is: All stars at a given time inherit the same abundance patterns of elements and therefore it is impossible to reproduce a scatter in the galactic abundances, which seems to be a crucial aspect, especially at low metallicities. As a consequence, instead of a spread of abundance distributions, curves with a single value for each [Fe/H] are observed. Utilizing the instantaneous mixing approximation leads thus also to a unique relation between galactic evolution time and metallicity [Fe/H], i.e. any [Fe/H] can be related to a specific time in the evolution of a galaxy and for each [Fe/H], due to the instantaneous mixing, only a mean value of [X/Fe] (X being the element of interest to follow in chemical evolution) is obtained. This (IMA) approach may be used to get a quick overview of the trends in chemical evolution with a considerably lower computational effort for such a model. For a detailed study of especially early chemical evolution, including the reproduction of spreads in abundance ratios due to local inhomogeneities, however, this approach is not sufficient.

2. Inhomogeneous galactic chemical evolution

Local inhomogeneities can only be produced if only limited amounts of ISM are polluted by and mixed with the ejecta of each event. The latter effect is of essential importance especially at low metallicities, where portions of the ISM are already polluted by stellar winds and supernovae, and others are not. Inhomogeneous mixing could produce larger element ratios in strongly polluted areas and smaller values in still less polluted ones. This means that the scatter in [X/Fe] at low metallicities can be a helpful asset in hinting to the origin of element X. Inhomogeneous mixing can experience similar [Fe/H] values in different locations of the Galaxy at different times

or different [Fe/H] values at the same time. In addition, different portions of the ISM are polluted by different types of events, leading to a scatter at the same metallicity, which can in fact be utilized as a constraint for these different stellar ejecta. This is especially the case in the very early galactic evolution ([Fe/H] < -3), when locally (out of a whole intitial mass function, IMF) only a few stars might have exploded and imprinted their stellar neighborhood with their ejecta. Thus, rare events, which produce large amounts of element X in each event, would cause a large scatter, which could be used as a very helpful constraint to identify the production site. Therefore, more advanced chemical evolution studies revoked the instantaneous mixing approximation (e.g. Chiappini *et al.*, 2001; Recchi *et al.*, 2001; Argast *et al.*, 2004; Spitoni *et al.*, 2009; Recchi *et al.*, 2009; van de Voort *et al.*, 2015; Cescutti *et al.*, 2015; Wehmeyer *et al.*, 2015; Shen *et al.*, 2015; Hirai *et al.*, 2015, 2017; Haynes and Kobayashi, 2018). For the reasons summarized above, specially for the origin of r-process elements like Eu, we think that only such inhomogeneous chemical evolution models should be utilized.

While some of the models mentioned here are of a more stochastic nature, Minchev *et al.* (2014) started with truly chemo "dynamical" galactic evolution models. These, as well as e.g. van de Voort *et al.* (2015); Hirai *et al.* (2015); Shen *et al.* (2015); Kobayashi (2016); Hirai *et al.* (2017); Haynes and Kobayashi (2018), are based on SPH simulations. They can model in a self-consistent way massive mergers of galactic subsystems (treated as infall in simpler models), energy feedback from stellar explosions causing outflows (and introduced as such in simpler models), radial migrations in disk galaxies, mixing and diffusion of matter in the ISM, and the initiation of a star formation dependence with progenitor mass. Thus, these global SPH approaches are on the one hand most suitable to model such environments. However, the mass and smoothing length utilized for the SPH particles will also determine the resolution and cause an artificial mixing on such scales which are not neccessarily related to the real mixing mechanisms. These effects go into the direction of the instantaneous mixing approximation on such scales. In reality a 10^{51} erg supernova explosion mixes via a Sedov blast wave only with about 5×10^4 $M_\odot$ of interstellar medium. Although different explosion energies and ejecta geometries are encountered, detailed simulations (Montes *et al.*, 2016) come to similar results for neutron star mergers. SPH particle masses or smoothing lengths can exceed these scales.

Inhomogeneous chem(odynam)ical evolution models for r-process elements, like Eu, have been provided by Argast *et al.* (2004), comparing neutron star mergers and core-collapse supernovae, by Cescutti *et al.* (2015); Wehmeyer *et al.* (2015), comparing MHD jet-SNe and regular core-collapse supernovae, and van de Voort *et al.* (2015); Shen *et al.* (2015); Hirai *et al.* (2015, 2017), only utilizing neutron star mergers. One of the main questions here is related to the problem of reproducing [Eu/Fe] at low(est) metallicities. Wehmeyer *et al.* (2015) treated the galactic chemical evolution of europium (Eu), iron (Fe) and α-elements, like e.g. oxygen (O), still utilizing a more classical stochastic approach with a parametrized infall of primordial matter, and a Schmidt law for star formation. This neglects (large scale turbulent) mixing effects and includes only those introduced by stellar explosions and the so initiated mixing with the surrounding ISM according to a Sedov-Taylor blast wave. However, the model permits inhomogeneities due to a local memory of the addition of stellar ejecta. This stochastic approach grasps the main features of the impact of the first stars and their (explosive) ejecta on the evolution of the heavy element enrichment. Haynes and Kobayashi (2018) did probably perform the most extensive simulations of all these approaches. Ojima *et al.* (2018), on the other hand, utilized a variation of sizes of galactic substructures of the scale of (ultrafaint) dwarf galaxies within an IMA approach, made use of related different star formation rates and different outflows according to their gravity, and added stochastically—within a Monte Carlo scheme—neutron star mergers in these substructures within the range of possible coalescence delay times. The merging of these substructures is expected to represent eventually the early Galaxy as a whole.

One of the major aspects within these approaches for the treatment of compact binary mergers is the connection of earlier supernova events, producing a neutron star and Fe ejecta, with the later delayed merger event and its r-process ejecta. Since explosive events give rise to nucleosynthesis, inside a supernova remnant bubble (given by a Sedov-Taylor blastwave) the abundances of metals are higher than outside such a remnant. A star which is born later *inside* such a remnant will inherit more metals than a star born *outside*. Thus, it is of high importance, *where* a star is born during galactic evolution, especially in the early phases. If the later merger is occurring within the supernova remnant bubble, producing large amounts of r-process matter, the [Fe/H] has been set already by the earlier supernova explosions and the related [Eu/Fe] ratios will appear at the appropriate [Fe/H]. This is the main question with respect to having large Eu contributions already at lowest metallicities. There are ways out of this connection: (a) neutron star kicks during the supernova explosions act in such a way that the actual neutron star mergers takes place outside the initial Fe pollution by the preceding supernovae, (b) neutron star - black hole mergers would have only experienced the Fe-ejecta of one supernova, (c) large scale turbulent mixing leads to the dilution of Fe on timescales shorter than the coalescence delay time of the mergers. Such effects are not (yet) necessarily treated correctly by present models.

C. Connecting observational constraints on r-process abundances with different astrophysical sites

In subsection VIII.A, we listed possible production sites for a strong r process. They need to fulfill the observational constraints: (i) in order to lead to a large scatter of r/Fe at low metallicities these events must be rare in comparison to regular core-collapse supernovae (this does not exclude the latter from being the site for a weak r process), and (ii) if they should be the dominant site responsible for the solar r-abundances, the combination of their ejecta mass and occurrence frequency must be able to match this requirement. Of the listed possible sites (e) magneto-rotational supernovae, (f) collapsars, and (g) compact binary mergers could possibly fulfill both criteria. (g) stays for a rare, observed and confirmed event with the ejecta amounts consistent with reproducing solar abundances. (e) and (f) are possible, still postulated, events. If the required high rotation rates and magnetic fields for magneto-rotational supernovae (leading to magnetars) can exist, they would eject similar amounts of r-process matter as binary mergers, and if they exist in reality they wil be rare. (f) collapsars, also known as hypernovae or observed as lGRBs, have been related to high ^{56}Ni ejecta, but recently also postulated to eject as much as 1 $M_\odot$ of r-process matter (Siegel and Metzger, 2017; Siegel *et al.*, 2018; Janiuk, 2018). In a such case, these events should be very rare, even a factor of 100 rarer than compact binary mergers.

A further requirement, in addition to the two discussed above (rarity and reproducing the total amount of solar r-abundances) is that galactic evolution modeling should reproduce the observed time or metallicity evolution. A number of inhomogeneous chemical evolution studies, which can follow local variations of abundances due to the specific contributions by individual explosions, have implemented this (Argast *et al.*, 2004; van de Voort *et al.*, 2015; Shen *et al.*, 2015; Wehmeyer *et al.*, 2015; Hirai *et al.*, 2015; Mennekens and Vanbeveren, 2016; Hirai *et al.*, 2017; Haynes and Kobayashi, 2018). There exists one difference between (e, f) and (g), in the first case the events result from the final phases of a single massive star, in the latter one or two prior supernovae (producing a neutron star and Fe-ejecta) are required, before—with a delay—(the delay or coalescence timescale) the merger can take place.

Therefore the question arises, whether the scatter of r-process elements like Eu compared to Fe, [Eu/Fe], at low metallicities (which covers more than two orders of magnitude, see Figs. 8 and 41, and hints at production sites with a low event rate) and its time evolution before approaching an average ratio only in the interval $-2 <$ [Fe/H] < -1, can be explained by all scenarios. The delay of approaching an average value in comparison to [Mg/Fe], where this takes place at [Fe/H] < -3, can be due to the much lower rate in comparison to the core-collapse SNe rate, causing the largely different metallicities where the approach to average values takes place. But the question is also whether the early appearance of high [Eu/Fe] values can be consistent with a "delayed" process like compact binary mergers. The supernovae responsible for producing at least one neutron star produce also Fe, which can shift the appearance of a typical r-process element like Eu to higher metallicities [Fe/H] (see Fig. 44). This effect has been discussed in inhomogeneous galactic evolution models utilizing neutron star mergers, i.e. events with two prior supernovae and their Fe-ejecta (Argast *et al.*, 2004; Cescutti *et al.*, 2015; Wehmeyer *et al.*, 2015; Haynes and Kobayashi, 2018). These authors come to the conclusion, also van de Voort *et al.* (2018), that neutron mergers have problems to explain [Eu/Fe] at lowest metallicities, while other inhomogenous models claim to do so (van de Voort *et al.*, 2015; Shen *et al.*, 2015; Hirai *et al.*, 2015; Ramirez-Ruiz *et al.*, 2015; Hirai *et al.*, 2017). This difference is probably related to resolution and mixing issues discussed in the previous subsubsection, which include uncertainties (and also possible solutions), but it should be noted that the high resolution run of van de Voort *et al.* (2015) as well as recent further investigations (van de Voort *et al.*, 2018) indicates the rise of [Eu/Fe] to occur at too high metallicities as well. Whether and how much the use of NS-BH mergers, which explode in an evironment polluted only with Fe by one prior supernova, improve this situation needs to be seen (Wehmeyer *et al.*, 2018). A different issue is the formation of the Galaxy from small substructures like (ultra-faint) dwarf galaxies, which, due to different gas densities, experience different star formation rates and, due to small gravity, the loss of metals from explosive events, both shifting the occurrence of abundance features to lower metallicities. An early simpler IMA approach by Ishimaru *et al.* (2015), recently extended by a stochastic inclusion of neutron star mergers, which are permitted to vary statistically with respect to coalescence time scales (Ojima *et al.*, 2018), seems also to provide a solution.

The previous investigations utilized coalescence delay times for neutron star mergers after the formation of the binary neutron star system with a narrow spread. Population synthesis studies, consistent with the occurrence of short-duration gamma-ray bursts (sGRBs, related to mergers) indicate that the possible delay times follow a distribution with a large spread, ranging over orders of magnitude with a t^{-1} behavior. Based on such a behavior, studies with simpler IMA modeling of chemical evolution (Côté *et al.*, 2017; Hotokezaka *et al.*, 2018; Côté *et al.*, 2018a) come to the conclusion that mergers would not be able to reproduce the early galactic evolution for metallicities [Fe/H] < -2, and not even the downturn at [Fe/H] $= -1$. Thus, problems would remain to explain the strong r process by NS-mergers alone. But the path to the binary merger is a complex one. The mass,

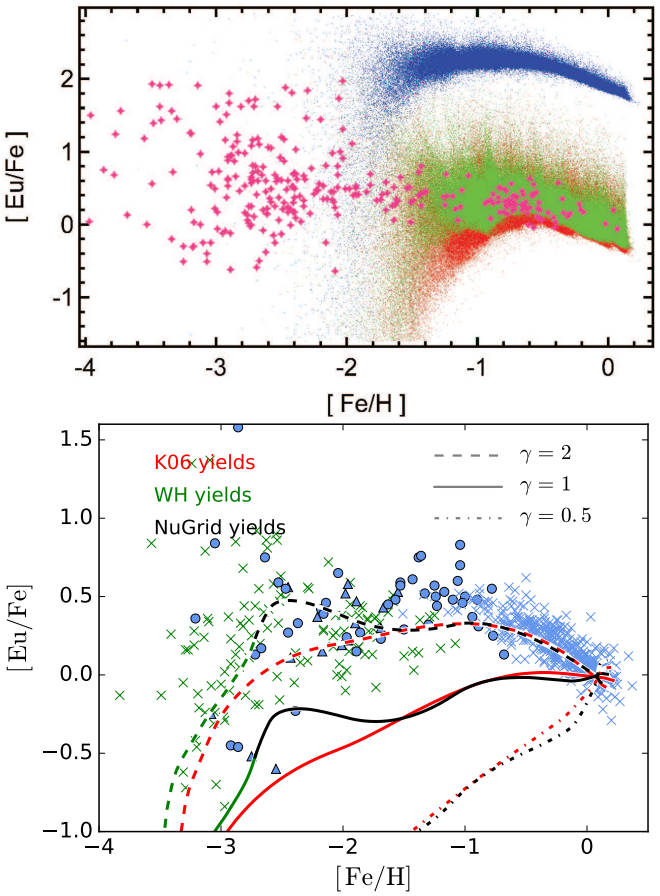

FIG. 44 top: Influence of coalescence timescale and neutron star merger probability on Eu-abundances in inhomogeneous galactic chemical evolution. Magenta stars represent observations. Red dots correspond to model star abundances as in (Argast *et al.*, 2004). The coalescence timescale utilized is 10^8 years with a typical probability consistent with population synthesis (Wehmeyer *et al.*, 2015). Green dots illustrate the effect on the abundances if the coalescence timescale is shorter (around 10^6 years). Blue dots show the abundance change if the probability of neutron star mergers is increased. bottom: results of a simpler galactic evolution approach with IMA by Côté *et al.* (2017) in comparison to observational data (crosses and circles), utilizing a set of supernova yields and delay time distributions for the binary merger following a power law $t^{-\gamma}$ in the range 10^7 to 10^{10} years. Population synthesis studies favor $\gamma = 1$. Within these treatments of galactic chemical evolution, none of the binary compact merger studies would permit a fit with observations of low metallicity stars in the metallicity range $-4 < [\mathrm{Fe/H}] < -2.5$.

ejecta, and explosion energy of the second supernova in a binary system have to be addressed for a full understanding (Müller *et al.*, 2018). This includes the fact that in the binary evolution neutron star kicks from supernova explosions could move the neutron star binary far out of the reach of the initial supernova remnants which polluted the local ISM with Ni and Fe (Fryer and Kalogera, 1997; Kalogera and Fryer, 1999; Abbott *et al.*, 2017b). If in such a way the merger event can be displaced from the original supernovae, Wehmeyer *et al.* (2018) finds that mergers could be made barely consistent with the [Eu/Fe] observations, if such displacement is taken into account and very short coalescence timescales of 10^6 yr are used. In addition, the difference between neutron star mergers and neutron star - black hole mergers, experiencing only the pollution by one prior supernova, has to be investigated (Wehmeyer *et al.*, 2018).

After this still somewhat inconclusive result with respect to the question whether neutron star mergers alone can provide the explanation for a strong r process throughout and also in the early Galaxy, there exist the other options (e and f) related to massive stars which can enter their ejecta immediately at the end of their stellar life and are possibly neglible Fe-producers. Thus, alternatively, a rare class of core-collapse supernovae (or collapsars?) might play a significant role, exploding early in galactic evolution. If producing also a solar r-process pattern, they could be responsible for explaining observations at low metallicities. Early suggestions, that so-called electron-capture supernovae (a) in the stellar mass range 8-10 $M_\odot$ (Kitaura *et al.*, 2006; Janka *et al.*, 2008; Wanajo *et al.*, 2009; Wanajo *et al.*, 2011) would be able to produce a strong r process, were never confirmed. They would also not correspond to rare events. However, other objects driven by strong magnetic fields and fast rotation (possibly about 1% or less of all core-collapse supernovae), leaving behind 10^{15} Gauss neutron stars (magnetars), could be important. Such magneto-rotational (MHD)jet-SNe (e) show similar characteristics in the amount of r-process ejecta and the occurrence frequency as neutron star mergers, but—because these objects result from massive single stars—they do not experience the delay of binary evolution (Winteler *et al.*, 2012; Nishimura *et al.*, 2015b, 2017; Mösta *et al.*, 2018; Halevi and Mösta, 2018). This means that they enter galactic evolution at lowest metallicities, resulting in a large scatter in r/Fe due to them being rare events. This can be seen in Fig. 45, which shows the result of a superposition of magneto-rotational MHD-jet supernovae and neutron star mergers. This way observations can be matched from lowest metallicities up to present. The very recent results by Siegel *et al.* (2018) and also Janiuk (2018) for collapsars (f) would point in the same direction. One aspect which is not clear here, is whether hypernovae, collapsars, lGRBs are a homogeneous class of objects and would all come with huge amounts of ^{56}Ni ejecta. This would in principle be contradictory to the observational findings of Fig. 43, indicating that strong r-process sites are not correlated with Fe-group ejecta, unless the relative overproductions of e.g. Fe vs. Eu with respect to solar abundances is negligible (which would be the case for ^{56}Ni ejecta of 0.5 $M_\odot$ and r-process ejecta of up to 1 $M_\odot$).

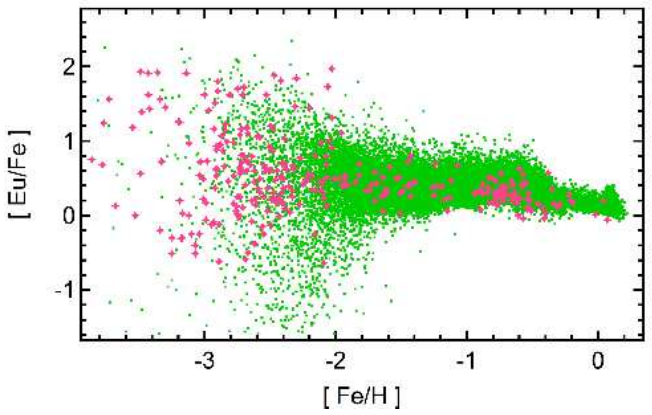

FIG. 45 Evolution of Eu-abundances in galactic chemical evolution models (Wehmeyer *et al.*, 2015) including both magneto-rotational supernovae and neutron star mergers as r-process sites. Magenta stars represent observations whereas green dots represent model stars. The combination of magneto-rotational MHD-jet supernovae - being of strong importance at low metallicities - early in the evolution of the Galaxy, and neutron star mergers permits a perfect fit with observations.

D. r-Process Cosmochronometers

A complete list of isotopes with half-lives in the range $10^7 - 10^{11}$ yr is given in Table II. They cover a time span from a lower limit in excess of the evolution time of massive stars up to (and beyond) the age of the universe. Such nuclei can be utilized as "chronometers" for processes in galactic evolution and also serve as a measure for the age of the galaxy (and thus as a lower limit for the age of the universe, see the earlier discussion in II.D). The list is not long. Two of the nuclei require predictions for the production of the ground and isomeric (^{92}Nb, ^{176}Lu). With the exception of ^{40}K, all of the remaining nuclei are heavier than the "Fe-group" and can only be made via neutron capture.

TABLE II Isotopes with half-lives in the range 10^7-10^{11} yr

Isoptope	Half-Life	Isoptope	Half-Life
^{40}K	1.3×10^9 yr	^{205}Pb	1.5×10^7 yr
^{87}Rb	4.8×10^{10} yr	^{232}Th	1.4×10^{10} yr
^{92}Nb	3.5×10^7 yr	^{235}U	7×10^8 yr
^{129}I	1.6×10^7 yr	^{236}U	2.3×10^7 yr
^{147}Sm	1.1×10^{11} yr	^{238}U	4.5×10^9 yr
^{176}Lu	3.7×10^{10} yr	^{244}Pu	8×10^7 yr
^{187}Re	4.4×10^{10} yr	^{247}Cm	1.6×10^7 yr

The nuclei with half-lives comparable to the age of the Galaxy/Universe, ^{232}Th and ^{238}U, are made in a single nucleosynthesis process (as well as all other actinide isotopes listed here). These elements, the heaviest ones occurring in nature beyond Bi, are all products of the r process. The possible astrophysical settings have been discussed in the previous sections. The question is how to predict reliable production ratios for these long-lived isotopes, if (a) not even the site is completely clear, and (b) even for a given site nuclear uncertainties enter. The abundances of especially these heaviest nuclei produced in the r process depend on mass models, β-decay properties (half-lives, delayed fission, delayed neutron emission), fission barriers and fragment distributions, and last but not least neutron captures, especially their rates during the r-process freeze-out, pointing also to the role direct capture plays in comparison to compound nuclear reactions (see e.g. Goriely and Martínez-Pinedo, 2015; Eichler *et al.*, 2015; Mendoza-Temis *et al.*, 2015, and the general discussion in sections IV and V).

Among the stars with observed Th and U, there exist a number of so-called actinide-boost stars with an enhanced ratio of Th/Eu and U/Eu in comparison to all other r-process enhanced stars (see e.g. Roederer *et al.*, 2009; Holmbeck *et al.*, 2018a), observed especially at low metallicities around [Fe/H] ≈ -3. While most of their element abundances, up to the third r-process peak, are consistent with solar-system r-abundances, the deviations occur essentially only for elements beyond the third r-process peak. This could point to either a different site than the one responsible for the solar-type r-process abundances or variations of conditions in the same site, dependent on still unknown aspects (Holmbeck *et al.*, 2018b).

Nevertheless, for many years such chronometers have been utilzed to attempt predictions for the age of the Galaxy as a lower limit for the age of the Universe (for early reviews see Fowler and Hoyle, 1960; Schramm and Wasserburg, 1970; Cowan *et al.*, 1991). This has been performed initially with simplified chemical evolution models via (i) the prediction of ^{232}Th/^{238}U and ^{235}U/^{238}U ratios in r-process calculations, (ii) applying them in galactic evolution models, which include assumptions about the histories of star formation rates and r-process production, and finally (iii) comparing these ratios with meteoritic data, which provide the Th/U and U/U ratios at the formation of the solar system. In addition for the early reviews on this method, mentioned above, see Panov *et al.* (2017) for recent investigations along these lines. An advantage (somewhat decreasing the nuclear uncertainties involved) is that ^{232}Th and ^{235,238}U are populated by α-decay chains und therefore uncertainties in the predictions of individual isotopes average out to some extent (Goriely and Clerbaux, 1999). Parametrized, so-called site-independent fits, based on a superposition of neutron densities which reproduce all solar r-process abundances from $A = 130$ through the actinides, have been utilized to predict their production ratios (Goriely and Arnould, 2001) (obtained in a sim-

ilar fashion as those in Fig. 15). Goriely and Janka (2016) have used adiabatic and steady-state neutrino-driven wind models and considered the superposition of a large number of contributing components to study the production of cosmochronometers. Alternatively to the ratio of long-lived actinide isotopes, also the ratios of e.g. ^{232}Th and ^{238}U to other (stable) r-process nuclei like Eu can be utilized to check for consistency. Other options include the ratio of Th and U to stable Pb, which has in addition to the s-process contribution (i) a direct r-process contribution to the ^{206,207,208}Pb isotopes (ii) a contribution due to fast α- and β-decay chains from unstable nuclei produced in the r process beyond Pb (decaying within less than 10^6 yr), and finally (iii) a contribution from the long-lived decay chains originating at ^{232}Th and ^{235,238}U (Roederer *et al.*, 2009; Frebel and Kratz, 2009).

Low-metallicity stars have the advantage that one can avoid uncertainties introduced by chemical evolution modeling. The metallicities of the halo stars for which neutron-capture element data have become available range from [Fe/H] = −3 to about −2. Typical, still simple (galactic chemical) evolution calculations suggest roughly the metallicity-age relation [Fe/H] = −1 at 10^9 yr, [Fe/H] = −2 at 10^8 yr, and [Fe/H] = −3 at 10^7 yr (if the instantaneous mixing approximation IMA could be applied at such low metallicities, see, e.g. Tsujimoto *et al.*, 1997; Chiappini *et al.*, 2000). Even if these estimates are uncertain by factors of 2–3, very low metallicity stars most certainly were born when the Galaxy was only 10^7–10^8 yr old, a tiny fraction of its present age. Thus, the neutron-capture elements observed in very low metallicity stars were generated in only one or at most a few prior nucleosynthesis episodes. If several events contributed, the time interval between these events had to be very short in comparison to Th decay ages. Thus, no error is made by simply adding these contributions, without considering decays, and treating them as a single r-process abundance distribution which undergoes decay from the time of its incorporation into a (low metallicity) star until its detection in present observations. Making use of the earlier mentioned, so-called site-independent, predictions for r-process production ratios, combined with the presently observed abundance ratios found in low-metallicity stars, can give an indication for the decay time of its radioactive isotopes since the star was born and polluted with an original r-process pattern. Typical results for ages of most low-metallicity r-process enhanced stars are in the range of 12–14 Gyr (Cowan *et al.*, 1999; Schatz *et al.*, 2002; Kratz *et al.*, 2004; Roederer *et al.*, 2009). This approach assumes that the production ratios of the site(s) responsible for these observations are consistent with those reproducing a solar r process.

Actinide boost stars are observed especially at low metallicities around [Fe/H] ≈ −3 (see Fig. 10 from Holmbeck *et al.*, 2018a). This could point to either a different site than the one responsible for the solar-type r-process abundances or variations of conditions in the same site, dependent on still unknown aspects. An interesting feature, affecting actinide to Eu ratios is related to the path of the r process and the timing when fission plays a role. Due to this the r-process results are dependent on the proton/nucleon ratio Y_e in the expanding matter. Holmbeck *et al.* (2018b) could show, with their nuclear input, that the actinide to Eu ratio is highest for a Y_e in the range 0.15, while lower Y_e's (as expected from the dynamic tidal ejecta of neutron star mergers) lead to smaller actinide to Eu ratios, as found in most r-enhanced stars. The Th/U ratio, reflecting abundances of nuclei relatively close in their mass, seems not that much affected. Present predictions for magneto-rotational supernovae lean more to higher Y_e values close to 0.15. This is still all very speculative and strongly affected by uncertainties in site specific conditions as well as in nuclear properties. However, it is intriguing to check how both types of abundance patterns can be observed in low-metallicity stars. Improved predictions for all the most probable main r-process sites, discussed in the previous section (plus possibly also exotic scenarios Fuller *et al.*, 2017) , can hopefully lead to a one-to-one connection between responsible production sites and observations (although still affected both by astrophysical site as well as nuclear uncertainties).

When applying the same (decay age) procedure to the actinide boost stars as in earlier investigations (Cowan *et al.*, 1999; Schatz *et al.*, 2002; Kratz *et al.*, 2004; Roederer *et al.*, 2009), in order to determine their age by assuming initial production ratios from the so-called site-independent analysis responsible for a solar r-process pattern, unreasonably low or even negative ages result, as can be seen in Fig. 10 on the right scale. Comparable ages in the range 12–14 Gyr are attained only if the higher Th/Eu (and other) production ratios are taken from nucleosynthesis conditions with $Y_e \approx 0.15$ (see Figs. 16 and 17 in Holmbeck *et al.*, 2018b). Similar results are found by Wu *et al.* (2018) and Eichler *et al.* (2018b). This is in line with chemical evolution findings (Wehmeyer *et al.*, 2015; Cescutti *et al.*, 2015; Côté *et al.*, 2017, 2018b; Hotokezaka *et al.*, 2018; Haynes and Kobayashi, 2018) that at low metallicities an additional (early occurring) r-process site is required before neutron star mergers can take over.

IX. SUMMARY AND CONCLUSIONS

Since the postulation of the r process by Burbidge *et al.* (1957) and Cameron (1957) many nuclear experiments and astronomical observations improved tremendously the available input and the constraints for continuous developments and improvements of the underlying theory and models. Here we will pass through the important features and the related present situation in nu-

clear physics, astrophysical modelling, constraints from astronomical observations and the understanding of the (chemical, i.e. abundance) evolution of our Galaxy. With respect to the NUCLEAR PHYSICS, which enters decisively in producing the abundance pattern of the r process, major achievements have been accomplished. This is related to experimental progress in accessing unstable nuclei far from stability, combined with a growing theoretical understanding of their properties. These enter in a number of fundamental ways:

1. *nuclear masses* far from stability and the behavior of shell closures are responsible for the location and the shape of the r-process peaks and subpeaks; close to shell closures the correct prediction of the shell gaps and the on- and offset of deformation plays a major role.

2. *β-decay properties*, like half-lives, are responsible for the speed with which the r process moves matter to heavier nuclei, with an impact (in combination with the path location determined by 1.) on the height of peaks and subpeaks; β-delayed neutron emission (affected by nuclear masses via neutron separation energies) leads, especially in the late phases during decay back to stability, to a smoothing of the abundance curve. In this final phase the energy production by β-decays is also important to understand the electromanetic emission which can be detected in astronomical observations.

3. *α-decays* are also important in the final phase, especially the decay-chains originating from actinide nuclei, powering the light emission detected in astronomical observations and determining the r-process Pb abundance.

4. *fission* enters strongly in the termination of the r process, causing fission-cycling which returns matter to lighter nuclei; the onset of fission (strongest probably near the $N = 184$ shell closure), or possible pathways in the nuclear chart to avoid it, determines the strength of fission cycling, the ratio of actinide to light and medium-mass r-process nuclei, and also the possibility to form superheavy nuclei; fission fragment distributions affect how masses are populated in the vicinity of the $A = 130$ peak, especially also whether substantial fractions can end in nuclei below $A = 130$; the amount of fission-neutrons released during the late phase of the r process, can shape the final abundance pattern.

5. last but not least, *neutron captures* (and their inverse photodisintegrations) are the substantial working horse for the rapid neutron capture process; fortunately, in environments with high neutron densities and temperatures responsible for the process, they occur on such a fast pace that a chemical equilibrium between neutron captures and photodisintegrations is attained, leading to an equilibrium compositon in each isotopic chain with maxima at the same neutron separation energy throughout the nuclear chart; this determines the r-process path and makes the connection to 1.; however, during the final declining phase of neutron densities, the so-called r-process freeze-out, this equilibrium cannot be maintained, and individual neutron captures affect the final abundance shape; here it plays an essential role that direct neutron capture probably wins over compound nucleus prescriptions, as it leads probably to higher reaction rates than predictions based on a compound nucleus picture far from stability; therefore, the above mentioned equilibrium holds probably longer during freeze-out than expected, but predictions and implementation of direct capture for neutron reactions are clearly needed (and presently not fully implemented).

In the investigation of all these aspects much progress has occurred, but major uncertainties are remaining, as experiments have touched nuclei in the r-process path only at a limited number of locations in the nuclear chart. However, the purely nuclear structure aspects are not the only ones to overcome, there exist further nuclear/particle physics, general relativity, magneto-hydrodynamiscs, atomic physics and numerical/computational challenges in MODELLING ASTROPHYSICAL SITES responsible for the production of r-process nuclei:

1. most environments expected to be sites of a strong r process involve objects at highest densities, whether related to core-collapse, compact binary mergers, or the inner areas of black hole accretion disks; the *nuclear and supra-nuclear equation of state* is of highest importance for modelling these sites, providing the pressure response during dynamic phases, the nuclear and particle composition, the existence of electron/positron pairs and their degeneracy, and last but not least determining maximum neutron star masses, which are important e.g. for answering the question whether in compact binary mergers a hypermassive neutron star exists intermittantly or even remains as a final outcome.

2. such dense environments have to be modelled in *general relativistic, high resolution multi-dimensional hydrodynamics* schemes in order to give provide a reliable outcome; this is highly challenging and computationally extremely expensive.

3. many of the discussed effects involve the modeling of *magnetic fields*, possibly as a major ingredient

to predict jet ejection; a decisive aspect is whether and how magnetic fields can be enhanced during these events, where the magneto-rotational instability plays a major role; high resolution magneto-hydrodynamics modeling is a field only at the brink of getting decent results for the modelling of complete astrophysical sites.

4. weak interactions, including electron/positron captures are essential, but at least of similar importance are *neutrino interactions with matter*; the correct treatment of multi-D neutrino transport plays a major role in determining the neutron to nucleon ratio Y_e, which is probably the key ingredient for attaining a successful r process; neutrino flavor transformations, especially via matter-neutrino resonances and fast pairwise flavor conversion, can play an essential role in compact binary mergers, a multi-D treatment for such complicated geometries is just at its infancy.

5. in addition to neutrino transport, general *radiation transport via photons* is important to predict the electromagnetic aftermath of explosions in order to make a connection to observational features like lightcurves and spectra; this involves still unkown opacities of heavy elements, but also the energy release of highly unstable radioactive matter after explosive nucleosynthesis has taken place.

Based on the presently available input for nuclear properties and the present status with respect to modelling POSSIBLE R-PROCESS SITES, three major options for sites of a strong r process have emerged:

1. models of *compact binary mergers* indicate that they are prolific sites of r-process nucleosynthesis, with about 10^{-2} $M_\odot$ of ejected r-process matter in the dynamic ejecta and a similar amount from accretion disk outflows; when including all components—dynamic ejecta, neutrino winds and viscous/secular accretions disk outflows—they produce not only the heaviest r-process nuclei but also significant amounts of the standard solar r-process abundances for mass numbers with $A < 130$; the first observation of a neutron star merger (GW170817), accompanied by the AT 2017gfo macronova/kilonova afterglow, makes this the first proven and confirmed production site of heavy r-process elements; neutron star - black hole mergers are also promising, but need to be confirmed.

2. there exist observational indications of 10^{15} Gauss neutron stars (magnetars); a rare class of *magneto-rotational core-collapse supernovae* could lead to such neutron stars with immense magnetic fields and related models produce r-process matter ejected in polar jets; however, predictions from stellar evolution about the distribution of magnetic fields and rotation rates before core-collapse are needed in order to understand the initial conditions, leading to such events, and investigating the role of the magneto-rotational instability (MRI) during the collapse/explosion phase is impossible without high resolution simulations. Thus, this is a promising site, but needs to be confirmed by observations.

3. very recent multi-D MHD simulation for *accretion disk outflows from collapsars*, i.e. objects which result from massive star evolution and end in the formation of a black hole, argue that large amounts of up to ($\approx$ 1 $M_\odot$) of r-process material can be ejected; further simulations are needed in order to understand whether the whole group of massive stars, leading to hypernovae, collapsars, and long-duration GRBs are a homogeneous class with the predicted outcome and observational confirmations related to the composition of ejecta would be extremely helpful.

4. while the three above mentioned sites are sites (or candidates) for a strong r process, producing heavy elements up to the actinides, there exist further options to produce a so-called *weak r process*, probably also synthesizing elements up to Eu, but with a steeper decline as a function of nuclear mass number than found in the solar system r-abundance pattern; such sites include electron capture supernovae, regular core-collapse supernovae, possibly also quark deconfinement supernovae.

All of these models have to confronted with and scrutinzed by ASTRONOMICAL OBSERVATIONS. An interesting aspect is that one of the listed and confirmed sites is related to binary systems, while the others are resulting from the evolution of massive single stars. Observations supporting and constraining r-process sites exist in a number of ways:

1. the total amount of *r-process matter existing in the solar system* (and the Galaxy) has to be explained together with the overall solar r-abundance pattern (although this could be a superposition of a multitude of events); it turns out that all three possible sites are rare events; if the predicted ejecta masses should be consistent with this requirement, the occurrence frequency of compact binary mergers as well as magneto-rotational supernovae should be between 1 event per 100 to 1000 regular supernovae; for mergers this would be consistent with population synthesis studies; collapsars should be even less frequent by a factor of about 100, which requires future investigations.

2. *radioactive tracers* like ^{244}Pu as well as ^{60}Fe are found in *deep sea sediments*; the production of ^{60}Fe in frequent events, related to regular core-collapse and electron capture supernovae, is supported by the latest contribution dating back about 2 million years; on the contrary, the amount of ^{244}Pu found in these sediments is lower than expected by about a factor of 100, if a quasi-continuous production of r-process elements is assumed; this points to substantial decay since the last addition and to much rarer events than supernovae, underlining the required rarity of events, consistent with all three possible production sites for a strong r process.

3. observations are not only related to explaining the solar abundances, in fact *observations indicate the presence of neutron-capture elements in halo stars at lowest metallicities*; in some cases these detections indicate a complete r-process abundance pattern, in other cases only a partial (or incomplete) r-process pattern is apparent (possibly indicating a weak r process origin), but it appears as though all of the early stars have some level of r-process enrichment; these abundance detections indicate nucleosynthesis early in the history of the Galaxy and provide important clues about the nature of the earliest stars.

4. observations of lowest metallicity stars in our Galaxy and (ultra-faint) dwarf galaxies show substantial variations in r-process elements, indicating a production site with a low event rate and consistent high amounts of r-process ejecta in order to explain solar abundances; this is also underlined by the *large scatter of Eu/Fe* (Eu being an r-process element and Fe stemming from core-collapse supernovae at these low metallicities) *seen in the earliest stars of the Galaxy*; this is explained by a not yet well mixed interstellar medium with respect to the ratio of products from regular core-collapse supernobvae and the rare r-process events.

5. due to the availability of experimental atomic data and high resolution, precision observations, r-process abundance determinations have improved much over time; this permitted also to detect *the presence of long-lived radioactive nuclei like Th and U*, making even a *"dating" of stellar ages* possible; the observed variations in the actinide to intermediate mass r-process elements like Eu, leading to so-called *actinide-boost stars*, concentrated at lowest metallicities, could even give clues about different r-process sites.

While the above observations indicate (a) a rare site for the strong r process, a requirement matched by all three candidates mentioned above, (b) the observations related to the overall evolution of heavy r-process elements in comparision to Fe, and especially its large scatter at low metallicities, require inhomogeneous GALACTIC EVOLUTION simulations, which can reproduce this behavior and might actually point to favored sites:

1. A major open question is: *can products of the neutron star merger r process alone explain the observations* of a large scatter of Eu/Fe and other r-process elements seen already at metallicities of [Fe/H] ≤ -3? As the supernovae which produce the neutron stars of a merger already lead to a substantial floor of Fe, they enhance [Fe/H]. Thus, the high [Eu/Fe] due to the new ejecta would then be seen first at the metallicity [Fe/H] inherited from the prior supernovae, if the merger ejecta are mixed with the same interstellar medium as the prior supernova ejecta. For a typical explosion energy of 10^{51} erg and typical densities of the interstellar medium, this mixing would occur via a Sedov-Taylor blast wave in a range of about 5×10^4 M$_\odot$. Although different energies are encountered in the case of neutron star mergers, recent investigations indicate that they would mix with a similar amount of interstellar medium. Stochastic inhomogeneous chemical evolution calculations, utilizing only this effect alone, show the appearance of Eu only at about [Fe/H] $= -2$ for neutron star mergers. It has to be investigated how this would be affected in the case of neutron star - black hole mergers, as they would only lead to Fe-ejecta by one prior supernova.

2. *Large-scale SPH simulations*, also addressing these issues, can suffer from resolution problems via the choice of the mass of the SPH particles involved as well as smoothing lengths applied. Both of these aspects affect the resolution and lead therefore (artificially) to more extended mixing than applied in case 1. above. Such lower resolution blurrs the metallicity behavior as it implies more extended mixing on the scales of the resolution. This would mix Fe with larger amounts of interstellar medium and thus also causes a lower [Fe/H] when the additional pollution by r-process ejecta takes place. While these resolution issues can be a disadvantage of such simulations, on the other hand they can also handle substantial turbulent mixing of interstellar medium matter in the early Galaxy. Some of these simulations seem to be able to reproduce the r-process behavior of low-metallicity observations with compact binary mergers, but the most recent ones also favor an additional site or source at lowest metallicities.

3. *Neutron star kicks*, resulting from a supernova explosion, could have the binary neutron star system

move out of its supernova remnants (polluted with Fe and Ni), and the merger event could take part in galactic regions unpolluted by Fe from earlier supernovae in the region of the final merger. This could permit the ejection of r-process matter in environments with a lower [Fe/H], also in the case of neutron star mergers. Preliminary simulations with stochastic inhomogeneous models (as in 1.) are able to reproduce observations, if coalescence delay times are as short as 1 Myr.

4. Another option is that early on, in *galactic substructures of the size of dwarf galaxies*, different star formation rates can exist combined with a loss of nucleosynthesis ejecta out of these galaxies due to smaller gravity. This can shift the behavior of the [Eu/Fe] ratio as a function of metallicity [Fe/H] to lower metallicities. When also considering a statistical distribution of (down to small) coalescence timescales in the individual substructures, the low-metallicity observations could possibly be matched, while the merging of these substructures within the early Galaxy at later times can be made consistent with the [Eu/Fe] decline (similar to alpha elements) at [Fe/H] $= -1$.

5. In somewhat simpler galactic evolution models, employing the instantaneous mixing approximation and *coalescence delay time distributions following a* t^{-1} *power law*, as expected from population synthesis studies and statistics of short duration gamma-ray bursts, apparently no model can reproduce the metallicity dependence of the r-process/Fe abundance ratios with neutron star mergers alone.

6. The discussion above underlines, that it is still inconclusive whether binary compact mergers alone can explain low metallicity observations, although they are probably responsible for the dominant amount of r-process products in the solar system and present Galaxy. *When introducing an additional component which acts at lowest metallicities, this yields a perfect fit to observations.* The detection of actinide boost stars, found in particular at metallicities as low as [Fe/H] ≈ -3, supports the argument for such an additional component with different nucleosynthesis conditions being active at such low metallicities.

This review of all aspects of the astrophysical r process, from nuclear physics via stellar (explosive) modeling, astronomical observations, as well as galactic evolution, has shown that substantial progress has been made since it was postulated in the 1950s. But it also shows that, despite the very first observation of an r-process production site (GW170817) in 2017, confirming neutron star mergers as probably the most important site, many open questions remain and further progress on all fronts is required in a truly interdisciplinary effort, in order to answer them.

Existing and upcoming nuclear facilities world-wide (FAIR, FRIB, HIAF, RAON, RIKEN, SPIRAL) will allow to produce neutron-rich nuclei along the r-process path and to determine their properties, including, for the first time, nuclei of the third r-process peak. Relativistic heavy-ion collision experiments envisioned for FAIR, NICA and RHIC will generate and investigate nuclear matter at the temperatures and densities as they exist in neutron-star mergers (and core-collapse supernovae). These exciting experimental prospectives will constrain and guide advances in global nuclear models, and together they will decisively reduce the nuclear uncertainties currently hampering r-process studies.

Observational programs targeting abundances in low-metallicity stars, like RAVE, Gaia, and APOGEE will be incorporated in future surveys such as SDSS V, 4MOST, and WEAVE. This will provide highest quality information about the chemical structure of the Galactic disc, the halo, and the bulge. Multimessenger astronomy with present and future gravitational wave detectors like LIGO, VIRGO, KAGRA, and IndIGO is expected to detect up to 10 compact binary mergers per year, which can be followed up with observations of related gamma-ray bursts and the electromagnetic afterglow. This permits to analyse the outcome of many sources with different viewing angles and will help our further understanding of this unique site, producing the heaviest elements in the Universe.

And finally, the advent of improved theoretical models of the nuclear equation of state, nuclei far from stability, stellar atmospheres, stellar evolution, stellar explosions, and state-of-the-art chemo-dynamical models of the Galaxy, plus by chance observational evidence for an additional (of the discussed or unexpected) r-process site, will hopefully point us to a clear understanding of the origin of the heavy elements from Fe to U.

In summary, we are living in exciting times for unravelling the mysteries of r-process nucleosynthesis.

ACKNOWLEDGMENTS

We thank a very large number of colleagues and friends for helpful collaborations and discussions, but especially Al Cameron and Willy Fowler should be mentioned here who motivated many of us to explore the topic of this review. This research was supported in part by: NASA grant HST-GO-14232 (JJC), NSF grant AST1616040 (CS), NASA grant NNX16AE96G and NSF grant AST-1516182 (JEL), NSF grant Phys-0758100 and the Joint Institute for Nuclear Astrophysics through NSF Grant Phys-0822648 (AA and MW), NSF award PHY-1430152 (JINA Center for the Evolution of the Elements AA,

JJC, and MW), the Extreme Matter Institute EMMI (KL and GMP), the Deutsche Forschungsgemeinschaft (DFG, German Research Foundation) - Projektnummer 279384907 - SFB 1245 (GMP), the Swiss SNF, an ERC Advanced Grant (FISH) and COST Actions NewCompstar (FKT) and ChETEC (FKT and GMP).

REFERENCES

Abbott, B. P., *et al.* (LIGO Scientific Collaboration and Virgo Collaboration) (2017a), Astrophys. J. Lett. **850**, L39.
Abbott, B. P., *et al.* (LIGO Scientific Collaboration and Virgo Collaboration, Fermi Gamma-ray Burst Monitor, INTEGRAL) (2017b), Astrophys. J. Lett. **848**, L13.
Abbott, B. P., *et al.* (LIGO Scientific Collaboration and Virgo Collaboration) (2017), Phys. Rev. Lett. **119**, 161101.
Abbott, B. P., *et al.* (2017a), Astrophys. J. Lett. **848**, L12.
Abbott, B. P., *et al.* (LIGO Scientific Collaboration and Virgo Collaboration) (2017b), Astrophys. J. Lett. **850**, L40.
Abbott, B. P., *et al.* (The LIGO Scientific Collaboration and the Virgo Collaboration) (2018), Phys. Rev. Lett. **121**, 161101.
Abbott, B. P., *et al.* (LIGO Scientific Collaboration and Virgo Collaboration) (2018), ArXiv e-prints arXiv:1805.11579 [gr-qc].
Aboussir, Y., J. M. Pearson, A. K. Dutta, and F. Tondeur (1995), At. Data Nucl. Data Tables **61**, 127.
Adrich, P., A. Klimkiewicz, M. Fallot, K. Boretzky, T. Aumann, D. Cortina-Gil, U. D. Pramanik, T. W. Elze, H. Emling, H. Geissel, M. Hellström, K. L. Jones, J. V. Kratz, R. Kulessa, Y. Leifels, C. Nociforo, R. Palit, H. Simon, G. Surówka, K. Sümmerer, and W. Waluś (LAND-FRS Collaboration) (2005), Phys. Rev. Lett. **95**, 132501.
Agramunt, J., J. L. Tain, M. B. Gómez-Hornillos, A. R. Garcia, F. Albiol, A. Algora, R. Caballero-Folch, F. Calviño, D. Cano-Ott, G. Cortés, C. Domingo-Pardo, T. Eronen, W. Gelletly, D. Gorelov, V. Gorlychev, H. Hakala, A. Jokinen, M. D. Jordan, A. Kankainen, V. Kolhinen, L. Kucuk, T. Martinez, P. J. R. Mason, I. Moore, H. Penttilä, Z. Podolyák, C. Pretel, M. Reponen, A. Riego, J. Rissanen, B. Rubio, A. Saastamoinen, A. Tarifeño-Saldivia, and E. Valencia (2016), Nuclear Instruments and Methods in Physics Research A **807**, 69.
Alhassid, Y., G. F. Bertsch, S. Liu, and H. Nakada (2000), Phys. Rev. Lett. **84**, 4313.
Alhassid, Y., S. Liu, and H. Nakada (1999), Phys. Rev. Lett. **83**, 4265.
Alhassid, Y., S. Liu, and H. Nakada (2007), Phys. Rev. Lett. **99** (16), 162504.
Anderson, M., E. W. Hirschmann, L. Lehner, S. L. Liebling, P. M. Motl, D. Neilsen, C. Palenzuela, and J. E. Tohline (2008), Phys. Rev. Lett. **100**, 191101.
Annala, E., T. Gorda, A. Kurkela, and A. Vuorinen (2018), Phys. Rev. Lett. **120**, 172703.
Antoniadis, J., P. C. C. Freire, N. Wex, T. M. Tauris, R. S. Lynch, M. H. van Kerkwijk, M. Kramer, C. Bassa, V. S. Dhillon, T. Driebe, J. W. T. Hessels, V. M. Kaspi, V. I. Kondratiev, N. Langer, T. R. Marsh, M. A. McLaughlin, T. T. Pennucci, S. M. Ransom, I. H. Stairs, J. van Leeuwen, J. P. W. Verbiest, and D. G. Whelan (2013), Science **340**, 1233232.
Aoki, M., Y. Ishimaru, W. Aoki, and S. Wanajo (2017), Astrophys. J. **837**, 8.
Aoki, W., T. C. Beers, Y. S. Lee, S. Honda, H. Ito, M. Takada-Hidai, A. Frebel, T. Suda, M. Y. Fujimoto, D. Carollo, and T. Sivarani (2013), Astron. J. **145**, 13.
Arcavi, I., G. Hosseinzadeh, D. A. Howell, C. McCully, D. Poznanski, D. Kasen, J. Barnes, M. Zaltzman, S. Vasylyev, D. Maoz, and S. Valenti (2017), Nature **551**, 64, arXiv:1710.05843 [astro-ph.HE].
Arcones, A., and H.-T. Janka (2011), Astron. & Astrophys. **526**, A160.
Arcones, A., H.-T. Janka, and L. Scheck (2007), Astron. & Astrophys. **467**, 1227.
Arcones, A., and G. Martínez-Pinedo (2011), Phys. Rev. C **83** (4), 045809.
Arcones, A., G. Martínez-Pinedo, L. F. Roberts, and S. E. Woosley (2010), Astron. & Astrophys. **522**, A25.
Arcones, A., and F. Montes (2011), Astrophys. J. **731**, 5.
Arcones, A., and F.-K. Thielemann (2013), J. Phys. G: Nucl. Part. Phys. **40**, 013201.
Ardevol-Pulpillo, R., H. T. Janka, O. Just, and A. Bauswein (2018), arXiv e-prints , arXiv:1808.00006arXiv:1808.00006 [astro-ph.HE].
Argast, D., M. Samland, F.-K. Thielemann, and Y.-Z. Qian (2004), Astron. & Astrophys. **416**, 997.
Arlandini, C., F. Käppeler, K. Wisshak, R. Gallino, M. Lugaro, M. Busso, and O. Straniero (1999), Astrophys. J. **525**, 886, astro-ph/9906266.
Armbruster, P., M. Asghar, J. P. Bocquet, R. Decker, H. Ewald, J. Greif, E. Moll, B. Pfeiffer, H. Schrader, F. Schussler, G. Siegert, and H. Wollnik (1976), Nuclear Instruments and Methods **139**, 213.
Arnett, W. D. (1980), Astrophys. J. **237**, 541.
Arnett, W. D. (1982), Astrophys. J. **253**, 785.
Arnould, M., and S. Goriely (2003), Phys. Rep. **384**, 1.
Arnould, M., S. Goriely, and K. Takahashi (2007), Phys. Rep. **450**, 97.
Arzhanov, A. (2017), *Microscopic nuclear mass model for r-process nucleosynthesis*, Ph.D. thesis (Technische Universität Darmstadt).
Asplund, M., N. Grevesse, A. J. Sauval, and P. Scott (2009), Annu. Rev. Astron. Astrophys. **47**, 481.
Atanasov, D., P. Ascher, K. Blaum, R. B. Cakirli, T. E. Cocolios, S. George, S. Goriely, F. Herfurth, H.-T. Janka, O. Just, M. Kowalska, S. Kreim, D. Kisler, Y. A. Litvinov, D. Lunney, V. Manea, D. Neidherr, M. Rosenbusch, L. Schweikhard, A. Welker, F. Wienholtz, R. N. Wolf, and K. Zuber (2015), Phys. Rev. Lett. **115** (23), 232501.
Audi, G., F. Kondev, M. Wang, B. Pfeiffer, X. Sun, J. Blachot, and M. MacCormick (2012), Chinese Phys. C **36**, 1157.
Audi, G., A. Wapstra, and C. Thibault (2003), Nucl. Phys. A **729**, 337.
Audouze, J., and B. M. Tinsley (1976), Annu. Rev. Astron. Astrophys. **14**, 43.
Avrigeanu, M., and V. Avrigeanu (2016), in *Journal of Physics Conference Series*, Journal of Physics Conference Series, Vol. 724, p. 012003.
Avrigeanu, V., and M. Avrigeanu (2015), Phys. Rev. C **91** (6), 064611.
Avrigeanu, V., M. Avrigeanu, and C. Mănăilescu (2014), Phys. Rev. C **90** (4), 044612.
Baade, W., and F. Zwicky (1934), Physical Review **46**, 76.
Baiotti, L., and L. Rezzolla (2017), Rep. Prog. Phys. **80**,

096901.
Baldo, M., and G. Burgio (2016), Prog. Part. Nucl. Phys. **91**, 203.
Banerjee, P., W. C. Haxton, and Y.-Z. Qian (2011), Phys. Rev. Lett. **106** (20), 201104, arXiv:1103.1193 [astro-ph.SR].
Banerjee, P., Y.-Z. Qian, A. Heger, and W. Haxton (2016), in *European Physical Journal Web of Conferences*, European Physical Journal Web of Conferences, Vol. 109, p. 06001, arXiv:1512.01523 [astro-ph.SR].
Barklem, P. S., N. Christlieb, T. C. Beers, V. Hill, M. S. Bessell, J. Holmberg, B. Marsteller, S. Rossi, F.-J. Zickgraf, and D. Reimers (2005), Astron. & Astrophys. **439**, 129.
Barnes, J., and D. Kasen (2013), Astrophys. J. **775**, 18.
Barnes, J., D. Kasen, M.-R. Wu, and G. Martínez-Pinedo (2016), Astrophys. J. **829**, 110, arXiv:1605.07218 [astro-ph.HE].
Battistini, C., and T. Bensby (2016), Astron. & Astrophys. **586**, A49, arXiv:1511.00966 [astro-ph.SR].
Bauge, E., J. P. Delaroche, and M. Girod (2001), Phys. Rev. C **63** (2), 024607.
Baumgarte, T. W., S. L. Shapiro, and M. Shibata (2000), Astrophys. J. Lett. **528**, L29.
Bauswein, A., T. W. Baumgarte, and H.-T. Janka (2013), Phys. Rev. Lett. **111**, 131101.
Bauswein, A., S. Goriely, and H.-T. Janka (2013), Astrophys. J. **773**, 78.
Bauswein, A., and H.-T. Janka (2012), Phys. Rev. Lett. **108**, 011101.
Bauswein, A., O. Just, H.-T. Janka, and N. Stergioulas (2017), Astrophys. J. Lett. **850**, L34.
Bauswein, A., and N. Stergioulas (2017), Mon. Not. Roy. Astron. Soc. **471**, 4956.
Bauswein, A., N. Stergioulas, and H.-T. Janka (2016), Eur. Phys. J. A **52**, 56.
Beard, M., E. Uberseder, R. Crowter, and M. Wiescher (2014), Phys. Rev. C **90** (3), 034619.
Beers, T. C., and N. Christlieb (2005), Annu. Rev. Astron. Astrophys. **43**, 531.
Belczynski, K., M. Dominik, T. Bulik, R. O'Shaughnessy, C. Fryer, and D. E. Holz (2010), Astrophys. J. Lett. **715**, L138.
Belczynski, K., R. O'Shaughnessy, V. Kalogera, F. Rasio, R. E. Taam, and T. Bulik (2008), Astrophys. J. **680**, L129.
Beloborodov, A. M. (2003), Astrophys. J. **588**, 931, astro-ph/0210522.
Beloborodov, A. M. (2008), in *American Institute of Physics Conference Series*, American Institute of Physics Conference Series, Vol. 1054, edited by M. Axelsson, pp. 51–70, arXiv:0810.2690.
Bengtsson, R., and W. M. Howard (1975), Physics Letters B **55**, 281.
Bensby, T., S. Feltzing, and M. S. Oey (2014), Astron. & Astrophys. **562**, A71, arXiv:1309.2631.
Bersten, M. C., and P. A. Mazzali (2017), "Light Curves of Type I Supernovae," in *Handbook of Supernovae*, edited by A. W. Alsabti and P. Murdin (Springer International Publishing, Cham).
Bethe, H. A. (1990), Rev. Mod. Phys. **62**, 801.
Bisterzo, S., R. Gallino, F. Käppeler, M. Wiescher, G. Imbriani, O. Straniero, S. Cristallo, J. Görres, and R. J. deBoer (2015), Mon. Not. Roy. Astron. Soc. **449**, 506, arXiv:1507.06798 [astro-ph.SR].
Bisterzo, S., C. Travaglio, M. Wiescher, F. Käppeler, and R. Gallino (2017), Astrophys. J. **835**, 97, arXiv:1701.01056 [astro-ph.SR].
Blake, J. B., and D. N. Schramm (1976), Astrophys. J. **209**, 846.
Blaum, K. (2006), Phys. Repts. **425**, 1.
Blaum, K., J. Dilling, and W. Nörtershäuser (2013), Physica Scripta Volume T **152** (1), 014017, arXiv:1210.4045 [physics.atom-ph].
Bohle, D., A. Richter, W. Steffen, A. E. L. Dieperink, N. Lo Iudice, F. Palumbo, and O. Scholten (1984), Phys. Lett. B **137**, 27.
Bollig, R., H.-T. Janka, A. Lohs, G. Martínez-Pinedo, C. J. Horowitz, and T. Melson (2017), Phys. Rev. Lett. **119**, 242702.
Borzov, I., and S. Goriely (2000), Phys. Rev. C **62**, 035501.
Borzov, I. N. (2003), Phys. Rev. C **67**, 025802.
Borzov, I. N., J. J. Cuenca-García, K. Langanke, G. Martínez-Pinedo, and F. Montes (2008), Nucl. Phys. A **814**, 159.
Bovard, L., D. Martin, F. Guercilena, A. Arcones, L. Rezzolla, and O. Korobkin (2017), Phys. Rev. D **96**, 124005.
Boyd, R. N., M. A. Famiano, B. S. Meyer, Y. Motizuki, T. Kajino, and I. U. Roederer (2012), Astrophys. J. **744**, L14, arXiv:1111.3985 [astro-ph.SR].
Brault, J. W. (1976), Journal of the Optical Society of America (1917-1983) **66**, 1081.
Brege, W., M. D. Duez, F. Foucart, M. B. Deaton, J. Caro, D. A. Hemberger, L. E. Kidder, E. O'Connor, H. P. Pfeiffer, and M. A. Scheel (2018), Phys. Rev. D **98**, 063009.
Brink, D. M. (1955), Ph.D. thesis (Oxford University).
Brink, D. M. (1957), Nucl. Phys. A **4**, 215.
Brown, B. A., and A. C. Larsen (2014), Phys. Rev. Lett. **113** (25), 252502, arXiv:1409.3492 [nucl-th].
Bruske, C., K. H. Burkard, W. Hüller, R. Kirchner, O. Klepper, and E. Roeckl (1981), Nuclear Instruments and Methods in Physics Research **186**, 61.
Burbidge, E. M., G. R. Burbidge, W. A. Fowler, and F. Hoyle (1957), Rev. Mod. Phys. **29**, 547.
Burbidge, G. R., F. Hoyle, E. M. Burbidge, R. F. Christy, and W. A. Fowler (1956), Phys. Rev. **103**, 1145.
Burris, D. L., C. A. Pilachowski, T. E. Armandroff, C. Sneden, J. J. Cowan, and H. Roe (2000), Astrophys. J. **544**, 302.
Burrows, A. (2013), Rev. Mod. Phys. **85**, 245.
Burrows, A., D. Vartanyan, J. C. Dolence, M. A. Skinner, and D. Radice (2018), ssr **214**, 33, arXiv:1611.05859 [astro-ph.SR].
Busso, M., R. Gallino, and G. J. Wasserburg (1999), Annu. Rev. Astron. Astrophys. **37**, 239.
Caballero, O. L., A. Arcones, I. N. Borzov, K. Langanke, and G. Martinez-Pinedo (2014), ArXiv e-prints arXiv:1405.0210 [nucl-th].
Caballero-Folch, R., C. Domingo-Pardo, J. Agramunt, A. Algora, F. Ameil, A. Arcones, Y. Ayyad, J. Benlliure, I. N. Borzov, M. Bowry, F. Calviño, D. Cano-Ott, G. Cortés, T. Davinson, I. Dillmann, A. Estrade, A. Evdokimov, T. Faestermann, F. Farinon, D. Galaviz, A. R. García, H. Geissel, W. Gelletly, R. Gernhäuser, M. B. Gómez-Hornillos, C. Guerrero, M. Heil, C. Hinke, R. Knöbel, I. Kojouharov, J. Kurcewicz, N. Kurz, Y. A. Litvinov, L. Maier, J. Marganiec, T. Marketin, M. Marta, T. Martínez, G. Martínez-Pinedo, F. Montes, I. Mukha, D. R. Napoli, C. Nociforo, C. Paradela, S. Pietri, Z. Podolyák, A. Prochazka, S. Rice, A. Riego, B. Rubio, H. Schaffner, C. Scheidenberger, K. Smith, E. Sokol, K. Steiger, B. Sun, J. L.

Taín, M. Takechi, D. Testov, H. Weick, E. Wilson, J. S. Winfield, R. Wood, P. Woods, and A. Yeremin (2016), Phys. Rev. Lett. **117**, 012501.
Cabezón, R. M., K.-C. Pan, M. Liebendörfer, T. Kuroda, K. Ebinger, O. Heinimann, F.-K. Thielemann, and A. Perego (2018), ArXiv e-prints arXiv:1806.09184 [astro-ph.HE].
Calvino, F., *et al.* (2014), *TDR BEta-deLayEd Neutron detector*, Tech. Rep. (FAIR).
Cameron, A. G. W. (1957), *Stellar Evolution, Nuclear Astrophysics, and Nucleogenesis*, Report CRL-41 (Chalk River).
Cameron, A. G. W. (1959), Astrophys. J. **129**, 676.
Cameron, A. G. W. (2003), Astrophys. J. **587**, 327.
Cameron, A. G. W., J. J. Cowan, and J. W. Truran (1983), Astrophys. Space Sci. **91**, 235.
Caurier, E., K. Langanke, G. Martínez-Pinedo, and F. Nowacki (1999), Nucl. Phys. A **653**, 439.
Caurier, E., G. Martínez-Pinedo, F. Nowacki, A. Poves, and A. P. Zuker (2005), Rev. Mod. Phys. **77**, 427.
Cayrel, R., E. Depagne, M. Spite, V. Hill, F. Spite, P. François, B. Plez, T. Beers, F. Primas, J. Andersen, B. Barbuy, P. Bonifacio, P. Molaro, and B. Nordström (2004), Astron. & Astrophys. **416**, 1117, astro-ph/0311082.
Cayrel, R., V. Hill, T. C. Beers, B. Barbuy, M. Spite, F. Spite, B. Plez, J. Andersen, P. Bonifacio, P. François, P. Molaro, B. Nordström, and F. Primas (2001), Nature **409**, 691, astro-ph/0104357.
Cescutti, G., D. Romano, F. Matteucci, C. Chiappini, and R. Hirschi (2015), Astron. & Astrophys. **577**, A139, arXiv:1503.02954.
Chawla, S., M. Anderson, M. Besselman, L. Lehner, S. L. Liebling, P. M. Motl, and D. Neilsen (2010), Phys. Rev. Lett. **105**, 111101.
Chen, B., J. Dobaczewski, K.-L. Kratz, K. Langanke, B. Pfeiffer, F.-K. Thielemann, and P. Vogel (1995), Phys. Lett. B **355**, 37.
Chiappini, C., F. Matteucci, and P. Padoan (2000), Astrophys. J. **528**, 711, arXiv:astro-ph/9908207.
Chiappini, C., F. Matteucci, and D. Romano (2001), Astrophys. J. **554**, 1044, arXiv:astro-ph/0102134.
Chornock, R., E. Berger, D. Kasen, P. S. Cowperthwaite, M. Nicholl, V. A. Villar, K. D. Alexander, P. K. Blanchard, T. Eftekhari, W. Fong, R. Margutti, P. K. G. Williams, J. Annis, D. Brout, D. A. Brown, H.-Y. Chen, M. R. Drout, B. Farr, R. J. Foley, J. A. Frieman, C. L. Fryer, K. Herner, D. E. Holz, R. Kessler, T. Matheson, B. D. Metzger, E. Quataert, A. Rest, M. Sako, D. M. Scolnic, N. Smith, and M. Soares-Santos (2017), Astrophys. J. Lett. **848**, L19.
Cizewski, J. A., A. Ratkiewicz, J. E. Escher, A. Lepailleur, S. D. Pain, and G. Potel (2018), in *European Physical Journal Web of Conferences*, European Physical Journal Web of Conferences, Vol. 165, p. 01013.
Clayton, D. D. (1968), *Principles of stellar evolution and nucleosynthesis* (New York: McGraw-Hill, 1968).
Cohen, J. G., N. Christlieb, A. McWilliam, S. Shectman, I. Thompson, G. J. Wasserburg, I. Ivans, M. Dehn, T. Karlsson, and J. Melendez (2004), Astrophys. J. **612**, 1107, astro-ph/0405286.
Cole, A. L., T. S. Anderson, R. G. T. Zegers, S. M. Austin, B. A. Brown, L. Valdez, S. Gupta, G. W. Hitt, and O. Fawwaz (2012), Phys. Rev. C **86**, 015809.
Côté, B., K. Belczynski, C. L. Fryer, C. Ritter, A. Paul, B. Wehmeyer, and B. W. O'Shea (2017), Astrophys. J. **836**, 230, arXiv:1610.02405.
Côté, B., M. Eichler, A. Arcones, C. J. Hansen, P. Simonetti, A. Frebel, C. L. Fryer, M. Pignatari, M. Reichert, K. Belczynski, and F. Matteucci (2018a), ArXiv e-prints arXiv:1809.03525 [astro-ph.HE].
Côté, B., C. L. Fryer, K. Belczynski, O. Korobkin, M. Chruślińska, N. Vassh, M. R. Mumpower, J. Lippuner, T. M. Sprouse, R. Surman, and R. Wollaeger (2018b), Astrophys. J. **855**, 99.
Coughlin, M. W., T. Dietrich, B. Margalit, and B. D. Metzger (2018), arXiv e-prints arXiv:1812.04803 [astro-ph.HE].
Coulter, D. A., R. J. Foley, C. D. Kilpatrick, M. R. Drout, A. L. Piro, B. J. Shappee, M. R. Siebert, J. D. Simon, N. Ulloa, D. Kasen, B. F. Madore, A. Murguia-Berthier, Y.-C. Pan, J. X. Prochaska, E. Ramirez-Ruiz, A. Rest, and C. Rojas-Bravo (2017), Science **358**, 1556, arXiv:1710.05452 [astro-ph.HE].
Council, N. R. (2003), *Connecting Quarks with the Cosmos: Eleven Science Questions for the New Century* (The National Academies Press, Washington, DC).
Cowan, J. J., A. G. W. Cameron, and J. W. Truran (1980), Astrophys. J. **241**, 1090.
Cowan, J. J., A. G. W. Cameron, and J. W. Truran (1983), Astrophys. J. **265**, 429.
Cowan, J. J., A. G. W. Cameron, and J. W. Truran (1985), Astrophys. J. **294**, 656.
Cowan, J. J., B. Pfeiffer, K.-L. Kratz, F.-K. Thielemann, C. Sneden, S. Burles, D. Tytler, and T. C. Beers (1999), Astrophys. J. **521**, 194.
Cowan, J. J., and W. K. Rose (1977), Astrophys. J. **212**, 149.
Cowan, J. J., C. Sneden, T. C. Beers, J. E. Lawler, J. Simmerer, J. W. Truran, F. Primas, J. Collier, and S. Burles (2005), Astrophys. J. **627**, 238.
Cowan, J. J., C. Sneden, S. Burles, I. I. Ivans, T. C. Beers, J. W. Truran, J. E. Lawler, F. Primas, G. M. Fuller, B. Pfeiffer, and K.-L. Kratz (2002), Astrophys. J. **572**, 861, astro-ph/0202429.
Cowan, J. J., and F.-K. Thielemann (2004), Physics Today **57**, 47.
Cowan, J. J., F.-K. Thielemann, and J. W. Truran (1991), Phys. Rep. **208**, 267.
Cowperthwaite, P. S., E. Berger, V. A. Villar, B. D. Metzger, M. Nicholl, R. Chornock, P. K. Blanchard, W. Fong, R. Margutti, M. Soares-Santos, K. D. Alexander, S. Allam, J. Annis, D. Brout, D. A. Brown, R. E. Butler, H.-Y. Chen, H. T. Diehl, Z. Doctor, M. R. Drout, T. Eftekhari, B. Farr, D. A. Finley, R. J. Foley, J. A. Frieman, C. L. Fryer, J. García-Bellido, M. S. S. Gill, J. Guillochon, K. Herner, D. E. Holz, D. Kasen, R. Kessler, J. Marriner, T. Matheson, E. H. Neilsen, Jr., E. Quataert, A. Palmese, A. Rest, M. Sako, D. M. Scolnic, N. Smith, D. L. Tucker, P. K. G. Williams, E. Balbinot, J. L. Carlin, E. R. Cook, F. Durret, T. S. Li, P. A. A. Lopes, A. C. C. Lourenço, J. L. Marshall, G. E. Medina, J. Muir, R. R. Muñoz, M. Sauseda, D. J. Schlegel, L. F. Secco, A. K. Vivas, W. Wester, A. Zenteno, Y. Zhang, T. M. C. Abbott, M. Banerji, K. Bechtol, A. Benoit-Lévy, E. Bertin, E. Buckley-Geer, D. L. Burke, D. Capozzi, A. Carnero Rosell, M. Carrasco Kind, F. J. Castander, M. Crocce, C. E. Cunha, C. B. D'Andrea, L. N. da Costa, C. Davis, D. L. DePoy, S. Desai, J. P. Dietrich, A. Drlica-Wagner, T. F. Eifler, A. E. Evrard, E. Fernandez, B. Flaugher, P. Fosalba, E. Gaztanaga, D. W. Gerdes, T. Giannantonio, D. A. Goldstein, D. Gruen, R. A. Gru-

endl, G. Gutierrez, K. Honscheid, B. Jain, D. J. James, T. Jeltema, M. W. G. Johnson, M. D. Johnson, S. Kent, E. Krause, R. Kron, K. Kuehn, N. Nuropatkin, O. Lahav, M. Lima, H. Lin, M. A. G. Maia, M. March, P. Martini, R. G. McMahon, F. Menanteau, C. J. Miller, R. Miquel, J. J. Mohr, E. Neilsen, R. C. Nichol, R. L. C. Ogando, A. A. Plazas, N. Roe, A. K. Romer, A. Roodman, E. S. Rykoff, E. Sanchez, V. Scarpine, R. Schindler, M. Schubnell, I. Sevilla-Noarbe, M. Smith, R. C. Smith, F. Sobreira, E. Suchyta, M. E. C. Swanson, G. Tarle, D. Thomas, R. C. Thomas, M. A. Troxel, V. Vikram, A. R. Walker, R. H. Wechsler, J. Weller, B. Yanny, and J. Zuntz (2017), Astrophys. J. Lett. **848**, L17.

Crease, R. P., and R. W. Seidel (2000), Physics Today **53** (1), 55.

Curtis, S., K. Ebinger, C. Fröhlich, M. Hempel, A. Perego, M. Liebendörfer, and F.-K. Thielemann (2018), ArXiv e-prints arXiv:1805.00498 [astro-ph.SR].

Cyburt, R. H., B. D. Fields, K. A. Olive, and T.-H. Yeh (2016), Rev. Mod. Phys. **88** (1), 015004, arXiv:1505.01076.

Davies, M. B., W. Benz, T. Piran, and F. K. Thielemann (1994), Astrophys. J. **431**, 742, astro-ph/9401032.

Davis, A. M., and K. D. McKeegan (2014), "Short-Lived Radionuclides and Early Solar System Chronology," in *Meteorites and Cosmochemical Processes*, edited by A. M. Davis, pp. 361–395.

De, S., D. Finstad, J. M. Lattimer, D. A. Brown, E. Berger, and C. M. Biwer (2018), Phys. Rev. Lett. **121**, 091102.

De Donder, E., and D. Vanbeveren (2004), New Astron. **9**, 1.

Demetriou, P., C. Grama, and S. Goriely (2002), Nucl. Phys. A **707**, 253.

Demetriou, P., C. Grama, and S. Goriely (2003), Nucl. Phys. A **718**, 510.

Demorest, P. B., T. Pennucci, S. M. Ransom, M. S. E. Roberts, and J. W. T. Hessels (2010), Nature **467**, 1081, arXiv:1010.5788v1.

Den Hartog, E. A., M. E. Wickliffe, and J. E. Lawler (2002), Astrophys. J. Suppl. **141**, 255.

Denissenkov, P. A., F. Herwig, U. Battino, C. Ritter, M. Pignatari, S. Jones, and B. Paxton (2017), Astrophys. J. **834**, L10, arXiv:1610.08541 [astro-ph.SR].

Desai, D., B. D. Metzger, and F. Foucart (2018), arXiv e-prints , arXiv:1812.04641arXiv:1812.04641 [astro-ph.HE].

Dessart, L., C. D. Ott, A. Burrows, S. Rosswog, and E. Livne (2009), Astrophys. J. **690**, 1681.

Diehl, R., and F. X. Timmes (1998), Publ. Astron. Soc. Pacific **110**, 637.

Dillmann, I., K.-L. Kratz, A. Wöhr, O. Arndt, B. A. Brown, P. Hoff, M. Hjorth-Jensen, U. Köster, A. N. Ostrowski, B. Pfeiffer, D. Seweryniak, J. Shergur, and W. B. Walters (2003), Phys. Rev. Lett. **91** (16), 162503.

Drout, M. R., A. L. Piro, B. J. Shappee, C. D. Kilpatrick, J. D. Simon, C. Contreras, D. A. Coulter, R. J. Foley, M. R. Siebert, N. Morrell, K. Boutsia, F. Di Mille, T. W.-S. Holoien, D. Kasen, J. A. Kollmeier, B. F. Madore, A. J. Monson, A. Murguia-Berthier, Y.-C. Pan, J. X. Prochaska, E. Ramirez-Ruiz, A. Rest, C. Adams, K. Alatalo, E. Bañados, J. Baughman, T. C. Beers, R. A. Bernstein, T. Bitsakis, A. Campillay, T. T. Hansen, C. R. Higgs, A. P. Ji, G. Maravelias, J. L. Marshall, C. Moni Bidin, J. L. Prieto, K. C. Rasmussen, C. Rojas-Bravo, A. L. Strom, N. Ulloa, J. Vargas-González, Z. Wan, and D. D. Whitten (2017), Science **358**, 1570, arXiv:1710.05443 [astro-ph.HE].

Duflo, J., and A. P. Zuker (1995), Phys. Rev. C **52**, R23.

Duncan, R. C., S. L. Shapiro, and I. Wasserman (1986), Astrophys. J. **309**, 141.

Duncan, R. C., and C. Thompson (1992), Astrophys. J. Lett. **392**, L9.

Duquette, D. W., S. Salih, and J. E. Lawler (1981), Physics Letters A **83**, 214.

Ebinger, K., S. Curtis, C. Fröhlich, M. Hempel, A. Perego, M. Liebendörfer, and F.-K. Thielemann (2018), ArXiv e-prints arXiv:1804.03182 [astro-ph.SR].

Eichler, D., M. Livio, T. Piran, and D. N. Schramm (1989), Nature **340**, 126.

Eichler, M., A. Arcones, A. Kelic, O. Korobkin, K. Langanke, T. Marketin, G. Martínez-Pinedo, I. Panov, T. Rauscher, S. Rosswog, C. Winteler, N. T. Zinner, and F.-K. Thielemann (2015), Astrophys. J. **808**, 30.

Eichler, M., K. Nakamura, T. Takiwaki, T. Kuroda, K. Kotake, M. Hempel, R. Cabezón, M. Liebendörfer, and F.-K. Thielemann (2018a), J. Phys. G: Nucl. Part. Phys. **45**, 014001.

Eichler, M., *et al.* (2018b), private communication.

Ejnisman, R., I. D. Goldman, K. S. Krane, P. Mohr, Y. Nakazawa, E. B. Norman, T. Rauscher, and J. Reel (1998), Phys. Rev. C **58**, 2531.

Eliseev, S., K. Blaum, M. Block, C. Droese, M. Goncharov, E. Minaya Ramirez, D. A. Nesterenko, Y. N. Novikov, and L. Schweikhard (2013), Phys. Rev. Lett. **110** (8), 082501.

Engel, J., M. Bender, J. Dobaczewski, W. Nazarewicz, and R. Surman (1999), Phys. Rev. C **60**, 014302.

Epstein, R. I., S. A. Colgate, and W. C. Haxton (1988), Phys. Rev. Lett. **61**, 2038.

Erler, J., K. Langanke, H. Loens, G. Martínez-Pinedo, and P.-G. Reinhard (2012), Phys. Rev. C **85** (2), 025802.

Ertl, T., H.-T. Janka, S. E. Woosley, T. Sukhbold, and M. Ugliano (2016), Astrophys. J. **818**, 124.

Escher, J. E., J. T. Burke, F. S. Dietrich, N. D. Scielzo, I. J. Thompson, and W. Younes (2012), Rev. Mod. Phys. **84**, 353.

Escher, J. E., and F. S. Dietrich (2006), Phys. Rev. C **74** (5), 054601.

Evans, P. A., S. B. Cenko, J. A. Kennea, S. W. K. Emery, N. P. M. Kuin, O. Korobkin, R. T. Wollaeger, C. L. Fryer, K. K. Madsen, F. A. Harrison, Y. Xu, E. Nakar, K. Hotokezaka, A. Lien, S. Campana, S. R. Oates, E. Troja, A. A. Breeveld, F. E. Marshall, S. D. Barthelmy, A. P. Beardmore, D. N. Burrows, G. Cusumano, A. D'Aì, P. D'Avanzo, V. D'Elia, M. de Pasquale, W. P. Even, C. J. Fontes, K. Forster, J. Garcia, P. Giommi, B. Grefenstette, C. Gronwall, D. H. Hartmann, M. Heida, A. L. Hungerford, M. M. Kasliwal, H. A. Krimm, A. J. Levan, D. Malesani, A. Melandri, H. Miyasaka, J. A. Nousek, P. T. O'Brien, J. P. Osborne, C. Pagani, K. L. Page, D. M. Palmer, M. Perri, S. Pike, J. L. Racusin, S. Rosswog, M. H. Siegel, T. Sakamoto, B. Sbarufatti, G. Tagliaferri, N. R. Tanvir, and A. Tohuvavohu (2017), Science **358**, 1565, arXiv:1710.05437 [astro-ph.HE].

Farouqi, K., K. Kratz, B. Pfeiffer, T. Rauscher, F. Thielemann, and J. W. Truran (2010), Astrophys. J. **712**, 1359.

Fattoyev, F. J., J. Piekarewicz, and C. J. Horowitz (2018), Phys. Rev. Lett. **120**, 172702.

Fernández, R., D. Kasen, B. D. Metzger, and E. Quataert (2015), Mon. Not. Roy. Astron. Soc. **446**, 750, arXiv:1409.4426 [astro-ph.HE].

Fernandez, R., and B. D. Metzger (2013), Mon. Not. Roy.

Astron. Soc. **435**, 502, 1304.6720.
Fernández, R., and B. D. Metzger (2016), Annu. Rev. Nucl. Part. Sci. **66**, 23, arXiv:1512.05435 [astro-ph.HE].
Fernández, R., A. Tchekhovskoy, E. Quataert, F. Foucart, and D. Kasen (2019), Mon. Not. Roy. Astron. Soc. **482**, 3373.
Fischer, T., N.-U. F. Bastian, M.-R. Wu, P. Baklanov, E. Sorokina, S. Blinnikov, S. Typel, T. Klähn, and D. B. Blaschke (2018a), Nature Astronomy **2**, 980.
Fischer, T., M. Hempel, I. Sagert, Y. Suwa, and J. Schaffner-Bielich (2014), European Physical Journal A **50**, 46, arXiv:1307.6190 [astro-ph.HE].
Fischer, T., G. Martínez-Pinedo, M.-R. Wu, A. Lohs, and Y.-Z. Qian (2018b), ArXiv e-prints arXiv:1804.10890 [astro-ph.HE].
Fischer, T., I. Sagert, G. Pagliara, M. Hempel, J. Schaffner-Bielich, T. Rauscher, F.-K. Thielemann, R. Käppeli, G. Martínez-Pinedo, and M. Liebendörfer (2011), Astrophys. J. Suppl. **194** (2), 39.
Fischer, T., S. C. Whitehouse, A. Mezzacappa, F.-K. Thielemann, and M. Liebendörfer (2010), Astron. & Astrophys. **517**, A80, arXiv:0908.1871 [astro-ph.HE].
Fischer, T., M.-R. Wu, G. Martínez-Pinedo, N.-U. Bastian, and D. Blaschke (2018), in preparation.
Fogelberg, B., H. Gausemel, K. A. Mezilev, P. Hoff, H. Mach, M. Sanchez-Vega, A. Lindroth, E. Ramström, J. Genevey, J. A. Pinston, and M. Rejmund (2004), Phys. Rev. C **70**, 034312.
Foglizzo, T., R. Kazeroni, J. Guilet, F. Masset, M. González, B. K. Krueger, J. Novak, M. Oertel, J. Margueron, J. Faure, N. Martin, P. Blottiau, B. Peres, and G. Durand (2015), Publ. Astron. Soc. Austr. **32**, e009.
Fontes, C., C. Fryer, A. Hungerford, P. Hakel, J. Colgan, D. Kilcrease, and M. Sherrill (2015), High Energy Density Phys. **16**, 53.
Fontes, C. J., C. L. Fryer, A. L. Hungerford, R. T. Wollaeger, S. Rosswog, and E. Berger (2017), arXiv e-prints arXiv:1702.02990 [astro-ph.HE].
Forssén, C., F. S. Dietrich, J. Escher, R. D. Hoffman, and K. Kelley (2007), Phys. Rev. C **75** (5), 055807, nucl-th/0703097.
Foucart, F., M. B. Deaton, M. D. Duez, L. E. Kidder, I. MacDonald, C. D. Ott, H. P. Pfeiffer, M. A. Scheel, B. Szilagyi, and S. A. Teukolsky (2013), Phys. Rev. D **87**, 084006.
Foucart, F., M. B. Deaton, M. D. Duez, E. O'Connor, C. D. Ott, R. Haas, L. E. Kidder, H. P. Pfeiffer, M. A. Scheel, and B. Szilagyi (2014a), Phys. Rev. D **90**, 024026, arXiv:1405.1121 [astro-ph.HE].
Foucart, F., M. B. Deaton, M. D. Duez, E. O'Connor, C. D. Ott, R. Haas, L. E. Kidder, H. P. Pfeiffer, M. A. Scheel, and B. Szilagyi (2014b), Phys. Rev. D **90**, 024026.
Foucart, F., M. D. Duez, L. E. Kidder, R. Nguyen, H. P. Pfeiffer, and M. A. Scheel (2018), Phys. Rev. D **98**, 063007.
Foucart, F., E. O'Connor, L. Roberts, M. D. Duez, R. Haas, L. E. Kidder, C. D. Ott, H. P. Pfeiffer, M. A. Scheel, and B. Szilagyi (2015), Phys. Rev. D **91**, 124021, arXiv:1502.04146 [astro-ph.HE].
Foucart, F., E. O'Connor, L. Roberts, L. E. Kidder, H. P. Pfeiffer, and M. A. Scheel (2016), Phys. Rev. D **94**, 123016.
Fowler, W. A., and F. Hoyle (1960), Annals of Physics **10**, 280.
François, P., E. Depagne, V. Hill, M. Spite, F. Spite, B. Plez, T. C. Beers, J. Andersen, G. James, B. Barbuy, R. Cayrel, P. Bonifacio, P. Molaro, B. Nordström, and F. Primas (2007), Astron. & Astrophys. **476**, 935, arXiv:0709.3454.
Frebel, A., N. Christlieb, J. E. Norris, C. Thom, T. C. Beers, and J. Rhee (2007), Astrophys. J. Lett. **660**, L117, astro-ph/0703414.
Frebel, A., and K.-L. Kratz (2009), in *The Ages of Stars*, IAU Symposium, Vol. 258, edited by E. E. Mamajek, D. R. Soderblom, and R. F. G. Wyse, pp. 449–456.
Frebel, A., and J. E. Norris (2015), Annu. Rev. Astron. Astrophys. **53**, 631.
Freiburghaus, C., J.-F. Rembges, T. Rauscher, E. Kolbe, F.-K. Thielemann, K.-L. Kratz, B. Pfeiffer, and J. J. Cowan (1999a), Astrophys. J. **516**, 381.
Freiburghaus, C., S. Rosswog, and F.-K. Thielemann (1999b), Astrophys. J. **525**, L121.
Frensel, M., M.-R. Wu, C. Volpe, and A. Perego (2017), Phys. Rev. D **95** (2), 023011, arXiv:1607.05938 [astro-ph.HE].
Frischknecht, U., R. Hirschi, M. Pignatari, A. Maeder, G. Meynet, C. Chiappini, F.-K. Thielemann, T. Rauscher, C. Georgy, and S. Ekström (2016), Mon. Not. Roy. Astron. Soc. **456**, 1803, arXiv:1511.05730 [astro-ph.SR].
Fröhlich, C., G. Martínez-Pinedo, M. Liebendörfer, F.-K. Thielemann, E. Bravo, W. R. Hix, K. Langanke, and N. T. Zinner (2006), Phys. Rev. Lett. **96**, 142502.
Fryer, C., and V. Kalogera (1997), Astrophys. J. **489**, 244, astro-ph/9706031.
Fryer, C. L., K. Belczynski, E. Ramirez-Ruiz, S. Rosswog, G. Shen, and A. W. Steiner (2015), Astrophys. J. **812**, 24, arXiv:1504.07605 [astro-ph.HE].
Fujibayashi, S., K. Kiuchi, N. Nishimura, Y. Sekiguchi, and M. Shibata (2018), Astrophys. J. **860**, 64.
Fujibayashi, S., Y. Sekiguchi, K. Kiuchi, and M. Shibata (2017), Astrophys. J. **846**, 114.
Fujimoto, S.-i., M.-a. Hashimoto, K. Arai, and R. Matsuba (2004), Astrophys. J. **614**, 847.
Fujimoto, S.-i., M.-a. Hashimoto, O. Koike, K. Arai, and R. Matsuba (2003), Astrophys. J. **585**, 418, astro-ph/0211171.
Fujimoto, S.-i., M.-a. Hashimoto, K. Kotake, and S. Yamada (2007), Astrophys. J. **656**, 382, astro-ph/0602460.
Fujimoto, S.-i., K. Kotake, S. Yamada, M.-a. Hashimoto, and K. Sato (2006), Astrophys. J. **644**, 1040, astro-ph/0602457.
Fujimoto, S.-i., N. Nishimura, and M.-a. Hashimoto (2008), Astrophys. J. **680**, 1350.
Fulbright, J. P. (2000), Astron. J. **120**, 1841, astro-ph/0006260.
Fuller, G. M., W. A. Fowler, and M. J. Newman (1980), Astrophys. J. Suppl. **42**, 447.
Fuller, G. M., A. Kusenko, and V. Takhistov (2017), Phys. Rev. Lett. **119**, 061101.
Geissel, H., P. Armbruster, K. H. Behr, A. Brünle, K. Burkard, M. Chen, H. Folger, B. Franczak, H. Keller, O. Klepper, B. Langenbeck, F. Nickel, E. Pfeng, M. Pfützner, E. Roeckl, K. Rykaczewski, I. Schall, D. Schardt, C. Scheidenberger, K.-H. Schmidt, A. Schröter, T. Schwab, K. Sümmerer, M. Weber, G. Münzenberg, T. Brohm, H.-G. Clerc, M. Fauerbach, J.-J. Gaimard, A. Grewe, E. Hanelt, B. Knödler, M. Steiner, B. Voss, J. Weckenmann, C. Ziegler, A. Magel, H. Wollnik, J. P. Dufour, Y. Fujita, D. J. Vieira, and B. Sherrill (1992), Nucl. Instruments Methods Phys. Res. Sect. B Beam Interact. with Mater. Atoms **70**, 286.
Giacomazzo, B., L. Rezzolla, and L. Baiotti (2009), Mon. Not. Roy. Astron. Soc. **399**, L164.
Giacomazzo, B., J. Zrake, P. C. Duffell, A. I. MacFadyen,

and R. Perna (2015), Astrophys. J. **809**, 39.
Gilroy, K. K., C. Sneden, C. A. Pilachowski, and J. J. Cowan (1988), Astrophys. J. **327**, 298.
Giuliani, S. A., G. Martínez-Pinedo, and L. M. Robledo (2018), Phys. Rev. C **97**, 034323.
Giuliani, S. A., Z. Matheson, W. Nazarewicz, E. Olsen, P.-G. Reinhard, J. Sadhukhan, B. Schuetrumpf, N. Schunck, and P. Schwerdtfeger (2019), Rev. Mod. Phys. in press.
Giuliani, S. A., L. M. Robledo, and R. Rodríguez-Guzmán (2014), Phys. Rev. C **90**, 054311.
Giunti, C., M. Laveder, Y. F. Li, Q. Y. Liu, and H. W. Long (2012), Phys. Rev. D **86**, 113014.
Goldstein, D. A., and D. Kasen (2018), Astrophys. J. **852**, L33.
Gómez-Hornillos, M. B., J. Rissanen, J. L. Taín, A. Algora, D. Cano-Ott, J. Agramunt, V. Gorlychev, R. Caballero, T. Martínez, L. Achouri, J. Äystö, G. Cortés, V. V. Elomaa, T. Eronen, A. García, J. Hakala, A. Jokinen, P. Karvonen, V. S. Kolhinen, I. Moore, M. Parlog, H. Penttilä, Z. Podolyak, C. Pretel, M. Reponen, V. Sonnenschein, and E. Valencia (2011), in *Journal of Physics Conference Series*, Journal of Physics Conference Series, Vol. 312, p. 052008.
Goriely, S. (1997), Astron. & Astrophys. **325**, 414.
Goriely, S. (1998), Phys. Lett. B **436**, 10.
Goriely, S. (1999), Astron. & Astrophys. **342**, 881.
Goriely, S. (2015), Eur. Phys. J. A **51** (2), 22.
Goriely, S., and M. Arnould (2001), Astron. & Astrophys. **379**, 1113, astro-ph/0111300.
Goriely, S., A. Bauswein, and H.-T. Janka (2011), Astrophys. J. **738**, L32.
Goriely, S., A. Bauswein, H. T. Janka, J. L. Sida, J. F. Lemaître, S. Panebianco, N. Dubray, and S. Hilaire (2014), in *American Institute of Physics Conference Series*, American Institute of Physics Conference Series, Vol. 1594, edited by S. Jeong, N. Imai, H. Miyatake, and T. Kajino, pp. 357–364.
Goriely, S., A. Bauswein, O. Just, E. Pllumbi, and H.-T. Janka (2015), Mon. Not. Roy. Astron. Soc. **452**, 3894.
Goriely, S., N. Chamel, and J. M. Pearson (2010), Phys. Rev. C **82**, 035804.
Goriely, S., N. Chamel, and J. M. Pearson (2016), Phys. Rev. C **93** (3), 034337.
Goriely, S., and B. Clerbaux (1999), Astron. & Astrophys. **346**, 798, astro-ph/9904409.
Goriely, S., and J.-P. Delaroche (2007), Physics Letters B **653**, 178.
Goriely, S., S. Hilaire, and M. Girod (2012), in *Journal of Physics Conference Series*, Journal of Physics Conference Series, Vol. 337, p. 012027.
Goriely, S., S. Hilaire, and A. J. Koning (2008), Phys. Rev. C **78** (6), 064307.
Goriely, S., S. Hilaire, A. J. Koning, M. Sin, and R. Capote (2009), Phys. Rev. C **79**, 024612.
Goriely, S., S. Hilaire, S. Péru, and K. Sieja (2018), Phys. Rev. C **98**, 014327.
Goriely, S., and H.-T. Janka (2016), Mon. Not. Roy. Astron. Soc. **459**, 4174.
Goriely, S., and E. Khan (2002), Nucl. Phys. A **706**, 217.
Goriely, S., E. Khan, and M. Samyn (2004), Nucl. Phys. A **739**, 331, nucl-th/0306005.
Goriely, S., and G. Martínez-Pinedo (2015), Nucl. Phys. A **944**, 158.
Goriely, S., J.-L. Sida, J.-F. Lemaître, S. Panebianco, N. Dubray, S. Hilaire, A. Bauswein, and H.-T. Janka (2013), Phys. Rev. Lett. **111**, 242502.
Görres, J., M. Wiescher, and F.-K. Thielemann (1995), Phys. Rev. C **51**, 392.
Grawe, H., K. Langanke, and G. Martínez-Pinedo (2007), Rep. Prog. Phys. **70**, 1525.
Grebenev, S. A., A. A. Lutovinov, S. S. Tsygankov, and C. Winkler (2012), Nature **490**, 373.
Greiner, J., P. A. Mazzali, D. A. Kann, T. Krühler, E. Pian, S. Prentice, F. Olivares E., A. Rossi, S. Klose, S. Taubenberger, F. Knust, P. M. J. Afonso, C. Ashall, J. Bolmer, C. Delvaux, R. Diehl, J. Elliott, R. Filgas, J. P. U. Fynbo, J. F. Graham, A. N. Guelbenzu, S. Kobayashi, G. Leloudas, S. Savaglio, P. Schady, S. Schmidl, T. Schweyer, V. Sudilovsky, M. Tanga, A. C. Updike, H. van Eerten, and K. Varela (2015), Nature **523**, 189, arXiv:1509.03279 [astro-ph.HE].
Griffin, R., B. Gustafsson, T. Vieira, and R. Griffin (1982), Mon. Not. Roy. Astron. Soc. **198**, 637.
Grossman, D., O. Korobkin, S. Rosswog, and T. Piran (2014), Mon. Not. Roy. Astron. Soc. **439**, 757, arXiv:1307.2943 [astro-ph.HE].
Guerrero, C., C. Domingo-Pardo, F. Käppeler, J. Lerendegui-Marco, F. R. Palomo, J. M. Quesada, and R. Reifarth (2017), European Physical Journal A **53**, 87.
Guilet, J., A. Bauswein, O. Just, and H.-T. Janka (2017), Mon. Not. Roy. Astron. Soc. **471**, 1879.
Guttormsen, M., R. Chankova, U. Agvaanluvsan, E. Algin, L. A. Bernstein, F. Ingebretsen, T. Lönnroth, S. Messelt, G. E. Mitchell, J. Rekstad, A. Schiller, S. Siem, A. C. Sunde, A. Voinov, and S. Ødegård (2005), Phys. Rev. C **71** (4), 044307, nucl-ex/0411051.
Guttormsen, M., T. Ramsøy, and J. Rekstad (1987), Nuclear Instruments and Methods in Physics Research A **255**, 518.
Halevi, G., and P. Mösta (2018), Mon. Not. Roy. Astron. Soc. 10.1093/mnras/sty797, arXiv:1801.08943 [astro-ph.HE].
Hannaford, P., and R. M. Lowe (1981), Journal of Physics B Atomic Molecular Physics **14**, L5.
Hansen, C. J., and F. Primas (2011), Astron. & Astrophys. **525**, L5.
Hansen, T. T., E. M. Holmbeck, T. C. Beers, V. M. Placco, I. U. Roederer, A. Frebel, C. M. Sakari, J. D. Simon, and I. B. Thompson (2018), Astrophys. J. **858**, 92.
Harikae, S., T. Takiwaki, and K. Kotake (2009), Astrophys. J. **704**, 354.
Hartmann, D., S. E. Woosley, and M. F. El Eid (1985), Astrophys. J. **297**, 837.
Hatarik, R., L. A. Bernstein, J. A. Cizewski, D. L. Bleuel, J. T. Burke, J. E. Escher, J. Gibelin, B. L. Goldblum, A. M. Hatarik, S. R. Lesher, P. D. O'Malley, L. Phair, E. Rodriguez-Vieitez, T. Swan, and M. Wiedeking (2010), Phys. Rev. C **81** (1), 011602.
Hausmann, M., F. Attallah, K. Beckert, F. Bosch, A. Dolinskiy, H. Eickhoff, M. Falch, B. Franczak, B. Franzke, H. Geissel, T. Kerscher, O. Klepper, H.-J. Kluge, C. Kozhuharov, K. E. G. Löbner, G. Münzenberg, F. Nolden, Y. N. Novikov, T. Radon, H. Schatz, C. Scheidenberger, J. Stadlmann, M. Steck, T. Winkler, and H. Wollnik (2000), Nuclear Instruments and Methods in Physics Research A **446**, 569.
Hausmann, M., J. Stadlmann, F. Attallah, K. Beckert, P. Beller, F. Bosch, H. Eickhoff, M. Falch, B. Franczak, B. Franzke, H. Geissel, T. Kerscher, O. Klepper, H.-J. Kluge, C. Kozhuharov, Y. A. Litvinov, K. E. G. Löbner,

G. Münzenberg, N. Nankov, F. Nolden, Y. N. Novikov, T. Ohtsubo, T. Radon, H. Schatz, C. Scheidenberger, M. Steck, Z. Sun, H. Weick, and H. Wollnik (2001), Hyperfine Interactions **132**, 289.
Haxton, W. C., K. Langanke, Y.-Z. Qian, and P. Vogel (1997), Phys. Rev. Lett. **78**, 2694.
Hayek, W., U. Wiesendahl, N. Christlieb, K. Eriksson, A. J. Korn, P. S. Barklem, V. Hill, T. C. Beers, K. Farouqi, B. Pfeiffer, and K.-L. Kratz (2009), Astron. & Astrophys. **504**, 511, arXiv:0910.0707 [astro-ph.SR].
Haynes, C., and C. Kobayashi (2018), ArXiv e-prints arXiv:1809.10991.
Hebeler, K., J. M. Lattimer, C. J. Pethick, and A. Schwenk (2013), Astrophys. J. **773**, 11.
Heger, A., C. L. Fryer, S. E. Woosley, N. Langer, and D. H. Hartmann (2003), Astrophys. J. **591**, 288.
Hewish, A., and S. E. Okoye (1965), Nature **207**, 59.
Hilaire, S., S. Goriely, M. Girod, A. J. Koning, R. Capote, and M. Sin (2010), in *European Physical Journal Web of Conferences*, European Physical Journal Web of Conferences, Vol. 2, p. 04005.
Hill, V., B. Plez, R. Cayrel, T. C. Beers, B. Nordström, J. Andersen, M. Spite, F. Spite, B. Barbuy, P. Bonifacio, E. Depagne, P. François, and F. Primas (2002), Astron. & Astrophys. **387**, 560, astro-ph/0203462.
Hillebrandt, W. (1978), Space Sci. Rev. **21**, 639.
Hillebrandt, W., T. Kodama, and K. Takahashi (1976), Astron. & Astrophys. **52**, 63.
Hillebrandt, W., M. Kromer, F. K. Röpke, and A. J. Ruiter (2013), Frontiers of Physics **8**, 116, arXiv:1302.6420 [astro-ph.CO].
Hillebrandt, W., F. K. Thielemann, H. V. Klapdor, and T. Oda (1981), Astron. & Astrophys. **99**, 195.
Hirai, Y., Y. Ishimaru, T. R. Saitoh, M. S. Fujii, J. Hidaka, and T. Kajino (2015), Astrophys. J. **814**, 41, arXiv:1509.08934.
Hirai, Y., Y. Ishimaru, T. R. Saitoh, M. S. Fujii, J. Hidaka, and T. Kajino (2017), Mon. Not. Roy. Astron. Soc. **466**, 2474, arXiv:1612.06861.
Hix, W. R., E. J. Lentz, S. W. Bruenn, A. Mezzacappa, O. E. B. Messer, E. Endeve, J. M. Blondin, J. A. Harris, P. Marronetti, and K. N. Yakunin (2016), Acta Phys. Pol. B **47**, 645.
Hix, W. R., and B. S. Meyer (2006), Nucl. Phys. A **777**, 188.
Hix, W. R., and F.-K. Thielemann (1999), J. Comput. Appl. Math. **109**, 321.
Hix, W. R., and F.-K. Thielemann (1999), Astrophys. J. **511**, 862.
Hoffman, R. D., S. E. Woosley, and Y.-Z. Qian (1997), Astrophys. J. **482**, 951.
Holmbeck, E. M., T. C. Beers, I. U. Roederer, V. M. Placco, T. T. Hansen, C. M. Sakari, C. Sneden, C. Liu, Y. S. Lee, J. J. Cowan, and A. Frebel (2018a), Astrophys. J. **859**, L24, arXiv:1805.11925 [astro-ph.SR].
Holmbeck, E. M., R. Surman, T. M. Sprouse, M. R. Mumpower, N. Vassh, T. C. Beers, and T. Kawano (2018b), ArXiv e-prints arXiv:1807.06662 [astro-ph.SR].
Honda, S., W. Aoki, Y. Ishimaru, and S. Wanajo (2007), Astrophys. J. **666**, 1189, arXiv:0705.3975.
Honda, S., W. Aoki, Y. Ishimaru, S. Wanajo, and S. G. Ryan (2006), Astrophys. J. **643**, 1180, astro-ph/0602107.
Honda, S., W. Aoki, T. Kajino, H. Ando, T. C. Beers, H. Izumiura, K. Sadakane, and M. Takada-Hidai (2004), Astrophys. J. **607**, 474, astro-ph/0402298.
Horowitz, C. J. (2002), Phys. Rev. D **65**, 043001.
Horowitz, C. J., A. Arcones, B. Côté, I. Dillmann, W. Nazarewicz, I. U. Roederer, H. Schatz, A. Aprahamian, D. Atanasov, A. Bauswein, J. Bliss, M. Brodeur, J. A. Clark, A. Frebel, F. Foucart, C. J. Hansen, O. Just, A. Kankainen, G. C. McLaughlin, J. M. Kelly, S. N. Liddick, D. M. Lee, J. Lippuner, D. Martin, J. Mendoza-Temis, B. D. Metzger, M. R. Mumpower, G. Perdikakis, J. Pereira, B. W. O'Shea, R. Reifarth, A. M. Rogers, D. M. Siegel, A. Spyrou, R. Surman, X. Tang, T. Uesaka, and M. Wang (2018), ArXiv e-prints arXiv:1805.04637 [astro-ph.SR].
Horowitz, C. J., G. Shen, E. O'Connor, and C. D. Ott (2012), Phys. Rev. C **86**, 065806.
Hosmer, P., H. Schatz, A. Aprahamian, O. Arndt, R. R. C. Clement, A. Estrade, K. Farouqi, K.-L. Kratz, S. N. Liddick, A. F. Lisetskiy, P. F. Mantica, P. Möller, W. F. Mueller, F. Montes, A. C. Morton, M. Ouellette, E. Pellegrini, J. Pereira, B. Pfeiffer, P. Reeder, P. Santi, M. Steiner, A. Stolz, B. E. Tomlin, W. B. Walters, and A. Wöhr (2010), Phys. Rev. C **82** (2), 025806, arXiv:1011.5255 [nucl-ex].
Hosmer, P. T., H. Schatz, A. Aprahamian, O. Arndt, R. R. C. Clement, A. Estrade, K.-L. Kratz, S. N. Liddick, P. F. Mantica, W. F. Mueller, F. Montes, A. C. Morton, M. Ouellette, E. Pellegrini, B. Pfeiffer, P. Reeder, P. Santi, M. Steiner, A. Stolz, B. E. Tomlin, W. B. Walters, and A. Wohr (2005), Phys. Rev. Lett. **94** (11), 112501.
Hotokezaka, K., P. Beniamini, and T. Piran (2018), International Journal of Modern Physics D **27**, 1842005, arXiv:1801.01141 [astro-ph.HE].
Hotokezaka, K., K. Kiuchi, K. Kyutoku, T. Muranushi, Y.-i. Sekiguchi, M. Shibata, and K. Taniguchi (2013a), Phys. Rev. D **88**, 044026.
Hotokezaka, K., K. Kiuchi, K. Kyutoku, H. Okawa, Y.-i. Sekiguchi, M. Shibata, and K. Taniguchi (2013b), Phys. Rev. D **87**, 024001.
Hotokezaka, K., K. Kyutoku, and M. Shibata (2013), Phys. Rev. D **87**, 044001.
Hotokezaka, K., T. Piran, and M. Paul (2015), Nature Physics **11**, 1042, arXiv:1510.00711 [astro-ph.HE].
Hotokezaka, K., R. Sari, and T. Piran (2017), Mon. Not. Roy. Astron. Soc. **468**, 91.
Hotokezaka, K., S. Wanajo, M. Tanaka, A. Bamba, Y. Terada, and T. Piran (2016), Mon. Not. Roy. Astron. Soc. **459**, 35.
Howard, W. M., and P. Möller (1980), At. Data Nucl. Data Tables **25**, 219.
Hüdepohl, L., B. Müller, H.-T. Janka, A. Marek, and G. G. Raffelt (2010), Phys. Rev. Lett. **104** (25), 251101.
Hulse, R. A., and J. H. Taylor (1975), Astrophys. J. **195**, L51.
Iliadis, C. (2007), *Nuclear Physics of Stars, by Christian Iliadis. ISBN 978-3-527-33648-7. Published by Wiley-VCH Verlag, Wenheim, Germany, 2007.* (Wiley-VCH Verlag).
Ishii, A., T. Shigeyama, and M. Tanaka (2018), Astrophys. J. **861**, 25, arXiv:1805.04909 [astro-ph.HE].
Ishimaru, Y., and S. Wanajo (1999), Astrophys. J. **511**, L33, astro-ph/9812067.
Ishimaru, Y., S. Wanajo, and N. Prantzos (2015), Astrophys. J. **804**, L35, arXiv:1504.04559.
Ivans, I. I., J. Simmerer, C. Sneden, J. E. Lawler, J. J. Cowan, R. Gallino, and S. Bisterzo (2006), Astrophys. J. **645**, 613.
Janiuk, A. (2014), Astron. & Astrophys. **568**, A105.
Janiuk, A. (2017), Astrophys. J. **837**, 39, arXiv:1609.09361 [astro-ph.HE].

Janiuk, A. (2018), private communication.
Janiuk, A., P. Sukova, and I. Palit (2018), ArXiv e-prints arXiv:1810.05261 [astro-ph.HE].
Janka, H., B. Müller, F. S. Kitaura, and R. Buras (2008), Astron. & Astrophys. **485**, 199, 0712.4237.
Janka, H.-T. (2016), "Neutrino emission from supernovae," in *Handbook of Supernovae*, edited by A. W. Alsabti and P. Murdin (Springer International Publishing, Cham).
Janka, H.-T. (2017), "Neutrino-driven explosions," in *Handbook of Supernovae*, edited by A. W. Alsabti and P. Murdin (Springer International Publishing, Cham).
Janka, H.-T., T. Melson, and A. Summa (2016), Annu. Rev. Nucl. Part. Sci. **66**, 341.
Jeukenne, J.-P., A. Lejeune, and C. Mahaux (1977), Phys. Rev. C **16**, 80.
Ji, A. P., and A. Frebel (2018), Astrophys. J. **856**, 138, arXiv:1802.07272 [astro-ph.SR].
Ji, A. P., A. Frebel, J. D. Simon, and A. Chiti (2016), Astrophys. J. **830**, 93, arXiv:1607.07447.
Johnson, C. W., S. E. Koonin, G. H. Lang, and W. E. Ormand (1992), Phys. Rev. Lett. **69**, 3157, nucl-th/9210014.
Jones, K. L., A. S. Adekola, D. W. Bardayan, J. C. Blackmon, K. Y. Chae, K. A. Chipps, J. A. Cizewski, L. Erikson, C. Harlin, R. Hatarik, R. Kapler, R. L. Kozub, J. F. Liang, R. Livesay, Z. Ma, B. H. Moazen, C. D. Nesaraja, F. M. Nunes, S. D. Pain, N. P. Patterson, D. Shapira, J. F. Shriner, M. S. Smith, T. P. Swan, and J. S. Thomas (2010), Nature **465**, 454, arXiv:1006.1576 [nucl-ex].
Jones, S., R. Hirschi, and K. Nomoto (2014), Astrophys. J. **797**, 83, arXiv:1412.2878 [astro-ph.SR].
Jones, S., C. Ritter, F. Herwig, C. Fryer, M. Pignatari, M. G. Bertolli, and B. Paxton (2016a), Mon. Not. Roy. Astron. Soc. **455**, 3848, arXiv:1510.07417 [astro-ph.SR].
Jones, S., F. K. Röpke, R. Pakmor, I. R. Seitenzahl, S. T. Ohlmann, and P. V. F. Edelmann (2016b), Astron. & Astrophys. **593**, A72.
Junghans, A. R., M. de Jong, H.-G. Clerc, A. V. Ignatyuk, G. A. Kudyaev, and K.-H. Schmidt (1998), Nucl. Phys. A **629**, 635.
Juodagalvis, A., K. Langanke, W. Hix, G. Martínez-Pinedo, and J. Sampaio (2010), Nucl. Phys. A **848**, 454.
Just, O., A. Bauswein, R. A. Pulpillo, S. Goriely, and H.-T. Janka (2015a), Mon. Not. Roy. Astron. Soc. **448**, 541.
Just, O., M. Obergaulinger, and H. T. Janka (2015b), Mon. Not. Roy. Astron. Soc. **453**, 3386.
Just, O., M. Obergaulinger, H.-T. Janka, A. Bauswein, and N. Schwarz (2016), Astrophys. J. **816**, L30, arXiv:1510.04288 [astro-ph.HE].
Kajino, T., and G. J. Mathews (2017), Rep. Prog. Phys. **80**, 084901.
Kalogera, V., and C. L. Fryer (1999), Astronomical and Astrophysical Transactions **18**, 515.
Kaplan, J. D., C. D. Ott, E. P. O'Connor, K. Kiuchi, L. Roberts, and M. Duez (2014), Astrophys. J. **790**, 19.
Käppeler, F. (1999), Prog. Part. Nucl. Phys. **43**, 419.
Käppeler, F., R. Gallino, S. Bisterzo, and W. Aoki (2011), rmp **83**, 157, arXiv:1012.5218 [astro-ph.SR].
Karakas, A. I., and J. C. Lattanzio (2014), Publ. Astron. Soc. Austr. **31**, e030, arXiv:1405.0062 [astro-ph.SR].
Kasen, D., N. R. Badnell, and J. Barnes (2013), Astrophys. J. **774**, 25, arXiv:1303.5788 [astro-ph.HE].
Kasen, D., and J. Barnes (2018), arXiv e-prints arXiv:1807.03319 [astro-ph.HE].
Kasen, D., and L. Bildsten (2010), Astrophys. J. **717**, 245, arXiv:0911.0680 [astro-ph.HE].
Kasen, D., B. Metzger, J. Barnes, E. Quataert, and E. Ramirez-Ruiz (2017), Nature **551**, 80.
Kasliwal, M. M., D. Kasen, R. M. Lau, D. A. Perley, S. Rosswog, E. O. Ofek, K. Hotokezaka, R.-R. Chary, J. Sollerman, A. Goobar, and D. L. Kaplan (2018), arXiv e-prints arXiv:1812.08708 [astro-ph.HE].
Kasliwal, M. M., E. Nakar, L. P. Singer, D. L. Kaplan, D. O. Cook, A. Van Sistine, R. M. Lau, C. Fremling, O. Gottlieb, J. E. Jencson, S. M. Adams, U. Feindt, K. Hotokezaka, S. Ghosh, D. A. Perley, P.-C. Yu, T. Piran, J. R. Allison, G. C. Anupama, A. Balasubramanian, K. W. Bannister, J. Bally, J. Barnes, S. Barway, E. Bellm, V. Bhalerao, D. Bhattacharya, N. Blagorodnova, J. S. Bloom, P. R. Brady, C. Cannella, D. Chatterjee, S. B. Cenko, B. E. Cobb, C. Copperwheat, A. Corsi, K. De, D. Dobie, S. W. K. Emery, P. A. Evans, O. D. Fox, D. A. Frail, C. Frohmaier, A. Goobar, G. Hallinan, F. Harrison, G. Helou, T. Hinderer, A. Y. Q. Ho, A. Horesh, W.-H. Ip, R. Itoh, D. Kasen, H. Kim, N. P. M. Kuin, T. Kupfer, C. Lynch, K. Madsen, P. A. Mazzali, A. A. Miller, K. Mooley, T. Murphy, C.-C. Ngeow, D. Nichols, S. Nissanke, P. Nugent, E. O. Ofek, H. Qi, R. M. Quimby, S. Rosswog, F. Rusu, E. M. Sadler, P. Schmidt, J. Sollerman, I. Steele, A. R. Williamson, Y. Xu, L. Yan, Y. Yatsu, C. Zhang, and W. Zhao (2017), Science **358**, 1559, arXiv:1710.05436 [astro-ph.HE].
Kaspi, V. M., and A. M. Beloborodov (2017), Annu. Rev. Astron. Astrophys. **55**, 261.
Kawaguchi, K., M. Shibata, and M. Tanaka (2018), Astrophys. J. **865**, L21.
Kelic, A., M. V. Ricciardi, and K.-H. Schmidt (2008), in *Dynamical Aspects of Nuclear Fission*, edited by J. Kliman, M. G. Itkis, and Š. Gmuca, pp. 203–215.
Kelic, A., M. Valentina Ricciardi, and K.-H. Schmidt (2009), arXiv e-prints arXiv:0906.4193 [nucl-th].
Kirby, E. N., J. G. Cohen, P. Guhathakurta, L. Cheng, J. S. Bullock, and A. Gallazzi (2013), Astrophys. J. **779**, 102, arXiv:1310.0814 [astro-ph.GA].
Kirsebom, O. S., S. Jones, D. F. Strömberg4, G. Martínez-Pinedo, K. Langanke, F. K. Röpke, B. A. Brown, T. Eronen, H. O. U. Fynbo, M. Hukkanen, A. Idini, A. Jokinen, A. Kankainen, I. Moore, H. Möller, S. T. Ohlmann, H. Penttila, K. Riisager, S. Rinta-Antila, W. H. Trzaska, and J. Äystö (2019), submitted.
Kirson, M. W. (2008), Nucl. Phys. A **798**, 29.
Kiss, G. G., P. Mohr, Z. Fülöp, D. Galaviz, G. Gyürky, Z. Elekes, E. Somorjai, A. Kretschmer, K. Sonnabend, A. Zilges, and M. Avrigeanu (2009), Phys. Rev. C **80** (4), 045807, arXiv:1012.2275 [nucl-ex].
Kitaura, F. S., H.-T. Janka, and W. Hillebrandt (2006), Astron. & Astrophys. **450**, 345.
Kiuchi, K., P. Cerdá-Durán, K. Kyutoku, Y. Sekiguchi, and M. Shibata (2015), Phys. Rev. D **92** (12), 124034, arXiv:1509.09205 [astro-ph.HE].
Kizivat, L.-T., G. Martínez-Pinedo, K. Langanke, R. Surman, and G. C. McLaughlin (2010), Phys. Rev. C **81**, 025802.
Klapdor, H. V., T. Oda, J. Metzinger, W. Hillebrandt, and F. K. Thielemann (1981), Zeitschrift fur Physik A Hadrons and Nuclei **299**, 213.
Knie, K., G. Korschinek, T. Faestermann, E. A. Dorfi, G. Rugel, and A. Wallner (2004), Phys. Rev. Lett. **93** (17), 171103.
Knöbel, R., M. Diwisch, F. Bosch, D. Boutin, L. Chen, C. Dimopoulou, A. Dolinskii, B. Franczak, B. Franzke,

H. Geissel, M. Hausmann, C. Kozhuharov, J. Kurcewicz, S. Litvinov, G. Martinez-Pinedo, M. Matoš, M. Mazzocco, G. Münzenberg, S. Nakajima, C. Nociforo, F. Nolden, T. Ohtsubo, A. Ozawa, Z. Patyk, W. Plaß, C. Scheidenberger, J. Stadlmann, M. Steck, B. Sun, T. Suzuki, P. Walker, H. Weick, M.-R. Wu, M. Winkler, and T. Yamaguchi (2016), Phys. Lett. B **754**, 288.

Kobayashi, C. (2016), in *The General Assembly of Galaxy Halos: Structure, Origin and Evolution*, IAU Symposium, Vol. 317, edited by A. Bragaglia, M. Arnaboldi, M. Rejkuba, and D. Romano, pp. 57–63.

Kobayashi, C., H. Umeda, K. Nomoto, N. Tominaga, and T. Ohkubo (2006), Astrophys. J. **653**, 1145.

Kodama, T., and K. Takahashi (1975), Nucl. Phys. A **239**, 489.

Kolbe, E., K. Langanke, G. Martínez-Pinedo, and P. Vogel (2003), J. Phys. G: Nucl. Part. Phys. **29**, 2569.

Koning, A. J., and J. P. Delaroche (2003), Nucl. Phys. A **713**, 231.

Koning, A. J., S. Hilaire, and S. Goriely (2008), Nucl. Phys. A **810**, 13.

Koonin, S. E., D. J. Dean, and K. Langanke (1997), Phys. Rep. **278**, 1, nucl-th/9602006.

Korobkin, O., S. Rosswog, A. Arcones, and C. Winteler (2012), Mon. Not. Roy. Astron. Soc. **426**, 1940.

Kotake, K., K. Sumiyoshi, S. Yamada, T. Takiwaki, T. Kuroda, Y. Suwa, and H. Nagakura (2012), Prog. Theor. Exp. Phys. **2012**, 01A301.

Koura, H., T. Tachibana, M. Uno, and M. Yamada (2005), Prog. Theor. Phys. **113**, 305.

Kozub, R. L., G. Arbanas, A. S. Adekola, D. W. Bardayan, J. C. Blackmon, K. Y. Chae, K. A. Chipps, J. A. Cizewski, L. Erikson, R. Hatarik, W. R. Hix, K. L. Jones, W. Krolas, J. F. Liang, Z. Ma, C. Matei, B. H. Moazen, C. D. Nesaraja, S. D. Pain, D. Shapira, J. F. Shriner, Jr., M. S. Smith, and T. P. Swan (2012), Phys. Rev. Lett. **109** (17), 172501.

Kramer, M. (2009), in *Cosmic Magnetic Fields: From Planets, to Stars and Galaxies*, IAU Symposium, Vol. 259, edited by K. G. Strassmeier, A. G. Kosovichev, and J. E. Beckman, pp. 485–492.

Kratz, K., J. Bitouzet, F. Thielemann, P. Moeller, and B. Pfeiffer (1993), Astrophys. J. **403**, 216.

Kratz, K.-L. (2001), Nucl. Phys. A **688**, 308, astro-ph/0012281.

Kratz, K.-L., K. Farouqi, and P. Möller (2014), Astrophys. J. **792**, 6, arXiv:1406.2529 [astro-ph.SR].

Kratz, K.-L., H. Gabelmann, W. Hillebrandt, B. Pfeiffer, K. Schlosser, and F.-K. Thielemann (1986), Z. Phys. A **325**, 489.

Kratz, K.-L., P. Möller, B. Pfeiffer, and W. B. Walters (2000), in *Capture Gamma-Rays and Related Studies*, Vol. 529, edited by S. Wender (AIP Conf. Proc.) p. 295.

Kratz, K.-L., B. Pfeiffer, J. J. Cowan, and C. Sneden (2004), New Astron. Rev. **48**, 105.

Kratz, K.-L., W. Rudolph, H. Ohm, H. Franz, M. Zendel, G. Herrmann, S. G. Prussin, F. M. Nuh, A. A. Shihab-Eldin, D. R. Slaughter, W. Halverson, and H. V. Klapdor (1979), Nucl. Phys. A **317**, 335.

Kratz, K.-L., A. Schröder, H. Ohm, M. Zendel, H. Gabelmann, W. Ziegert, P. Peuser, G. Jung, B. Pfeiffer, K. D. Wünsch, H. Wollnik, C. Ristori, and J. Crançon (1982), Zeitschrift fur Physik A Hadrons and Nuclei **306**, 239.

Kratz, K.-L., F.-K. Thielemann, W. Hillebrandt, P. Möller, V. Harms, A. Wohr, and J. W. Truran (1988), J. Phys. G **14**, S331.

Kratz, K.-L., W. Ziegert, W. Hillebrandt, and F.-K. Thielemann (1983), Astron. & Astrophys. **125**, 381.

Kugler, E., D. Fiander, B. Johnson, H. Haas, A. Przewloka, H. L. Ravn, D. J. Simon, K. Zimmer, and Isolde Collaboration (1992), Nuclear Instruments and Methods in Physics Research B **70**, 41.

Kulkarni, S. R. (2005), arXiv e-prints arXiv:astro-ph/0510256 [astro-ph].

Kurcewicz, J., F. Farinon, H. Geissel, S. Pietri, C. Nociforo, A. Prochazka, H. Weick, J. S. Winfield, A. Estradé, P. R. P. Allegro, A. Bail, G. Bélier, J. Benlliure, G. Benzoni, M. Bunce, M. Bowry, R. Caballero-Folch, I. Dillmann, A. Evdokimov, J. Gerl, A. Gottardo, E. Gregor, R. Janik, A. Kelić-Heil, R. Knöbel, T. Kubo, Y. A. Litvinov, E. Merchan, I. Mukha, F. Naqvi, M. Pfützner, M. Pomorski, Z. Podolyák, P. H. Regan, B. Riese, M. V. Ricciardi, C. Scheidenberger, B. Sitar, P. Spiller, J. Stadlmann, P. Strmen, B. Sun, I. Szarka, J. Taïeb, S. Terashima, J. J. Valiente-Dobón, M. Winkler, and P. Woods (2012), Physics Letters B **717**, 371, arXiv:1112.0521 [nucl-ex].

Kuroda, T., K. Kotake, T. Takiwaki, and F.-K. Thielemann (2018), Mon. Not. Roy. Astron. Soc. **477**, L80, arXiv:1801.01293 [astro-ph.HE].

Kyutoku, K., K. Ioka, H. Okawa, M. Shibata, and K. Taniguchi (2015), Phys. Rev. D **92**, 044028.

Kyutoku, K., K. Ioka, and M. Shibata (2013), Phys. Rev. D **88** (4), 041503, arXiv:1305.6309 [astro-ph.HE].

Kyutoku, K., K. Kiuchi, Y. Sekiguchi, M. Shibata, and K. Taniguchi (2018), Phys. Rev. D **97**, 023009, arXiv:1710.00827 [astro-ph.HE].

Landau, L. D. (1932), Phys. Z. Sowjetunion **1**, 285.

Langanke, K. (1998), Phys. Lett. B **438**, 235.

Langanke, K. (2006), Nucl. Phys. A **778**, 233.

Langanke, K., and E. Kolbe (2001), At. Data. Nucl. Data Tables **79**, 293.

Langanke, K., and E. Kolbe (2002), At. Data. Nucl. Data Tables **82**, 191.

Langanke, K., and G. Martínez-Pinedo (2000), Nucl. Phys. A **673**, 481.

Langanke, K., and G. Martínez-Pinedo (2001), At. Data. Nucl. Data Tables **79**, 1.

Langanke, K., and G. Martínez-Pinedo (2003), Rev. Mod. Phys. **75**, 819.

Larsen, A. C., R. Chankova, M. Guttormsen, F. Ingebretsen, S. Messelt, J. Rekstad, S. Siem, N. U. H. Syed, S. W. Ødegård, T. Lönnroth, A. Schiller, and A. Voinov (2006), Phys. Rev. C **73** (6), 064301, nucl-ex/0511054.

Larsen, A. C., and S. Goriely (2010), Phys. Rev. C **82** (1), 014318, arXiv:1211.6257 [nucl-ex].

Larsen, A. C., S. Goriely, L. A. Bernstein, D. L. Bleuel, A. Bracco, B. A. Brown, F. Camera, T. K. Eriksen, S. Frauendorf, F. Giacoppo, M. Guttormsen, A. Görgen, S. Harissopulos, S. Leoni, S. N. Liddick, F. Naqvi, H. T. Nyhus, S. J. Rose, T. Renstrøm, R. Schwengner, S. Siem, A. Spyrou, G. M. Tveten, A. V. Voinov, and M. Wiedeking (2015), Acta Physica Polonica B **46**, 509.

Larsen, A. C., M. Guttormsen, R. Chankova, F. Ingebretsen, T. Lönnroth, S. Messelt, J. Rekstad, A. Schiller, S. Siem, N. U. H. Syed, and A. Voinov (2007), Phys. Rev. C **76** (4), 044303, arXiv:0706.0533 [nucl-ex].

Larson, N., S. N. Liddick, M. Bennett, A. Bowe, A. Chemey, C. Prokop, A. Simon, A. Spyrou, S. Suchyta, S. J. Quinn, S. L. Tabor, P. L. Tai, V. Tripathi, and J. M. VonMoss

(2013), Nuclear Instruments and Methods in Physics Research A **727**, 59.
Lattimer, J. M. (2012), Annu. Rev. Nucl. Part. Sci. **62**, 485.
Lattimer, J. M. (2014), Nucl. Phys. A **928**, 276.
Lattimer, J. M., and M. Prakash (2016), Phys. Rep. **621**, 127.
Lattimer, J. M., and D. N. Schramm (1974), Astrophys. J. **192**, L145.
Lattimer, J. M., and D. N. Schramm (1976), Astrophys. J. **210**, 549.
Lawler, J. E., E. A. Den Hartog, C. Sneden, and J. J. Cowan (2006), Astrophys. J. Suppl. **162**, 227.
Lawler, J. E., E. A. Hartog, C. Sneden, and J. J. Cowan (2008), Canadian Journal of Physics **86**, 1033.
Lawler, J. E., C. Sneden, J. J. Cowan, I. I. Ivans, and E. A. Den Hartog (2009), Astrophys. J. Suppl. **182**, 51.
Lee, W. H., and E. Ramirez-Ruiz (2007), New J. Phys. **9**, 17.
Lehner, L., S. L. Liebling, C. Palenzuela, O. L. Caballero, E. O'Connor, M. Anderson, and D. Neilsen (2016), Class. Quantum Gravity **33**, 184002, arXiv:1603.00501 [gr-qc].
Leist, B., W. Ziegert, M. Wiescher, K.-L. Kratz, and F.-K. Thielemann (1985), Zeitschrift fur Physik A Hadrons and Nuclei **322**, 531.
Lhersonneau, G., H. Gabelmann, B. Pfeiffer, and K.-L. Kratz (1995), Zeitschrift für Phys. A Atoms Nucl. **352**, 293.
Li, H.-N., W. Aoki, S. Honda, G. Zhao, N. Christlieb, and T. Suda (2015), Research in Astronomy and Astrophysics **15**, 1264, arXiv:1506.05200 [astro-ph.SR].
Li, L.-X., and B. Paczyński (1998), Astrophys. J. **507**, L59, astro-ph/9807272.
Liddick, S. N., A. Spyrou, B. P. Crider, F. Naqvi, A. C. Larsen, M. Guttormsen, M. Mumpower, R. Surman, G. Perdikakis, D. L. Bleuel, A. Couture, L. Crespo Campo, A. C. Dombos, R. Lewis, S. Mosby, S. Nikas, C. J. Prokop, T. Renstrom, B. Rubio, S. Siem, and S. J. Quinn (2016), Phys. Rev. Lett. **116** (24), 242502.
Liebendörfer, M., M. Rampp, H.-T. Janka, and A. Mezzacappa (2005), Astrophys. J. **620**, 840, astro-ph/0310662.
Liebendörfer, M., S. C. Whitehouse, and T. Fischer (2009), Astrophys. J. **698**, 1174, arXiv:0711.2929.
Limongi, M., and A. Chieffi (2018), Astrophys. J. Suppl. **237**, 13, arXiv:1805.09640 [astro-ph.SR].
Lippuner, J., R. Fernández, L. F. Roberts, F. Foucart, D. Kasen, B. D. Metzger, and C. D. Ott (2017), Mon. Not. Roy. Astron. Soc. **472**, 904.
Lippuner, J., and L. F. Roberts (2015), Astrophys. J. **815**, 82.
Lippuner, J., and L. F. Roberts (2017), Astrophys. J. Suppl. **233**, 18.
Litvinov, Y. A., H. Geissel, Y. N. Novikov, Z. Patyk, T. Radon, C. Scheidenberger, F. Attallah, K. Beckert, F. Bosch, M. Falch, B. Franzke, M. Hausmann, T. Kerscher, O. Klepper, H.-J. Kluge, C. Kozhuharov, K. E. G. Löbner, G. Münzenberg, F. Nolden, M. Steck, and H. Wollnik (2004), Nucl. Phys. A **734**, 473.
Litvinova, E., and N. Belov (2013), Phys. Rev. C **88** (3), 031302, arXiv:1302.4478 [nucl-th].
Litvinova, E., H. Loens, K. Langanke, G. Martínez-Pinedo, T. Rauscher, P. Ring, F. Thielemann, and V. Tselyaev (2009), Nucl. Phys. A **823**, 26.
Liu, M., N. Wang, Y. Deng, and X. Wu (2011), Phys. Rev. C **84**, 014333.
Liu, Y. T., S. L. Shapiro, Z. B. Etienne, and K. Taniguchi (2008), Phys. Rev. D **78**, 024012.
Livio, M., and P. Mazzali (2018), physrep **736**, 1, arXiv:1802.03125 [astro-ph.SR].
Lodders, K., H. Palme, and H.-P. Gail (2009), Landolt Börnstein , 44arXiv:0901.1149 [astro-ph.EP].
Loens, H., K. Langanke, G. Martínez-Pinedo, T. Rauscher, and F.-K. Thielemann (2008), Phys. Lett. B **666**, 395.
Loens, H. P., K. Langanke, G. Martínez-Pinedo, and K. Sieja (2012), Eur. Phys. J. A **48**, 34.
Lorusso, G., S. Nishimura, Z. Y. Xu, A. Jungclaus, Y. Shimizu, G. S. Simpson, P.-A. Söderström, H. Watanabe, F. Browne, P. Doornenbal, G. Gey, H. S. Jung, B. Meyer, T. Sumikama, J. Taprogge, Z. Vajta, J. Wu, H. Baba, G. Benzoni, K. Y. Chae, F. C. L. Crespi, N. Fukuda, R. Gernhäuser, N. Inabe, T. Isobe, T. Kajino, D. Kameda, G. D. Kim, Y.-K. Kim, I. Kojouharov, F. G. Kondev, T. Kubo, N. Kurz, Y. K. Kwon, G. J. Lane, Z. Li, A. Montaner-Pizá, K. Moschner, F. Naqvi, M. Niikura, H. Nishibata, A. Odahara, R. Orlandi, Z. Patel, Z. Podolyák, H. Sakurai, H. Schaffner, P. Schury, S. Shibagaki, K. Steiger, H. Suzuki, H. Takeda, A. Wendt, A. Yagi, and K. Yoshinaga (2015), Phys. Rev. Lett. **114**, 192501.
Ludwig, P., S. Bishop, R. Egli, V. Chernenko, B. Deneva, T. Faestermann, N. Famulok, L. Fimiani, J. M. Gómez-Guzmán, K. Hain, G. Korschinek, M. Hanzlik, S. Merchel, and G. Rugel (2016), Proceedings of the National Academy of Science **113**, 9232.
MacFadyen, A. I., and S. E. Woosley (1999), Astrophys. J. **524**, 262, astro-ph/9810274.
MacFadyen, A. I., S. E. Woosley, and A. Heger (2001), Astrophys. J. **550**, 410, astro-ph/9910034.
Malkus, A., J. P. Kneller, G. C. McLaughlin, and R. Surman (2012), Phys. Rev. D **86** (8), 085015, arXiv:1207.6648 [hep-ph].
Malkus, A., G. C. McLaughlin, and R. Surman (2016), Phys. Rev. D **93** (4), 045021, arXiv:1507.00946 [hep-ph].
Mamdouh, A., J. Pearson, M. Rayet, and F. Tondeur (2001), Nucl. Phys. A **679**, 337.
Maoz, D., F. Mannucci, and G. Nelemans (2014), Annu. Rev. Astron. Astrophys. **52**, 107, arXiv:1312.0628.
Margalit, B., and B. Metzger (2017), Astrophys. J. Lett. **850**, L19.
Marketin, T., L. Huther, and G. Martínez-Pinedo (2016a), Phys. Rev. C **93** (2), 025805, arXiv:1507.07442 [nucl-th].
Marketin, T., L. Huther, J. Petković, N. Paar, and G. Martínez-Pinedo (2016b), in *American Institute of Physics Conference Series*, American Institute of Physics Conference Series, Vol. 1743, p. 040006.
Marketin, T., D. Vretenar, and P. Ring (2007), Phys. Rev. C **75**, 024304.
Marshall, J., *et al.* (DES Collaboration) (2018), arXiv e-prints arXiv:1812.01022.
Martin, D., A. Arcones, W. Nazarewicz, and E. Olsen (2016), Phys. Rev. Lett. **116**, 121101.
Martin, D., A. Perego, A. Arcones, F.-K. Thielemann, O. Korobkin, and S. Rosswog (2015), Astrophys. J. **813**, 2, arXiv:1506.05048 [astro-ph.SR].
Martin, D., A. Perego, W. Kastaun, and A. Arcones (2018), Class. Quantum Gravity **35**, 034001.
Martin, W. C., R. Zalubas, and L. Hagan (1971), *Atomic Energy Levels - The Rare Earth Elements, Nat. Ref. Data Ser. 60* (National Bureau of Standards, Washington: US GPO).
Martínez-Pinedo, G., T. Fischer, and L. Huther (2014), J. Phys. G: Nucl. Part. Phys. **41**, 044008.

Martínez-Pinedo, G., T. Fischer, K. Langanke, A. Lohs, A. Sieverding, and M.-R. Wu (2016), "Neutrinos and Their Impact on Core-Collapse Supernova Nucleosynthesis," in *Handbook of Supernovae*, edited by A. W. Alsabti and P. Murdin (Springer International Publishing, Cham).
Martínez-Pinedo, G., T. Fischer, A. Lohs, and L. Huther (2012), Phys. Rev. Lett. **109**, 251104.
Martínez-Pinedo, G., D. Mocelj, N. Zinner, A. Kelić, K. Langankea, I. Panov, B. Pfeiffer, T. Rauscher, K.-H. Schmidt, and F.-K. Thielemann (2007), Prog. Part. Nucl. Phys. **59**, 199.
Mashonkina, L., N. Christlieb, and K. Eriksson (2014), Astron. & Astrophys. **569**, A43, arXiv:1407.5379 [astro-ph.SR].
Mathews, G. J., A. Mengoni, F.-K. Thielemann, and W. A. Fowler (1983), Astrophys. J. **270**, 740.
Matteucci, F. (2012), *Chemical Evolution of Galaxies*, Astronomy and Astrophysics Library (Springer-Verlag, Berlin Heidelberg).
Matteucci, F., and C. Chiappini (2001), New Astron. Rev. **45**, 567.
Matteucci, F., and L. Greggio (1986), Astron. & Astrophys. **154**, 279.
Matteucci, F., D. Romano, A. Arcones, O. Korobkin, and S. Rosswog (2014), Mon. Not. Roy. Astron. Soc. **438**, 2177, arXiv:1311.6980.
McConnell, J. R., and W. L. Talbert (1975), Nuclear Instruments and Methods **128**, 227.
McFadden, L., and G. R. Satchler (1966), Nucl. Phys. A **84**, 177.
McKinney, J. C., A. Tchekhovskoy, and R. D. Blandford (2013), Science **339**, 49, arXiv:1211.3651 [astro-ph.CO].
McLaughlin, G. C., J. M. Fetter, A. B. Balantekin, and G. M. Fuller (1999), Phys. Rev. C **59**, 2873.
McLaughlin, G. C., and R. Surman (2005), Nucl. Phys. A **758**, 189.
Mendoza-Temis, J. J. (2017), *Nuclear masses and their impact in r-process nucleosynthesis*, Ph.D. thesis (Technische Universität Darmstadt).
Mendoza-Temis, J. J., M.-R. Wu, K. Langanke, G. Martínez-Pinedo, A. Bauswein, and H.-T. Janka (2015), Phys. Rev. C **92**, 055805.
Mennekens, N., and D. Vanbeveren (2014), Astron. & Astrophys. **564**, A134, arXiv:1307.0959 [astro-ph.SR].
Mennekens, N., and D. Vanbeveren (2016), Astron. & Astrophys. **589**, A64, arXiv:1601.06966 [astro-ph.SR].
Mention, G., M. Fechner, T. Lasserre, T. Mueller, D. Lhuillier, *et al.* (2011), Phys. Rev. D **83**, 073006.
Merrill, P. W. (1952), Astrophys. J. **116**, 21.
Metzger, B. D. (2017a), Living Reviews in Relativity **20**, 3.
Metzger, B. D. (2017b), ArXiv e-prints arXiv:1710.05931 [astro-ph.HE].
Metzger, B. D., A. Arcones, E. Quataert, and G. Martínez-Pinedo (2010a), Mon. Not. Roy. Astron. Soc. **402**, 2771.
Metzger, B. D., A. Bauswein, S. Goriely, and D. Kasen (2015), Mon. Not. Roy. Astron. Soc. **446**, 1115.
Metzger, B. D., and E. Berger (2012), Astrophys. J. **746**, 48.
Metzger, B. D., and R. Fernández (2014), Mon. Not. Roy. Astron. Soc. **441**, 3444, arXiv:1402.4803 [astro-ph.HE].
Metzger, B. D., G. Martínez-Pinedo, S. Darbha, E. Quataert, A. Arcones, D. Kasen, R. Thomas, P. Nugent, I. V. Panov, and N. T. Zinner (2010b), Mon. Not. Roy. Astron. Soc. **406**, 2650.
Metzger, B. D., A. L. Piro, and E. Quataert (2009), Mon. Not. Roy. Astron. Soc. **396**, 304.
Metzger, B. D., T. A. Thompson, and E. Quataert (2008), Astrophys. J. **676**, 1130.
Metzger, B. D., T. A. Thompson, and E. Quataert (2018), Astrophys. J. **856**, 101.
Meyer, B. S. (1993), Phys. Rep. **227**, 257.
Meyer, B. S., G. J. Mathews, W. M. Howard, S. E. Woosley, and R. D. Hoffman (1992), Astrophys. J. **399**, 656.
Meyer, B. S., G. C. McLaughlin, and G. M. Fuller (1998), Phys. Rev. C **58**, 3696.
Meyer, B. S., and D. N. Schramm (1988), in *Origin and Distribution of the Elements*, edited by G. J. Mathews, p. 610.
Minchev, I., C. Chiappini, and M. Martig (2014), Astron. & Astrophys. **572**, A92, arXiv:1401.5796.
Mirizzi, A. (2015), prd **92** (10), 105020, arXiv:1506.06805 [hep-ph].
Mirizzi, A., G. Mangano, and N. Saviano (2015), Phys. Rev. D **92** (2), 021702, arXiv:1503.03485 [hep-ph].
Mirizzi, A., I. Tamborra, H.-T. Janka, N. Saviano, K. Scholberg, R. Bollig, L. Hüdepohl, and S. Chakraborty (2016), Nuovo Cimento Rivista Serie **39**, 1, arXiv:1508.00785 [astro-ph.HE].
Mocelj, D., T. Rauscher, G. Martínez-Pinedo, K. Langanke, L. Pacearescu, A. Faessler, F.-K. Thielemann, and Y. Alhassid (2007), Phys. Rev. C **75**, 045805.
Mohr, P., G. Gyürky, and Z. Fülöp (2017), Phys. Rev. C **95** (1), 015807, arXiv:1701.02290 [nucl-th].
Mohr, P., G. G. Kiss, Z. Fülöp, D. Galaviz, G. Gyürky, and E. Somorjai (2013), At. Data Nucl. Data Tables **99**, 651, arXiv:1212.2891 [nucl-ex].
Möller, P., W. D. Myers, H. Sagawa, and S. Yoshida (2012a), Phys. Rev. Lett. **108** (5), 052501.
Möller, P., J. R. Nix, and K.-L. Kratz (1997), At. Data. Nucl. Data Tables **66**, 131.
Möller, P., J. R. Nix, W. D. Myers, and W. J. Swiatecki (1995), At. Data Nucl. Data Tables **59**, 185.
Möller, P., B. Pfeiffer, and K.-L. Kratz (2003), Phys. Rev. C **67**, 055802.
Möller, P., B. Pfeiffer, and K.-L. Kratz (2003), Phys. Rev. C **67** (5), 055802.
Möller, P., A. J. Sierk, R. Bengtsson, H. Sagawa, and T. Ichikawa (2012b), At. Data Nucl. Data Tables **98**, 149.
Möller, P., A. J. Sierk, T. Ichikawa, A. Iwamoto, and M. Mumpower (2015), Phys. Rev. C **91** (2), 024310.
Möller, P., A. J. Sierk, T. Ichikawa, and H. Sagawa (2016), At. Data Nucl. Data Tables **109**, 1.
Montes, F., A. Estrade, P. T. Hosmer, S. N. Liddick, P. F. Mantica, A. C. Morton, W. F. Mueller, M. Ouellette, E. Pellegrini, P. Santi, H. Schatz, A. Stolz, B. E. Tomlin, O. Arndt, K.-L. Kratz, B. Pfeiffer, P. Reeder, W. B. Walters, A. Aprahamian, and A. Wöhr (2006), Phys. Rev. C **73** (3), 035801.
Montes, G., E. Ramirez-Ruiz, J. Naiman, S. Shen, and W. H. Lee (2016), Astrophys. J. **830**, 12.
Moore, C. E. (1971), *Atomic Energy Levels, Nat. Ref. Data Ser. 60* (National Bureau of Standards, Washington: US GPO).
Most, E. R., L. R. Weih, L. Rezzolla, and J. Schaffner-Bielich (2018), Phys. Rev. Lett. **120**, 261103.
Mösta, P., C. D. Ott, D. Radice, L. F. Roberts, E. Schnetter, and R. Haas (2015), Nature **528**, 376.
Mösta, P., S. Richers, C. D. Ott, R. Haas, A. L. Piro, K. Boydstun, E. Abdikamalov, C. Reisswig, and E. Schnetter

(2014), Astrophys. J. **785**, L29.
Mösta, P., L. F. Roberts, G. Halevi, C. D. Ott, J. Lippuner, R. Haas, and E. Schnetter (2018), Astrophys. J. **864**, 171, arXiv:1712.09370 [astro-ph.HE].
Mueller, E. (1986), Astron. & Astrophys. **162**, 103.
Müller, B. (2016), Publ. Astron. Soc. Austr. **33**, e048.
Müller, B., D. W. Gay, A. Heger, T. M. Tauris, and S. A. Sim (2018), Mon. Not. Roy. Astron. Soc. **479**, 3675, arXiv:1803.03388 [astro-ph.SR].
Mumpower, M. R., T. Kawano, T. M. Sprouse, N. Vassh, E. M. Holmbeck, R. Surman, and P. Moller (2018), ArXiv e-prints arXiv:1802.04398 [nucl-th].
Mumpower, M. R., T. Kawano, J. L. Ullmann, M. Krtička, and T. M. Sprouse (2017a), Phys. Rev. C **96** (2), 024612, arXiv:1706.07504 [nucl-th].
Mumpower, M. R., G. C. McLaughlin, R. Surman, and A. W. Steiner (2017b), Journal of Physics G Nuclear Physics **44** (3), 034003, arXiv:1609.09858 [nucl-th].
Mumpower, M. R., R. Surman, D.-L. Fang, M. Beard, P. Möller, T. Kawano, and A. Aprahamian (2015), Phys. Rev. C **92** (3), 035807, arXiv:1505.07789 [nucl-th].
Mumpower, M. R., R. Surman, G. C. McLaughlin, and A. Aprahamian (2016), Prog. Part. Nucl. Phys. **86**, 86.
Münzel, J., H. Wollnik, B. Pfeiffer, and G. Jung (1981), Nuclear Instruments and Methods in Physics Research **186**, 343.
Mustafa, M. G., M. Blann, A. V. Ignatyuk, and S. M. Grimes (1992), Phys. Rev. C **45**, 1078.
Mustonen, M. T., and J. Engel (2016), Phys. Rev. C **93** (1), 014304, arXiv:1510.02136 [nucl-th].
Myers, W. D., and W. J. Świaţecki (1999), Phys. Rev. C **60**, 014606.
Nadyozhin, D. K., and I. V. Panov (2007), Astronomy Letters **33**, 385.
Nagataki, S. (2011), International Journal of Modern Physics D **20**, 1975.
Nagataki, S., R. Takahashi, A. Mizuta, and T. Takiwaki (2007), Astrophys. J. **659**, 512, astro-ph/0608233.
Nakada, H., and Y. Alhassid (1997), Phys. Rev. Lett. **79**, 2939.
Nakamura, K., T. Kajino, G. J. Mathews, S. Sato, and S. Harikae (2015), Astron. & Astrophys. **582**, A34.
Nakamura, T., H. Umeda, K. Iwamoto, K. Nomoto, M.-a. Hashimoto, W. R. Hix, and F.-K. Thielemann (2001), Astrophys. J. **555**, 880, astro-ph/0011184.
Nakar, E. (2007), Phys. Rep. **442**, 166.
Neufcourt, L., Y. Cao, W. Nazarewicz, and F. Viens (2018), Phys. Rev. C **98**, 034318.
Nicholl, M., E. Berger, D. Kasen, B. D. Metzger, J. Elias, C. Briceño, K. D. Alexander, P. K. Blanchard, R. Chornock, P. S. Cowperthwaite, T. Eftekhari, W. Fong, R. Margutti, V. A. Villar, P. K. G. Williams, W. Brown, J. Annis, A. Bahramian, D. Brout, D. A. Brown, H.-Y. Chen, J. C. Clemens, E. Dennihy, B. Dunlap, D. E. Holz, E. Marchesini, F. Massaro, N. Moskowitz, I. Pelisoli, A. Rest, F. Ricci, M. Sako, M. Soares-Santos, and J. Strader (2017a), Astrophys. J. Lett. **848**, L18.
Nicholl, M., J. Guillochon, and E. Berger (2017b), Astrophys. J. **850**, 55, arXiv:1706.00825 [astro-ph.HE].
Nishimura, N., T. Rauscher, R. Hirschi, A. S. J. Murphy, G. Cescutti, and C. Travaglio (2018), Mon. Not. Roy. Astron. Soc. **474**, 3133, arXiv:1711.09098 [astro-ph.SR].
Nishimura, N., H. Sawai, T. Takiwaki, S. Yamada, and F.-K. Thielemann (2017), Astrophys. J. **836**, L21.
Nishimura, N., T. Takiwaki, and F.-K. Thielemann (2015a), Astrophys. J. **810**, 109, arXiv:1501.06567 [astro-ph.SR].
Nishimura, N., T. Takiwaki, and F.-K. Thielemann (2015b), Astrophys. J. **810**, 109, arXiv:1501.06567 [astro-ph.SR].
Nishimura, S., K. Kotake, M.-a. Hashimoto, S. Yamada, N. Nishimura, S. Fujimoto, and K. Sato (2006), Astrophys. J. **642**, 410, astro-ph/0504100.
Nolden, F., P. Hülsmann, Y. A. Litvinov, P. Moritz, C. Peschke, P. Petri, M. S. Sanjari, M. Steck, H. Weick, J. X. Wu, Y. D. Zang, S. H. Zhang, and T. C. Zhao (2011), Nuclear Instruments and Methods in Physics Research A **659**, 69.
Nomoto, K. (2017), "Nucleosynthesis in Hypernovae Associated with Gamma-Ray Bursts," in *Handbook of Supernovae, ISBN 978-3-319-21845-8. Springer International Publishing AG, 2017, p. 1931*, edited by A. W. Alsabti and P. Murdin, p. 1931.
Nomoto, K., C. Kobayashi, and N. Tominaga (2013), Annu. Rev. Astron. Astrophys. **51**, 457.
Nomoto, K., and S.-C. Leung (2017a), "Electron Capture Supernovae from Super Asymptotic Giant Branch Stars," in *Handbook of Supernovae*, edited by A. W. Alsabti and P. Murdin (Springer International Publishing, Cham).
Nomoto, K., and S.-C. Leung (2017b), "Thermonuclear Explosions of Chandrasekhar Mass White Dwarfs," in *Handbook of Supernovae*, edited by A. W. Alsabti and P. Murdin (Springer International Publishing, Cham).
Nomoto, K., F.-K. Thielemann, and S. Miyaji (1985), Astron. & Astrophys. **149**, 239.
Nomoto, K., N. Tominaga, H. Umeda, C. Kobayashi, and K. Maeda (2006), Nuclear Physics A **777**, 424, astro-ph/0605725.
Nunokawa, H., J. T. Peltoniemi, A. Rossi, and J. W. F. Valle (1997), Phys. Rev. D **56**, 1704.
Obergaulinger, M., M. A. Aloy, and E. Müller (2010), Astron. & Astrophys. **515**, A30.
Obergaulinger, M., O. Just, and M. A. Aloy (2018), J. Phys. G: Nucl. Part. Phys. **45**, 084001.
Oechslin, R., H.-T. Janka, and A. Marek (2007), Astron. & Astrophys. **467**, 395, astro-ph/0611047.
Oechslin, R., S. Rosswog, and F.-K. Thielemann (2002), Phys. Rev. D **65**, 103005.
Oechslin, R., K. Uryū, G. Poghosyan, and F. K. Thielemann (2004), Mon. Not. Roy. Astron. Soc. **349**, 1469.
Oertel, M., M. Hempel, T. Klähn, and S. Typel (2017), Rev. Mod. Phys. **89**, 015007.
Ojima, T., Y. Ishimaru, S. Wanajo, N. Prantzos, and P. François (2018), Astrophys. J. **865**, 87, arXiv:1808.03390.
Ono, M., M. Hashimoto, S. Fujimoto, K. Kotake, and S. Yamada (2012), Prog. Theor. Phys. **128**, 741.
Orford, R., N. Vassh, J. A. Clark, G. C. McLaughlin, M. R. Mumpower, G. Savard, R. Surman, A. Aprahamian, F. Buchinger, M. T. Burkey, D. A. Gorelov, T. Y. Hirsh, J. W. Klimes, G. E. Morgan, A. Nystrom, and K. S. Sharma (2018), Phys. Rev. Lett. **120**, 262702.
Ormand, W. E. (1997), Phys. Rev. C **56**, R1678.
Otsuki, K., A. Burrows, G. Martinez-Pinedo, S. Typel, K. Langanke, and M. Matos (2010), in *American Institute of Physics Conference Series*, American Institute of Physics Conference Series, Vol. 1238, edited by H. Susa, M. Arnould, S. Gales, T. Motobayashi, C. Scheidenberger, and H. Utsunomiya, pp. 240–242.

Otsuki, K., H. Tagoshi, T. Kajino, and S. Wanajo (2000), Astrophys. J. **533**, 424.
Özel, F., and P. Freire (2016), Annu. Rev. Astron. Astrophys. **54**, 401.
Özen, C., Y. Alhassid, and H. Nakada (2015), Phys. Rev. C **91** (3), 034329.
Pagel, B. E. J. (2009), *Nucleosynthesis and Chemical Evolution of Galaxies, by Bernard E. J. Pagel, Cambridge, UK: Cambridge University Press, 2009*.
Pain, S. D., J. A. Cizewski, R. Hatarik, K. L. Jones, J. S. Thomas, D. W. Bardayan, J. C. Blackmon, C. D. Nesaraja, M. S. Smith, R. L. Kozub, and M. S. Johnson (2007), Nuclear Instruments and Methods in Physics Research B **261**, 1122.
Palenzuela, C., S. L. Liebling, D. Neilsen, L. Lehner, O. L. Caballero, E. O'Connor, and M. Anderson (2015), Phys. Rev. D **92**, 044045.
Pan, K.-C., M. Liebendörfer, S. M. Couch, and F.-K. Thielemann (2018a), Astrophys. J. **857**, 13, arXiv:1710.01690 [astro-ph.HE].
Pan, K.-C., C. Mattes, E. P. O'Connor, S. M. Couch, A. Perego, and A. Arcones (2018b), ArXiv e-prints arXiv:1806.10030 [astro-ph.HE].
Panov, I. V., E. Kolbe, B. Pfeiffer, T. Rauscher, K.-L. Kratz, and F.-K. Thielemann (2005), Nucl. Phys. A **747**, 633, astro-ph/0412654.
Panov, I. V., I. Y. Korneev, Y. S. Lutostansky, and F.-K. Thielemann (2013), Phys. Atom. Nuclei **76**, 88.
Panov, I. V., I. Y. Korneev, T. Rauscher, G. Martínez-Pinedo, A. Kelić-Heil, N. T. Zinner, and F. Thielemann (2010), Astron. & Astrophys. **513**, A61.
Panov, I. V., I. Y. Korneev, and F.-K. Thielemann (2008), Astronomy Letters **34**, 189.
Panov, I. V., Y. S. Lutostansky, M. Eichler, and F.-K. Thielemann (2017), Phys. Atom. Nuclei **80**, 657.
Panov, I. V., Y. S. Lutostansky, and F.-K. Thielemann (2016), Nucl. Phys. A **947**, 1.
Panov, I. V., and F.-K. Thielemann (2004), Astronomy Letters **30**, 647.
Papenfort, L. J., R. Gold, and L. Rezzolla (2018), Phys. Rev. D **98**, 104028.
Perego, A., D. Radice, and S. Bernuzzi (2017a), Astrophys. J. **850**, L37.
Perego, A., S. Rosswog, R. M. Cabezón, O. Korobkin, R. Käppeli, A. Arcones, and M. Liebendörfer (2014), Mon. Not. Roy. Astron. Soc. **443**, 3134, arXiv:1405.6730 [astro-ph.HE].
Perego, A., H. Yasin, and A. Arcones (2017b), J. Phys. G: Nucl. Part. Phys. **44**, 084007.
Pereira, J., S. Hennrich, A. Aprahamian, O. Arndt, A. Becerril, T. Elliot, A. Estrade, D. Galaviz, R. Kessler, K.-L. Kratz, G. Lorusso, P. F. Mantica, M. Matos, P. Möller, F. Montes, B. Pfeiffer, H. Schatz, F. Schertz, L. Schnorrenberger, E. Smith, A. Stolz, M. Quinn, W. B. Walters, and A. Wöhr (2009), Phys. Rev. C **79** (3), 035806, arXiv:0902.1705 [nucl-ex].
Pereira, J., P. Hosmer, G. Lorusso, P. Santi, A. Couture, J. Daly, M. Del Santo, T. Elliot, J. Görres, C. Herlitzius, K.-L. Kratz, L. O. Lamm, H. Y. Lee, F. Montes, M. Ouellette, E. Pellegrini, P. Reeder, H. Schatz, F. Schertz, L. Schnorrenberger, K. Smith, E. Stech, E. Strandberg, C. Ugalde, M. Wiescher, and A. Wöhr (2010), Nucl. Instruments Methods Phys. Res. Sect. A Accel. Spectrometers, Detect. Assoc. Equip. **618**, 275.
Petermann, I., K. Langanke, G. Martínez-Pinedo, I. V. Panov, P.-G. Reinhard, and F.-K. Thielemann (2012), Eur. Phys. J. A **48**, 122.
Pfeiffer, B., K.-L. Kratz, F.-K. Thielemann, and W. B. Walters (2001), Nucl. Phys. A **693**, 282.
Pian, E., *et al.* (2017), Nature **551**, 67.
Pinto, P. A., and R. G. Eastman (2000a), Astrophys. J. **530**, 744.
Pinto, P. A., and R. G. Eastman (2000b), Astrophys. J. **530**, 757.
Piran, T. (2004), Rev. Mod. Phys. **76**, 1143.
Piran, T., E. Nakar, and S. Rosswog (2013), Mon. Not. Roy. Astron. Soc. **430**, 2121.
Pitrou, C., A. Coc, J.-P. Uzan, and E. Vangioni (2018), Phys. Rep. **754**, 1.
Placco, V. M., E. M. Holmbeck, A. Frebel, T. C. Beers, R. A. Surman, A. P. Ji, R. Ezzeddine, S. D. Points, C. C. Kaleida, T. T. Hansen, C. M. Sakari, and A. R. Casey (2017), Astrophys. J. **844**, 18, arXiv:1706.02934 [astro-ph.SR].
Pllumbi, E., I. Tamborra, S. Wanajo, H. T. Janka, and L. Hüdepohl (2015), Astrophys. J. **808**, 188.
Potel, G., F. M. Nunes, and I. J. Thompson (2015), Phys. Rev. C **92** (3), 034611.
Price, D. J., and S. Rosswog (2006), Science **312**, 719.
Pruet, J., R. D. Hoffman, S. E. Woosley, H.-T. Janka, and R. Buras (2006), Astrophys. J. **644**, 1028.
Pruet, J., T. A. Thompson, and R. D. Hoffman (2004), Astrophys. J. **606**, 1006, astro-ph/0309278.
Pruet, J., S. E. Woosley, and R. D. Hoffman (2003), Astrophys. J. **586**, 1254, astro-ph/0209412.
Qian, Y.-Z. (2014), J. Phys. G: Nucl. Part. Phys. **41**, 044002.
Qian, Y. Z., W. C. Haxton, K. Langanke, and P. Vogel (1997), Phys. Rev. C **55**, 1532.
Qian, Y.-Z., P. Vogel, and G. J. Wasserburg (1998), Astrophys. J. **506**, 868.
Qian, Y.-Z., P. Vogel, and G. J. Wasserburg (1999), Astrophys. J. **524**, 213.
Qian, Y.-Z., and G. J. Wasserburg (2007), Phys. Rep. **442**, 237.
Qian, Y.-Z., and S. E. Woosley (1996), Astrophys. J. **471**, 331.
Quinn, M., A. Aprahamian, J. Pereira, R. Surman, O. Arndt, T. Baumann, A. Becerril, T. Elliot, A. Estrade, D. Galaviz, T. Ginter, M. Hausmann, S. Hennrich, R. Kessler, K.-L. Kratz, G. Lorusso, P. F. Mantica, M. Matos, F. Montes, B. Pfeiffer, M. Portillo, H. Schatz, F. Schertz, L. Schnorrenberger, E. Smith, A. Stolz, W. B. Walters, and A. Wöhr (2012), Phys. Rev. C **85** (3), 035807, arXiv:1112.5055 [nucl-ex].
Radice, D., F. Galeazzi, J. Lippuner, L. F. Roberts, C. D. Ott, and L. Rezzolla (2016), Mon. Not. Roy. Astron. Soc. **460**, 3255.
Radice, D., A. Perego, K. Hotokezaka, S. Bernuzzi, S. A. Fromm, and L. F. Roberts (2018a), ArXiv e-prints arXiv:1809.11163 [astro-ph.HE].
Radice, D., A. Perego, K. Hotokezaka, S. A. Fromm, S. Bernuzzi, and L. F. Roberts (2018b), ArXiv e-prints arXiv:1809.11161 [astro-ph.HE].
Radon, T., H. Geissel, G. Münzenberg, B. Franzke, T. Kerscher, F. Nolden, Y. N. Novikov, Z. Patyk, C. Scheidenberger, F. Attallah, K. Beckert, T. Beha, F. Bosch, H. Eickhoff, M. Falch, Y. Fujita, M. Hausmann, F. Herfurth, H. Irnich, H. C. Jung, O. Klepper, C. Kozhuharov, Y. A. Litvinov, K. E. G. Löbner, F. Nickel, H. Reich, W. Schwab,

B. Schlitt, M. Steck, K. Sümmerer, T. Winkler, and H. Wollnik (2000), Nucl. Phys. A **677**, 75.
Raman, S., B. Fogelberg, J. A. Harvey, R. L. Macklin, P. H. Stelson, A. Schröder, and K.-L. Kratz (1983), Phys. Rev. C **28**, 602.
Ramirez-Ruiz, E., M. Trenti, M. MacLeod, L. F. Roberts, W. H. Lee, and M. I. Saladino-Rosas (2015), Astrophys. J. **802**, L22.
Rauscher, T. (2011), International Journal of Modern Physics E **20**, 1071, arXiv:1010.4283 [nucl-th].
Rauscher, T. (2013), Phys. Rev. C **88** (3), 035803, arXiv:1308.5816 [astro-ph.SR].
Rauscher, T., N. Dauphas, I. Dillmann, C. Fröhlich, Z. Fülöp, and G. Gyürky (2013), Reports on Progress in Physics **76** (6), 066201, arXiv:1303.2666 [astro-ph.SR].
Rauscher, T., and F.-K. Thielemann (2000), At. Data Nucl. Data Tables **75**, 1, astro-ph/0004059.
Rauscher, T., and F.-K. Thielemann (2001), At. Data Nucl. Data Tables **79**, 47, nucl-th/0104003.
Rauscher, T., F.-K. Thielemann, and K.-L. Kratz (1997), Phys. Rev. C **56**, 1613.
Ravn, H. L., S. Sundell, and L. Westgaard (1975), Nuclear Instruments and Methods **123**, 131.
Recchi, S., F. Calura, and P. Kroupa (2009), Astron. & Astrophys. **499**, 711, arXiv:0903.2395.
Recchi, S., F. Matteucci, and A. D'Ercole (2001), Mon. Not. Roy. Astron. Soc. **322**, 800, astro-ph/0002370.
Reddy, B. E., D. L. Lambert, and C. Allende Prieto (2006), Mon. Not. Roy. Astron. Soc. **367**, 1329, astro-ph/0512505.
Reddy, B. E., J. Tomkin, D. L. Lambert, and C. Allende Prieto (2003), Mon. Not. Roy. Astron. Soc. **340**, 304, astro-ph/0211551.
Rehse, S. J., R. Li, T. J. Scholl, A. Sharikova, R. Chatelain, R. A. Holt, and S. D. Rosner (2006), Canadian Journal of Physics **84**, 723.
Reifarth, R., K. Göbel, T. Heftrich, M. Weigand, B. Jurado, F. Käppeler, and Y. A. Litvinov (2017), Phys. Rev. Accel. Beams **20**, 044701.
Reifarth, R., C. Lederer, and F. Käppeler (2014), Journal of Physics G Nuclear Physics **41**, 053101, arXiv:1403.5670 [astro-ph.IM].
Reifarth, R., and Y. A. Litvinov (2014), Physical Review Accelerators and Beams **17** (1), 014701, arXiv:1312.3714 [nucl-ex].
Reiter, M. P., S. Ayet San Andrés, J. Lippuner, S. Nikas, C. Andreoiu, C. Babcock, B. R. Barquest, J. Bollig, T. Brunner, T. Dickel, J. Dilling, I. Dillmann, E. Dunling, G. Gwinner, L. Graham, C. Hornung, R. Klawitter, B. Kootte, A. A. Kwiatkowski, Y. Lan, D. Lascar, K. G. Leach, E. Leistenschneider, G. Martínez-Pinedo, J. E. McKay, S. F. Paul, W. R. Plaß, L. Roberts, H. Schatz, C. Scheidenberger, A. Sieverding, R. Steinbrügge, R. Thompson, M. E. Wieser, C. Will, and D. Welch (2018), arXiv e-prints arXiv:1810.11561 [nucl-ex].
Rembges, F., C. Freiburghaus, T. Rauscher, F.-K. Thielemann, H. Schatz, and M. Wiescher (1997), Astrophys. J. **484**, 412, astro-ph/9701217.
Renaud, M., J. Vink, A. Decourchelle, F. Lebrun, P. R. den Hartog, R. Terrier, C. Couvreur, J. Knödlseder, P. Martin, N. Prantzos, A. M. Bykov, and H. Bloemen (2006), Astrophys. J. Lett. **647**, L41.
Rezzolla, L., E. R. Most, and L. R. Weih (2018), Astrophys. J. **852**, L25.
Richers, S., H. Nagakura, C. D. Ott, J. Dolence, K. Sumiyoshi, and S. Yamada (2017), Astrophys. J. **847**, 133, arXiv:1706.06187 [astro-ph.HE].
Ripley, J. L., B. D. Metzger, A. Arcones, and G. Martínez-Pinedo (2014), Mon. Not. Roy. Astron. Soc. **438**, 3243.
Roberts, L. F. (2012), Astrophys. J. **755**, 126.
Roberts, L. F., D. Kasen, W. H. Lee, and E. Ramirez-Ruiz (2011), Astrophys. J. **736**, L21.
Roberts, L. F., J. Lippuner, M. D. Duez, J. A. Faber, F. Foucart, J. C. Lombardi, Jr., S. Ning, C. D. Ott, and M. Ponce (2017), Mon. Not. Roy. Astron. Soc. **464**, 3907.
Roberts, L. F., and S. Reddy (2017), Phys. Rev. C **95**, 045807.
Roberts, L. F., S. Reddy, and G. Shen (2012), Phys. Rev. C **86**, 065803.
Roberts, L. F., G. Shen, V. Cirigliano, J. A. Pons, S. Reddy, and S. E. Woosley (2012), Phys. Rev. Lett. **108**, 061103.
Roberts, L. F., S. E. Woosley, and R. D. Hoffman (2010), Astrophys. J. **722**, 954.
Rodríguez, T. R., A. Arzhanov, and G. Martínez-Pinedo (2015), Phys. Rev. C **91**, 044315.
Roederer, I. U. (2013), Astron. J. **145**, 26.
Roederer, I. U. (2017), Astrophys. J. **835**, 23, arXiv:1611.05886.
Roederer, I. U., J. J. Cowan, A. I. Karakas, K.-L. Kratz, M. Lugaro, J. Simmerer, K. Farouqi, and C. Sneden (2010a), Astrophys. J. **724**, 975, arXiv:1009.4496 [astro-ph.SR].
Roederer, I. U., A. I. Karakas, M. Pignatari, and F. Herwig (2016), Astrophys. J. **821**, 37, arXiv:1603.00036 [astro-ph.SR].
Roederer, I. U., K.-L. Kratz, A. Frebel, N. Christlieb, B. Pfeiffer, J. J. Cowan, and C. Sneden (2009), Astrophys. J. **698**, 1963, arXiv:0904.3105 [astro-ph.SR].
Roederer, I. U., and J. E. Lawler (2012), Astrophys. J. **750**, 76, arXiv:1204.3901 [astro-ph.SR].
Roederer, I. U., J. E. Lawler, J. J. Cowan, T. C. Beers, A. Frebel, I. I. Ivans, H. Schatz, J. S. Sobeck, and C. Sneden (2012), Astrophys. J. Suppl. **747**, L8, arXiv:1202.2378 [astro-ph.SR].
Roederer, I. U., H. Schatz, J. E. Lawler, T. C. Beers, J. J. Cowan, A. Frebel, I. I. Ivans, C. Sneden, and J. S. Sobeck (2014), Astrophys. J. **791**, 32, arXiv:1406.4554 [astro-ph.SR].
Roederer, I. U., C. Sneden, J. E. Lawler, and J. J. Cowan (2010b), Astrophys. J. **714**, L123, arXiv:1003.4522 [astro-ph.SR].
Rolfs, C., and W. Rodney (1988), *Cauldrons in the Cosmos: Nuclear Astrophysics* (University of Chicago Press, Chicago).
Rosswog, S. (2005), Astrophys. J. **634**, 1202, astro-ph/0508138.
Rosswog, S. (2007), Mon. Not. Roy. Astron. Soc. **376**, L48.
Rosswog, S. (2015), Int. J. Mod. Phys. D **24**, 1530012.
Rosswog, S., M. B. Davies, F.-K. Thielemann, and T. Piran (2000), Astron. & Astrophys. **360**, 171.
Rosswog, S., U. Feindt, O. Korobkin, M.-R. Wu, J. Sollerman, A. Goobar, and G. Martinez-Pinedo (2017), Class. Quantum Gravity **34** (10), 104001.
Rosswog, S., O. Korobkin, A. Arcones, F.-K. Thielemann, and T. Piran (2014), Mon. Not. Roy. Astron. Soc. **439**, 744.
Rosswog, S., M. Liebendörfer, F.-K. Thielemann, M. B. Davies, W. Benz, and T. Piran (1999), Astron. & Astrophys. **341**, 499, astro-ph/9811367.

Rosswog, S., J. Sollerman, U. Feindt, A. Goobar, O. Korobkin, R. Wollaeger, C. Fremling, and M. M. Kasliwal (2018), Astron. & Astrophys. **615**, A132.
Rrapaj, E., J. W. Holt, A. Bartl, S. Reddy, and A. Schwenk (2015), Phys. Rev. C **91**, 035806.
Ruffert, M., and H.-T. Janka (2001), Astron. & Astrophys. **380**, 544.
Ruffert, M., H.-T. Janka, and G. Schaefer (1996), Astron. & Astrophys. **311**, 532, astro-ph/9509006.
Ruffert, M., H.-T. Janka, K. Takahashi, and G. Schaefer (1997), Astron. & Astrophys. **319**, 122.
Ruiz, M., S. L. Shapiro, and A. Tsokaros (2018), Phys. Rev. D **97**, 021501.
Sadhukhan, J., K. Mazurek, A. Baran, J. Dobaczewski, W. Nazarewicz, and J. A. Sheikh (2013), Phys. Rev. C **88**, 064314.
Sadhukhan, J., W. Nazarewicz, and N. Schunck (2016), Phys. Rev. C **93** (1), 011304, arXiv:1510.08003 [nucl-th].
Sagert, I., T. Fischer, M. Hempel, G. Pagliara, J. Schaffner-Bielich, A. Mezzacappa, F.-K. Thielemann, and M. Liebendörfer (2009), Phys. Rev. Lett. **102** (8), 081101, arXiv:0809.4225.
Salih, S., and J. E. Lawler (1983), Phys Rev A **28**, 3653.
Sato, K. (1974), Progress of Theoretical Physics **51**, 726.
Schäfer, F. P., W. Schmidt, and J. Volze (1966), Applied Physics Letters **9**, 306.
Schatz, H., R. Toenjes, B. Pfeiffer, T. C. Beers, J. J. Cowan, V. Hill, and K.-L. Kratz (2002), Astrophys. J. **579**, 626, astro-ph/0104335.
Schiller, A., L. Bergholt, M. Guttormsen, E. Melby, J. Rekstad, and S. Siem (2000), Nuclear Instruments and Methods in Physics Research A **447**, 498, nucl-ex/9910009.
Schmidt, K.-H., and B. Jurado (2018), Rep. Prog. Phys. **81**, 106301.
Schmidt, K.-H. H., B. Jurado, C. Amouroux, and C. Schmitt (2016), Nucl. Data Sheets **131**, 107.
Schmitt, C., K.-H. Schmidt, and B. Jurado (2018), Phys. Rev. C **98**, 044605.
Schramm, D. N. (1973), Astrophys. J. **185**, 293.
Schramm, D. N., and G. J. Wasserburg (1970), Astrophys. J. **162**, 57.
Schwengner, R., S. Frauendorf, and B. A. Brown (2017), Phys. Rev. Lett. **118** (9), 092502.
Schwengner, R., S. Frauendorf, and A. C. Larsen (2013), Phys. Rev. Lett. **111** (23), 232504, arXiv:1310.7667 [nucl-th].
Seeger, P. A., W. A. Fowler, and D. D. Clayton (1965), Astrophys. J. Suppl. **11**, 121.
Seitenzahl, I., and D. Townsley (2017), "Nucleosynthesis in Thermonuclear Supernovae," in *Handbook of Supernovae*, edited by A. W. Alsabti and P. Murdin (Springer International Publishing, Cham).
Seitenzahl, I. R., F. X. Timmes, and G. Magkotsios (2014), Astrophys. J. **792**, 10.
Sekiguchi, Y., K. Kiuchi, K. Kyutoku, and M. Shibata (2011), Phys. Rev. Lett. **107**, 051102.
Sekiguchi, Y., K. Kiuchi, K. Kyutoku, and M. Shibata (2015), Phys. Rev. D **91** (6), 064059, arXiv:1502.06660 [astro-ph.HE].
Sekiguchi, Y., K. Kiuchi, K. Kyutoku, M. Shibata, and K. Taniguchi (2016), Phys. Rev. D **93** (12), 124046, arXiv:1603.01918 [astro-ph.HE].
Sekiguchi, Y., and M. Shibata (2011), Astrophys. J. **737**, 6, arXiv:1009.5303 [astro-ph.HE].
Shafer, T., J. Engel, C. Fröhlich, G. C. McLaughlin, M. Mumpower, and R. Surman (2016), Phys. Rev. C **94**, 055802.
Shen, S., R. J. Cooke, E. Ramirez-Ruiz, P. Madau, L. Mayer, and J. Guedes (2015), Astrophys. J. **807**, 115, arXiv:1407.3796.
Shetrone, M., K. A. Venn, E. Tolstoy, F. Primas, V. Hill, and A. Kaufer (2003), aj **125**, 684, astro-ph/0211167.
Shetrone, M. D., M. Bolte, and P. B. Stetson (1998), aj **115**, 1888.
Shibagaki, S., T. Kajino, G. J. Mathews, S. Chiba, S. Nishimura, and G. Lorusso (2016), apj **816**, 79, arXiv:1505.02257 [astro-ph.SR].
Shibata, M. (2018), "Mass ejection from neutron star mergers," Talk at the EMMI Rapid Reaction Task Force: The physics of neitron star mergers at GSI/FAIR.
Shibata, M., S. Fujibayashi, K. Hotokezaka, K. Kiuchi, K. Kyutoku, Y. Sekiguchi, and M. Tanaka (2017), Phys. Rev. D **96**, 123012.
Shibata, M., and K. Taniguchi (2011), Living Reviews in Relativity **14**, 6.
Shibata, M., and K. Uryū (2006), Phys. Rev. D **74**, 121503.
Shibata, M., and K. b. o. Uryū (2000), Phys. Rev. D **61**, 064001.
Siegel, D. M., J. Barnes, and B. D. Metzger (2018), ArXiv e-prints arXiv:1810.00098 [astro-ph.HE].
Siegel, D. M., and B. D. Metzger (2017), Phys. Rev. Lett. **119**, 231102.
Siegel, D. M., and B. D. Metzger (2018), Astrophys. J. **858**, 52.
Sieja, K. (2017), Phys. Rev. Lett. **119** (5), 052502.
Sieja, K. (2018), Phys. Rev. C **98**, 064312.
Sieverding, A., G. Martínez-Pinedo, L. Huther, K. Langanke, and A. Heger (2018), Astrophys. J. **865**, 143.
Simmerer, J., C. Sneden, J. J. Cowan, J. Collier, V. M. Woolf, and J. E. Lawler (2004), Astrophys. J. **617**, 1091, astro-ph/0410396.
Siqueira Mello, C., M. Spite, B. Barbuy, F. Spite, E. Caffau, V. Hill, S. Wanajo, F. Primas, B. Plez, R. Cayrel, J. Andersen, B. Nordström, C. Sneden, T. C. Beers, P. Bonifacio, P. François, and P. Molaro (2013), Astron. & Astrophys. **550**, A122, arXiv:1212.0211 [astro-ph.SR].
Smartt, S. J., T.-W. Chen, A. Jerkstrand, M. Coughlin, E. Kankare, S. A. Sim, M. Fraser, C. Inserra, K. Maguire, K. C. Chambers, M. E. Huber, T. Krühler, G. Leloudas, M. Magee, L. J. Shingles, K. W. Smith, D. R. Young, J. Tonry, R. Kotak, A. Gal-Yam, J. D. Lyman, D. S. Homan, C. Agliozzo, J. P. Anderson, C. R. Angus, C. Ashall, C. Barbarino, F. E. Bauer, M. Berton, M. T. Botticella, M. Bulla, J. Bulger, G. Cannizzaro, Z. Cano, R. Cartier, A. Cikota, P. Clark, A. De Cia, M. Della Valle, L. Denneau, M. Dennefeld, L. Dessart, G. Dimitriadis, N. Elias-Rosa, R. E. Firth, H. Flewelling, A. Flörs, A. Franckowiak, C. Frohmaier, L. Galbany, S. González-Gaitán, J. Greiner, M. Gromadzki, A. N. Guelbenzu, C. P. Gutiérrez, A. Hamanowicz, L. Hanlon, J. Harmanen, K. E. Heintz, A. Heinze, M.-S. Hernandez, S. T. Hodgkin, I. M. Hook, L. Izzo, P. A. James, P. G. Jonker, W. E. Kerzendorf, S. Klose, Z. Kostrzewa-Rutkowska, M. Kowalski, M. Kromer, H. Kuncarayakti, A. Lawrence, T. B. Lowe, E. A. Magnier, I. Manulis, A. Martin-Carrillo, S. Mattila, O. McBrien, A. Müller, J. Nordin, D. O'Neill, F. Onori, J. T. Palmerio, A. Pastorello, F. Patat, G. Pignata, P. Podsiadlowski, M. L. Pumo, S. J. Prentice, A. Rau, A. Razza,

A. Rest, T. Reynolds, R. Roy, A. J. Ruiter, K. A. Rybicki, L. Salmon, P. Schady, A. S. B. Schultz, T. Schweyer, I. R. Seitenzahl, M. Smith, J. Sollerman, B. Stalder, C. W. Stubbs, M. Sullivan, H. Szegedi, F. Taddia, S. Taubenberger, G. Terreran, B. van Soelen, J. Vos, R. J. Wainscoat, N. A. Walton, C. Waters, H. Weiland, M. Willman, P. Wiseman, D. E. Wright, Ł. Wyrzykowski, and O. Yaron (2017), Nature **551**, 75, arXiv:1710.05841 [astro-ph.HE].

Sneden, C., and J. J. Cowan (2003), Sience **299** (5603), 70.

Sneden, C., J. J. Cowan, and R. Gallino (2008), Annu. Rev. Astron. Astrophys. **46**, 241.

Sneden, C., J. J. Cowan, J. E. Lawler, I. I. Ivans, S. Burles, T. C. Beers, F. Primas, V. Hill, J. W. Truran, G. M. Fuller, B. Pfeiffer, and K.-L. Kratz (2003), Astrophys. J. **591**, 936, astro-ph/0303542.

Sneden, C., J. E. Lawler, J. J. Cowan, I. I. Ivans, and E. A. Den Hartog (2009), Astrophys. J. Suppl. **182**, 80.

Sneden, C., A. McWilliam, G. W. Preston, J. J. Cowan, D. L. Burris, and B. J. Armosky (1996), Astrophys. J. **467**, 819.

Sneden, C., and M. Parthasarathy (1983), Astrophys. J. **267**, 757.

Sneden, C., G. W. Preston, A. McWilliam, and L. Searle (1994), Astrophys. J. Lett. **431**, L27.

Soares-Santos, M., D. E. Holz, J. Annis, R. Chornock, K. Herner, E. Berger, D. Brout, H.-Y. Chen, R. Kessler, M. Sako, S. Allam, D. L. Tucker, R. E. Butler, A. Palmese, Z. Doctor, H. T. Diehl, J. Frieman, B. Yanny, H. Lin, D. Scolnic, P. Cowperthwaite, E. Neilsen, J. Marriner, N. Kuropatkin, W. G. Hartley, F. Paz-Chinchón, K. D. Alexander, E. Balbinot, P. Blanchard, D. A. Brown, J. L. Carlin, C. Conselice, E. R. Cook, A. Drlica-Wagner, M. R. Drout, F. Durret, T. Eftekhari, B. Farr, D. A. Finley, R. J. Foley, W. Fong, C. L. Fryer, J. García-Bellido, M. S. S. Gill, R. A. Gruendl, C. Hanna, D. Kasen, T. S. Li, P. A. A. Lopes, A. C. C. Lourenço, R. Margutti, J. L. Marshall, T. Matheson, G. E. Medina, B. D. Metzger, R. R. Muñoz, J. Muir, M. Nicholl, E. Quataert, A. Rest, M. Sauseda, D. J. Schlegel, L. F. Secco, F. Sobreira, A. Stebbins, V. A. Villar, K. Vivas, A. R. Walker, W. Wester, P. K. G. Williams, A. Zenteno, Y. Zhang, T. M. C. Abbott, F. B. Abdalla, M. Banerji, K. Bechtol, A. Benoit-Lévy, E. Bertin, D. Brooks, E. Buckley-Geer, D. L. Burke, A. Carnero Rosell, M. Carrasco Kind, J. Carretero, F. J. Castander, M. Crocce, C. E. Cunha, C. B. D'Andrea, L. N. da Costa, C. Davis, S. Desai, J. P. Dietrich, P. Doel, T. F. Eifler, E. Fernandez, B. Flaugher, P. Fosalba, E. Gaztanaga, D. W. Gerdes, T. Giannantonio, D. A. Goldstein, D. Gruen, J. Gschwend, G. Gutierrez, K. Honscheid, B. Jain, D. J. James, T. Jeltema, M. W. G. Johnson, M. D. Johnson, S. Kent, E. Krause, R. Kron, K. Kuehn, S. Kuhlmann, O. Lahav, M. Lima, M. A. G. Maia, M. March, R. G. McMahon, F. Menanteau, R. Miquel, J. J. Mohr, R. C. Nichol, B. Nord, R. L. C. Ogando, D. Petravick, A. A. Plazas, A. K. Romer, A. Roodman, E. S. Rykoff, E. Sanchez, V. Scarpine, M. Schubnell, I. Sevilla-Noarbe, M. Smith, R. C. Smith, E. Suchyta, M. E. C. Swanson, G. Tarle, D. Thomas, R. C. Thomas, M. A. Troxel, V. Vikram, R. H. Wechsler, J. Weller, Dark Energy Survey, and Dark Energy Camera GW-EM Collaboration (2017), Astrophys. J. Lett. **848**, L16, arXiv:1710.05459 [astro-ph.HE].

Söderström, P.-A., S. Nishimura, P. Doornenbal, G. Lorusso, T. Sumikama, H. Watanabe, Z. Y. Xu, H. Baba, F. Browne, S. Go, G. Gey, T. Isobe, H.-S. Jung, G. D. Kim, Y.-K. Kim, I. Kojouharov, N. Kurz, Y. K. Kwon, Z. Li, K. Moschner, T. Nakao, H. Nishibata, M. Nishimura, A. Odahara, H. Sakurai, H. Schaffner, T. Shimoda, J. Taprogge, Z. Vajta, V. Werner, J. Wu, A. Yagi, and K. Yoshinaga (2013), Nuclear Instruments and Methods in Physics Research B **317**, 649.

Sørensen, M., H. Svensmark, and U. Gråe Jørgensen (2017), ArXiv e-prints arXiv:1708.08248 [astro-ph.SR].

Sorokin, P. P., and J. R. Lankard (1966), IBM Res. Develop. **10**, 187.

Spitoni, E., F. Matteucci, S. Recchi, G. Cescutti, and A. Pipino (2009), Astron. & Astrophys. **504**, 87, arXiv:0906.3400.

Spyrou, A., A. C. Larsen, S. N. Liddick, F. Naqvi, B. P. Crider, A. C. Dombos, M. Guttormsen, D. L. Bleuel, A. Couture, L. Crespo Campo, R. Lewis, S. Mosby, M. R. Mumpower, G. Perdikakis, C. J. Prokop, S. J. Quinn, T. Renstrøm, S. Siem, and R. Surman (2017), Journal of Physics G Nuclear Physics **44** (4), 044002.

Spyrou, A., S. N. Liddick, A. C. Larsen, M. Guttormsen, K. Cooper, A. C. Dombos, D. J. Morrissey, F. Naqvi, G. Perdikakis, S. J. Quinn, T. Renstrøm, J. A. Rodriguez, A. Simon, C. S. Sumithrarachchi, and R. G. T. Zegers (2014), Phys. Rev. Lett. **113** (23), 232502, arXiv:1408.6498 [nucl-ex].

Steinberg, E. P., and B. D. Wilkins (1978), Astrophys. J. **223**, 1000.

Steiner, A. W., M. Hempel, and T. Fischer (2013), Astrophys. J. **774**, 17, arXiv:1207.2184 [astro-ph.SR].

Steiner, A. W., J. M. Lattimer, and E. F. Brown (2016), European Physical Journal A **52**, 18, arXiv:1510.07515 [astro-ph.HE].

Sukhbold, T., T. Ertl, S. E. Woosley, J. M. Brown, and H.-T. Janka (2016), Astrophys. J. **821**, 38.

Sumiyoshi, K., M. Terasawa, G. J. Mathews, T. Kajino, S. Yamada, and H. Suzuki (2001), Astrophys. J. **562**, 880, astro-ph/0106407.

Sun, B., R. Knöbel, Y. A. Litvinov, H. Geissel, J. Meng, K. Beckert, F. Bosch, D. Boutin, C. Brandau, L. Chen, I. J. Cullen, C. Dimopoulou, B. Fabian, M. Hausmann, C. Kozhuharov, S. A. Litvinov, M. Mazzocco, F. Montes, G. Münzenberg, A. Musumarra, S. Nakajima, C. Nociforo, F. Nolden, T. Ohtsubo, A. Ozawa, Z. Patyk, W. R. Plaß, C. Scheidenberger, M. Steck, T. Suzuki, P. M. Walker, H. Weick, N. Winckler, M. Winkler, and T. Yamaguchi (2008), Nucl. Phys. A **812**, 1.

Sun, B.-H., and J. Meng (2008), Chinese Physics Letters **25**, 2429, arXiv:0807.2509 [nucl-th].

Surman, R., O. L. Caballero, G. C. McLaughlin, O. Just, and H.-T. Janka (2014), J. Phys. G: Nucl. Part. Phys. **41** (4), 044006, arXiv:1312.1199 [astro-ph.SR].

Surman, R., J. Engel, J. R. Bennett, and B. S. Meyer (1997), Phys. Rev. Lett. **79**, 1809.

Surman, R., G. C. McLaughlin, and W. R. Hix (2006), Astrophys. J. **643**, 1057, astro-ph/0509365.

Surman, R., G. C. McLaughlin, M. Ruffert, H.-T. Janka, and W. R. Hix (2008), Astrophys. J. **679**, L117, arXiv:0803.1785.

Suzuki, T., T. Yoshida, T. Kajino, and T. Otsuka (2012), Phys. Rev. C **85**, 015802.

Svanberg, S., J. Larsson, A. Persson, and C.-G. Wahlström (1994), Phys. Sscr **49**, 187.

Symbalisty, E., and D. N. Schramm (1982), Astrophys. J. **22**, 143.

Symbalisty, E. M. D., D. N. Schramm, and J. R. Wilson (1985), Astrophys. J. **291**, L11.
Tachibana, T., M. Yamada, and Y. Yoshida (1990), Prog. Theor. Phys. **84**, 641.
Takahashi, K., J. Witti, and H.-T. Janka (1994), Astron. & Astrophys. **286**, 857.
Takiwaki, T., and K. Kotake (2011), Astrophys. J. **743**, 30, arXiv:1004.2896 [astro-ph.HE].
Takiwaki, T., K. Kotake, and K. Sato (2009), Astrophys. J. **691**, 1360, arXiv:0712.1949.
Talbert, W. L., F. K. Wohn, J. C. Hill, A. R. Landin, M. A. Cullison, and R. L. Gill (1979), Nuclear Instruments and Methods **161**, 431.
Tanaka, M. (2016), Adv. Astron. **2016**, 634197.
Tanaka, M., and K. Hotokezaka (2013), Astrophys. J. **775**, 113.
Tanaka, M., D. Kato, G. Gaigalas, P. Rynkun, L. Radžiūtė, S. Wanajo, Y. Sekiguchi, N. Nakamura, H. Tanuma, I. Murakami, and H. A. Sakaue (2018), Astrophys. J. **852**, 109.
Tanaka, M., Y. Utsumi, P. A. Mazzali, N. Tominaga, M. Yoshida, Y. Sekiguchi, T. Morokuma, K. Motohara, K. Ohta, K. S. Kawabata, F. Abe, K. Aoki, Y. Asakura, S. Baar, S. Barway, I. A. Bond, M. Doi, T. Fujiyoshi, H. Furusawa, S. Honda, Y. Itoh, M. Kawabata, N. Kawai, J. H. Kim, C.-H. Lee, S. Miyazaki, K. Morihana, H. Nagashima, T. Nagayama, T. Nakaoka, F. Nakata, R. Ohsawa, T. Ohshima, H. Okita, T. Saito, T. Sumi, A. Tajitsu, J. Takahashi, M. Takayama, Y. Tamura, I. Tanaka, T. Terai, P. J. Tristram, N. Yasuda, and T. Zenko (2017), Publ. Astron. Soc. Japan **69**, 102, arXiv:1710.05850 [astro-ph.HE].
Tanvir, N. R., A. J. Levan, A. S. Fruchter, J. Hjorth, R. A. Hounsell, K. Wiersema, and R. L. Tunnicliffe (2013), Nature **500**, 547, arXiv:1306.4971 [astro-ph.HE].
Tanvir, N. R., A. J. Levan, C. González-Fernández, O. Korobkin, I. Mandel, S. Rosswog, J. Hjorth, P. D'Avanzo, A. S. Fruchter, C. L. Fryer, T. Kangas, B. Milvang-Jensen, S. Rosetti, D. Steeghs, R. T. Wollaeger, Z. Cano, C. M. Copperwheat, S. Covino, V. D'Elia, A. de Ugarte Postigo, P. A. Evans, W. P. Even, S. Fairhurst, R. Figuera Jaimes, C. J. Fontes, Y. I. Fujii, J. P. U. Fynbo, B. P. Gompertz, J. Greiner, G. Hodosan, M. J. Irwin, P. Jakobsson, U. G. Jørgensen, D. A. Kann, J. D. Lyman, D. Malesani, R. G. McMahon, A. Melandri, P. T. O'Brien, J. P. Osborne, E. Palazzi, D. A. Perley, E. Pian, S. Piranomonte, M. Rabus, E. Rol, A. Rowlinson, S. Schulze, P. Sutton, C. C. Thöne, K. Ulaczyk, D. Watson, K. Wiersema, and R. A. M. J. Wijers (2017), Astrophys. J. Lett. **848**, L27, arXiv:1710.05455 [astro-ph.HE].
Tauris, T. M., M. Kramer, P. C. C. Freire, N. Wex, H.-T. Janka, N. Langer, P. Podsiadlowski, E. Bozzo, S. Chaty, M. U. Kruckow, E. P. J. van den Heuvel, J. Antoniadis, R. P. Breton, and D. J. Champion (2017), Astrophys. J. **846**, 170.
Terasawa, M., K. Langanke, T. Kajino, G. J. Mathews, and E. Kolbe (2004), Astrophys. J. **608**, 470.
Terasawa, M., K. Sumiyoshi, T. Kajino, G. J. Mathews, and I. Tanihata (2001), Astrophys. J. **562**, 470.
Tews, I., J. Margueron, and S. Reddy (2018), Phys. Rev. C **98**, 045804.
Thielemann, F.-K., M. Arnould, and W. Hillebrandt (1979), Astron. & Astrophys. **74**, 175.
Thielemann, F.-K., A. G. W. Cameron, and J. J. Cowan (1989), in *50 Years with Nuclear Fission*, American Nuclear Society, ISBN: 978-0-89448-578-7, edited by J. Behrens and A. Carlson, p. 592.
Thielemann, F.-K., M. Eichler, I. V. Panov, M. Pignatrari, and B. Wehmeyer (2017a), "Making the Heaviest Elements in a Rare Class of Supernovae," in *Handbook of Supernovae*, edited by A. W. Alsabti and P. Murdin (Springer International Publishing, Cham).
Thielemann, F.-K., M. Eichler, I. V. Panov, and B. Wehmeyer (2017b), Annu. Rev. Nucl. Part. Sci. **67**, 253.
Thielemann, F.-K., A. Heger, R. Hirschi, M. Liebendörfer, and R. Diehl (2018), in *Astrophysics with Radioactive Istopes, Berlin Springer Verlag*, Astrophysics and Space Science Library, Berlin Springer Verlag, Vol. 453, edited by R. Diehl, D. H. Hartmann, and N. Prantzos, pp. 173–286, arXiv:1008.2144 [astro-ph.HE].
Thielemann, F.-K., R. Hirschi, M. Liebendörfer, and R. Diehl (2011), in *Lecture Notes in Physics, Berlin Springer Verlag*, Lecture Notes in Physics, Berlin Springer Verlag, Vol. 812, edited by R. Diehl, D. H. Hartmann, and N. Prantzos, pp. 153–232, arXiv:1008.2144 [astro-ph.HE].
Thielemann, F.-K., J. Metzinger, and H. V. Klapdor (1983), Zeitschrift für Phys. A Atoms Nucl. **309**, 301.
Thielemann, F.-K., *et al.* (2011), Prog. Part. Nucl. Phys. **66** (2), 346.
Thompson, T. A., A. Burrows, and B. S. Meyer (2001), Astrophys. J. **562**, 887.
Timmes, F. X. (1999), Astrophys. J. Suppl. **124**, 241.
Timmes, F. X., S. E. Woosley, and T. A. Weaver (1995), Astrophys. J. Suppl. **98**, 617.
Tinsley, B. M. (1980), fcp **5**, 287.
Tornyi, T. G., M. Guttormsen, T. K. Eriksen, A. Görgen, F. Giacoppo, T. W. Hagen, A. Krasznahorkay, A. C. Larsen, T. Renstrøm, S. J. Rose, S. Siem, and G. M. Tveten (2014), Phys. Rev. C **89** (4), 044323.
Travaglio, C., D. Galli, R. Gallino, M. Busso, F. Ferrini, and O. Straniero (1999), Astrophys. J. **521**, 691.
Travaglio, C., R. Gallino, E. Arnone, J. Cowan, F. Jordan, and C. Sneden (2004), Astrophys. J. **601**, 864.
Travaglio, C., T. Rauscher, A. Heger, M. Pignatari, and C. West (2018), Astrophys. J. **854**, 18, arXiv:1801.01929 [astro-ph.SR].
Truran, J. W., J. J. Cowan, and A. G. W. Cameron (1978), Astrophys. J. **222**, L63.
Tsujimoto, T., Y. Yoshii, K. Nomoto, F. Matteucci, F.-K. Thielemann, and M. Hashimoto (1997), Astrophys. J. **483**, 228, astro-ph/9702205.
Ural, U., G. Cescutti, A. Koch, J. Kleyna, S. Feltzing, and M. I. Wilkinson (2015), Mon. Not. Roy. Astron. Soc. **449**, 761, arXiv:1502.04133.
van de Voort, F., E. Quataert, P. F. Hopkins, D. Kereš, and C.-A. Faucher-Giguère (2015), Mon. Not. Roy. Astron. Soc. **447**, 140, arXiv:1407.7039.
van de Voort, F., *et al.* (2018), private communication.
Vangioni, E., S. Goriely, F. Daigne, P. François, and K. Belczynski (2016), Mon. Not. Roy. Astron. Soc. **455**, 17, arXiv:1501.01115 [astro-ph.HE].
Vassh, N., R. Vogt, R. Surman, J. Randrup, T. Sprouse, M. Mumpower, P. Jaffke, D. Shaw, E. Holmbeck, Y. Zhu, and G. McLaughlin (2018), arXiv e-prints , arXiv:1810.08133arXiv:1810.08133 [nucl-th].
Venn, K. A., E. Tolstoy, A. Kaufer, E. D. Skillman, S. M. Clarkson, S. J. Smartt, D. J. Lennon, and R. P. Kudritzki (2003), aj **126**, 1326, astro-ph/0306160.
Vilen, M., J. M. Kelly, A. Kankainen, M. Brodeur, A. Apra-

hamian, L. Canete, T. Eronen, A. Jokinen, T. Kuta, I. D. Moore, M. R. Mumpower, D. A. Nesterenko, H. Penttilä, I. Pohjalainen, W. S. Porter, S. Rinta-Antila, R. Surman, A. Voss, and J. Äystö (2018), Phys. Rev. Lett. **120** (26), 262701.

Villar, V. A., P. S. Cowperthwaite, E. Berger, P. K. Blanchard, S. Gomez, K. D. Alexander, R. Margutti, R. Chornock, T. Eftekhari, G. G. Fazio, J. Guillochon, J. L. Hora, M. Nicholl, and P. K. G. Williams (2018), Astrophys. J. Lett. **862**, L11, arXiv:1805.08192 [astro-ph.HE].

Villar, V. A., J. Guillochon, E. Berger, B. D. Metzger, P. S. Cowperthwaite, M. Nicholl, K. D. Alexander, P. K. Blanchard, R. Chornock, T. Eftekhari, W. Fong, R. Margutti, and P. K. G. Williams (2017), Astrophys. J. Lett. **851**, L21.

Vink, J., J. M. Laming, J. S. Kaastra, J. A. M. Bleeker, H. Bloemen, and U. Oberlack (2001), Astrophys. J. Lett. **560**, L79.

Vlasenko, A., and G. C. McLaughlin (2018), Phys. Rev. D **97**, 083011.

Wallner, A., T. Faestermann, J. Feige, C. Feldstein, K. Knie, G. Korschinek, W. Kutschera, A. Ofan, M. Paul, F. Quinto, G. Rugel, and P. Steier (2015), Nature Communications **6**, 5956.

Wallner, A., J. Feige, N. Kinoshita, M. Paul, L. K. Fifield, R. Golser, M. Honda, U. Linnemann, H. Matsuzaki, S. Merchel, G. Rugel, S. G. Tims, P. Steier, T. Yamagata, and S. R. Winkler (2016), Nature **532**, 69.

Wanajo, S. (2006), Astrophys. J. **647**, 1323.

Wanajo, S. (2007), Astrophys. J. **666**, L77.

Wanajo, S. (2018), Astrophys. J. **868**, 65.

Wanajo, S., and Y. Ishimaru (2006), Nucl. Phys. A **777**, 676.

Wanajo, S., and H.-T. Janka (2012a), Astrophys. J. **746**, 180, arXiv:1106.6142 [astro-ph.SR].

Wanajo, S., and H.-T. Janka (2012b), Astrophys. J. **746**, 180.

Wanajo, S., H.-T. Janka, and B. Müller (2011), Astrophys. J. **726** (2), L15.

Wanajo, S., H.-T. Janka, and B. Müller (2013), Astrophys. J. **774**, L6.

Wanajo, S., T. Kajino, G. J. Mathews, and K. Otsuki (2001), Astrophys. J. **554**, 578.

Wanajo, S., B. Müller, H.-T. Janka, and A. Heger (2018), Astrophys. J. **852**, 40.

Wanajo, S., K. Nomoto, H. Janka, F. S. Kitaura, and B. Müller (2009), Astrophys. J. **695**, 208.

Wanajo, S., Y. Sekiguchi, N. Nishimura, K. Kiuchi, K. Kyutoku, and M. Shibata (2014), Astrophys. J. **789**, L39.

Wanderman, D., and T. Piran (2015), Mon. Not. Roy. Astron. Soc. **448**, 3026, arXiv:1405.5878 [astro-ph.HE].

Wang, M., G. Audi, A. Wapstra, F. Kondev, M. MacCormick, X. Xu, and B. Pfeiffer (2012), Chinese Phys. C **36** (12), 1603.

Wang, N., M. Liu, and X. Wu (2010), Phys. Rev. C **81** (5), 059902.

Waxman, E., E. O. Ofek, D. Kushnir, and A. Gal-Yam (2018), Mon. Not. Roy. Astron. Soc. **481**, 3423.

Way, K., and E. P. Wigner (1948), Phys. Rev. **73**, 1318.

Wehmeyer, B., M. Pignatari, and F.-K. Thielemann (2015), Mon. Not. Roy. Astron. Soc. **452**, 1970, arXiv:1501.07749.

Wehmeyer, B., *et al.* (2018), private communication.

Weisberg, J. M., and Y. Huang (2016), Astrophys. J. **829**, 55.

Westin, J., C. Sneden, B. Gustafsson, and J. J. Cowan (2000), Astrophys. J. **530**, 783, astro-ph/9910376.

Whaling, W., M. T. Carle, and M. L. Pitt (1993), J. Quant Spec. Rad. Trans. **50**, 7.

Wheeler, J. C., J. J. Cowan, and W. Hillebrandt (1998), Astrophys. J. **493**, L101.

Wheeler, J. C., C. Sneden, and J. W. Truran, Jr. (1989), Annu. Rev. Astron. Astrophys. **27**, 279.

Winteler, C., R. Käppeli, A. Perego, A. Arcones, N. Vasset, N. Nishimura, M. Liebendörfer, and F.-K. Thielemann (2012), Astrophys. J. **750**, L22.

Wisshak, K., F. Voss, C. Arlandini, F. Käppeler, and L. Kazakov (2000), Phys. Rev. C **61** (6), 065801.

Witti, J., H.-T. Janka, and K. Takahashi (1994), Astron. & Astrophys. **286**, 841.

Wojczuk, K., and A. Janiuk (2018), in *XXXVIII Polish Astronomical Society Meeting*, Vol. 7, edited by A. Różańska, pp. 337–340.

Woosley, S. E., D. H. Hartmann, R. D. Hoffman, and W. C. Haxton (1990), Astrophys. J. **356**, 272.

Woosley, S. E., and A. Heger (2007), Phys. Rep. **442**, 269, astro-ph/0702176.

Woosley, S. E., A. Heger, and T. A. Weaver (2002), Rev. Mod. Phys. **74**, 1015.

Woosley, S. E., and R. D. Hoffman (1992), Astrophys. J. **395**, 202.

Woosley, S. E., J. R. Wilson, G. J. Mathews, R. D. Hoffman, and B. S. Meyer (1994), Astrophys. J. **433**, 229.

Wu, J., S. Nishimura, G. Lorusso, P. Möller, E. Ideguchi, P.-H. Regan, G. S. Simpson, P.-A. Söderström, P. M. Walker, H. Watanabe, Z. Y. Xu, H. Baba, F. Browne, R. Daido, P. Doornenbal, Y. F. Fang, N. Fukuda, G. Gey, T. Isobe, Z. Korkulu, P. S. Lee, J. J. Liu, Z. Li, Z. Patel, V. Phong, S. Rice, H. Sakurai, L. Sinclair, T. Sumikama, M. Tanaka, A. Yagi, Y. L. Ye, R. Yokoyama, G. X. Zhang, D. S. Ahn, T. Alharbi, N. Aoi, F. L. Bello Garrote, G. Benzoni, A. M. Bruce, R. J. Carroll, K. Y. Chae, Z. Dombradi, A. Estrade, A. Gottardo, C. J. Griffin, N. Inabe, D. Kameda, H. Kanaoka, I. Kojouharov, F. G. Kondev, T. Kubo, S. Kubono, N. Kurz, I. Kuti, S. Lalkovski, G. J. Lane, E. J. Lee, T. Lokotko, G. Lotay, C.-B. Moon, D. Murai, H. Nishibata, I. Nishizuka, C. R. Nita, A. Odahara, Z. Podolyák, O. J. Roberts, H. Schaffner, C. Shand, Y. Shimizu, H. Suzuki, H. Takeda, J. Taprogge, S. Terashima, Z. Vajta, and S. Yoshida (2017a), Phys. Rev. Lett. **118**, 072701.

Wu, M.-R., J. Barnes, G. Martínez-Pinedo, and B. D. Metzger (2018), Phys. Rev. Lett. accepted, arXiv:1808.10459 [astro-ph.HE].

Wu, M.-R., R. Fernández, G. Martínez-Pinedo, and B. D. Metzger (2016), Mon. Not. Roy. Astron. Soc. **463**, 2323.

Wu, M.-R., T. Fischer, L. Huther, G. Martínez-Pinedo, and Y.-Z. Qian (2014), Phys. Rev. D **89**, 061303(R).

Wu, M.-R., Y.-Z. Qian, G. Martínez-Pinedo, T. Fischer, and L. Huther (2015), Phys. Rev. D **91**, 065016.

Wu, M.-R., and I. Tamborra (2017), Phys. Rev. D **95**, 103007.

Wu, M.-R., I. Tamborra, O. Just, and H.-T. Janka (2017b), Phys. Rev. D **96**, 123015.

Wu, Y., and A. MacFadyen (2018), Astrophys. J. **869**, 55.

Wünsch, K.-d. (1978), Nuclear Instruments and Methods **155**, 347.

Xu, Y., and S. Goriely (2012), Phys. Rev. C **86** (4), 045801.

Xu, Y., S. Goriely, A. J. Koning, and S. Hilaire (2014), Phys. Rev. C **90** (2), 024604.

Yakovlev, D. G., P. Haensel, G. Baym, and C. Pethick (2013), Physics Uspekhi **56**, 289.

Yan, X. L., K. Blaum, Y. A. Litvinov, X. L. Tu, H. S. Xu, Y. H. Zhang, X. H. Zhou, ESR, and CSRe Collaborations on In-Ring Mass Measurements (2016), in *Journal of Physics Conference Series*, Journal of Physics Conference Series, Vol. 665, p. 012053.

Yee, R. M., N. D. Scielzo, P. F. Bertone, F. Buchinger, S. Caldwell, J. A. Clark, C. M. Deibel, J. Fallis, J. P. Greene, S. Gulick, D. Lascar, A. F. Levand, G. Li, E. B. Norman, M. Pedretti, G. Savard, R. E. Segel, K. S. Sharma, M. G. Sternberg, J. Van Schelt, and B. J. Zabransky (2013), Phys. Rev. Lett. **110** (9), 092501.

Yeh, T.-R., D. D. Clark, G. Scharff-Goldhaber, R. E. Chrien, L.-J. Yuan, M. Shmid, R. L. Gill, A. E. Evans, H. Dautet, and J. Lee (1983), in *Nuclear Data for Science and Technology*, edited by K. H. Böckhoff (Springer Netherlands, Dordrecht) pp. 261–264.

Yong, D., J. E. Norris, G. S. Da Costa, L. M. Stanford, A. I. Karakas, L. J. Shingles, R. Hirschi, and M. Pignatari (2017), Astrophys. J. **837**, 176, arXiv:1702.07087 [astro-ph.SR].

Zampieri, L. (2017), "Light Curves of Type II Supernovae," in *Handbook of Supernovae*, edited by A. W. Alsabti and P. Murdin (Springer International Publishing, Cham).

Zhang, C. L., B. Schuetrumpf, and W. Nazarewicz (2016), Phys. Rev. C **94** (6), 064323, arXiv:1607.00422 [nucl-th].

Zhi, Q., E. Caurier, J. J. Cuenca-García, K. Langanke, G. Martínez-Pinedo, and K. Sieja (2013), Phys. Rev. C **87**, 025803.

Zhu, Y., R. T. Wollaeger, N. Vassh, R. Surman, T. M. Sprouse, M. R. Mumpower, P. Möller, G. C. McLaughlin, O. Korobkin, T. Kawano, P. J. Jaffke, E. M. Holmbeck, C. L. Fryer, W. P. Even, A. J. Couture, and J. Barnes (2018), Astrophys. J. **863**, L23.

Zhu, Y. L., A. Perego, and G. C. McLaughlin (2016), Phys. Rev. D **94** (10), 105006, arXiv:1607.04671 [hep-ph].

Zrake, J., and A. I. MacFadyen (2013), Astrophys. J. **769**, L29.